LUND UNIVERSITY

Vibration transmission in lightweight buildings

Numerical prediction models

Flodén, Ola

2016

Document Version:
Publisher's PDF, also known as Version of record

LUND UNIVERSITY

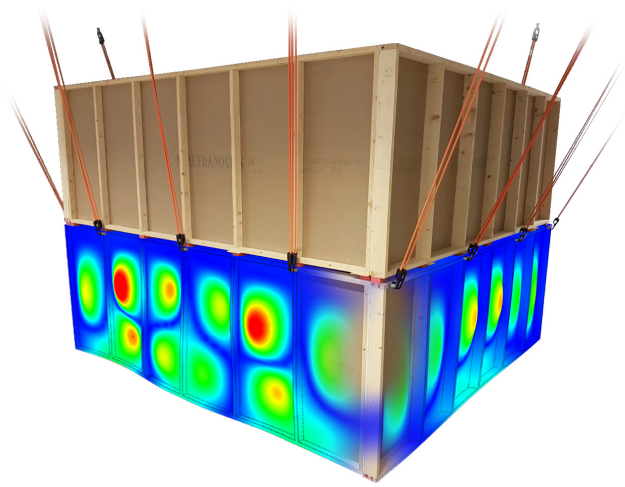

VIBRATION TRANSMISSION IN LIGHTWEIGHT BUILDINGS

Numerical prediction models

OLA FLODÉN

Structural Mechanics

Doctoral Thesis

DEPARTMENT OF CONSTRUCTION SCIENCES
DIVISION OF STRUCTURAL MECHANICS

ISRN LUTVDG/TVSM--16/1028--SE (1-180) | ISSN 0281-6679
ISBN 978-91-7753-082-4 (print) | ISBN 978-91-7753-083-1 (pdf)
DOCTORAL THESIS

VIBRATION TRANSMISSION IN LIGHTWEIGHT BUILDINGS

Numerical prediction models

OLA FLODÉN

Printed by Media-Tryck LU, Lund, Sweden, December 2016 *(Pl)*.

For information, address:
Division of Structural Mechanics,
Faculty of Engineering LTH, Lund University, Box 118, SE-221 00 Lund, Sweden.
Homepage: www.byggmek.lth.se

Acknowledgements

The work presented in this thesis was carried out at the Department of Construction Sciences at Lund University. The financial support provided by the Silent Spaces and Urban Tranquility projects, parts of the EU programs Interreg IVA and Interreg V, is gratefully acknowledged.

I would like to thank my supervisors Prof. Kent Persson and Prof. Göran Sandberg for all their work and continuous support along the way towards finalising this thesis. I am also grateful to my colleagues at the Division of Structural Mechanics for always creating a good atmosphere and making the working days enjoyable. Especially to Håkan Hansson for all the encouraging banter. Furthermore, I would like to thank the graphics magician Bo Zadig for all his help with illustrations and for providing a soundtrack to my working days. I would also like to thank Anders Sjöström for his help in the lab and for a short but pleasant stint as office mates. A special thank you is directed to Peter Persson and Juan Negreira who have not only become two of my best friends, but have also supported me in my work more than could ever be expected of any friend or colleague.

Finally, I would like to thank my family, especially my parents Kristina and Ingvar, for their endless support throughout my life and for always being there when needed. Nothing else has meant as much to me.

Lund, December 2016
Ola Flodén

Abstract

Wood buildings currently account for 10–15% of the newly produced multi-family housings in Sweden and their construction is increasing rapidly. Although modern wood buildings fulfil the requirements for sound insulation specified in building regulations, studies have shown that residents in wood buildings are more disturbed by noise and vibrations than are residents in conventional concrete buildings. Especially problematic is the transmission of low-frequency structure-borne sound between storeys and rooms. During the last few decades, the vibroacoustic comfort of residents has improved as a result of the efforts to reduce noise and vibration transmission. However, there are no reliable models for predicting the noise and vibration transmission in the buildings. If accurate and efficient numerical models were available, they would facilitate the optimisation of existing measures for noise and vibration reduction and the development of novel types of measures. The objective of the research presented in this thesis is to develop such models.

The thesis work focuses on the numerical modelling of low-frequency vibration transmission from a source to a receiving room. Accurate models of the structural vibrations are valuable for predicting structure-borne sound as well as floor vibrations. Two main topics are discussed in the thesis: model validation to ensure accurate predictions and dynamic substructuring to improve the computational efficiency. The studies were performed using example cases representing parts of timber volume element buildings. Such buildings are constructed by stacking pre-fabricated volume elements with elastomeric vibration isolators between storeys to reduce vibration transmission. The timber volume element buildings account for a large part of the construction of multi-storey wood buildings in Sweden.

An important step towards validating the numerical models is to perform model correlations to unveil errors and update the models. In the thesis, a model correlation study for the low-frequency vibration transmission in an experimental wooden building structure is presented. It was found that deterministic methods are relevant for creating the models provided that measurement data for calibration purposes is available. Based on the observations made in the correlation studies, important modelling parameters are discussed and modelling guidelines are presented. The studies presented in the thesis also consider the modelling of air and insulation in cavities of wood buildings, which were found to have appreciable effect on the vibration transmission.

A strategy for dynamic substructuring of wood buildings is suggested in the thesis. It involves methods for model order reduction and for interface reduction of substructure models, and uses coupling elements to represent elastomeric vibration isolators between building elements. It was shown that by performing the model reduction in the suggested manner, the computation times of numerical analyses can be reduced significantly without having an appreciable effect on the accuracy of the model predictions.

Several uncertainties in the modelling remain, but the results and conclusions presented in the thesis are important steps towards enabling the prediction of vibration transmission by use of numerical models.

Keywords: vibration transmission, structure-borne sound, wood buildings, numerical modelling, finite element method, structure-acoustic coupling, model validation, model calibration, dynamic substructuring, model order reduction

Populärvetenskaplig sammanfattning

Ljud från grannar är ett återkommande problem för boende i flerfamiljshus. Problemen är generellt mer omfattande för de som bor i flervåningshus byggda i trä, en byggnadstyp som blir allt vanligare i Sverige. Många av de boende i trähus upplever även att störande vibrationer är vanligt förekommande i trähus. För att designa byggnader med förbättrad boendemiljö avseende ljud och vibrationer behövs metoder för att prediktera spridningen mellan rum och våningsplan. I avhandlingen presenteras forskning som bidrar till att utveckla datormodeller för sådana prediktioner.

Fram till 1994 var det förbjudet att bygga flervåningshus i trä i Sverige. Sedan förbudet avskaffades har de blivit allt vanligare och står idag för 10–15% av den totala nybyggnationen av flerfamiljshus i Sverige. En stor andel av trähusen tillverkas genom att prefabricera volymelement i fabriker. Volymelementen transporteras sedan till byggarbetsplatser där de staplas för att bilda flervåningshus. Detta leder till en snabb och kostnadseffektiv byggprocess som är möjlig tack vare trähusens låga vikt. Det finns flera miljömässiga fördelar med att bygga i trä, exempelvis att den låga vikten leder till minskad bränsleförbrukning vid transporter och att koldioxid lagras i byggnaderna. För att byggandet i trä ska öka på lång sikt är det viktigt att boendemiljön i trähus anses vara tillfredsställande. En del i att uppnå det är att minska risken för störande ljud och vibrationer.

I tidigare studier har det undersökt hur boende i olika typer av byggnader uppfattar ljud och vibrationer som orsakas av olika typer av källor. Studierna har visat att boende i trähus ofta störs av ljud som orsakas av stötar mot golv i grannlägenheter, exempelvis fotsteg. För boende i konventionella betonghus är sådana problem inte lika vanligt förekommande. I nyproducerade flervåningshus i trä används ofta gummikomponenter för att minska överföringen av ljud och vibrationer mellan lägenheter. Dock saknas det kunskap om hur gummikomponenterna bör designas för att verka optimalt. För att öka kunskapen är det till stor nytta att datormodeller som kan generera korrekta prediktioner är tillgängliga. Med hjälp av datormodeller kan gummikomponenternas reducerande effekt optimeras och andra typer av ljud- och vibrationsisolerande åtgärder kan utvecklas. Alternativet till datormodeller är att bygga experimentella prototyper, vilket är såväl dyrt som tidskrävande. Genom att använda datormodeller kan studier utföras både tids- och kostnadseffektivt. Tidsaspekten är viktig för att möjliggöra simuleringar inom tidsramen för en konventionell designprocess.

Forskningen som presenteras i avhandlingen bidrar till att utveckla tidseffektiva datormodeller som kan användas till att generera korrekta prediktioner. Noggrannheten i prediktioner utvecklas genom att korrelera simulerade resultat mot mätningar på experimentella byggnadsstrukturer. Tidsåtgången för beräkningar minskas genom att använda metoder för att reducera storleken på datormodeller. Målet med modellreduktion är att minska beräkningstiden utan att göra avkall på noggrannheten i prediktioner.

Contents

I Introduction and overview **xiii**

1 Introduction **1**
1.1 Aim and objective . . . 4
1.2 Procedure for model development . . . 4
1.3 Outline . . . 6

2 Noise and vibrations in wood buildings **7**
2.1 Wood as construction material . . . 7
2.1.1 Mechanical properties of wood . . . 8
2.1.2 Engineered wood products . . . 10
2.1.3 Construction of multi-storey wood buildings . . . 10
2.2 Noise and vibration transmission in buildings . . . 11
2.2.1 Building regulations . . . 13
2.2.2 Vibroacoustic issues in residential wood buildings . . . 14
2.2.3 Noise and vibration reduction measures . . . 15
2.3 Numerical prediction models . . . 16
2.3.1 Modelling strategies . . . 17
2.3.2 Deterministic methods . . . 19
2.3.3 Model reduction . . . 19

3 Governing theory **21**
3.1 Structure-acoustic equations . . . 21
3.1.1 Structural domain . . . 22
3.1.2 Acoustic domain . . . 23
3.1.3 Coupling of domains . . . 24
3.2 Finite element method . . . 24
3.2.1 Weak formulation . . . 24
3.2.2 Finite element formulation . . . 25
3.3 Analysis of structural dynamic systems . . . 27
3.3.1 Free vibrations . . . 28
3.3.2 Harmonic excitation . . . 29
3.3.3 Damped systems . . . 30
3.3.4 Nonlinear systems . . . 33
3.4 Experimental modal analysis . . . 34
3.4.1 Frequency response measurements . . . 35

3.4.2 Modal parameter estimation . . . 37

4 Model validation **39**
4.1 General procedure in structural dynamics . . . 39
4.1.1 Calibrations . . . 41
4.1.2 Correlations . . . 41
4.1.3 Applying the procedure to low-frequency vibration transmission in wood buildings . . . 42
4.2 Literature review on numerical modelling of low-frequency vibrations in wood buildings . . . 42
4.2.1 Summary . . . 45
4.3 Conclusions in appended publications . . . 46

5 Dynamic substructuring **49**
5.1 Theoretical background . . . 50
5.1.1 Model order reduction . . . 50
5.1.2 Interface reduction . . . 51
5.2 Strategy used in thesis . . . 51
5.3 Conclusions in appended publications . . . 52

6 Summary of appended publications **55**
6.1 Paper A . . . 55
6.2 Paper B . . . 56
6.3 Paper C . . . 56
6.4 Paper D . . . 57
6.5 Paper E . . . 58
6.6 Paper F . . . 58

7 Concluding remarks **61**
7.1 Conclusions and contributions . . . 61
7.1.1 Model validation . . . 62
7.1.2 Dynamic substructuring . . . 62
7.2 Proposals for future work . . . 63

References **65**

II Appended publications **71**

Paper A
Numerical investigation of vibration reduction in multi-storey lightweight buildings.
Ola Flodén, Kent Persson, Göran Sandberg.
In: Dynamics of Civil Structures, Vol 2: 443–453. Springer International Publishing, 2015.

Paper B
The effect of modelling acoustic media in cavities of lightweight building structures on the transmission of structural vibrations.
Ola Flodén, Juan Negreira, Kent Persson, Göran Sandberg.
Engineering Structures 83: 7–16, 2015.

Paper C
Numerical and experimental studies on scale models of lightweight building structures.
Ola Flodén, Kent Persson, Göran Sandberg.
In: Dynamics of Coupled Structures, Vol 4: 173–180. Springer International Publishing, 2016.

Paper D
A multi-level model correlation approach for low-frequency vibration transmission in wood structures.
Ola Flodén, Kent Persson, Göran Sandberg.
Submitted for publication.

Paper E
Modelling of elastomeric vibration isolators in dynamic substructuring.
Ola Flodén, Kent Persson, Göran Sandberg.
Submitted for publication.

Paper F
Reduction methods for the dynamic analysis of substructure models of lightweight building structures.
Ola Flodén, Kent Persson, Göran Sandberg.
Computers & Structures 138: 49–61, 2014.

Part I

Introduction and overview

1 Introduction

Multi-storey wood buildings entered the construction market in Sweden following a revision of the building regulations in the year of 1994. Until then, the construction of wood buildings more than two storeys in height was prohibited. Today, 10–15% of the newly built multi-family housings in Sweden are made of wood, and their construction is increasing rapidly [1]. Although modern wood buildings fulfil the requirements for sound insulation specified in building regulations, studies have shown that residents in wood buildings are more disturbed by noise and vibrations than are residents in conventional concrete buildings [2–4]. In other words, current requirements do not properly reflect the annoyance of residents in wood buildings. Specific problems include the transmission of low-frequency structure-borne sound between apartments, caused by sources such as footsteps, dropped objects and vibrating machines.

During the last few decades, the vibroacoustic comfort of residents in wood buildings has improved as a result of the efforts made to reduce noise and vibration transmission. An example of a reduction measure is the use of elastomeric vibration isolators between building elements. The isolators are used in, for example, timber volume element (TVE) buildings, which represent the building system that dominates the Swedish market for multi-storey wood buildings [1]. TVE buildings are constructed by stacking prefabricated volume elements with elastomeric vibration isolators between them, as illustrated in Figure 1.1. However, as there are no reliable prediction models, the performance of such isolators has not yet been optimised. If accurate and efficient numerical models were available, parametric studies and design optimisations could be performed in a time efficient manner and at a low cost. Numerical simulations could increase the understanding of the physics involved in noise and vibration transmission as the results from such models can be evaluated in detail. This would facilitate the optimisation of existing measures for noise and vibration reduction and the development of novel types of measures.

The prediction of structure-borne sound in buildings can be divided into three tasks: (1) predicting the input force caused by the source, (2) predicting the transmission of structural vibrations from the source to the receiving room, and (3) predicting the sound radiation caused by the structural vibrations in the receiving room. Figure 1.2 illustrates the source, the vibration transmission and the sound radiation. The research presented in this thesis focuses on the

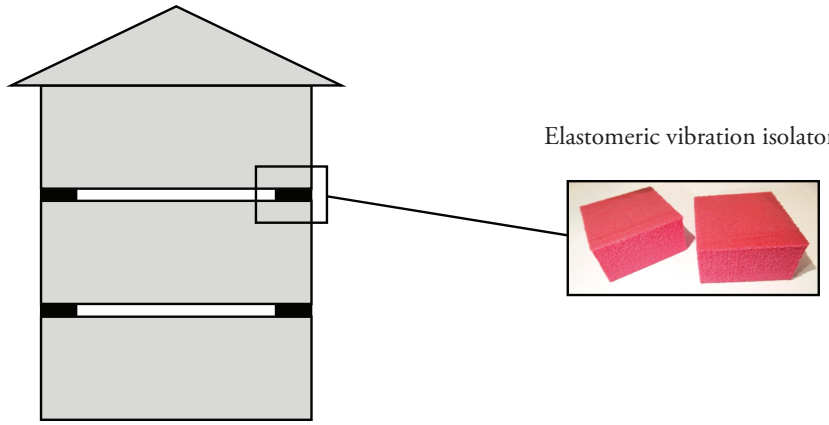

Figure 1.1: *Illustration of TVE building system with elastomeric vibration isolators separating the volume elements [5].*

numerical modelling of low-frequency vibration transmission, i.e., the second predictive task. Accurate models of structural vibrations can be used to predict structure-borne sound as well as floor vibrations.

Studies on human annoyance caused by noise and vibrations indicate that frequencies below 100 Hz are particularly problematic for residents in wood buildings [2]. Hence, it is important to enable predictions at those frequencies. Standardised prediction models for noise and vibration transmission in buildings, which are described in [6], are based on statistical energy analysis (SEA) methods; these methods consider the energy flow between subsystems and require high modal density of the subsystems to yield accurate results. This is not the case at lower frequencies in which small sets of vibration modes govern the response. Low-frequency vibrations can instead be analysed using deterministic methods such as the finite element (FE) method. Compared to SEA methods, deterministic methods have the advantage of allowing for a more detailed description of the structure under study and therefore facilitate studies on design modifications. An issue in the modelling of wood buildings is that variations in both the material parameters of wood and in the mechanical behaviour of joints are large. Such variations can be accounted for in FE models by using stochastic methods such as Monte Carlo simulations. The effects of variations and uncertainties increase at higher frequencies, which mean that deterministic models become less meaningful. Therefore, above a certain frequency, a less detailed modelling strategy such as SEA must be accepted. The question then is at which frequencies are the deterministic strategies relevant. The studies presented in this thesis are an important step towards answering that question.

At present there are no reliable numerical models for predicting low-frequency vibration transmission in wood buildings. There are, however, several publications that investigate different aspects involved in such modelling, for example, the properties of elastomeric vibration isolators and how to model joints between structural parts. Still, numerous uncertainties remain, including how to deal with the effects of many details present in real buildings (for example,

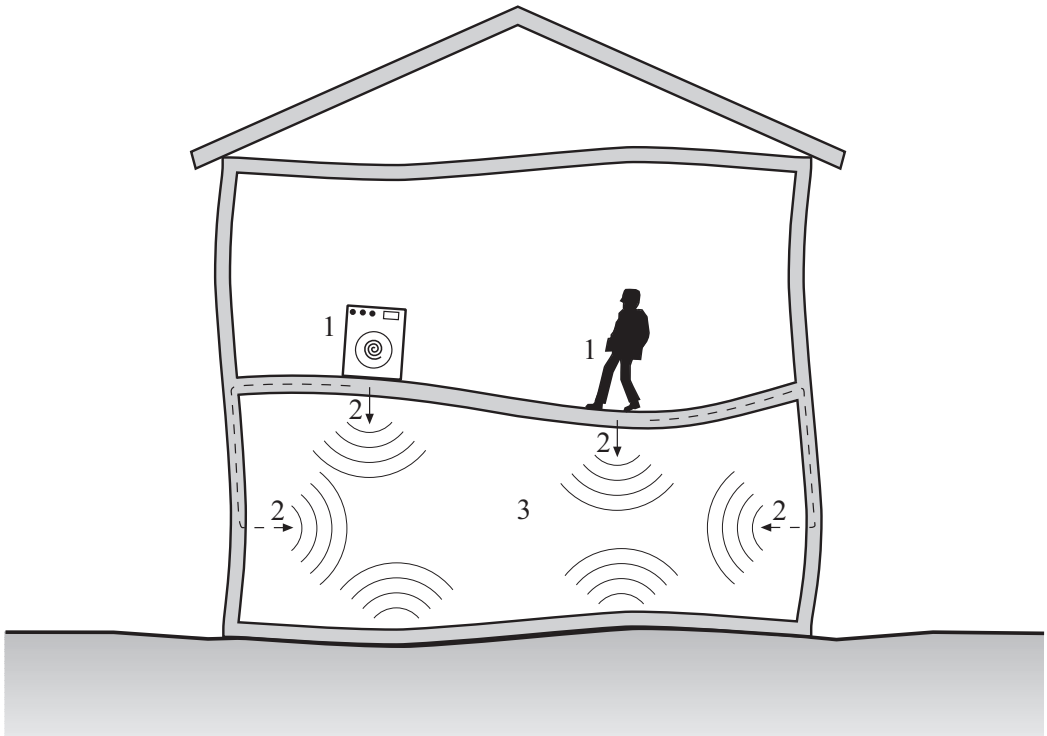

Figure 1.2: *Illustration of (1) the sources, (2) the vibration transmission, and (3) the sound radiation involved in structure-borne sound transmission in buildings.*

windows, doors, interior walls and floor surfaces). Another uncertainty is how to deal with the effects of variations in the material parameters of wood and in the mechanical behaviour of joints, which cause variations in the dynamic behaviour among buildings with identical geometry. To investigate these uncertainties, it is preferable to use a reference model that has been correlated to measurements. Although several publications present model correlation studies, they consider rather simple building structures such as a single floor. The results presented in this thesis can be used to establish reference models representing larger parts of buildings.

Accurately assessing the dynamic behaviour of wood buildings requires the use of models representing the building geometry in considerable detail. The resulting FE models contain many degrees of freedom (DoFs) and can easily exceed the limits of computer capacity, at least if computations are to be performed within a reasonable time in the context of a design process. A widely used methodology to reduce the size of numerical models is dynamic substructuring wherein models are divided into substructures that are reduced in size and assembled to form reduced global models. The reduction of substructures can be performed using different methods for model order reduction, and the division into substructures can be accomplished in different manners. Suitable strategies for substructure division of wood buildings and methods for model order reduction are discussed in the thesis.

1.1 AIM AND OBJECTIVE

The aim of the research discussed in this thesis is to create numerical prediction models that can be used for designing multi-storey wood buildings with improved vibroacoustic comfort for residents. The thesis work focuses on the prediction of low-frequency vibration transmission between storeys and rooms considering frequencies up to 100 Hz. The overall objective is to develop models that are accurate and efficient. In relation to this objective, two main topics are discussed in the thesis:

1. Model validation to ensure accurate model predictions
2. Dynamic substructuring to perform model reduction and thereby improve the computational efficiency of the models

The objective in Paper A is to investigate the effects of different design choices for elastomeric vibration isolators on vibration transmission in wood buildings; the paper is not part of the model development. The objective of Paper B is to investigate the effects of modelling air and insulation in the cavities of multi-storey wood buildings on vibration transmission predictions. Paper C presents methods for designing scaled-size experimental building structures through the use of numerical analyses. The objective is to obtain scaled-size structures that preserve the dynamic characteristics of full-scale structures. The objective of Paper D is to develop an FE model of a scaled-size building structure by calibrating and correlating the model to measured data. The FE model is intended for use as a reference model for investigations on the effects of variations and uncertainties in the modelling of vibration transmission in wood buildings.

Papers E and F deal with dynamic substructuring of wood buildings; Paper E addresses the coupling of substructure models, while Paper F discusses the model order reduction of substructures. Paper E presents a procedure for creating reduced coupling elements that represent elastomeric vibration isolators in dynamic substructuring. The purpose of developing the procedure is to enable coupling of substructures at a small number of interface DoFs, which is important in achieving successful model order reductions. The objective of Paper F is to evaluate the performance of a wide range of methods for model order reduction by comparing their accuracy and computational cost when applied to FE models of wooden building structures.

1.2 PROCEDURE FOR MODEL DEVELOPMENT

Figure 1.3 shows the procedure adopted in this thesis to develop accurate and efficient numerical prediction models for vibration transmission in wood buildings. The procedure involves two main topics: model validation and dynamic substructuring. Model validation is the process of assessing and developing the accuracy in model predictions, while dynamic substructuring is employed to reduce the computation times without impairing the accuracy of model

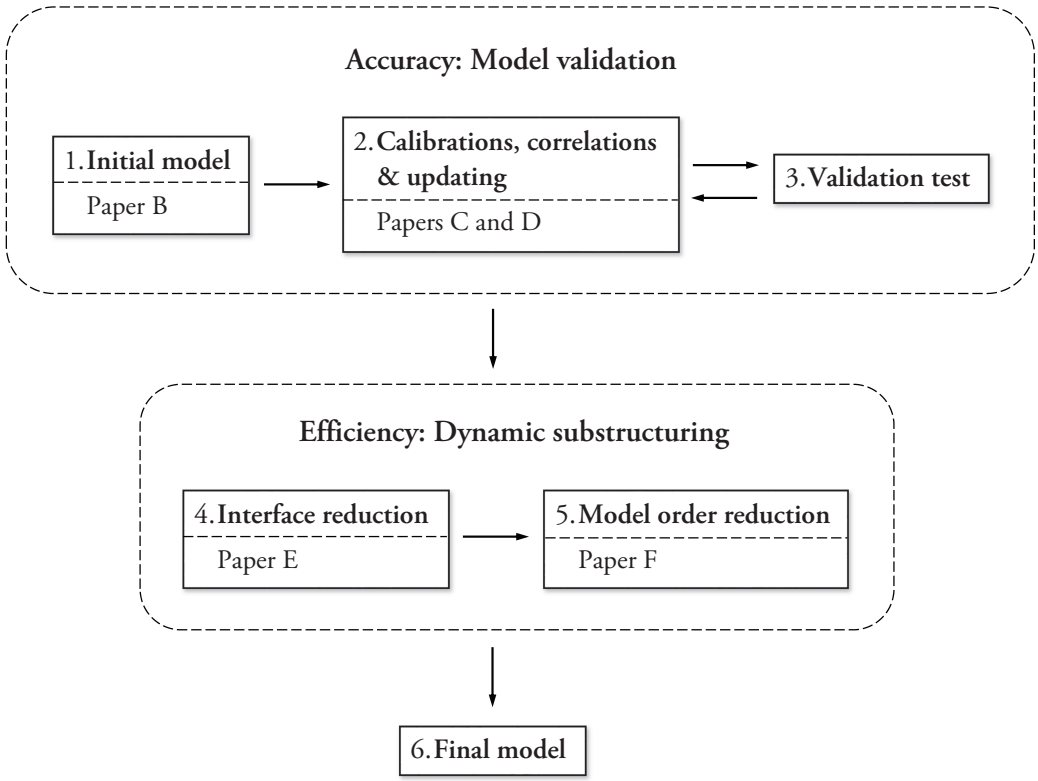

Figure 1.3: *The procedure adopted in the thesis to develop numerical prediction models.*

predictions. For a general structural dynamics problem, the procedure can be summarised as follows:

1. **Initial model.** The first step in developing a numerical model is to create an initial model based on previous research. The aspects to be considered in the modelling process are, for example, assumptions about physical phenomena, analytical descriptions of mechanical behaviour and numerical methods for calculating the response.

2. **Calibrations, correlations & updating.** The initial model is updated by performing calibrations and correlations to experimental results. In the context of model development, calibration can be defined as the tuning of model parameters to match experimental results. Correlation can be defined as the process of unveiling and reducing errors in modelling. Calibrations and correlations are usually performed for subcomponents of structures.

3. **Validations test.** The accuracy of model predictions is tested by comparing them with results from validation experiments. If the model fails a validation test, it must be up-

dated and tested again. Model validation can therefore involve iterations of calibrations, correlations and validation tests.

4. **Interface reduction.** Once the numerical model has passed validation testing, it can be reduced by employing dynamic substructuring in which the model is divided into a set of substructure models. The number of interface DoFs for each substructure is reduced by employing methods for interface reduction.

5. **Model order reduction.** The number of DoFs for each substructure is reduced further by employing methods for model order reduction. The interface DoFs are preserved in the reduction while the number of internal DoFs are reduced.

6. **Final model.** The reduced substructure models are assembled to form a reduced model of the complete structure. The final model can be used in design processes to perform accurate and efficient analyses of various design proposals.

In the appended publications, various aspects of the model development process are discussed; Figure 1.3 shows the steps in the procedure to which the appended publications have contributed. Paper A does not deal with model development and is therefore not included in Figure 1.3. The paper presents a conceptual study that uses models that have not been validated by experimental data. Paper B is placed in the "'Initial model"' step in Figure 1.3 as it presents numerical studies on the effects of conceptual assumptions in the modelling process and does not involve any calibrations or correlations to experimental data. Although Paper C does not discuss calibrations or correlations either, it is placed in the second step as it is a pre-study to the correlation study presented in Paper D.

1.3 OUTLINE

The thesis is divided into two main parts. The first part presents an overview of the work, which is divided into seven chapters, while the second part contains the six appended publications.

Chapter 2 presents an extensive background to and motivation for the research, including discussions on vibroacoustic issues in wood buildings and different methods for creating numerical prediction models. Chapter 3 gives a theoretical background to the numerical and experimental methods used in the research. The two main topics in the thesis, model validation and dynamic substructuring, are discussed in Chapters 4 and 5, respectively. Chapter 6 contains a summary of each appended publication. Conclusions of the thesis work and its contributions to the research field are presented in Chapter 7, along with proposals for future work.

2 Noise and vibrations in wood buildings

This chapter contains an extensive background to and motivation for the research presented in this thesis. An introduction to wood as a construction material for multi-storey buildings is given first. Terminologies used to describe noise and vibrations in residential buildings are then introduced, and the vibroacoustic issues that are of special concern for wood buildings are highlighted. Following this, measures for reducing noise and vibrations and the need to establish accurate and efficient numerical models to predict their effects are discussed. Finally, different methods for creating numerical prediction models are discussed to motivate the choice of methods used in the research.

2.1 WOOD AS CONSTRUCTION MATERIAL

In reaction to a number of urban fires, a ban on the construction of wood buildings more than two storeys in height was introduced in Sweden in 1874 [7]. The ban was maintained for over a century before it was lifted following a revision of the building regulations in 1994, leading to the reintroduction of such buildings. In a publication by the Swedish government in 2004 [7], the use of wood as construction material is promoted; the study presented a vision of wood as a natural choice of material for construction, not only in Sweden but also in the rest of Europe. Wood is attractive as a construction material for a number of economic and environmental reasons, many of which are related to its lightweight properties. For example, the use of wood lowers the costs involved in transportation and assembly and can reduce the loads on the foundations by up to 50% compared to conventional concrete buildings [8]. The environmental advantages of using wood were demonstrated in [9] in which it was found that the energy consumption during the complete lifecycle of wood buildings is lower than that of concrete buildings of comparable size. Moreover, the lightweight properties of wood make it suitable as a construction material for prefabrication of planar and volume elements. Prefabrication has a number of advantages, for example, more time- and cost-effective assembling, better conditions for construction workers, less material wastage and lessened sensitivity to weather conditions.

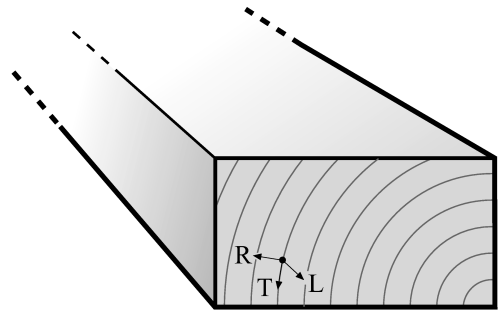

Figure 2.1: Illustration of the annual ring pattern in wood and a cylindrical coordinate system aligned with the pattern. L, R and T are the longitudinal, radial and tangential directions, respectively.

The reintroduction of multi-storey wood buildings has led to a number of challenges for engineers in the construction industry. One example is fire safety, which was the motivation behind the historic restrictions on constructing multi-storey wood buildings. In [10], it is stated that considerable research regarding fire safety is still needed, although such issues do not rule out the use of wood in multi-storey buildings. Another challenge is the one considered in the thesis: vibroacoustic comfort.

2.1.1 Mechanical properties of wood

The strength-to-density ratio of wood is high compared to other construction materials, for example, concrete or steel [11]. Consequently, wood structures are generally lighter than concrete or steel structures that have the same load-bearing capacity. Hence, wood is referred to as a lightweight construction material.

Wood is a natural material; its mechanical properties depend on the way trees grow. Every season, the stem grows outwards, adding a new layer of fibres directed in the lengthwise direction of the stem. This results in the material structure seen in Figure 2.1, with layers of annual rings. The cylindrical coordinate system in the figure indicates the longitudinal, radial and tangential directions (L, R and T, respectively), which are often used to define the mechanical properties of wood. The longitudinal axis is aligned with the fibres, while the radial and tangential directions are defined with respect to the annual rings. The mechanical properties display large variations in the size-scales of the fibres and annual rings. In engineering applications, however, wood is frequently regarded as a homogenous material with orthotropic material behaviour [12]. If the strains are below the limit of proportionality, wood can be considered linear elastic. Since the strains are small for human-induced structural vibration, the assumptions of linear elastic and homogenous material properties are employed in the thesis for the numerical modelling of wood. The constitutive relation for a linear elastic orthotropic

material with respect to cylindrical coordinates is given by (see, for example, [12])

$$\begin{bmatrix} \varepsilon_{LL} \\ \varepsilon_{RR} \\ \varepsilon_{TT} \\ \gamma_{LR} \\ \gamma_{LT} \\ \gamma_{RT} \end{bmatrix} = \begin{bmatrix} \frac{1}{E_L} & \frac{-\nu_{RL}}{E_R} & \frac{-\nu_{TL}}{E_T} & 0 & 0 & 0 \\ \frac{-\nu_{LR}}{E_L} & \frac{1}{E_R} & \frac{-\nu_{TR}}{E_T} & 0 & 0 & 0 \\ \frac{-\nu_{LT}}{E_L} & \frac{-\nu_{RT}}{E_R} & \frac{1}{E_T} & 0 & 0 & 0 \\ 0 & 0 & 0 & \frac{1}{G_{LR}} & 0 & 0 \\ 0 & 0 & 0 & 0 & \frac{1}{G_{LT}} & 0 \\ 0 & 0 & 0 & 0 & 0 & \frac{1}{G_{RT}} \end{bmatrix} \begin{bmatrix} \sigma_{LL} \\ \sigma_{RR} \\ \sigma_{TT} \\ \tau_{LR} \\ \tau_{LT} \\ \tau_{RT} \end{bmatrix}, \tag{2.1}$$

which can be written more compactly as

$$\boldsymbol{\varepsilon} = \mathbf{C}\boldsymbol{\sigma}, \tag{2.2}$$

where $\boldsymbol{\varepsilon}$ is the elastic strain vector, $\boldsymbol{\sigma}$ is the stress vector and $\mathbf{C}$ is a constitutive matrix containing twelve material parameters. As the material is assumed to be elastic, $\mathbf{C}$ is symmetric. This results in

$$\frac{\nu_{RL}}{E_R} = \frac{\nu_{LR}}{E_L}; \qquad \frac{\nu_{TL}}{E_T} = \frac{\nu_{LT}}{E_L}; \qquad \frac{\nu_{TR}}{E_T} = \frac{\nu_{RT}}{E_R}, \tag{2.3}$$

which means that the number of independent elastic parameters is reduced to nine. In Paper D, the material parameters of spruce were determined based on figures gathered from literature and from the calibration of numerical models to experimental results. It was found that E_L for wood beams made of spruce is approximately 11,000 MPa, which is more than an order of magnitude larger than the values for E_R and E_T (approximately 700 MPa each). The same differences were found for the shear moduli, where G_{LT} and G_{LR} are approximately 700 MPa and G_{RT} is about 70 MPa. As the distribution of the annual ring pattern in the cross-section of a beam is random, it is impossible for many engineering applications to distinguish between the radial and tangential directions. Therefore, it is often assumed that $E_T = E_R$, $G_{LT} = G_{LR}$ and $\nu_{LT} = \nu_{LR}$, which reduces the number of independent parameters to six. Furthermore, the calibrations performed in Paper D reveal that the low-frequency dynamics of wood beams, in terms of bending and torsional modes, are basically governed by E_L and $G_{LT} = G_{LR}$.

There is a large variation in elastic parameters among wood beams. In Paper D, the parameters of 90 wood beams (made of spruce and of type G4-2 according to the Swedish standard SS-EN 1611-1 [13]) were identified. The standard deviation of E_L was found to be 18% of the mean value, although the beams were tested in a controlled climate by the same person using the same equipment. There are several reasons for these large variations; for example, the beams were sawn from different parts of the stem, and the fibres were not perfectly aligned with the axial direction of the beams. In addition to variations among wood beams, the parameters depend to a great extent on the moisture content in the wood [14].

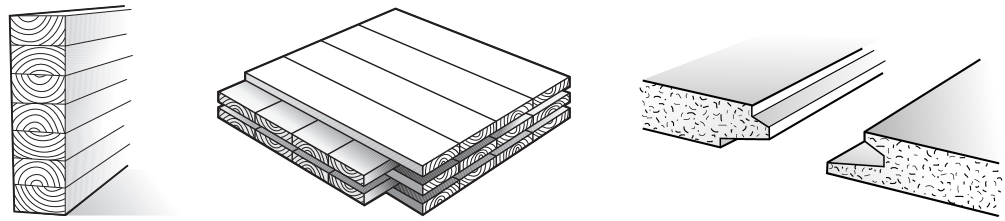

(a) Glulam. (b) CLT. (c) Particleboard.

Figure 2.2: *Examples of engineered wood products.*

2.1.2 Engineered wood products

Raw sawn wood as a construction material have several drawbacks, for example, the high orthotropy, the variations in material properties and the limitations in dimensions caused by the geometry of timber logs. Sawn wood is therefore often transformed into engineered wood products, which include a wide range of products manufactured by bonding wood constituents with adhesives [15]. Figure 2.2 shows examples of engineered wood products that are common in the construction industry: glue-laminated (glulam) beams, cross-laminated timber (CLT) panels and particleboards. Glulam beams consist of several layers of glued wood beams and can be used to create large and curved structural members. CLT panels are made by gluing layers of boards with each layer placed cross-wise to the adjacent layers. Particleboards are created by pressing wood chips or saw dust together with glue under high heat and pressure. Engineered wood products can be produced in sizes other than those possible from raw sawn wood. Such products are also more homogeneous and thus have material properties that show less variation. One disadvantage of engineered wood, compared to raw sawn wood, is that products, in general, are more expensive per weight.

2.1.3 Construction of multi-storey wood buildings

Three main types of multi-storey wood building systems can be identified [8]:

- *Column-beam systems*: frameworks of massive timber components, for example, glulam beams and columns.
- *Plate systems*: plate components made of massive wood laminates, for example, CLT panels.
- *Wood frame systems*: panels, such as particleboards and plasterboards, mounted on frames of wood beams.

The construction of buildings can be performed using different methods involving different degrees of prefabrication. Three main categories can be identified [8]:

Figure 2.3: *A TVE ready for transportation to construction site.*

- *On-site construction*: complete assembling procedure performed at the construction site.
- *Prefabricated planar elements*: industrially produced planar elements assembled at the construction site.
- *Prefabricated volume elements*: industrially produced volume elements assembled at the construction site.

Following the revision of the Swedish building regulations in 1994, multi-storey wood buildings were initially constructed on-site. However, a trend toward a high degree of prefabrication has been observed in recent years [8]. Prefabricated planar and volume elements often consist of wood-framed systems, owing to their light weight. In several of the appended publications, TVE buildings (which are described below) are used as example cases. In 2015, a total of 25,000 apartments were constructed in Sweden [16], with TVE buildings accounting for approximately 3,000 of these, and their construction is increasing rapidly [1].

Timber volume element buildings

The conceptual layout of a TVE building is illustrated in Figure 1.1. Each TVE contains a small apartment or part of a larger apartment. The floor, ceiling and walls consist of wood-frames covered with particleboards or plasterboards or both. As much of the construction work as possible is performed at the factory, including electrical installations, flooring, wardrobes etc. An example of a TVE is shown in Figure 2.3. At the construction site, the prefabricated TVEs are stacked to form complete buildings. In between the TVEs, elastomeric vibration isolators are placed to reduce the vibration transmission between storeys. The only additional connection is through a number of steel tie plates, ensuring the global stability of the buildings.

2.2 NOISE AND VIBRATION TRANSMISSION IN BUILDINGS

The noise transmission between storeys and rooms in residential buildings can be caused by many different types of sources, such as footsteps, vibrating machines and speakers. The noise

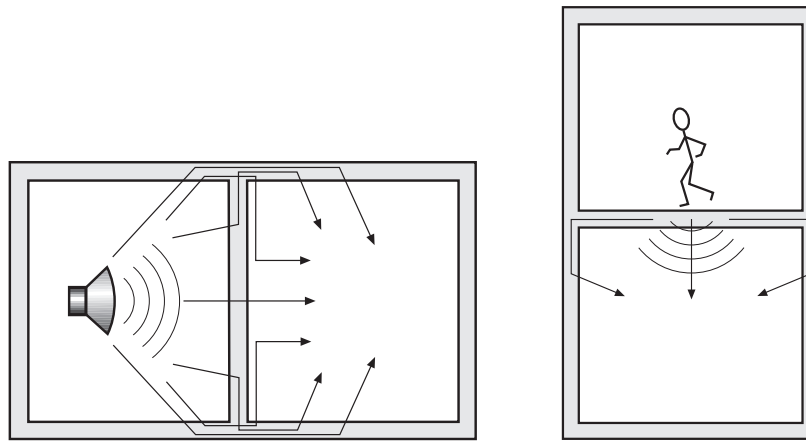

(**a**) Airborne sound source. (**b**) Impact sound source.

Figure 2.4: *Illustration of airborne and impact sound sources and examples of possible transmission paths for the structural vibrations.*

can be transmitted as airborne sound through leakages or as structure-borne sound, i.e. vibrations that propagate through the structure and induce noise in adjacent rooms. While sound leakages can be prevented through sealing, it is more complicated to reduce structure-borne sound.

Based on the type of sound source, two types of sound insulation performance of buildings is distinguished in standards and building regulations: airborne sound insulation and impact sound insulation. Examples of airborne sound sources are speech and speakers, and examples of impact sound sources are footsteps and dropped objects. Standardised procedures for measuring airborne sound insulation and impact sound insulation involve speakers and tapping machines, respectively, as sound sources. Standardised tapping machines contain five hammers placed in a row and are used to generate series of impacts.

Figure 2.4 illustrates airborne and impact sound sources and possible paths for the transmission of structural vibration between storeys and rooms. In the thesis, the term structure-borne sound is used to describe noise induced by structural vibrations irrespective of the type of sound source causing the vibrations. It should be noted that noise from airborne sound sources can be transmitted as structure-borne sound, and that noise from impact sound sources can be transmitted as airborne sound.

Both the structural vibrations and the noise they induce can cause annoyance for residents. The extent of such issues is a consequence of the following factors:

- *Load spectrum*: sources excite buildings with different levels of energy at different frequencies. For example, speakers induce vibrations at a wide range of frequencies while vibrating machines typically generate vibrations at specific frequencies. The load spec-

trum depends on the interaction between the source and structure.

- *Sensitivity of buildings*: the vibration amplitudes in a building resulting from a given load spectrum depend on the building's sensitivity to vibrations at different frequencies. If the load spectrum contains high levels of energy at frequencies to which the building is more sensitive, it will result in higher vibration amplitudes, which in turn cause higher noise levels.
- *Human perception*: the extent to which noise and vibrations are problematic depends on human perception. Building regulations and sound classifications provide limit values and guidelines for noise and vibration levels that are intended to reflect the number of satisfied residents.

To design residential buildings with adequate vibroacoustic performance, an understanding of all the three aforementioned factors is important. Sources and human perception are inputs to the design process, while the sensitivity of a building is a consequence of the design itself. In residential buildings, it is normally the annoyance of residents that is of concern. In other types of buildings, such as hospitals or research facilities, there are additional aspects to be considered; such buildings may house vibration-sensitive equipment, for example, microscopes and eye-lasers, associated with vibration requirements.

2.2.1 Building regulations

The regulations regarding airborne and impact sound insulation in residential buildings are defined in terms of standardised single-value descriptors that can be determined through standardised measurement procedures. These single-value descriptors are intended to reflect the sound insulation performance of the building elements in question over the entire frequency range of interest. The current descriptors for airborne and impact sound insulation are defined in the international standard ISO 717:2013 [17]. The measurement procedures for laboratory and field measurements are defined in ISO 10140:2010 [18] and ISO 16283:2014 [19], respectively. These standards provide details on, for example, sound sources, microphone positions and how to calculate the single-value descriptors. Building regulations in different countries state national limits for the measured descriptors, with large differences in limit values existing among the regulations in different European countries [20]. Such regulations differ not only in the allowed sound pressure levels but also in the descriptors used. The ISO standards define several descriptors and spectrum adaptation terms to account for low-frequency sound. These regulations are normally defined for frequencies above 100 Hz, and the adaptation terms can be used to extend the frequency range down to 50 Hz. In addition to regulations, several European countries have introduced sound classification schemes [21] that describe different quality classes for sound insulation.

The first regulations were introduced in the 1950s. Some of these were formulated in relation to constructions that were considered to provide adequate sound insulation; for example "a

sound insulation as good as a 1/1 stone brick wall" [22]. In several countries, requirements that were specified by considering the performance of existing buildings have essentially remained unchanged [20]. Ideally, the descriptors used in building regulations should correlate well with subjective ratings by residents, and the limit values should reflect the number of satisfied residents. There is, however, not much evidence that building regulations adequately reflect the annoyance of residents. Several studies on the correlation between the measured values of descriptors and subjective ratings from residents have been performed; a compilation of such studies can be found in [21], in which it is concluded that the correlations between measured values and subjective ratings are, in general, considerably low.

Standardised procedures for measuring and evaluating floor vibrations are presented in ISO 2631-1:1997 [23] and ISO 2631-2:2003 [24]. These standards do not specify any sources or single-value descriptors but instead describe procedures for measuring ambient vibrations and how to weight the measured spectra. Regulations on floor vibrations in wood buildings are given in Eurocode 1995-1-1:2004 [25]. These regulations are based on the work presented in [26] wherein the measured springiness and vibrations were compared to subjective ratings and are applicable to floors with fundamental frequencies above 8 Hz. For floors with lower fundamental frequencies, there is no guidance in the Eurocode except for limit values of static deflection. Furthermore, it is stated in ISO 2631-2 that "at present it is not possible to give guidance on acceptable magnitudes of vibration until more information has been collected". However, recent studies have investigated the validity of different indicators of human annoyance to floor vibrations [27], which is an important step towards more comprehensive and relevant regulations.

2.2.2 Vibroacoustic issues in residential wood buildings

Compared to buildings with heavier load-bearing systems, it is in general more difficult to construct lightweight buildings in such a way that noise and vibrations do not become a common source of annoyance among residents. This is related to the fact that a lightweight structure, in general, responds with higher vibration amplitudes than a heavier structure does for a given load. In some multi-storey wood buildings, many residents perceive impact sound as annoying even though the building fulfils the regulations; see, for example, [2,3,28–32]. Residents often describe the noise caused by impacts as low frequency "thumps" [28]. In [2], ten buildings were investigated by measuring sound insulation parameters and collecting subjective ratings from residents. The airborne and impact sound insulation between storeys was measured according to ISO standards and evaluated in terms of single-value descriptors for frequencies above 50 Hz. Eight of the investigated buildings have load-bearing structures made out of either traditional wood frames or CLT plate systems. The ratings indicate that the degree of annoyance with respect to impact sound is higher for those living in wood buildings than for the residents in a concrete building included in the study. Moreover, the correlation between impact sound insulation above 50 Hz and the annoyance of residents is weak for the wood buildings. The correlation was improved from 32 to 85% in terms of the coefficient of determination, R^2, when the lower limit of the frequency range was changed to 20 Hz in the evaluation of the

measurements. These observations emphasise the need for improved low-frequency impact sound insulation in wood buildings.

The ratings in [2] indicate that the degree of annoyance with respect to noise from airborne sound sources is substantially lower than the degree of annoyance with respect to impact sound. This observation is supported by the study presented in [3] in which ratings from residents in ten buildings (five wood and five concrete) were collected. The study shows that there is no difference in ratings regarding noise from airborne sound sources between residents in wood buildings and those in concrete buildings. In terms of impact sound, however, the ratings are considerably worse among residents in wood buildings, with about 60% of the residents considering impact sounds to be at least somewhat disturbing and 25–30% considering it to be very disturbing. The corresponding figures for noise from airborne sound sources are 20 and 5–10%, respectively.

A study on the annoyance arising from floor vibrations in seven multi-storey wood buildings is presented in [4]. It was found that, in general, residents in wood buildings are disturbed by vibrations; a majority of the residents consider the vibrations to be at least somewhat disturbing, with up to 25% of the residents in each building considering the vibrations to be very disturbing.

2.2.3 Noise and vibration reduction measures

To reduce the amount of noise and vibrations transmitted in buildings, different measures can be taken. In [33], different types of vibration reduction measures for floor structures are discussed. One example is the tuned mass damper (TMD), which consists of a mass mounted to the vibrating structure with an elastic material in-between. TMDs are tuned to have certain natural frequencies, and are thus effective in reducing vibrations caused by single vibration modes. Two other examples discussed in the paper are the semi-active absorber, which changes its damping properties rapidly to adjust for changes in the excitation, and the active control system, which drives the system using a shaker and feedback loops to control the input force. Both these methods can potentially reduce the vibrations further than TMDs can, but are in practice too expensive for standardised use in the building industry. TMDs are expensive as well, as they need to be tuned for each installation, but can be used if severe vibration problems are discovered in existing buildings. However, TMDs are less useful for dealing with structure-borne sound transmission between storeys and rooms since such transmission, in general, involves large frequency ranges containing many vibration modes.

In [5], measurements on full-scale buildings were carried out to investigate the effects of different measures for reducing impact sound in TVE buildings. The impact sound insulation was measured according to ISO standards and evaluated in terms of single-value descriptors for frequencies above 50 Hz. Measures that were found to be effective are, for example, additional layers of plasterboards on floors and the use of floating floors, which are constructed by placing layers of mineral wool between the load-bearing beams and the boards covering the

beams. Measures that were found to be less effective are, for example, the use of heavier mineral wools as insulation (compared to conventional types) or use of larger cavities between floors and ceilings. The effect of using elastomeric vibration isolators between storeys was tested for a two-storey experimental setup, comparing the cases with and without elastomers in the junctions. It was found that the elastomers increase the noise transmission; a 1 dB difference was observed in the descriptor used for evaluating the impact sound. The majority of the tested measures were found to affect the impact sound descriptors with less than 2 dB when evaluated according to ISO standards. This should be compared to the variance of 1.1 dB between constructions with identical geometry, as reported in the paper.

In [34], an experimental investigation of the effect of elastomeric vibration isolators in junctions of wood buildings is presented. A mock-up consisting of a floor structure supported by three walls was used to study the vibration transmission from the floor to the walls of the storey below. Marked differences in the behaviour were found for certain eigenmodes when inserting elastomeric isolators, as compared to a setup with the floor mounted directly onto the walls. For example, it was found that the damping is larger for mode shapes where large deformations occur in the elastomer layers. It was also concluded that elastomers can worsen the structure-borne sound insulation at low frequencies (20–70 Hz), possibly due to shear resonances in the elastomer layers. This conclusion is supported by the numerical investigation in the appended Paper A, where the effects of varying the material parameters of elastomer layers were investigated. The material parameters were varied within a range of realistic values, and it was concluded that when stiff elastomers are used (to fulfil static requirements in the buildings), the vibration transmission can be higher compared to a corresponding building without elastomers. These conclusions point out the need for a careful design of the elastomeric vibration isolators, and that it can be preferable to develop other types of isolators for wood buildings.

2.3 NUMERICAL PREDICTION MODELS

Numerical models are valuable in the development of novel measures for reducing noise and vibrations and for the optimisation of existing measures. The alternative of using experimental prototypes is both time-consuming and costly. Another benefit of using numerical simulations is that they provide additional insight into the physics governing noise and vibration transmission; the results of simulations can be visualised in more detail than experimental results, and parametric studies can demonstrate the effects of changes in design parameters.

The objective in developing numerical prediction models is to establish accurate and efficient models with respect to their use. Because low-frequency structure-borne sound is a proven cause of annoyance for residents in multi-storey wood buildings, it is of particular importance to enable its prediction. The prediction of structure-borne sound can be divided into three tasks: (1) predicting the input force caused by the source, (2) predicting the transmission of structural vibrations from the source to the receiving room, and (3) predicting the sound

pressure caused by the structural vibrations in the receiving room. In [35], numerical studies employing a 2D FE model showed that the sound pressure in rooms of multi-storey wood buildings has a negligible effect on transmitted vibrations. This means that the second predictive task can be carried out independent of the third task. This thesis focuses on the second predictive task. The models discussed in the thesis are thus used for predicting the transmission of low-frequency structural vibrations from a source to a receiving room. Such models are useful in predicting structure-borne sound as well as floor vibrations.

The accuracy required from model predictions depends on the specific use of the models. If absolute vibration levels are sought, the requirements are likely to differ from those in comparative studies such as the investigation of the relative effects of vibration reduction measures. Another concern when developing numerical models is computation time. If the computation time for each simulation can be reduced, engineers can perform more extensive analyses, and the overall design process can be faster. In developing numerical models, there is a trade-off between accuracy and computation time; this trade-off must be considered when choosing methods for creating the models and when performing the discretisations involved in numerical modelling.

2.3.1 Modelling strategies

The first step in developing models for predicting low-frequency vibrations in wood buildings is to choose an adequate modelling strategy and suitable numerical methods. Methodologies and methods for analysing the dynamics of structures have been developed in various engineering disciplines. One such methodology is multibody system dynamics, which is often used in, for example, aerospace engineering, vehicle design, biomechanics and robotics [36]. In its classical form, multibody system dynamics considers systems as assemblies of rigid bodies connected through, for example, springs, dampers and different types of joints. This methodology was developed for systems undergoing large displacements and rotations compared to the elastic deformations of the subcomponents. Consequently, multibody system dynamics is not well-suited for analysing vibrations in buildings, which are characterised by small displacements and elastic deformations of the structural components. Instead, a continuum mechanical formulation resulting in partial differential equations (PDEs) describing the dynamics of the system should be adopted for buildings.

Approximate solutions to PDEs can be sought using different methods, which are more or less suitable depending on the frequency range of interest. Figure 2.5 illustrates a typical frequency response function (FRF) for structural vibrations, divided into the low- and high frequency ranges. In the low-frequency range, the modal density is low and the response is governed by a small set of vibration modes. Detailed analyses of the low-frequency response can be performed using deterministic methods such as the FE method [37, 38] and the boundary element (BE) method [39, 40]. The FE and BE methods approximate the exact solutions of PDEs in both space and time. In the high-frequency region illustrated in Figure 2.5, the modal density is higher. Using deterministic methods to calculate high-frequency vibrations is computationally

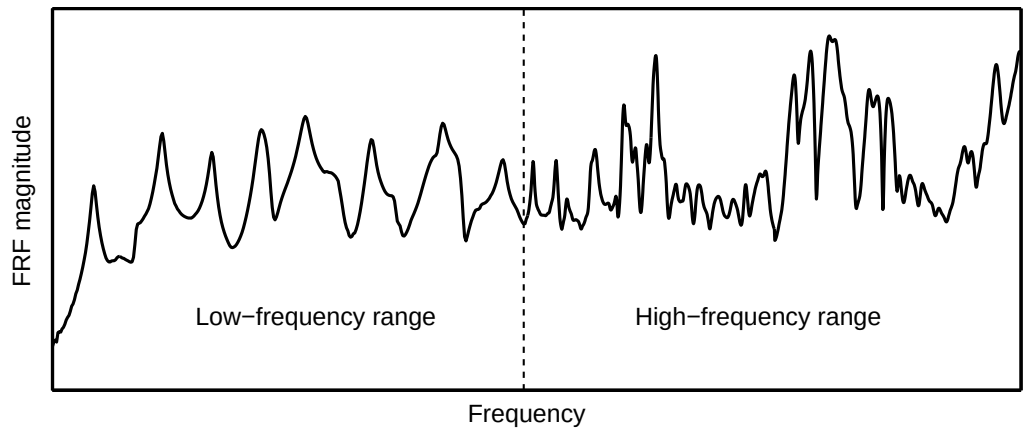

Figure 2.5: *Example of FRF for structural vibrations. The low- and high-frequency ranges are illustrated.*

expensive because it requires high resolution in both space and time. Furthermore, model predictions at high frequencies are sensitive to variations and uncertainties in the structure under study. Consequently, deterministic methods are less meaningful at higher frequencies, and a less detailed methodology must be accepted. SEA methods (see, for example, [41,42]) are often used to analyse high-frequency vibrations. In SEA, the energy flow between subsystems and their internal dissipation is considered; the energy flow is governed by the difference in vibrational energy between subsystems and is averaged over frequency bands. The vibrational energy in a subsystem depends on the modal density, which is often calculated using theoretical formulas. The validity of SEA methods relies on several assumptions, for example, that the modal density in the subsystems is high. This can result in large errors in the low-frequency region, where the modal density is low.

It can be challenging to choose suitable numerical methods for the transition region between the low- and high-frequency ranges. The choice of methods should be based on the extent to which variations and uncertainties affect the model output. Variations can be considered in deterministic models by using Monte Carlo simulations [43] in which probabilistic distributions of model parameters are propagated to the model output. If the variations in the model output are small, deterministic methods are suitable. For a specific structure, the variations can be reduced by performing calibrations of model parameters. However, it is common for models to be used to predict the behaviour of several structures with identical geometry, in which case the models must account for variations among the structures. This is the case when designing wood buildings, whose dynamic behaviour is affected by large variations in, for example, the material properties of wood and the mechanical behaviour of joints. The thesis work considers the development of deterministic models and investigates the possibilities and limitations of using them to model low-frequency vibrations in wood buildings.

2.3.2 Deterministic methods

The FE and BE methods are essentially the two methods used in structural mechanics for creating deterministic numerical models based on continuum mechanical formulations. The BE method is based on discretisations of the domain boundaries and generates system matrices that are fully populated and non-symmetric [39]. The FE method, in turn, discretises the entire domain, resulting in models that contain larger numbers of DoFs than BE models do. The system matrices of FE models are sparse and symmetric, which means that the number of DoFs in BE models must be considerably smaller than that in FE models to achieve similar computation times. The BE method is well-suited for infinite geometries because they can be treated as exteriors to the domain boundaries. BE models for infinite problems, therefore, contain fewer DoFs than FE models, which must discretise large parts of infinite geometries. On the other hand, the BE method is not suitable for problems involving complex geometries, material inhomogeneity and high surface-to-volume ratios [39], all of which are characteristic of wood buildings. Correspondingly, the FE method is employed in this thesis for developing numerical models for predicting low-frequency vibration transmission in wood buildings.

2.3.3 Model reduction

The FE models considered in this thesis contain large numbers of DoFs and require long computation times for analysis. To employ the models in a design process, it is often necessary to reduce the size of the models by using one of the many methods for model order reduction available in the literature. Such methods require analyses of the full FE models to establish reduced models. To avoid analyses of full FE models, which can be very time-consuming, dynamic substructuring [44] can be used. In dynamic substructuring, models are divided into substructures that are reduced in size and assembled to form reduced global models. An advantage of performing a reduction at the substructure level is that when details in the models are modified, only the substructures affected by the changes have to be updated. Dynamic substructuring is employed in the thesis for the reduction of models of low-frequency vibration transmission in wood buildings.

3 Governing theory

This chapter presents a theoretical background to the numerical and experimental methods used in the appended publications. The first topic covered in the chapter is the mathematical and numerical modelling of structure-acoustic systems. Structure-acoustic interaction is employed in the thesis to account for air and insulation in cavities of wood buildings. Section 3.1 presents the PDEs resulting from continuum mechanical formulations in the structural and acoustic domains. By employing such formulations, the engineering problems are described by PDEs supplemented with boundary conditions (BCs), and initial conditions if the transient response is sought. The PDEs are often too complex to be solved by analytical methods. Instead, the solutions are approximated by using numerical methods such as the FE method. In Section 3.2, the FE formulation of structure-acoustic systems is presented. The FE formulation results in equation systems whose solutions approximate the solutions of the PDEs. The equation systems can be used to analyse the responses of structures subjected to dynamic loading. Such analyses are covered in Section 3.3. Free vibrations and responses to harmonic loading are discussed, which leads to the formulation of eigenvalue problems and steady-state dynamics. These are the two analysis methods used in the appended publications. Furthermore, a brief discussion on nonlinear effects in structural dynamics is included in the section to introduce phenomena that cannot be explained by linear analysis. It can be important to recognise symptoms of nonlinearities when analysing measurement data since many experimental methods are based on assumptions of linearity. Experimental modal analysis (EMA) is covered in Section 3.4, where methods used in the thesis work for frequency response measurements and modal parameter estimation are discussed.

3.1 STRUCTURE-ACOUSTIC EQUATIONS

In this section, the governing equations for continuum mechanical formulations of the structural and acoustic domains and of the coupling between domains are derived. Continuum mechanics is a branch of mechanics where the physical behaviour of solids and fluids is modelled by considering the matter as continuously distributed, as opposed to modelling the matter as discrete particles. Further reading on continuum mechanics can be found in, for example, [45, 46]. In the derivations below, quantities belonging to the structural and acoustic

domains are denoted by subscripts s and f, respectively.

3.1.1 Structural domain

By considering Newton's second law of motion for the continuum formulation of a solid, the differential equation of motion for a body occupying the domain Ω_s can be obtained as [46]

$$\tilde{\boldsymbol{\nabla}}^T \boldsymbol{\sigma}_s + \mathbf{b}_s = \rho_s \frac{\partial^2 \mathbf{u}_s}{\partial t^2}, \tag{3.1}$$

where

$$\tilde{\boldsymbol{\nabla}}^T = \begin{bmatrix} \frac{\partial}{\partial x} & 0 & 0 & \frac{\partial}{\partial y} & \frac{\partial}{\partial z} & 0 \\ 0 & \frac{\partial}{\partial y} & 0 & \frac{\partial}{\partial x} & 0 & \frac{\partial}{\partial z} \\ 0 & 0 & \frac{\partial}{\partial z} & 0 & \frac{\partial}{\partial x} & \frac{\partial}{\partial y} \end{bmatrix}, \quad \boldsymbol{\sigma}_s = \begin{bmatrix} \sigma_{xx} \\ \sigma_{yy} \\ \sigma_{zz} \\ \sigma_{xy} \\ \sigma_{xz} \\ \sigma_{yz}, \end{bmatrix}, \quad \mathbf{b}_s = \begin{bmatrix} b_x \\ b_y \\ b_z \end{bmatrix}, \quad \mathbf{u}_s = \begin{bmatrix} u_x \\ u_y \\ u_z \end{bmatrix}.$$

$\boldsymbol{\sigma}_s$ is the vector representation of the stresses, ρ_s is the mass density, $\mathbf{b}_s$ is the body force vector and $\mathbf{u}_s$ is the displacement vector. $\boldsymbol{\sigma}_s$, $\mathbf{b}_s$ and $\mathbf{u}_s$ depend on spatial coordinates, x, y and z, and on time, t. Viscous forces are not considered here; methods for including such forces are discussed in Section 3.3.3. By assuming small deformations, the vector representation of the strains is given by

$$\boldsymbol{\varepsilon}_s = \begin{bmatrix} \varepsilon_{xx} & \varepsilon_{yy} & \varepsilon_{zz} & \gamma_{xy} & \gamma_{xz} & \gamma_{yz} \end{bmatrix}^T = \tilde{\boldsymbol{\nabla}} \mathbf{u}_s. \tag{3.2}$$

If linear elastic material behaviour is assumed, the stresses are given by

$$\boldsymbol{\sigma}_s = \mathbf{D}_s \boldsymbol{\varepsilon}_s = \mathbf{D}_s \tilde{\boldsymbol{\nabla}} \mathbf{u}_s, \tag{3.3}$$

where $\mathbf{D}_s$ is the constitutive matrix. An example of a constitutive relation is the one defined in Equation (2.1) for the orthotropic behaviour of wood. At the domain boundary $\partial\Omega_s$, a surface traction vector, $\mathbf{t}_s$, is defined. The surface tractions are related to the stresses according to

$$\mathbf{t}_s = \begin{bmatrix} t_x \\ t_y \\ t_z \end{bmatrix} = \begin{bmatrix} \sigma_{xx} n_x + \sigma_{xy} n_y + \sigma_{xz} n_z \\ \sigma_{xy} n_x + \sigma_{yy} n_y + \sigma_{yz} n_z \\ \sigma_{xz} n_x + \sigma_{yz} n_y + \sigma_{zz} n_z \end{bmatrix}, \tag{3.4}$$

where n_x, n_y and n_z are the components of the boundary normal vector $\mathbf{n}_s$, pointing outwards from $\partial\Omega_s$. BCs are defined at $\partial\Omega_s$ by prescribing the displacements and surface tractions,

$$\begin{aligned} \mathbf{u}_s &= \mathbf{u}_{bc} \qquad \text{on } \partial\Omega_{s,u}, \\ \mathbf{t}_s &= \mathbf{t}_{bc} \qquad \text{on } \partial\Omega_{s,t}, \end{aligned} \tag{3.5}$$

where $\mathbf{u}_{bc}$ and $\mathbf{t}_{bc}$ are known quantities and $\partial\Omega_{s,u}$ and $\partial\Omega_{s,t}$ are separated parts of the domain boundary which together constitute the complete boundary $\partial\Omega_s$. By supplementing Equation (3.1) with the BCs in Equation (3.5), a fully defined problem in three-dimensional structural mechanics is obtained. If the transient response to dynamic loading is sought, initial conditions need to be defined.

3.1.2 Acoustic domain

The equations that govern the acoustic fluid domain are derived by assuming the fluid to be inviscid and irrotational, in addition to the assumption of small displacements. The motion of an acoustic fluid can be described by using different primary variables, such as the fluid displacement or a fluid displacement potential. In the equations presented here, the acoustic pressure is used as primary variable. With the stated assumptions, the pressure field in an acoustic fluid is governed by the equation of motion [47]

$$\rho_{0,f} \frac{\partial^2 \mathbf{u}_f}{\partial t^2} + \boldsymbol{\nabla} p_f = 0 \tag{3.6}$$

and the continuity equation

$$\frac{\partial p_f}{\partial t} + \rho_{0,f} c_{0,f}^2 \boldsymbol{\nabla} \cdot \frac{\partial \mathbf{u}_f}{\partial t} = 0, \tag{3.7}$$

where $\rho_{0,f}$ is the static density, $c_{0,f}$ is the speed of sound, p_f is the acoustic pressure and $\boldsymbol{\nabla}$ is the gradient operator. p_f and $\mathbf{u}_f$ depend on spatial coordinates, x, y and z, and on time t. By differentiating Equation (3.7) with respect to time and inserting the resulting equation into Equation (3.6), the wave equation in the acoustic fluid domain is obtained as

$$\frac{1}{c_{0,f}^2} \frac{\partial^2 p_f}{\partial t^2} - \boldsymbol{\nabla}^2 p_f = 0. \tag{3.8}$$

The BCs at $\partial\Omega_f$ can be defined in terms of a pressure

$$\mathbf{p}_f = \mathbf{p}_{bc} \qquad \text{on } \partial\Omega_{f,p}, \tag{3.9}$$

where $\mathbf{p}_{bc}$ is a known quantity and $\partial\Omega_{f,p}$ is the part of the domain boundary where the pressure is prescribed. A pressure described to zero represents a free surface, while a non-zero pressure represents a sound source. Another type of BC is to prescribe the pressure gradient normal to the domain boundary

$$\mathbf{n}_f^T \boldsymbol{\nabla} p_f = 0 \qquad \text{on } \partial\Omega_{f,\nabla p}, \tag{3.10}$$

where $\partial\Omega_{f,\nabla p}$ is the part of the boundary where the pressure gradient is prescribed. Such BC represents a rigid surface. A third type of BC is to define a surface impedance, imposed through the equation

$$\mathbf{n}_f^T \dot{\mathbf{u}}_f = \frac{1}{c_1} \dot{p}_f + \frac{1}{c_2} p_f \qquad \text{on } \partial\Omega_{f,i}, \tag{3.11}$$

where c_1 and c_2 are coefficients and $\partial\Omega_{f,i}$ is the part of the domain boundary where surface impedance is modelled.

The above equations are suitable for modelling the acoustic pressure field in air. To accurately represent the acoustic pressure in porous materials, the interaction between the porous structures and the air needs to be considered. There are several porous material models available in the literature, both empirical and analytical. Such models are discussed in the appended Paper B.

3.1.3 Coupling of domains

When structure-acoustic interaction is modelled, the boundary $\partial\Omega_{sf}$ is introduced, which is the part of the structural and acoustic domain boundaries where coupling occurs. At $\partial\Omega_{sf}$, there is a continuity in displacement,

$$\mathbf{n}_f^T \mathbf{u}_s = \mathbf{n}_f^T \mathbf{u}_f, \tag{3.12}$$

and in pressure,

$$\mathbf{n}_f^T \mathbf{t}_s = -p_f. \tag{3.13}$$

3.2 FINITE ELEMENT METHOD

Problems encountered in many engineering fields are described by PDEs, originating from different types of balance laws. The PDEs derived in Section 3.1 for the structural and acoustic domains are just two examples. In practice, it is not feasible to solve the PDEs analytically. Therefore, numerical methods such as the FE method are employed to find approximate solutions. In the FE method, the geometry is divided into elements that together form an FE mesh. An example of an FE mesh for a structure-acoustic system is shown in Figure 3.1. Each element contains a number of nodes, which are associated with discrete values of the sought field variables – the nodal DoFs. Within the elements, the field variables are assumed to vary according to selected shape functions. The shape functions are often chosen as polynomials of various degree. If linear shape functions are used, the approximate solution varies linearly within each element. The FE formulation results in an equation system in which the nodal DoFs are the unknowns. The size of the FE mesh affects the size of the resulting equation system. A very fine mesh, i.e. small elements, results in a good approximation of the field variables at the expense of obtaining a large equation system. When using the FE method, the practicing engineer has to make a trade-off between the accuracy of the approximations and the computation time of the analyses.

In this section, the FE formulation for the structural and acoustic domains and for the coupling between the domains is presented. For a more detailed description of the FE method, see for example [37, 38]. The FE formulation of structure-acoustic systems is discussed in more detail in, for example, [47].

3.2.1 Weak formulation

The first step in deriving the FE formulation is to rephrase the problem from being described by PDEs and BCs to the so-called weak formulation. For the structural domain, the weak formulation is derived by first pre-multiplying Equation (3.1) with a vector of arbitrary weight functions,

$$\mathbf{v}_s^T(x, y, z) = \begin{bmatrix} v_x & v_y & v_z \end{bmatrix}, \tag{3.14}$$

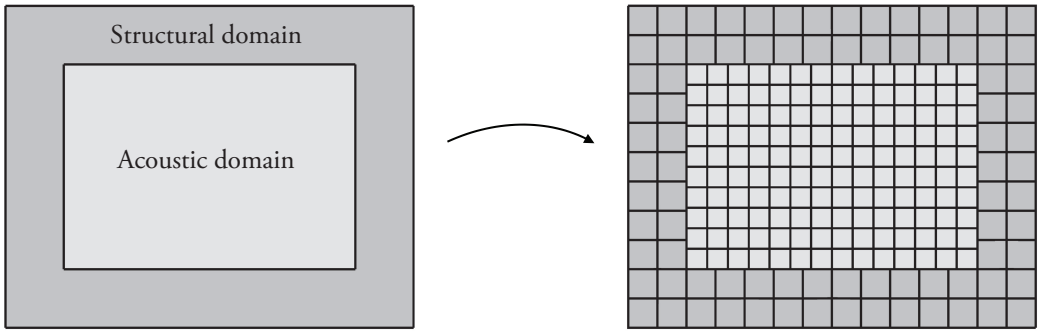

Figure 3.1: *Example of an FE mesh for a structure-acoustic system.*

and integrating over the region Ω_s. This results in

$$\int_{\Omega_s} \mathbf{v}_s^T \left(\tilde{\boldsymbol{\nabla}}^T \boldsymbol{\sigma}_s + \mathbf{b}_s - \rho_s \frac{\partial^2 \mathbf{u}_s}{\partial t^2} \right) \mathrm{d}V = 0. \tag{3.15}$$

By applying the Green-Gauss theorem, the first term in the integral can be re-written as

$$\int_{\Omega_s} \mathbf{v}_s^T \tilde{\boldsymbol{\nabla}}^T \boldsymbol{\sigma}_s \mathrm{d}V = \int_{\partial\Omega_s} \mathbf{v}_s^T \mathbf{t}_s \mathrm{d}S - \int_{\Omega_s} (\tilde{\boldsymbol{\nabla}} \mathbf{v}_s)^T \boldsymbol{\sigma}_s \mathrm{d}V. \tag{3.16}$$

Inserting the above expression into Equation (3.15) results in

$$\int_{\Omega_s} \mathbf{v}_s^T \rho_s \frac{\partial^2 \mathbf{u}_s}{\partial t^2} \mathrm{d}V + \int_{\Omega_s} (\tilde{\boldsymbol{\nabla}} \mathbf{v}_s)^T \boldsymbol{\sigma}_s \mathrm{d}V = \int_{\partial\Omega_s} \mathbf{v}_s^T \mathbf{t}_s \mathrm{d}S + \int_{\Omega_s} \mathbf{v}_s^T \mathbf{b}_s \mathrm{d}V, \tag{3.17}$$

which together with the BCs in Equation (3.5) is the weak formulation in the structural domain. The prescribed surface tractions can be inserted in the integral equation.

The weak formulation in the acoustic domain is obtained similarly; Equation (3.8) is pre-multiplied with the scalar-valued weight function $v_f\left(x, y, z\right)$, integrated over the region $\boldsymbol{\Omega}_f$ and re-written using the Green-Gauss theorem. The weak formulation can then be obtained as

$$\int_{\Omega_f} v_f \frac{1}{c_{0,f}^2} \frac{\partial^2 p_f}{\partial t^2} \mathrm{d}V + \int_{\Omega_f} (\boldsymbol{\nabla} v_f)^T \boldsymbol{\nabla} p_f \mathrm{d}V = \int_{\partial\Omega_f} v_f \mathbf{n}_f^T \boldsymbol{\nabla} p_f \mathrm{d}S \tag{3.18}$$

together with the BCs in Equations (3.9–3.11). The prescribed pressure gradients can be inserted in the integral equation.

3.2.2 Finite element formulation

So far, no approximations to the solutions of Equations (3.1) and (3.8) have been introduced; the weak formulations are equivalent to the PDEs. In the structural domain, the following

approximation of the displacements is introduced:

$$\mathbf{u}_s = \mathbf{N}_s \mathbf{a}_s \,, \tag{3.19}$$

where $\mathbf{N}_s(x, y, z) \in \mathbb{R}^{3\times n_s}$ contains the global shape functions, $\mathbf{a}_s(t) \in \mathbb{R}^{n_s\times 1}$ contains the nodal displacements and n_s is the number of nodal displacements. By using Galerkin's method, the arbitrary weight functions are selected as

$$\mathbf{v}_s = \mathbf{N}_s \mathbf{c}, \tag{3.20}$$

where $\mathbf{c}$ is a vector containing arbitrary constants. Insertion of Equations (3.3), (3.19) and (3.20) into Equation (3.17) (and using that $\mathbf{a}_s$ is independent of spatial coordinates and that $\mathbf{c}$ is arbitrary) results in the FE formulation for a linear elastic solid,

$$\int_{\Omega_s} \mathbf{N}_s^T \rho_s \mathbf{N}_s \mathrm{d}V \ddot{\mathbf{a}}_s + \int_{\Omega_s} (\tilde{\boldsymbol{\nabla}}\mathbf{N}_s)^T \mathbf{D}_s \tilde{\boldsymbol{\nabla}}\mathbf{N}_s \mathrm{d}V \mathbf{a}_s = \int_{\Omega_s} \mathbf{N}_s^T \mathbf{b}_s \mathrm{d}V + \int_{\partial\Omega_s} \mathbf{N}^T \mathbf{t}_s \mathrm{d}S. \tag{3.21}$$

The equation can be written more compactly as

$$\mathbf{M}_s \ddot{\mathbf{a}}_s + \mathbf{K}_s \mathbf{a}_s = \mathbf{f}_{s,l} + \mathbf{f}_{s,b} = \mathbf{f}_s \,, \tag{3.22}$$

where

$$\begin{aligned} \mathbf{M}_s &= \int_{\Omega_s} \mathbf{N}_s^T \rho_s \mathbf{N}_s \, \mathrm{d}V, & \mathbf{K}_s &= \int_{\Omega} (\tilde{\boldsymbol{\nabla}}\mathbf{N}_s)^T \mathbf{D}_s \tilde{\boldsymbol{\nabla}}\mathbf{N}_s \, \mathrm{d}V, \\ \mathbf{f}_{s,l} &= \int_{\Omega_s} \mathbf{N}_s^T \mathbf{b}_s \, \mathrm{d}V, & \mathbf{f}_{s,b} &= \int_{\partial\Omega_s} \mathbf{N}_s^T \mathbf{t}_s \, \mathrm{d}S. \end{aligned} \tag{3.23}$$

$\mathbf{M}_s$, $\mathbf{K}_s$, $\mathbf{f}_{s,l}$ and $\mathbf{f}_{s,b}$ are referred to as the mass matrix, the stiffness matrix, the body force vector and the boundary force vector, respectively. The BCs in Equation (3.5) are introduced in Equation (3.22) by prescribing nodal values in $\mathbf{a}_s$ and $\mathbf{f}_{s,b}$.

The FE formulation for an acoustic fluid is obtained in a corresponding way. The approximation

$$\mathbf{p}_f = \mathbf{N}_f \mathbf{a}_f \tag{3.24}$$

is introduced, where $\mathbf{N}_f(x, y, z) \in \mathbb{R}^{1\times n_f}$ contains the global shape functions, $\mathbf{a}_f(t) \in \mathbb{R}^{n_f\times 1}$ contains the nodal pressures and n_f is the number of nodal pressures. Through employing Galerkin's method, the FE formulation in the acoustic domain can be obtained as

$$\mathbf{M}_f \ddot{\mathbf{a}}_f + \mathbf{K}_f \mathbf{a}_f = \mathbf{f}_{f,b} \,, \tag{3.25}$$

where

$$\begin{aligned} \mathbf{M}_f &= \frac{1}{c_{0,f}^2} \int_{\Omega_f} \mathbf{N}_f^T \mathbf{N}_f \, \mathrm{d}V, & \mathbf{K}_f &= \int_{\Omega_f} (\boldsymbol{\nabla}\mathbf{N}_f)^T \boldsymbol{\nabla}\mathbf{N}_f \, \mathrm{d}V, \\ \mathbf{f}_{f,b} &= \int_{\partial\Omega_f} \mathbf{N}_f^T \mathbf{n}_f^T \boldsymbol{\nabla} p_f \, \mathrm{d}S. \end{aligned} \tag{3.26}$$

To arrive at the FE formulation for a structure-acoustic system, the spatial coupling matrix

$$\mathbf{H}_{sf} = \int_{\partial\Omega_{sf}} \mathbf{N}_s^T \mathbf{n}_f \mathbf{N}_f \, \mathrm{d}S \tag{3.27}$$

is introduced. With use of $\mathbf{H}_{sf}$ and Equation (3.6), the boundary force vectors at $\partial\Omega_{sf}$ can be rewritten as

$$\mathbf{f}_{f,b} = \mathbf{H}_{sf}\mathbf{a}_f \,, \tag{3.28}$$

and

$$\mathbf{f}_{s,b} = -\rho_{0,f}\mathbf{H}_{sf}^T \ddot{\mathbf{a}}_s . \tag{3.29}$$

By inserting Equations (3.28) and (3.29) into Equations (3.22) and (3.25), the coupled structure-acoustic FE formulation is obtained as

$$\begin{bmatrix} \mathbf{M}_s & \mathbf{0} \\ \rho_{0,f}\mathbf{H}_{sf}^T & \mathbf{M}_f \end{bmatrix} \begin{bmatrix} \ddot{\mathbf{a}}_s \\ \ddot{\mathbf{a}}_f \end{bmatrix} + \begin{bmatrix} \mathbf{K}_s & -\mathbf{H}_{sf} \\ \mathbf{0} & \mathbf{K}_f \end{bmatrix} \begin{bmatrix} \mathbf{a}_s \\ \mathbf{a}_f \end{bmatrix} = \begin{bmatrix} \mathbf{f}_{s,l} \\ \mathbf{0} \end{bmatrix} + \begin{bmatrix} \mathbf{f}_{s,b} \\ \mathbf{f}_{f,b} \end{bmatrix}, \tag{3.30}$$

where $\mathbf{f}_{s,b}$ and $\mathbf{f}_{f,b}$ contain contributions from the parts of the domain boundaries $\partial\Omega_s$ and $\partial\Omega_f$, respectively, that are separated from the interface boundary $\partial\Omega_{sf}$.

3.3 ANALYSIS OF STRUCTURAL DYNAMIC SYSTEMS

This section considers the analysis of structural dynamic systems of the form shown in Equation (3.22). Such systems have more than one unknown and are referred to as multi-DoF (MDoF) systems. Free vibrations and responses to harmonic loading are discussed, which leads to the introduction of two analysis methods: eigenvalue analysis and steady-state analysis. The latter is a frequency-domain method, but can be used to predict the time-domain response of linear systems through Fourier transformations. Steady-state analysis is applicable also to acoustic systems and coupled structure-acoustic systems. The eigenvalue analysis discussed here is, however, not directly applicable to coupled structure-acoustic systems of the form in Equation (3.30) since their system matrices are asymmetric. Eigenvalue analysis of such systems can be performed using the methods discussed in, for example, [48].

In Sections 3.3.1 and 3.3.2, undamped systems are considered. Damping is introduced in Section 3.3.3. The theory presented is based on assumptions of linearity, which were introduced already in the continuum mechanical formulation in Section 3.1. Typically, such assumptions are adequate for analysing vibrations in residential buildings. Nonlinear behaviour in structural dynamics is discussed briefly in Section 3.3.4. Further reading about the analysis of structural dynamic systems can be found in, for example, [49, 50]. In the derivations below, the subscripts used in the previous section (to indicate structural and acoustic domains) are dropped.

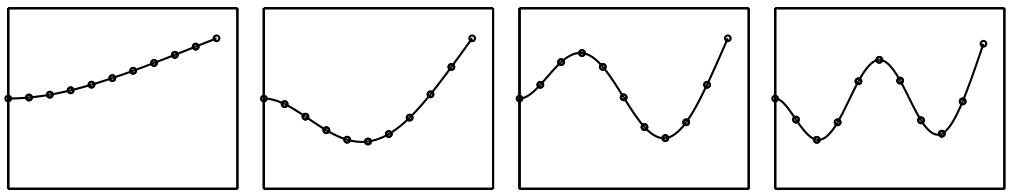

(a) 1st eigenmode. (b) 2nd eigenmode. (c) 3rd eigenmode. (d) 4th eigenmode.

Figure 3.2: *The first four eigenmodes of an FE model of a 2D cantilever beam.*

3.3.1 Free vibrations

It is assumed here that no external loads are acting on the structure. This results in the motion of the structure being determined by the initial conditions, i.e. the prescribed displacements and velocities at $t = 0$. For free undamped vibrations, the MDoF system is reduced to the homogeneous differential equation

$$\mathbf{M}\ddot{\mathbf{a}}(t) + \mathbf{K}\mathbf{a}(t) = 0. \tag{3.31}$$

This equation can be solved by assuming the harmonic solution

$$\mathbf{a}(t) = \hat{A}e^{i\omega t}\Phi, \tag{3.32}$$

where $\hat{A}$ is the complex amplitude, i is the complex number, ω is the angular frequency and Φ is a constant vector. Differentiation of Equation (3.32) and insertion into Equation (3.31) results in the eigenvalue problem

$$(\mathbf{K} - \omega^2\mathbf{M})\Phi = 0, \tag{3.33}$$

which has non-trivial solutions given by

$$\det(\mathbf{K} - \omega^2\mathbf{M}) = 0. \tag{3.34}$$

For an MDoF system containing n DoFs, there are n solutions, $\omega_j = \omega_1, ..., \omega_n$, referred to as the eigenfrequencies of the system. Each eigenfrequency has a corresponding eigenmode, or mode shape, Φ_j, which can be determined through Equation (3.33). As an example, Figure 3.2 shows the first four eigenmodes of an FE model of a 2D cantilever beam. The set of n eigenmodes form an orthogonal basis. Consequently, the solution to Equation (3.31) can be expressed as a sum of the eigenmodes:

$$\mathbf{a}(t) = \sum_{j=1}^{n} q_j(t)\Phi_j, \tag{3.35}$$

where

$$q_j(t) = \hat{q}_j e^{i\omega_j t}. \tag{3.36}$$

$\hat{q}_j$ is the complex amplitude of the jth eigenmode, determined by use of the initial conditions. For a given set of initial conditions, the amplitudes of the eigenmodes are determined uniquely. Equation (3.35) is referred to as the modal decomposition of $\mathbf{a}(t)$.

3.3.2 Harmonic excitation

Harmonic excitation of the undamped MDoF system is assumed, i.e.

$$\mathbf{M}\ddot{\mathbf{a}}(t) + \mathbf{K}\mathbf{a}(t) = \hat{\mathbf{f}}e^{i\omega t}, \tag{3.37}$$

where $\hat{\mathbf{f}}$ is a constant complex-valued vector describing the load distribution. The solution to Equation (3.37) is a sum of the complimentary and particular solutions. The complimentary solution is of the form given in Equation (3.35) and depends on the initial conditions. The particular solution does not depend on the initial conditions, and is derived by assuming a harmonic response

$$\mathbf{a}(t) = \hat{\mathbf{a}}e^{i\omega t}, \tag{3.38}$$

where $\hat{\mathbf{a}}$ is a constant complex-valued vector. This results in the equation of motion in the frequency domain for an undamped system

$$\mathbf{D}(\omega)\hat{\mathbf{a}} = \hat{\mathbf{f}}, \tag{3.39}$$

where the dynamic stiffness matrix $\mathbf{D}(\omega)$ is given by

$$\mathbf{D}(\omega) = -\omega^2\mathbf{M} + \mathbf{K}. \tag{3.40}$$

Equation (3.39) is often rewritten in terms of FRFs by inverting the dynamic stiffness matrix, $\mathbf{D}^{-1}(\omega) = \mathbf{H}(\omega)$, which results in

$$\hat{\mathbf{a}} = \mathbf{H}(\omega)\hat{\mathbf{f}}. \tag{3.41}$$

Each FRF in $\mathbf{H}(\omega)$ describes the complex vibration amplitude in a certain DoF when applying a harmonic load with unit amplitude in another (or the same) DoF. Deriving the response amplitude $\hat{\mathbf{a}}$ for harmonic loading is referred to as steady-state dynamic analysis.

By pre-multiplying Equation (3.39) with the eigenmodes Φ_k^T, where $k = 1, \ldots, n$, and employing the modal decomposition

$$\hat{\mathbf{a}} = \sum_{j=1}^{n} \hat{r}_j \Phi_j, \tag{3.42}$$

the following equation is obtained:

$$-\omega^2 \sum_{j=1}^{n} \Phi_k^T \mathbf{M} \Phi_j \hat{r}_j + \sum_{j=1}^{n} \Phi_k^T \mathbf{K} \Phi_j \hat{r}_j = \Phi_k^T \hat{\mathbf{f}}, \tag{3.43}$$

The eigenmodes are orthogonal in the scalar products $\Phi_k^T \mathbf{M} \Phi_j$ and $\Phi_k^T \mathbf{K} \Phi_j$. Consequently, only for $j = k$ are the terms in the summations non-zero. This results in n uncoupled single-DoF (SDoF) systems, given by

$$-\omega^2 \bar{m}_j \hat{r}_j + \bar{k}_j \hat{r}_j = \bar{f}_j, \tag{3.44}$$

where

$$\bar{m}_j = \Phi_j^T \mathbf{M} \Phi_j, \quad \bar{k}_j = \Phi_j^T \mathbf{K} \Phi_j, \quad \bar{f}_j = \Phi_j^T \hat{\mathbf{f}}, \tag{3.45}$$

for $j = 1, ..., n$. Each SDoF system describes the amplitude of an eigenmode. The SDoF systems have the solution

$$\hat{r}_j = \frac{\bar{f}_j}{\bar{k}_j} \frac{1}{1 - \left(\omega/\omega_j\right)^2}, \tag{3.46}$$

where

$$\omega_j = \sqrt{\frac{\bar{k}_j}{\bar{m}_j}}. \tag{3.47}$$

The particular solution to Equation (3.37) can now be obtained through Equations (3.38), (3.42) and (3.46) as

$$\mathbf{a}(t) = e^{i\omega t} \sum_{j=1}^{n} \frac{\bar{f}_j}{\bar{k}_j} \frac{1}{1 - \left(\omega/\omega_j\right)^2} \Phi_j \,. \tag{3.48}$$

Hence, the particular solution for the MDoF system is a sum of the responses for the modal SDoF systems. The FRF for each SDoF system is given by

$$H(\omega) = \frac{1}{\bar{k}_j} \frac{1}{1 - \left(\omega/\omega_j\right)^2}. \tag{3.49}$$

The magnitude of the FRF is infinite when the excitation frequency is equal to the eigenfrequency, $\omega = \omega_j$. This is a phenomenon called resonance. Infinite vibration amplitudes can of course not occur in real structures; damping and nonlinearities will prevent such behaviour.

3.3.3 Damped systems

Damping is included in numerical models to represent the energy dissipation occurring in dynamical systems. The dissipation can be caused by, for example, friction in joints or internal losses in materials. Damping is introduced in the equation of motion through the damping matrix $\mathbf{C}$,

$$\mathbf{M}\ddot{\mathbf{a}}(t) + \mathbf{C}\dot{\mathbf{a}}(t) + \mathbf{K}\mathbf{a}(t) = \mathbf{f}(t). \tag{3.50}$$

Constructing the damping matrix is not as straightforward as constructing the stiffness matrix, which is built by considering the stiffness properties of individual structural components. The damping properties of materials are not as well established, and the energy dissipation in joints

is difficult to measure. Instead, the damping matrix is often constructed using modal damping ratios of the structure, which are obtained through measurements. Damping matrices can be divided into two types: classical and non-classical. Classical damping matrices are, as opposed to non-classical matrices, diagonalised by a modal decomposition of the system. This enables MDoF systems to be separated into n uncoupled SDoF equations, as was done in Equation (3.43) for the undamped case. Hence, it is of interest to study the effect of damping on the response of SDoF systems. The damped SDoF system is given by

$$m\ddot{a}(t) + c\dot{a}(t) + ka(t) = f(t), \tag{3.51}$$

where m, c, k, $a(t)$ and $f(t)$ are scalar-valued coefficients and variables. The equation can be rewritten as

$$\ddot{a}(t) + 2\zeta\omega_n\dot{a}(t) + \omega_n^2 a(t) = f(t), \tag{3.52}$$

where ω_n is the eigenfrequency for the undamped case and ζ is the damping ratio. These are defined as

$$\omega_n = \sqrt{\frac{k}{m}}, \qquad \zeta = \frac{c}{c_{cr}} = \frac{c}{2m\omega_n}, \tag{3.53}$$

where c_{cr} is the critical damping. For $c > c_{cr}$, a damped SDOF system returns to its static equilibrium position without overshooting when external forces are removed. For $c < c_{cr}$, vibrations around the equilibrium position occur instead. The free vibration response of a damped SDoF system is of the form

$$a(t) = \hat{A}e^{i\omega_D t - \zeta\omega_n t}, \tag{3.54}$$

where ω_D is the eigenfrequency for the damped system, given by

$$\omega_D = \omega_n\sqrt{1-\zeta^2}. \tag{3.55}$$

For relatively low damping ratios (for example $\zeta < 0.2$, which is common in many structural dynamic problems), $\omega_D \approx \omega_n$, i.e. the eigenfrequencies are unaffected by the damping. The term $e^{-\zeta\omega_n t}$ in Equation (3.54) makes the oscillations decay exponentially at a rate governed by the damping ratio.

Through derivations similar to those presented for the undamped case, it can be shown that the FRF for the damped SDoF system is complex-valued and given by

$$H(\omega) = \frac{1}{\omega_n^2\left[\left(1-(\omega/\omega_n)^2\right) + 2i\zeta\,(\omega/\omega_n)\right]}. \tag{3.56}$$

In Figure 3.3, the magnitude of the FRF is plotted for $\omega_n = 1$, and for different values of the damping ratio. It can be observed that a lower value of the damping ratio results in a narrower and higher resonance peak.

The FRFs for the MDoF system in Equation (3.50) are given by superposition of the FRFs for the modal SDoF systems. An example is shown in Figure 3.4. The FRFs of a structural

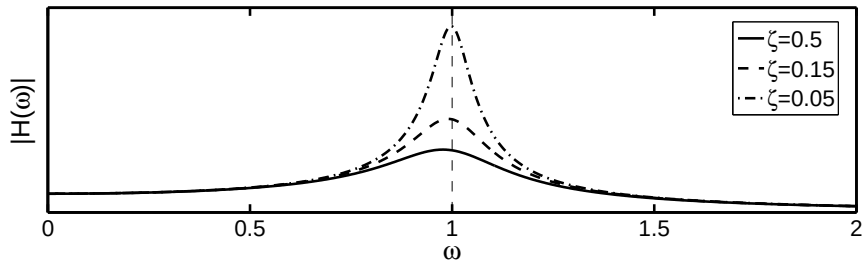

Figure 3.3: The magnitude of an FRF for a damped SDoF system with $\omega_n = 1$, and for different values of the damping ratio, ζ.

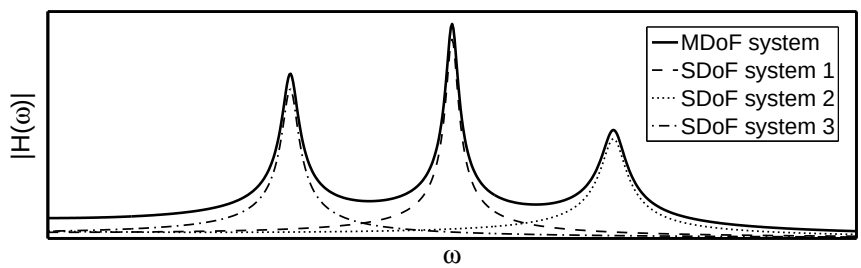

Figure 3.4: Example of an FRF magnitude for a damped MDoF system. The dashed lines illustrate the contributions from three modal SDoF systems.

dynamic system, which can be determined through steady-state analyses, unveil the sensitivity of the system at different frequencies and positions. The shape of the FRFs are in turn governed by the eigenfrequencies and mode shapes of the system. This highlights that eigenvalue and steady-state analyses are central in structural dynamic analysis.

Rayleigh damping

A frequently employed method for constructing damping matrices is Rayleigh damping [50], which produces classical damping matrices. Rayleigh damping uses a linear combination of the mass and stiffness matrices to construct the damping matrix,

$$\mathbf{C} = a_0\mathbf{M} + a_1\mathbf{K}, \tag{3.57}$$

where a_0 and a_1 are coefficients. With use of Equation (3.53), it can be shown that the damping ratio of the nth mode is given by

$$\zeta_n = \frac{a_0}{2\omega_n} + \frac{a_1\omega_n}{2}. \tag{3.58}$$

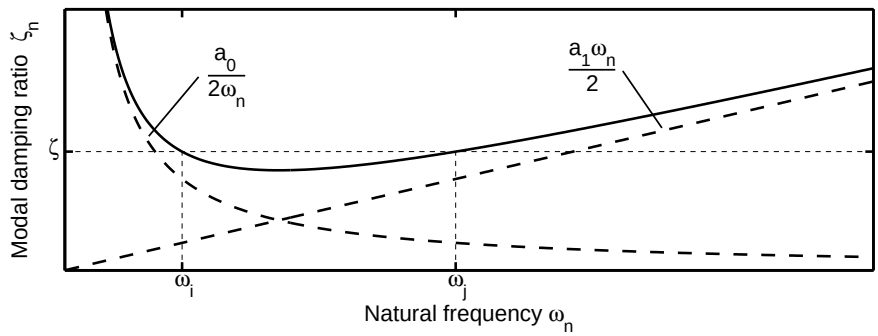

Figure 3.5: The modal damping ratio ζ_n as function of natural frequency ω_n for a Rayleigh damping model with $\zeta_i = \zeta_j = \zeta$. The two dashed curves show the mass and stiffness proportional damping.

With known values of the modal damping ratios ζ_i and ζ_j for eigenmodes Φ_i and Φ_j, the coefficients a_0 an a_1 can be determined through Equation (3.58). If $\zeta_i = \zeta_j = \zeta$, the coefficients are given by

$$a_0 = \zeta \frac{2\omega_i \omega_j}{\omega_i + \omega_j}, \tag{3.59}$$

and

$$a_1 = \zeta \frac{2}{\omega_i + \omega_j}. \tag{3.60}$$

Figure 3.5 shows the modal damping ratio ζ_n as function of natural frequency ω_n when $\zeta_i = \zeta_j = \zeta$. The two dashed curves illustrate the contributions from the mass and stiffness matrices. The mass matrix dominates at lower frequencies and the stiffness matrix provides the major contribution at higher frequencies.

3.3.4 Nonlinear systems

Modal superposition is an important feature of linear systems since it makes it possible to describe MDoF systems in terms of sets of SDoF systems. This is an advantage from a computational point-of-view and facilitates the understanding of dynamic systems. When analysing nonlinear systems, however, modal superposition is no longer possible. Nonlinear systems can exhibit complex phenomena which do not occur in linear systems. Examples are bifurcations, superharmonics and internal resonances [51]. Typical sources of nonlinearities in structures are: geometric nonlinearities due to large deformations, material nonlinearities in the stress-strain laws and nonlinear BCs due to, for example, loose joints or clearances.

All structures in real life are inherently nonlinear; linear models are just approximations of the nonlinear behaviour. For many problems, however, the nonlinear effects are negligible and linear assumptions are valid. In general, the effects of nonlinearities increase as the vibration

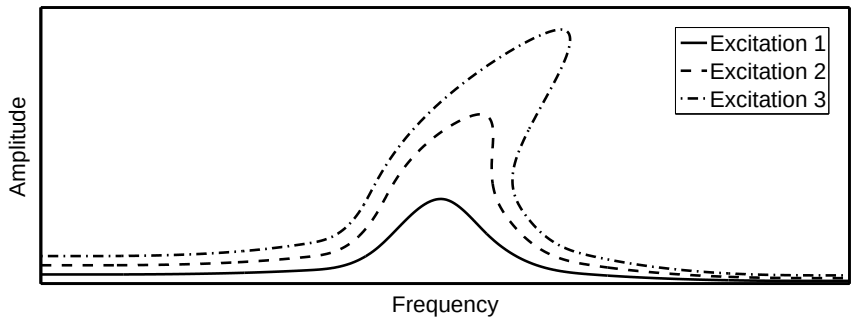

Figure 3.6: *Frequency response amplitude of a nonlinear system with hardening behaviour. The different curves show the response to excitations with different magnitude. Excitation 1 has the lowest input energy and Excitation 3 has the highest.*

energy increases, although there are exceptions, such as dry friction, where nonlinearities are important also at very low energy levels. When developing a linear model, it is important to recognise symptoms of nonlinearities in experimental data. If nonlinear behaviour is detected, the experiments can be re-designed to avoid triggering the nonlinearities. However, it may be the case that nonlinearities are important in the system under study and that a linear model is insufficient.

A fundamental difference between nonlinear and linear systems is that for single-harmonic excitation, a nonlinear system generally responds with multi-harmonic vibrations. This means that the concept of FRFs, which is defined for linear systems, is inapplicable to nonlinear systems. Furthermore, the response of nonlinear systems depends on the vibration energy. An example of the frequency response of a nonlinear system at different excitation levels is shown in Figure 3.6. The system has a hardening behaviour; the resonance peak distorts towards higher frequencies at higher energy levels. Such frequency response can affect the quality of EMA (described in Section 3.4); for example, the modal parameter estimation can result in the estimation of two linear eigenmodes from one nonlinear resonance peak.

Further reading on nonlinear structural dynamics can be found in, for example, [51, 52].

3.4 EXPERIMENTAL MODAL ANALYSIS

EMA can be used to determine the modal parameters of experimental structures. The modal parameters include eigenfrequencies, mode shapes, modal damping ratios, modal stiffness and modal mass. These are determined by fitting theoretical responses of linear systems to measured data.

(a) Shakers. (b) Impact hammers. (c) Accelerometers.

Figure 3.7: *Examples of equipment that can be used for EMA.*

3.4.1 Frequency response measurements

Let $x_m(t)$ and $y_n(t)$ be the measured discrete time signals of a force in measurement DoF m and the vibration response in measurement DoF n, respectively. By using the fast Fourier transform (FFT) [53], the frequency domain representations of the discrete signals, $X_m(\omega)$ and $Y_n(\omega)$, can be obtained. The FRF between the input force and the vibration response can be calculated as

$$H_{mn}(\omega) = \frac{Y_n(\omega)}{X_m(\omega)}. \tag{3.61}$$

There are several methods for measuring FRFs of experimental structures, involving different excitation sources. Two common types of sources are impact hammers and shakers, shown in Figure 3.7. Both types of sources have integrated force sensors to measure the input to the structures. Impact hammers generate short force pulses, whereas shakers can generate different types of signals, such as single harmonics, burst chirp and burst random; the different force signals are illustrated in Figure 3.8. Shakers are attached to the structures using thin rods to transfer forces only in the axial direction. The input forces generated by hammers depend on the stiffness of the hammer tip; stiffer tips generate input forces with more high-frequency content.

Both $Y_n(\omega)$ and $X_m(\omega)$ contain noise that deteriorates the quality of the measurements. It is important to choose an excitation source that leads to high signal-to-noise ratios, so that well-estimated FRFs can be obtained. This requires force inputs with sufficiently high energy levels for all frequencies of interest. On the other hand, if the energy input is too high, nonlinear behaviour of the experimental structure can be triggered. This leads to distorted frequency responses, as discussed in Section 3.3.4. Such responses are not suitable as input to linear modal parameter estimations.

Vibrations are usually measured in terms of accelerations using piezoelectric accelerometers, shown in Figure 3.7. In testing with an impact hammer, it is typical that only a few accelerometers are placed on the structure in question. The accelerometers are placed in a few fixed positions while the structure is excited with the hammer in a large number of points. In shaker

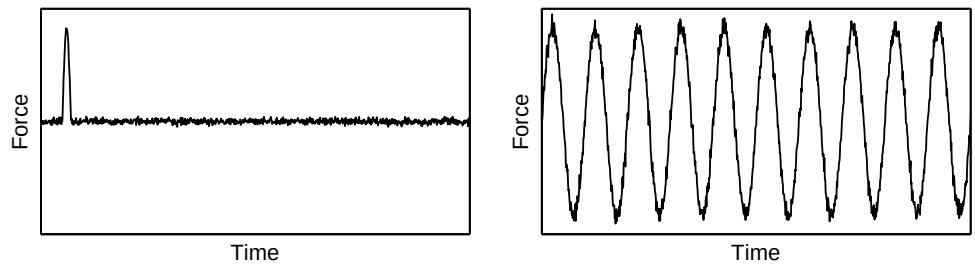

(**a**) Impulse. (**b**) Single harmonic.

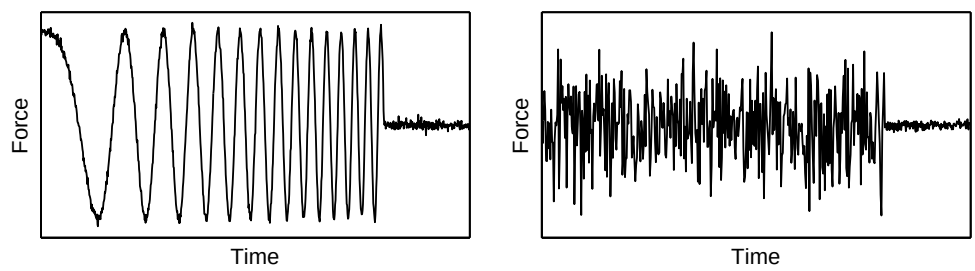

(**c**) Burst chirp. (**d**) Burst random.

Figure 3.8: *Examples of different types of force signals for EMA.*

testing, the shakers are typically placed in one or a few points while a larger number of accelerometers are distributed over the structure. According to the reciprocity theorem [54], which is valid for linear systems, $H_{mn}(\omega) = H_{nm}(\omega)$. Hence, the same information about the system can be retrieved using either method since using a shaker in DoF m and measuring the accelerations in DoF n is equivalent to using an impact hammer in DoF n and measuring the accelerations in DoF m.

There are, however, several practical differences between hammer and shaker testing. Impact testing generally requires less instrumentation than shaker testing since only a few accelerometers are needed. In shaker testing, it has to be ensured that the main body of the shaker is isolated from the structure to avoid that reaction forces are transmitted back to the structure when it is excited. When using impact hammers, or generating burst signals with shakers, too short time records can result in leakage. Leakage occurs when the transient response has not decayed enough at the end of the record, which deteriorates the quality of the FFT (since FFT assumes periodic signals). On the other hand, too long time records can result in low signal-to-noise ratios. The effects of leakage can be reduced by windowing the time signals [55], which is performed to reduce the amplitudes at the start and the end of the signals. Figure 3.9 illustrates the use of an exponential window for a transient acceleration signal. The errors stemming from low-signal-to-noise ratio can be reduced by repeating the measurements and averaging the resulting FRFs.

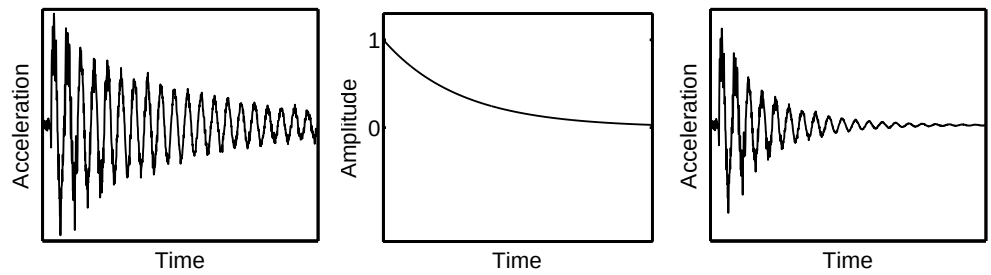

(a) Time signal. (b) Window. (c) Windowed time signal.

Figure 3.9: *Example of windowing for time signals; exponential window applied to transient acceleration response.*

The results of EMA are often used as input to calibrations and correlations of FE models. To accurately model the experimental structure, it is important to have good knowledge of the BCs during testing. Often, free or fixed BCs are approximated in experimental setups. Free BCs are in theory obtained when the experimental structure is completely free floating, which of course is impossible in practise. Instead, the structure can be suspended by soft rubber bands or similar. If the frequencies of the rigid body modes due to the elastic suspension are much lower than the eigenfrequencies of the structure, it can be assumed as free floating. Fixed BCs can be difficult to achieve since the stiffness of the supports and of the connections between supports and experimental structure must be much higher than the stiffness of the structure. An alternative type of BC is to employ flexible supports with known properties, which can be used as input to FE models when calibrating and correlating these to measured data.

More detailed information about frequency response measurements can be found in [56, 57] and theoretical descriptions of the methods involved are presented in, for example, [58].

3.4.2 Modal parameter estimation

There are several methods for estimating modal parameters from measured data. A review of different methods is presented in [59]. Essentially, the methods provide different ways of fitting theoretical responses of linear systems to measured data. Most methods employ measured FRFs as input, either directly in the frequency domain or in the time domain by using impulse response functions that are obtained through inverse FFT of the FRFs. To illustrate the concept of modal parameter estimation, an FRF of a linear system can be separated into the contributions from modal responses as

$$H(\omega) = \sum_{k=1}^{n} \frac{r_k}{i\omega - \lambda_k} + \frac{r_k^*}{i\omega - \lambda_k^*}, \tag{3.62}$$

where

$$\lambda_k = \zeta_k + i\omega_k. \tag{3.63}$$

n is the number of modes in the linear system, r_k is the modal participation factor and, ζ_k and ω_k are the modal damping ratio and eigenfrequency, respectively. The superscript '*' denotes the complex conjugate. The modal participation factors depend on the mode shapes of the system. The separation of an FRF into modal responses is illustrated in Figure 3.4. The modal parameters of an experimental structure can be estimated by adjusting the modal parameters in Equation (3.62) to obtain an FRFs that is as close to the measured FRF as possible. Equations of the form in Equation (3.62) are often solved by first estimating the damping ratios and eigenfrequencies, and then solving for the mode shapes in a subsequent step. Usually, there is more data available than required to determine the modal parameters. The parameters can in such cases be estimated by formulating an over-determined system and minimising the errors between synthesised and measured FRFs by, for example, using least squares methods.

The methods for modal parameter estimation found in the literature employ different expressions for the FRFs, or for impulse response functions, but are based on the same principles. The methods are discussed in terms of a unified framework in [59], highlighting their similarities.

4 Model validation

Model validation is defined by the American Society for Mechanical Engineers (ASME) as *"the process of determining the degree to which a model is an accurate representation of the real world from the perspective of the intended uses of the model"* [60]. No model is an exact representation of the real world; instead, the question is how accurate the model predictions are required to be and if that accuracy can be achieved.

The numerical models considered in this thesis are used for predicting low-frequency vibration transmission between storeys and rooms in wood building. The FE method was used for creating the numerical models; the choice of method is motivated in Section 2.3. This chapter discusses the validation of FE models to experimental results, which involves calibrations and correlations of the models. First, a general procedure for model validation in structural dynamics is presented to provide a framework for the research discussed in the chapter and to define different terms used in the context of model validation. Second, a review of published research on the numerical modelling of low-frequency vibrations in wood buildings is presented. Finally, the conclusions drawn in the appended publications are discussed. The studies discussed in the chapter have in common that they aim at developing the accuracy of the numerical models.

4.1 GENERAL PROCEDURE IN STRUCTURAL DYNAMICS

In published research discussing comparisons of numerical and experimental results, terms such as validation, calibration, correlation and updating are sometimes used interchangeably and different authors use different definitions. This section is included in the chapter to define the terms according to how they used in the thesis and to introduce a framework for the research discussed in Sections 4.2 and 4.3. The suggested procedure is discussed with respect to a single model validation study, but can be projected on the whole research field of numerical modelling of low-frequency vibration transmission in wood buildings.

Before performing the simulations and experiments involved in a validation procedure, a number of decisions need to be made. The following steps should be considered in the planning of a model validation [61]:

1. **Specify the model use.** A clear definition of the model use is important, and it affects all of the subsequent steps.

2. **Specify the physical system response measures.** These are quantities that are functions of the system response and are used for comparing model predictions to results of validation experiments. Examples include maximum vibration amplitudes and root mean square (RMS) values.

3. **Specify the validation metrics,** which are the mathematical methods for comparing simulated response measures to measured response measures. The validation metrics often involve probabilistic and statistical data. Further information on methods for evaluating such data can be found in, for example, [62, 63].

4. **Specify the domain of comparison,** i.e., the ranges of physical and model parameters. In structural dynamic analysis, it is important to define the frequency range of interest and the maximum vibration amplitudes. Extrapolation of the model predictions outside the domain of comparison should be done with caution. For example, if maximum vibration amplitudes are specified such that no nonlinear behaviour is triggered, predictions at higher vibration amplitudes should not be performed unless it can be ensured that the nonlinear effects remain negligible.

5. **Specify the validation experiments.** These experiments are used for performing validation tests in which model predictions are compared to experimental results. The results of validation experiments should not be used for calibrations or correlations.

6. **Specify the adequacy criteria,** i.e., the tolerance for discrepancies between model predictions and results from validation experiments. If the adequacy criteria are fulfilled, the model is deemed valid.

7. **Specify the conceptual model,** which consists of the physical phenomena considered in the model and the set of assumptions made. For example, the assumptions of linear behaviour and structure-acoustic coupling made in the continuum mechanical formulation in Section 3.1 are part of the conceptual model.

8. **Specify the mathematical model.** The PDEs derived in Section 3.1 are examples of mathematical descriptions of conceptual models. In addition, other modelling data such as initial conditions and loads must be described mathematically.

9. **Specify the computational model.** This involves the discretisations and solution algorithms, for example, those discussed in Sections 3.2 and 3.3, used for computing approximate solutions to the mathematical model. It should be ensured that the errors in the approximate solutions are small compared to the adequacy criteria.

10. **Specify the calibration and correlation experiments,** discussed further in Sections 4.1.1 and 4.1.2, respectively.

Once a validation procedure is planned, measurements and simulations can be performed. An initial computational model is created, and measurements needed for calibrations, correlations and validations are carried out. Then, calibration and correlation studies are performed to update the model. Finally, the calibrated and correlated model is used for performing validation tests in which model predictions are compared to results from validation experiments. If the model validation fails, the conceptual, mathematical and computational models must be revised to identify potential sources of error. The model is then updated to reduce the errors, and new validation tests are performed. Hence, validation procedures involve iterations of calibrations, correlations and validations.

4.1.1 Calibrations

Calibration is the procedure of improving estimates of uncertain model parameters [64]. It is usually performed for subsystems of the model to isolate errors in specific parameters. The first step in calibration is to perform sensitivity analyses to study the effects of uncertain parameters on the model output. Only the parameters that show a notable effect on the model output are optimised further. These parameters are optimised by minimising the difference between the model output and the corresponding experimental results. The objective function in the optimisations can, for example, be the frequency difference for an eigenmode. The optimisations are often subjected to constraints such as minimum and maximum values for the parameters, and it must be ensured that the optimisations result in global minima of the objective function so that local minima are avoided. For this purpose, interval searches in which the objective function is evaluated for a set of parameter values within the allowed intervals can be employed. Interval searches provide approximate solutions to the global minima. If a more accurate solution is desired, iterative methods such as Newton's method [65] can be used.

4.1.2 Correlations

According to [64], the term correlation in structural dynamics originates from the one-to-one correlation of eigenmodes from simulations and experiments. However, correlation can be defined in a much broader sense; here it is considered to be any type of comparison between simulated and experimental results with the goal of unveiling and reducing modelling errors. This differs from calibration, which involves optimising model parameters, and validation, in which the quality of the final model predictions are tested. Correlations are generally performed for subsystems of a model as performing correlations for a complete model can cause difficulties in identifying different sources of errors and distinguishing their effects.

Correlations can be carried out in many different ways, for example, by comparing simulated and measured mode shapes of subsystems to identify the least correlated modes. Differences in eigenfrequencies and mode shapes can guide the engineer towards the sources of error. Typically, correlation studies can unveil deficient modelling of joints, improper BCs or invalid assumptions regarding the physical phenomena governing the dynamic response of structures.

Examples of invalid assumptions are the use of incorrect material models and the exclusion of structure-acoustic interaction when it has a significant effect on the response.

4.1.3 Applying the procedure to low-frequency vibration transmission in wood buildings

Existing methods and guidelines for modelling low-frequency vibration transmission in wood buildings are insufficient for creating accurate numerical models. The focus of the research presented in the thesis is therefore not on performing pure validation tests of models but rather on investigating the effects of different uncertainties in the modelling. Nevertheless, it is important to keep in mind the ultimate use of the models so that the investigations are relevant to the development of models that can eventually be validated against measurements on real buildings.

Based on the discussion in Section 2.3, several of the steps in planning a model validation study can be specified for the models considered in the thesis. As the **model use** is defined as predicting the transmission of low-frequency structural vibrations from a source to a receiving room, it is natural to define the **response measures** as the FRFs between the input force at the source and the vibration response in the receiving room. The **domain of comparison** in the thesis is frequencies below 100 Hz (except in Paper B, in which frequencies up to 200 Hz are considered). A **conceptual assumption** made in the thesis as well as the publications referenced in Section 4.2 is that the vibrations are of small amplitude. This implies that nonlinearities can be neglected, and linear models can be used. This assumption is made because vibration sources in residential buildings, such as footfalls and vibrating machines, generate vibrations of relatively low amplitude. The **mathematical models** are based on the PDEs derived in Section 3.1 and the **computational models** are obtained using the FE method and dynamic substructuring. The **calibrations and correlations** performed in Paper D as well as in several of the publications discussed in Section 4.2 are mostly based on comparisons of simulated and measured eigenfrequencies and mode shapes.

4.2 LITERATURE REVIEW ON NUMERICAL MODELLING OF LOW-FREQUENCY VIBRATIONS IN WOOD BUILDINGS

In this section, the state-of-the-art in terms of numerical modelling of low-frequency structure-borne sound and vibration transmission in wood buildings is reviewed. The referenced publications can be seen in the context of the model validation procedure presented in Section 4.1; they present calibrations, correlations and validation tests that contribute to the validation of numerical models of wood buildings. Of the studies discussed in the section, those in [66–69] consider all three tasks in the prediction of structure-borne sound: predicting the input force, predicting the vibration transmission and predicting the resulting sound pressure in the receiving room. These publications aim at developing models that describe standardised tests

for impact sound insulation in which tapping machines are used as vibration sources, and they present comparisons between predicted and measured sound levels that can be regarded as validation tests. In the remaining studies discussed in this section, namely those in [70–77], the focus is on the modelling of structural vibrations. These publications present calibration and correlation studies where the modelling of different details in wood buildings are investigated.

In [66], FE models for predicting the impact sound generated by standardised tapping machines were developed and compared with results from laboratory measurements. The structures that were studied consisted of wood-framed floors with particleboard surfaces and inner ceilings of plasterboards attached to the wood frames of the floors. The FE models include air and insulation inside cavities between floors and underlying ceilings, and they account for the interaction between tapping machine and floor structure. Calibrations were performed to optimise material parameters and stiffness parameters of joints. The objective function for the optimisations was based on the difference between the FRFs from simulations and measurements. Probabilistic models were established for the optimised parameters and included in stochastic models of the building structures. Monte Carlo simulations were used to determine variations in the output of the stochastic models. The sound pressure in the receiving room was predicted by applying the vibration field in the ceiling surface as BCs on the fluid boundary, i.e., by assuming a one-way coupling. The model predictions were compared with laboratory impact sound measurements following ISO standards [18] for frequencies up to 200 Hz. Simulations were performed for a deterministic model and a stochastic model, with the results from the latter model presented in terms of confidence intervals. Although the predictions displayed trends similar to the measured trends, they were not convincing around the first resonance frequency. It is difficult to point out any dominating source of error as no eigenvalue analyses were performed, and the third-octave bands can comprise several resonances. An important conclusion from these studies is that the force spectrum of the tapping machine can be regarded as deterministic, i.e. the force spectrum can be calculated using a deterministic model of the floor.

A study similar to the one in [66] is presented in [67] in which three topics are discussed in more detail: prediction of the force spectrum, modelling of damping and calculation of the sound pressure in the receiving room. The FE modelling of the structure is, however, not explained in great detail. As in [66], the pressure field in the receiving room was calculated using the vibrations on the ceiling surface as BCs. Predicted impact sound levels are presented in third-octave bands between 50–2000 Hz and compared to results from several measurements on similar (but not identical) floors tested in different laboratories. In the paper, the measured impact sound levels are presented in intervals calculated as the mean value of the sound pressure ±2 standard deviations, which result in ranges of up to 15 dB per third-octave band. Therefore, it is difficult to draw any conclusions regarding the accuracy of the predictions.

In [68], a CLT floor with a suspended ceiling was investigated. The study focused on the FE modelling of the structure and on the prediction of radiated sound power into the receiving room. The floor consisted of four CLT plates with joints between them modelled using linear springs. Calibrations were performed to optimise the spring stiffness of the joints and the

material parameters of wood. The errors between simulated and measured eigenfrequencies were used as objective function in the optimisations. Comparisons of predicted and measured sound power in the receiving room for frequencies up to 150 Hz revealed that the trends were similar. However, the measured data displayed a more resonant behaviour, and a number of the measured resonance peaks were not captured in the simulations. Furthermore, the measured velocities were used as inputs to the prediction of radiated sound power, yielding a good correlation with the measured sound power and thereby validating the modelling of sound radiation employed in the paper. All results in the paper are presented in terms of FRFs, but the spatial distribution of the load is not stated. The results of the parameter optimisations in [68] are presented in [69], along with an investigation regarding the effects of air in the cavity between the floor and the suspended ceiling. The authors concluded that it is necessary to model the air using acoustic finite elements as the use of simpler spring representations is insufficient to capture the resonant behaviour of the air cavity.

In [70], modelling of low-frequency vibrations in wooden T-junctions (joints between wood beams and particleboards) was investigated by comparing FE models with each other and with measurements on four mock-ups. All comparisons were made in terms of eigenfrequencies and mode shapes. The effects of using different models for the screws and glue between plates and beams were studied. It was concluded, for example, that when glue is used in the joints between beams and boards it is valid to assume full interaction in FE models by constraining their respective DoFs to each other. This conclusion is supported by the results in [71], in which experimental and numerical modal analyses were carried out for a wooden floor-wall structure. The structure in [71] had screwed and glued joints between particleboards and beams, and a good correlation in terms of eigenfrequencies and mode shapes was observed for the first eigenmodes of the structure. No alternative methods for modelling the joints were tested, although doing so could possibly have improved the results. An alternative model of joints between wood beams and plate materials was introduced in [72] and employed in [73,74] for floors without glue in the joints. The model is based on the use of withdrawal modulus and slip modulus that represent the linear elasticity of joints in the axial and in-plane directions, respectively. Such models can also be used for joints between wood beams and plasterboards in ceilings and walls as the plasterboards are typically screwed to the beams without any glue in between. In [73], FE models were developed for predicting the fundamental frequency of wood floors. Models were created for 22 experimentally tested floors consisting of wood frames covered with plywood or oriented strand board (OSB), some of which had lateral reinforcement between the wood beams. Material properties of the wood beams were determined from measurements on each beam. Values of the slip modulus were taken from literature, whereas the values for the withdrawal modulus were determined from static measurements on several types of joints. Sensitivity analyses showed that the fundamental frequency is insensitive to changes in the withdrawal modulus. The slip modulus, however, has a larger effect on the fundamental frequency. Similar models were developed in [74], although without measuring the material properties of each beam. The correlation in eigenfrequencies and mode shapes was studied for the first five modes of six experimentally investigated floors, and it was concluded that modelling the elasticity in joints and supports is important for improving model accur-

acy. The correlation between simulations and measurements was, however, relatively poor also when elastic joints and supports were modelled.

In [75], an FE model was created for an experimental wooden assembly consisting of a floor connected to three underlying walls through elastomeric vibration isolators. The elastomeric isolators resembled those found in TVE buildings, as shown in Figure 1.1. The simulated mode shapes were compared to results from EMA, and discrepancies between the two mode sets were identified. For example, the building parts interacted more in the measured mode shapes. The authors pointed out the modelling of elastomers as a likely source of error; the elastomers were modelled using spring-dashpots in three directions without taking the rotational stiffness into account and neglecting any frequency-dependence of the elastomer properties. In [76], an elastomer connection similar to those found in many wood buildings was studied experimentally and numerically for frequencies below 100 Hz. The experimental structure consisted of an elastomer strip connected to steel parts on two sides. The steel parts are rigid in the frequency range of interest. Numerical modal analyses of the setup showed that using the elastomers' static stiffness in the model resulted in large errors, which led to the conclusion that it is necessary to model the dynamic properties of elastomers. In [77], a procedure for determining the frequency-dependent viscoelastic properties of elastomers was presented. The procedure combines results from FE analyses with experimental data provided by manufacturers valid for the specific geometry of the tested elastomers and for the BCs applied during the tests. The procedure in [77] can be employed to extract material properties from such data, enabling the creation of three-dimensional and frequency-dependent models of elastomers without the need to perform calibrations for each specific shape and set of BCs. The use of three-dimensional models naturally accounts for the rotational stiffness of the elastomer connections.

4.2.1 Summary

The results and conclusions in the publications discussed in Section 4.2 can be summarised as follows:

- None of the developed models for predicting structure-borne sound generated accurate predictions, although comparisons have been performed for simplified laboratory setups.
- The radiated sound power in the receiving room caused by structure-borne sound sources can be predicted with high accuracy using measured vibrations in the receiving room as input. Considering the previous bullet, this highlights that the uncertainty in the predictions of structure-borne sound lies within the modelling of the vibration transmission.
- The force spectrum generated by a standardised tapping machine can be predicted using a deterministic FE model of the structure. Variations in model parameters have a negligible effect on the force spectrum.

- When glue is used in the joints between wood beams and particleboards, full interaction can be assumed in the models.
- For joints without glue between beams and plates, it may be necessary to model the elasticity between these parts.
- Elastomeric vibration isolators in wood buildings must be modelled in detail by considering dynamic material parameters and rotational stiffness. Linear translational spring-dampers systems are insufficient for obtaining accurate results.
- Air-filled cavities in wood buildings affect the vibration transmission and should be considered in models. This conclusion is based on correlation studies for a structure without insulation in the cavity between the floor and ceiling.

It should be noted that some of the aforementioned conclusions are based on single publications in which simplified laboratory setups representing specific types of wood buildings were studied. Therefore, the conclusions are not necessarily applicable to all types of wood buildings; it may be necessary to test their validity in future correlation and validation studies.

4.3 CONCLUSIONS IN APPENDED PUBLICATIONS

In this section, the results and conclusions presented in Papers B, C and D are discussed. A summary of each paper is found in Chapter 6. The conclusions are based on example cases representing parts of TVE buildings.

There are several uncertainties that must be investigated before reliable models for predicting vibration transmission in multi-storey wood buildings can be established. One example is the effect of variations between structures with identical geometry, caused by, for example, the material properties of wood and the mechanical properties of joints. Another uncertainty that needs to be addressed is the effect of details and irregularities such as windows, floors, inner walls and surface layers. To investigate the effects of different variations and uncertainties, it is necessary to first develop a deterministic numerical model that has been correlated to measurements for use as a reference model. This was one of the objectives of the studies presented in the appended Papers C and D in which a wooden building structure representing part of a two-storey TVE building was investigated numerically and experimentally.

Paper C presents a procedure for determining the dimensions of scaled-size experimental structures. The procedure is based on analytical calculations and FE simulations. The simulated results for scaled-size structures were correlated to results for corresponding full-size structures to ensure accurate scaling. The procedure was applied to a wooden building structure representing part of a two-storey TVE building. The structure was scaled down from a volume of $4.0\times3.6\times2.8$ m^3 to $2.6\times2.4\times1.9$ m^3, which is a reduction of 70%. The eigenfrequencies and mode shapes of the structure were preserved with high accuracy in the scaling, and a reasonable accuracy was obtained for the FRFs between storeys.

In Paper D, model correlations were performed for the scaled-size wooden building structure developed in Paper C. Calibrations and correlations between simulated and measured results were performed using a multi-level approach. In the paper, important model parameters are discussed and modelling guidelines are suggested. These can be summarised as follows:

- It is important to use optimised material parameters for each individual wood beam to accurately simulate the mode shapes of floors, ceilings, walls and room structures for frequencies up to 100 Hz. Consequently, if Monte Carlo simulations are performed for the variations in material parameters of wood, random parameters should be generated for each individual beam.
- Joints between wood beams and particleboards can be modelled as fully interacting when they are both screwed and glued, as they were in the experimental structure. This observation agrees with the conclusions from previous research (see Section 4.2.1).
- It is erroneous to model the joints between wood beams and plasterboards as fully interacting when they are screwed and not glued, as they were in the experimental structure. The joints should instead be modelled by using elasticity for the rotational coupling.
- Elasticity in rotational coupling should also be used for modelling the joints between floors and walls, ceilings and walls, and different walls.
- It is important to model acoustic media in the cavities between floors and ceilings, particularly at higher frequencies. The floor-ceiling cavity in the experimental structure contained only air, with no insulation.

It was concluded that the dynamic behaviour of the experimental structure is to a great extent captured by the developed model. The simulated and measured results display similar amplitudes and resonance peaks, although appreciable discrepancies were found for transmission between storeys for frequencies above 50 Hz. Potential error sources are discussed in the paper. It was concluded that it is relevant to employ deterministic models to predict the vibration transmission provided that measurement data for calibration purposes is available.

The effect of modelling acoustic media in the cavities of wood buildings was investigated in more detail in Paper B wherein air and insulation were included in the numerical models. Air in the cavities alone was first modelled, resulting in significantly increased vibration transmission from a floor to the underlying room (in agreement with the studies in Paper D). The floor vibrations were, however, not affected to any appreciable extent when including air alone. Next, both air and insulation were modelled, with the latter modelled using a porous material model. The insulation had a dampening affect compared to the model with only air, both for the floor vibrations and for the transmission to the lower room. Comparing the model with both air and insulation in cavities to the model without acoustic media revealed that floor vibrations were reduced by about 15%, and the transmission to the underlying room was increased by a factor of up to 100 for frequencies below 100 Hz. The main conclusion from these

studies is that it is important to consider air and insulation in the cavities of wood buildings when modelling low-frequency vibration transmission between storeys and rooms. The effect of acoustic media is already distinct at very low frequencies, around the first resonances of the buildings.

5 Dynamic substructuring

The FE models discussed in Chapter 4 contain a large number of DoFs, which results in long computation times. For example, the FE model developed in Paper D representing a part of a two-storey TVE building contained 2.3 million DoFs. Steady-state analysis of the model at one frequency took 260 s when using the solver implemented in Abaqus/Standard 6.13 on an Intel Xeon E5-2650 eight-core processor of 2.0 GHz with 62 GB of RAM available. This means that a sweep of steady-state analyses of the model up to 100 Hz in steps of 1 Hz would take 7 hours. Such computation times are often problematic in the context of a design process. A parametric study can involve tens or hundreds of analyses and if each analysis takes 7 hours, the total computation time is several days or weeks. Consequently, there is a need to reduce the computation times for FE models of wood buildings. Dynamic substructuring is used in the thesis to perform the reduction.

Dynamic substructuring is a methodology frequently used for reducing large numerical models of structural dynamic systems. The methodology is illustrated in Figure 5.1. It is based on the division of structures into substructures that are reduced in size and assembled to form reduced global models. Dynamic substructuring provides a flexible and practical framework. It enables the combination of full numerical models and reduced order models of the substructures. The framework also allows for integration of experimental substructures represented by measured data into assemblies of numerical models. A description of the historic development of substructuring and a classification of methods is presented in [44].

In Sections 5.1.1 and 5.1.2, the theoretical background to model reduction through dynamic substructuring is presented. Section 5.2 describes how the framework for dynamic substructuring is applied to FE models of wood buildings. Conclusions of the studies on substructuring presented in the appended Papers E and F are discussed in Section 5.3.

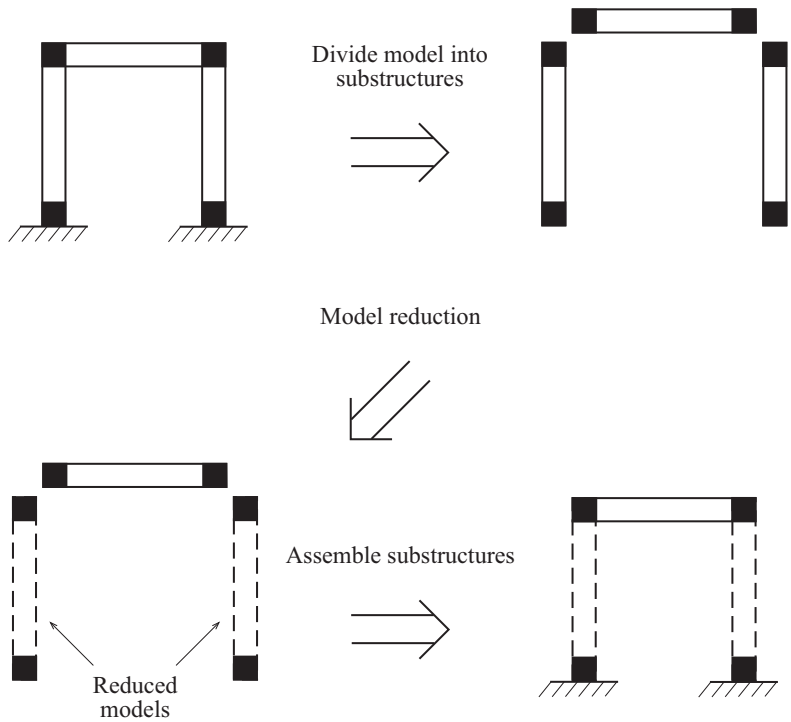

Figure 5.1: Illustration of model order reduction through dynamic substructuring when applied to a simple frame structure.

5.1 THEORETICAL BACKGROUND

5.1.1 Model order reduction

If a linear FE model is divided into substructures, each substructure is represented by the equation of motion in Equation (3.50). In this section, the reduction of one substructure containing n DoFs is considered. The objective of model order reduction is to obtain a system of m DoFs (where $m << n$) that preserves the dynamic characteristics of the full equation system. The general approach is to approximate the state vector using the transformation $\mathbf{a}(t) = \mathbf{T}\mathbf{a}_R(t)$, where $\mathbf{T} \in \mathbb{R}^{n\times m}$ is the transformation matrix and $\mathbf{a}_R(t) \in \mathbb{R}^{m\times 1}$ is the reduced state vector. This is a Ritz approximation [78] and the columns of the transformation matrix is the basis vectors. Applying the transformation to Equation (3.50) results in

$$\mathbf{M}_R\ddot{\mathbf{a}}_R(t) + \mathbf{C}_R\dot{\mathbf{a}}_R(t) + \mathbf{K}_R\mathbf{a}_R(t) = \mathbf{f}_R(t), \tag{5.1}$$

where the reduced mass, damping and stiffness matrices, $\mathbf{M}_R, \mathbf{C}_R, \mathbf{K}_R \in \mathbb{R}^{m\times m}$, respectively, and the reduced load vector $\mathbf{f}_R(t) \in \mathbb{R}^{m\times 1}$ are given by

$$\mathbf{M}_R = \mathbf{T}^T\mathbf{M}\mathbf{T}, \quad \mathbf{C}_R = \mathbf{T}^T\mathbf{C}\mathbf{T}, \quad \mathbf{K}_R = \mathbf{T}^T\mathbf{K}\mathbf{T}, \quad \mathbf{f}_R(t) = \mathbf{T}^T\mathbf{f}(t). \tag{5.2}$$

In the recent decades, many different methods for model order reduction have been proposed in the literature. The methods offer different ways of constructing the reduced basis in the transformation matrix. The theoretical background to a wide range of methods is presented in Paper F. The DoFs in the reduced state vector can be divided into two categories: interface DoFs and generalised coordinates. Interface DoFs can be, for example, displacements or forces in the nodes of the substructure interfaces. Generalised coordinates generally have no physical interpretation other than being amplitudes of basis vectors contained in the transformation matrix. The coupling of substructures is normally realised by tying the interface DoFs of neighbouring substructures to each other using Lagrange multipliers [37]. This enforces the compatibility requirements and force equilibrium. Such a coupling procedure requires that the interface DoFs are preserved in the model order reduction. Reduction methods preserving the interface DoFs are referred to as structure-preserving. The research presented in Papers E and F considers only structure-preserving methods.

5.1.2 Interface reduction

The reduced system matrices resulting from a model order reduction are, in general, densely populated. This means that the computation time increases faster compared to full FE models (which have sparse system matrices) as the number of DoFs increases. If substructure models have large numbers of interface DoFs, it is necessary to perform interface reduction before model order reductions are carried out. There are essentially two methodologies for reducing the number of interface DoFs of substructures. The first is based on the concept of interface modes; deformation shapes of the interfaces that are extracted from eigenmodes of the substructure assembly [79]. The coupling of adjacent substructures is then realised by coupling the sets of generalised coordinates through Lagrange multipliers. Two drawbacks of this methodology are that it is not structure preserving and that the substructures cannot be reduced separately. In the second methodology, an additional node referred to as condensation node [80] is introduced for each interface surface. A condensation node represents the motion of its interface surface and has both translational and rotational DoFs, resulting in six DoFs per interface. The coupling of adjacent substructures is then realised by coupling the condensation nodes through Lagrange multipliers. The condensation nodes can be coupled to the DoFs of their respective interface surfaces using different methods. The theoretical background to such coupling methods is presented in Paper E.

5.2 STRATEGY USED IN THESIS

Dynamic substructuring of wood buildings is considered in Papers E and F. A summary of each paper is found in Chapter 6. Paper E considers interface reduction and coupling of substructure models, while Paper F discusses methods for model order reduction of the substructures.

The division into substructures can be accomplished in different manners and affects both the

accuracy and the computational efficiency of the reduced models. Since the reduced system matrices generally are densely populated, it is important to ensure that the substructures have a small number of DoFs to avoid long computation times. In the thesis, wood buildings are divided into substructures at the interfaces between elastomeric vibration isolators and wood components. For TVE buildings, illustrated in Figure 1.1, this approach means that each volume element is considered as a substructure. There are several benefits from performing the substructure division in such manner. First of all, those interfaces are often small compared to the complete geometry, which is an advantage when striving for a small number of interface DoFs. Second, the large difference in stiffness between elastomers and wood components is beneficial for the interface reduction described in Paper E; this is explained in more detail in the paper. Third, by performing the division at the interfaces between elastomers and wood components, the elastomers are excluded from the substructures. Instead, the elastomers can be treated as coupling elements, which is discussed in Paper E. This is necessary when modelling frequency-dependent material properties of elastomers since most methods for model order reduction require constant system matrices. In summary, the strategy for dividing wood buildings into substructures employed in the thesis results in substructure models with a small number of interface DoFs and enables the modelling of frequency-dependent properties of elastomers.

5.3 CONCLUSIONS IN APPENDED PUBLICATIONS

In Paper E, a procedure for creating reduced coupling elements representing elastomeric vibration isolators is presented. Figure 5.2 illustrates the coupling elements and how they are used to couple substructures models. The coupling elements replace 3D FE models of elastomers and are able to represent frequency-dependent material properties and the rotational stiffness in elastomeric connections. The developed procedure involves methods for interface reduction and for reduction of the number of internal DoFs of elastomers. The methods for interface reduction are based on the use of condensation nodes, which results in six DoFs representing each interface surface. The interface reduction is performed both for elastomers and for the substructures they are connected to. The coupling of substructures is then realised by tying the condensation nodes at the coupling elements to the condensation nodes at the substructures using Lagrange multipliers. In the paper, an FE model comprising a wood floor and a wood ceiling with elastomeric vibration isolators between them was used as an example case. Based on the studies of the example case, several conclusions were drawn regarding the accuracy of different methods for interface reduction and for reduction of internal DoFs of elastomers. For example, it was concluded that the optimal method for interface reduction of elastomers is another method than the optimal method for wood components.

In Paper F, a wide range of methods for model order reduction were compared in terms of their effects on the accuracy and computational time of analyses. Two FE models of wood floors were used as example cases. The comparative studies provide guidance in the selection of suitable methods for reducing FE models of wooden building structures. For example,

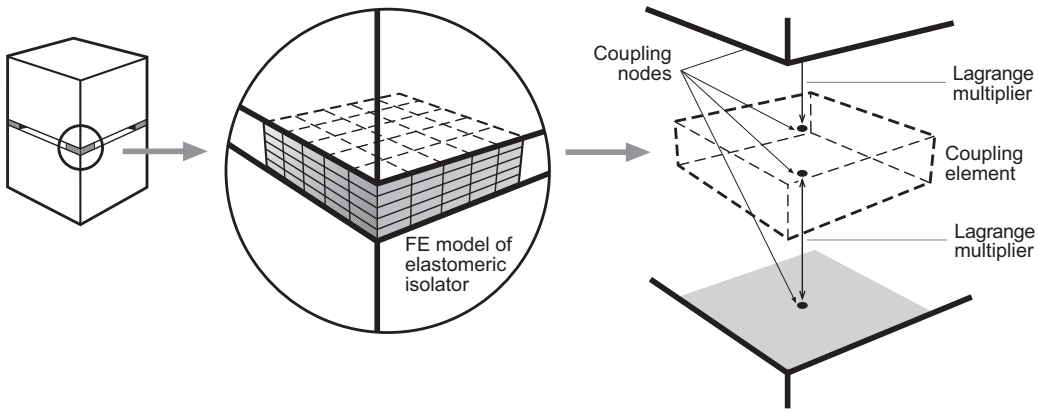

Figure 5.2: *Illustration of coupling elements representing elastomeric vibration isolators in dynamic substructuring.*

the component mode synthesis (CMS) method by Craig-Bampton and the Krylov subspace version of CMS were found to produce reduced models with similar accuracy and computation time. The former method is widely used in structural dynamics, while the latter has emerged as an alternative in recent years.

In Paper E, the example model studied was reduced by combining the reduction methods suggested in Papers E and F. By performing the reduction, the computation time for steady-state analyses of the full model was reduced by 99.8% while only introducing errors of about 1% in the simulated vibration transmission for frequencies up to 100 Hz. This demonstrates the potential of using the strategy suggested in the thesis for dynamic substructuring of FE models of wood buildings.

6 Summary of appended publications

6.1 PAPER A

Numerical investigation of vibration reduction in multi-storey lightweight buildings.
Ola Flodén, Kent Persson, Göran Sandberg.
In: Dynamics of Civil Structures, Vol 2: 443–453. Springer International Publishing, 2015.

Summary

A numerical study on the effects of different design choices for elastomeric vibration isolators in wood buildings is presented. The vibration transmission in a two-storey TVE building was simulated using an FE model. Only the structural transmission was considered, i.e. acoustic media in the cavity between floor and ceiling was not modelled. The amount of transmitted vibrations was compared for different designs of the elastomeric isolators, which were in the shape of blocks and placed along the walls between the storeys. Two design choices were studied: the placement of the elastomers and their material properties. The properties were varied within realistic ranges and the placement was varied while keeping constant distances between the blocks. It was found that the transmission from a floor to the ceiling of the storey below, in general, increases with the stiffness of the elastomers. It was observed that the use of relatively stiff elastomers can cause increased vibration transmission at frequencies between 50–100 Hz compared to a setup without elastomeric isolators. The placement of the elastomers was found to have negligible effect on the vibration transmission. The floor vibrations were not affected by the design of the elastomeric isolators.

Contributions by Ola Flodén

Ola Flodén was the main author of the paper, planned research tasks, performed the FE modelling and analyses, and drew conclusions that were presented.

6.2 PAPER B

The effect of modelling acoustic media in cavities of lightweight building structures on the transmission of structural vibrations.
Ola Flodén, Juan Negreira, Kent Persson, Göran Sandberg.
Engineering Structures 83: 7–16, 2015.

Summary

A numerical investigation regarding the effects of air and insulation in cavities of multi-storey wood buildings on the vibration transmission is presented. TVE buildings were used as example case for studying the vibration transmission from a floor structure to the storey below for frequencies up to 100 Hz. An FE model without acoustic media was compared to two other models: one model including air and insulation and one model including air alone. It was found that the modelling of air alone results in a more resonant system and higher vibration amplitudes. Compared to the model without acoustic media, the model with both air and insulation introduces a dampening effect for the floor vibrations, while the transmission to the lower room is increased significantly. The main conclusion in the paper is that the air and insulation inside cavities should be considered in numerical analysis of vibration transmission in multi-storey wood buildings.

Contributions by Ola Flodén

Ola Flodén contributed was the main author of the paper, planned research tasks, performed the main part of the FE modelling and analyses, and drew conclusions that were presented.

6.3 PAPER C

Numerical and experimental studies on scale models of lightweight building structures.
Ola Flodén, Kent Persson, Göran Sandberg.
In: Dynamics of Coupled Structures, Vol 4: 173–180. Springer International Publishing, 2016.

Summary

A procedure for scaling the size of experimental building structures for vibration measurements is presented. The objective of developing the scaling procedure is to enable the design of scaled-size structures which preserve the dynamic behaviour of full-size structures. The procedure is based on analytical expressions for the dynamic bending of beams and involves FE modelling of the scaled-size and full-size structures to correlate their eigenfrequencies, mode shapes and vibration transmission. As an example case, a wooden building structure representing part of a two-storey TVE building was used. The volume of the structure was scaled down from

4.0×3.6×2.8 m^3 to 2.6×2.4×1.9 m^3, i.e. by 70%, through employing the scaling procedure. It was found that the eigenfrequencies and mode shapes below 100 Hz were well-preserved in the scaling. The vibration transmission in the scaled-size and full-size structures were found to be well-correlated for frequencies up to 50 Hz.

Contributions by Ola Flodén

Ola Flodén was the main author of the paper, planned research tasks, performed the analytical and FE calculations, and drew conclusions that were presented.

6.4 PAPER D

A multi-level model correlation approach for low-frequency vibration transmission in wood structures.

Ola Flodén, Kent Persson, Göran Sandberg.

Submitted for publication.

Summary

A multi-level model correlation approach for low-frequency vibration transmission in wood buildings is presented. The approach is based on calibrations and correlations between simulations and measurements at four levels: structural components (viz. beams and boards), planar structures (viz. floors, ceilings and walls), room structures and the complete structure. As an example case, the scaled-size experimental structure designed in Paper C was used. Based on observations made in the studies, important model parameters are discussed and modelling guidelines are suggested. The results were used to discuss the accuracy of deterministic models in the special case that detailed information regarding material parameters and mechanical behaviour of joints is available. The results indicate that the dynamic behaviour of the experimental structure is to a great extent captured by the developed model. Therefore, it was concluded that it is relevant to employ deterministic models to predict the vibration transmission provided that measurement data for calibration purposes is available. The developed model can be used as a reference model for investigations on the effects of variations and uncertainties in the modelling, and on the possibilities and limitations of using deterministic methods.

Contributions by Ola Flodén

Ola Flodén was the main author of the paper, planned research tasks, performed the experimental and numerical analyses, and drew conclusions that were presented.

6.5 PAPER E

Modelling of elastomeric vibration isolators in dynamic substructuring.
Ola Flodén, Kent Persson, Göran Sandberg.
Submitted for publication.

Summary

A procedure for creating coupling elements that represent elastomeric vibration isolators in dynamic substructuring is presented. The coupling elements are constructed on the basis of 3D FE models of elastomers, and are intended for use in assembling reduced substructure models. The developed procedure involves methods for interface reduction and for reduction of the number of internal DoFs of elastomers. The interface reduction is performed both for elastomers and for the substructures they are connected to. An FE model comprising a floor and a ceiling with elastomeric isolators between them was used as example case. The effects of using different reduction methods to create the coupling elements were investigated. Also, the effects of including different modelling features, such as rotational coupling and frequency-dependent material properties, in the coupling elements were investigated. It was found that the procedure for creating coupling elements can be used for establishing accurate and efficient assemblies of reduced substructure models provided that suitable reduction methods are employed.

Contributions by Ola Flodén

Ola Flodén was the main author of the paper, planned research tasks, performed the FE modelling and analyses, and drew conclusions that were presented.

6.6 PAPER F

Reduction methods for the dynamic analysis of substructure models of lightweight building structures.
Ola Flodén, Kent Persson, Göran Sandberg.
Computers & Structures 138: 49–61, 2014.

Summary

A comparative study of different methods for model order reduction when applied to substructure models of wood buildings is presented. A wide range of methods in the literature were compared for two example cases, both being FE models of wooden floor structures. The comparisons were made by studying the errors in eigenfrequencies, mode shapes and predicted vibration transmission through the floors. The latter was performed when applying realistic BCs, imposed by coupling the reduced models to FE models of wood-framed walls. Conclusions were drawn regarding the relative accuracy and computation time of the reduced models.

For example, the CMS method by Craig-Bampton and the Krylov subspace version of CMS were found to result in similar accuracy and computation time. The former method is widely used in structural dynamics, while the latter has emerged as an alternative in recent years.

Contributions by Ola Flodén

Ola Flodén was the main author of the paper, planned research tasks, implemented the methods for model order reduction, performed the FE modelling and analyses, and drew conclusions that were presented.

7 Concluding remarks

The aim of the research discussed in the thesis is to create accurate and efficient prediction models that can be used for designing multi-storey wood buildings with improved vibroacoustic comfort for residents. The thesis work focused on the prediction of low-frequency vibration transmission between storeys and rooms. Such models can be used to predict structure-borne sound as well as floor vibrations. The presented research is a part of the development of accurate and efficient numerical models. Several uncertainties in the modelling remain, but the results and conclusions presented in the thesis are important steps towards enabling the prediction of vibration transmission by use of numerical models. Two main conclusions of the studies are: (1) that deterministic models are relevant for predicting the vibration transmission below 100 Hz, provided that measurement data for calibration purposes is available, and (2) that the suggested strategy for dynamic substructuring can be used to reduce the computation times significantly without having an appreciable effect on the accuracy of the model predictions.

The conclusions of the studies presented in the appended publications and their contributions to the research field are discussed in more detail in this chapter, along with proposals for future work.

7.1 CONCLUSIONS AND CONTRIBUTIONS

The studies in Paper A contribute to the research field by increasing knowledge regarding the effects of design choices for elastomeric vibration isolators in wood buildings. Elastomeric isolators are widely used in the construction industry, but knowledge of their effect on the dynamic behaviour of wood buildings and how they should be designed to optimise the vibration reduction is limited. In the paper, results from numerical parametric studies were used to show that overly stiff elastomers can result in amplifications of vibration transmission between storeys at frequencies between 50–100 Hz. This highlights the need for a careful design of elastomeric isolators and that it can be preferable to develop other types of vibration isolators for wood buildings.

The contributions of the research presented in Papers B–D are related to the development of accurate numerical models, while the research presented in Papers E and F considers the

computational efficiency of the models. The conclusions were based on studies of example cases representing parts of TVE buildings.

7.1.1 Model validation

Paper C presents a procedure for determining the dimensions of scaled-size experimental building structures. For the example case studied, it was found that the procedure can be used to establish scaled-size structures with well-preserved dynamic characteristics and significantly reduced dimensions compared to full-scale structures. The procedure is well-suited for model correlation studies, such as the one presented in Paper D, in which it is important that the dynamic characteristics are well-preserved in the scaling but absolute vibration levels are of less importance. By employing the procedure for future model correlation studies, these can be performed at a lower cost and with greater time-efficiency. For model validation tests, however, measurements on real buildings should be used instead.

The correlation study presented in Paper D is an important step towards establishing accurate models for analysing low-frequency vibration transmission in wood buildings. It was found that the developed deterministic model could reproduce the vibration transmission in the experimental structure to a great extent. In the paper, discussions on important model parameters and modelling guidelines are presented that provide valuable input to future studies. The developed numerical model can be used as a reference model for investigations on the effects of variations and uncertainties in the modelling of low-frequency vibrations in wood buildings.

One of the findings in Paper D was that the correlation between simulated and measured vibrations is improved by modelling the air in the cavity between the floor and the ceiling as an acoustic medium. The effects of modelling acoustic media in the cavities of wood buildings was investigated in more detail in Paper B in which both air and insulation were considered in numerical models. It was concluded that the predicted vibration transmission from a floor to the underlying storey is increased substantially by including air and insulation in the model. The effects were found to be less significant for floor vibrations, which were slightly damped. The results presented in Papers B and D show that the inclusion of acoustic media in models has a considerable effect on the vibration transmission and that the effect is distinct already at very low frequencies, around the first resonances of the buildings.

7.1.2 Dynamic substructuring

The conclusions in Papers E and F contribute to a framework for establishing computationally efficient reduced substructure models of wood buildings. The procedure presented in Paper E can be employed to create coupling elements representing elastomeric vibration isolators. The use of the coupling elements results in substructure models with a small number of interface DoFs, which is crucial for obtaining reduced substructure models that are computationally efficient. In the paper, an example case consisting of a floor and a ceiling with elastomeric

isolators between them was studied. It was found that using the procedure for creating coupling elements allowed substantial reduction of the number of interface DoFs of the substructure models without introducing errors of any appreciable size. Furthermore, the procedure allows for the modelling of frequency-dependent properties of elastomers, which is not possible using conventional substructuring techniques. Paper F provides guidelines for selecting methods for model order reduction of substructure models of wooden building structures. The guidelines are based on comparisons of a wide range of methods in terms of their effects on the accuracy and efficiency of the reduced models.

The potential of combining the reduction methods suggested in Papers E and F was demonstrated for the example case in Paper E. The computation time for steady-state analyses of the full model was reduced by 99.8% while only introducing errors of about 1% in the simulated vibration transmission for frequencies below 100 Hz.

7.2 PROPOSALS FOR FUTURE WORK

The proposals presented here are related to the further development of the numerical models discussed in the thesis. However, the model developed in Paper D is accurate enough to study the physics involved in low-frequency vibration transmission in wood buildings. The model can be used in studies on novel types of vibration isolators for wood buildings.

An important continuation of the research presented in the thesis is to investigate the effects that variations and uncertainties in the modelling have on the predicted vibrations. The correlated model developed in Paper D is suitable for use as a reference model for such investigations. Examples of variations and uncertainties that are relevant to study are:

- The variations in material parameters of wood. It was concluded in Paper D that it is important to use optimised material parameters for each individual wood beam to accurately simulate the mode shapes of floors, ceilings, walls and room structures below 100 Hz. Therefore, variations should be considered for each individual beam as opposed to varying the parameters simultaneously for all beams.
- The variations in the mechanical behaviour of joints between beams and plates and between floor, walls and ceiling in each room.
- The level of detail in the models. It can, for example, be investigated how modelling of windows, doors, interior walls and surface layers affect the model predictions.
- The BCs applied to the models. The model developed in Paper D represents part of a two-storey building and was developed for free BCs because the experimental structure was suspended from soft rubber bands. It should be investigated how the modelling of larger parts of buildings and the use of different BCs affect predictions.

Whereas variations in the material parameters of wood are well-known, the understanding of variations in the mechanical behaviour of joints is not as extensive. To determine statistical distributions for model parameters for joints, model calibrations can be performed for a series of simplified experimental setups. Once statistical distributions have been established, their effects can be considered through Monte Carlo simulations in which variations are propagated from the model input to the model output. Monte Carlo simulations can be performed by considering the stochastic parameters both individually and simultaneously. By considering the parameters one at a time, the necessity for modelling them stochastically can be assessed; by considering the parameters simultaneously, the total variation in the model predictions can be determined.

The modelling of air and insulation in cavities should be investigated further. In the investigations presented in Paper B, no correlations between simulations and measurements were carried out. Correlations should be performed for experimental setups containing insulation to identify porous material models that are suitable for modelling low-frequency vibration transmission. Furthermore, it would be interesting to investigate if air and insulation in cavities can be modelled in a simpler fashion than by using acoustic finite elements. An example of a simpler approach would be to use spring-dashpot systems.

Through further model correlation studies and investigations on the effects of variations and uncertainties, the accuracy of model prediction will be improved. Eventually, model validation tests should be performed by comparing predictions to a series of measurements on real buildings. Through such testing, it can be determined if the developed models are able to predict the variations in dynamic behaviour among buildings with identical geometry.

The dynamic substructuring methods discussed in Papers E and F provide a framework for creating reduced models that are computationally efficient. As these studies were performed without considering air and insulation in cavities, the integration of air and insulation into the framework should be further investigated. However, before performing these investigations, the modelling of air and insulation in cavities should be further investigated. If such investigations reveal that the effects of air and insulation can be modelled accurately using spring-dashpot systems, these can be integrated with the substructure division employed in Papers E and F; the spring-dashpots can be considered as coupling elements in the same way as the elastomeric vibration isolators. If it is found that acoustic finite elements are required to obtain accurate predictions, it will be necessary to modify the strategy for performing substructure division.

References

[1] Freij, J. (2016), *Genombrott för flerfamiljshus i trä*, in: *Skog & Ekonomi – Nyheter från Danske Bank, Nummer 1*, Danske Bank Sweden, Stockholm.

[2] Ljunggren, F., Simmons, S., Hagberg, K. (2014), *Correlation between sound insulation and occupants' perception – Proposal of alternative single number ratings of impact sound*, Applied Acoustics **85**, 57–68.

[3] Simmons, S., Hagberg, K., Backman, K. (2011), *Acoustical performance of apartment buildings – Resident's survey and field measurements, Report 2011:58*, SP Technical Research Institute of Sweden, Stockholm.

[4] Jarnerö, K., Bard, D., Simmons, C. (2013), *Vibration performance of apartment buildings with wooden lightweight framework – Residents survey and field measurements, Report 2013:17*, SP Technical Research Institute of Sweden, Stockholm.

[5] Ljunggren, F., Ågren, A. (2011), *Potential solutions to improved sound performance of volume based lightweight multi-storey timber buildings*, Appl Acoust **72**, 231–240.

[6] Swedish Standards Institute (2000), *SS-EN 12354: Building acoustics – Estimation of acoustic performance of buildings from the performance of elements*, SIS, Stockholm, Sweden.

[7] Swedish Ministry of Enterprise, Energy and Communications (2004), *Mer trä i byggandet – Underlag för en nationell strategi att främja användning av trä i byggande, Ds 2004:1*, Government Offices of Sweden, Stockholm.

[8] Stehn, L., Rask, L.O., Nygren, I., Östman, B. (2008), *Byggandet av flervåningshus i trä – Erfarenheter efter tre års observation av träbyggandets utveckling*, Luleå University of Technology, Sweden.

[9] Gustavsson, L., Pingoud, K., Sathre, R. (2006), *Carbon dioxide balance of wood substitution: comparing concrete- and wood-framed buildings*, Mitigation and Adaption Strategies for Global Change **11**, 667–691.

[10] Bisby, L.A., Frangi, A. (2015), *Special issue on timber in fire*, Fire Technology **451**, 1275–1277.

[11] Labonnote, N. (2005), *Damping in timber structures*, Ph.D. thesis, Norwegian University of Science and Technology, Trondheim.

[12] Persson, K. (2000), *Micromechanical modelling of wood and fibre properties*, Ph.D. thesis, Lund University, Sweden.

[13] Swedish Standards Institute (2000), *SS-EN 1611-1: Sawn timber – Appearance grading of softwoods – Part 1: European spruces, firs, pines and Douglas firs*, SIS, Stockholm, Sweden.

[14] Gerhards, C.C. (1982), *Effect of moisture and temperature on the mechanical properties of wood: an analysis of immediate effects*, Wood and Fiber Science **14(1)**, 4–36.

[15] Thelandersson, S. (2003), *Introduction: Wood as construction material*, in: Timber Engineering, John Wiley & Sons, Chichester, UK.

[16] Statistics Sweden (2016-09-05), *http://www.scb.se/sv_/Hitta-statistik/Statistik-efter-amne/Boende-byggande-och-bebyggelse*, SCB, Stockholm, Sweden.

[17] International Organization for Standardization (2013), *ISO 717: Acoustics – Rating of sound insulation in buildings and of building elements*, ISO, Geneva, Switzerland.

[18] International Organization for Standardization (2010), *ISO 10140: Acoustics – Laboratory measurement of sound insulation of building elements*, ISO, Geneva, Switzerland.

[19] International Organization for Standardization (2014), *ISO 16283: Acoustics – Field measurement of sound insulation in buildings and of building elements*, ISO, Geneva, Switzerland.

[20] Rasmussen, B. (2010), *Sound insulation between dwellings – Requirements in building regulations in Europe*, Applied Acoustics **71**, 373–385.

[21] Rasmussen, B., Machimbarrena, M. (eds.) (2014), *Building acoustics throughout Europe. Volume 1: Towards a common framework in building acoustics throughout Europe*, COST Action TU0901.

[22] Rasmussen, B., Rindel, J.H. (2010), *Sound insulation between dwellings – Descriptors applied in building regulations in Europe*, Applied Acoustics **71**, 171–180.

[23] International Organization for Standardization (1997), *ISO 2631-1: Mechanical vibration and shock – Evaluation of human exposure to whole-boy vibration – Part 1: General requirements*, ISO, Geneva, Switzerland.

[24] International Organization for Standardization (2003), *ISO 2631-2: Mechanical vibration and shock – Evaluation of human exposure to whole-body vibration – Part 2: Vibrations in buildings (1 Hz to 80 Hz)*, ISO, Geneva, Switzerland.

[25] European Committee for Standardization (2004), *EN 1995-1-1: Eurocode 5: Design of timber structures – Part 1-1: General – Common rules and rules for building*, CEN, Brussels, Belgium.

[26] Ohlsson, S.V. (1982), *Floor vibrations and human discomfort*, Ph.D. thesis, Chalmers University of Technology, Gothenburg, Sweden.

[27] Negreira, J., Trollé, A., Jarnerö, K., Sjökvist, L.G., Bard, D. (2015), *Low frequency vibroacoustic investigation of wooden T-junctions*, Journal of Sound and Vibration **340**, 383–408.

[28] Hveem, S. (2000), *Nordic multi-storey timber buildings for residential housing*, in: *Proceedings of Internoise 2000*, Nice, France.

[29] Forssén, J., Kropp, W., Brunskog, J., Ljunggren, S., Bard, D., Sandberg, G., Ljunggren, F., Ågren, A., Hallström, O., Dybro, H., Larsson, K., Tillberg, K., Sjökvist, L.G., Östman, B., Hagberg, K., Bolmsvik, Å., Olsson, A., Ekstrand, C.G., Johansson, M. (2008), *Acoustics in wooden buildings – State of the art 2008, Vinnova project 2007-01653, Report 2008:16*, SP Technical Research Institute of Sweden, Stockholm.

[30] Hveem, S., Homb, A., Hagberg, K., Rindel, J.H. (1996), *Low-frequency footfall noise in multi-storey timber frame buildings, Report 1996:12E*, NKB Work and Committee Reports, Helsinki, Finland.

[31] Sipari, P. (2000), *Sound insulation of multi-storey houses – A summary of Finnish impact sound insulation results*, Building Acoustics **7(1)**, 15–30.

[32] Guigou-Carter, C., Balanant, N., Villenave, M. (2014), *Acoustic comfort evaluation in lightweight wood-based buildings*, in: *Proceedings of Forum Acusticum 2014*, Krakow, Poland.

[33] Ljunggren, F., Ågren, A. (2002), *Development of a new damper to reduce resonant vibrations in lightweight steel joist floors*, Applied Acoustics **63**, 1267–1280.

[34] Bolmsvik, Å., Brandt, A. (2013), *Damping assessment of light wooden assembly with and without damping material*, Engineering Structures **49**, 434–447.

[35] Andersen, L., Kirkegaard, P.H., Dickow, K.A., Kiel, N., Persson, K. (2012), *Influence of wall surface and air modelling in finite-element analysis of sound transmission between rooms in lightweight buildings*, in: *Proceedings of Internoise 2012/ASME NCAD meeting*, New York, US.

[36] Schiehlen, W. (1997), *Multibody system dynamics: Roots and perspectives*, Multibody System Dynamics **1**, 149–188.

[37] Bathe, K.J. (1996), *Finite element procedures*, Prentice Hall, New York, US.

[38] Zienkiewicz, O.C., Taylor, R.L. (1994), *The finite element method, 5th ed.*, MacGraw-Hill, London.

[39] Katsikadelis, J.T. (2002), *Boundary elements – Theory and application*, Elsevier Science Ltd, Oxford, UK.

[40] Ali, A., Rajakumar, C. (2004), *The boundary element method – Applications in sound and vibration*, CRC Press, Boca Raton, US.

[41] Lyon, R.H., DeJong, R.G. (1995), *Theory and application of statistical energy analysis – Second edition*, Butterworth-Heinemann, Newton, US.

[42] Le Bot, A. (2015), *Foundation of statistical energy analysis in vibroacoustics*, Oxford University Press, Oxford, UK.

[43] Mooney, C.Z. (1997), *Monte Carlo simulation*, Sage Publications, Thousand Oaks, US.

[44] de Clerk, D., Rixen, D.J., Voormeeren, S.N. (2008), *General framework for dynamic substructuring: history, review and classification of techniques*, AIAA Journal **46(5)**, 1169–1181.

[45] Gurtin, M.E. (1981), *An introduction to continuum mechanics*, Academic press, New York, US.

[46] Holzapfel, G.A. (2000), *Nonlinear solid mechanics: a continuum approach for engineering*, John Wiley & Sons, Chichester, UK.

[47] Sandberg, G., Ohayon, R. (2008), *Computational aspects of structural acoustics and vibrations*, CISM Courses and Lectures, vol. 505, Springer Wien, New York, US.

[48] Sandberg, G. (1995), *A new strategy for solving fluid-structure problems*, International Journal for Numerical Methods in Engineering **38**, 357–370.

[49] Craig, R.R., Kurdila, A.J. (2006), *Fundamentals of structural dynamics*, John Wiley & Sons, New Jersey, US.

[50] Chopra, A.K. (2007), *Dynamics of structures: theory and application to earthquake engineering 3d ed*, Prentice Hall, New Jersey, US.

[51] Kerschen, G., Worden, K., Vakakis, F., Golinval, J.C. (2006), *Past, present and future of nonlinear system identification in structural dynamics*, Mechanical Systems and Signal Processing **20**, 505–592.

[52] Worden, K., Tomlinson, G.R. (2000), *Nonlinearity in structural dynamics*, Institute of Physics Publishing, London, UK.

[53] Cooley, J.W., Tukey, J.W. (1965), *An algorithm for the machine calculation of complex fourier series*, Mathematics of Computation **19(90)**, 297–301.

[54] Rayleigh, J. (1877), *The theory of sound*, Macmillan, London, UK.

[55] Halvorsen, W.G., Brown, D.L. (1977), *Impulse technique for structural frequency response testing*, Sound and Vibration **11(11)**, 8–21.

[56] Agilent Technologies (2000), *The fundamentals of modal testing*, Application Note 243-3, Agilent Technologies, US.

[57] Avitabile, P. (2001), *Experimental modal analysis*, Sound and Vibration **35**, 20–31.

[58] Brandt, A. (2011), *Noise and vibration analysis: signal analysis and experimental procedures*, John Wiley & Sons, Chichester, UK.

[59] Allemang, R.J., Brown, D.L. (1998), *A unified matrix polynomial approach to modal identification*, Journal of Sound and Vibration **211(3)**, 301–322.

[60] American Society of Mechanical Engineers (2006), *Guide for the verification and validation in computational solid mechanics*, ASME, New York, US.

[61] Paez, T. (2009), *Introduction to model validation*, in: *Proceedings of IMAC XXVII*, Orlando, US.

[62] Paez, T., Swiler, L. (2009), *Probabilistic methods in model validation*, in: *Proceedings of IMAC XXVII*, Orlando, US.

[63] Swiler, L., Paez, T., Mayes, R. (2009), *Probabilistic methods in model validation*, in: *Proceedings of IMAC XXVII*, Orlando, US.

[64] Mayes, R. (2009), *Model correlation and calibration*, in: *Proceedings of IMAC XXVII*, Orlando, US.

[65] Antoniou, A., Wu-Sheng, L. (2007), *Practical optimization – Algorithms and engineering applications*, Springer Science+Business Media, LLC, New York, US.

[66] Cougenanff, C. (2015), *Robust design of lightweight wood-based systems in linear vibroacoustics*, Ph.D. thesis, Universite Paris-Est, France.

[67] Rabold, A. (2008), *FEM based prediction model for the impact sound level of floors*, in: *Acoustics'08*, Paris, France.

[68] Kohrmann, M., Buchschmid, M., Müller, G., Vøltl, R., Schanda, U. (2013), *Numerical models for the prediction of vibro-acoustical characteristics of light-weighted ceiling*, in: *Proceedings of Internoise 2013*, Innsbruck, Austria.

[69] Buchschmid, M., Müller, G., Kohrmann, M., Schanda, U. (2015), *Vibroacoustic investigation of light-weight ceilings – Modeling aspects and design guidelines*, in: *Proceedings of Euronoise 2015*, Maastricht, Netherlands.

[70] Negreira, J., Sjöström, A., Bard, D. (2016), *Low frequency vibroacoustic investigation of wooden T-junctions*, Applied Acoustics **105**, 1–12.

[71] Ejenstam, J., Flodén, O. (2011), *Vibration analyses of a wooden floor-wall structure – Experimental and finite element studies*, Master's thesis, Lund University, Sweden.

[72] Thomson, E.G., Goodman, J.P., Vanderbilt, M.D. (1975), *Finite element analysis of layered wood systems*, Journal of the Structural Division **101**(**12**), 2659–2672.

[73] Jiang, L., Hu, L., Chui, Y.H. (2004), *Finite-element model for wood-based floors with lateral reinforcement*, Journal of Structural Engineering **130**(**7**), 1097–1107.

[74] Weckendorf, J. (2009), *Dynamic response of structural timber flooring systems*, Ph.D. thesis, Edinburgh Napier University, Scotland.

[75] Bolmsvik, Å., Linderholt, A., Brandt, A., Ekevid, T. (2014), *FE modelling of light weight wooden assemblies – Parameter study and comparison between analyses and experiments*, Engineering Structures **73**, 125–142.

[76] Bolmsvik, Å., Linderholt, A. (2015), *Damping elastomers for wooden constructions – Dynamic properties*, Wood Material Science & Engineering **10**(**3**), 245–255.

[77] Negreira, J., Austrell, P.E., Flodén, O., Bard, D. (2014), *Characterisation of an elastomer for noise and vibration insulation in lightweight timber buildings*, Building Acoustics **21**(**4**), 251–276.

[78] Arnold, R.R., Citerley, R.L., Chargin, M., Galant, D. (1985), *Application of Ritz vectors for dynamic analysis of large structures*, Computers & Structures **21**(**3**), 461–467.

[79] Tran, D.M. (2001), *Component mode synthesis methods using interface modes. Application to structures with cyclic symmetry*, Computers & Structures **79**(**2**), 209–222.

[80] Heirman, G.H.K., Desmet, W. (2010), *Interface reduction of flexible bodies for efficient modeling of body flexibility in multibody dynamics*, Computers & Structures **24**(**2**), 219–234.

Part II

Appended publications

Paper A

Chapter 45
Numerical Investigation of Vibration Reduction in Multi-storey Lightweight Buildings

Ola Flodén, Kent Persson, and Göran Sandberg

Abstract In order to reduce the vibration transmission in multi-storey wood buildings, it is common to insert viscoelastic elastomer materials between parts of the buildings. The studies presented here investigate to which extent different design choices for the elastomer layers affect the isolation of low-frequency vibrations (0–100 Hz). A finite element model of two storeys of a multi-storey wood building, involving blocks of elastomer material in between the storeys, was used to perform numerical investigations. Parametric studies were carried out, considering different properties of the elastomer material and different placements of the elastomer blocks. Considering the transmission from the floor of the upper storey to the underlying ceiling, the material properties of the elastomer material were found to affect the vibration levels appreciably. A too stiff elastomer material can result in an amplification of the vibration levels in the ceiling for certain frequencies, whilst a less stiff material, in general, reduces the vibration transmission. The placement of the elastomer blocks was varied by shifting the position of the blocks while maintaining their centre-to-centre distance, resulting in a small effect on the vibration levels.

Keywords Wooden buildings • Impact sound • Vibration reduction • Elastomer materials • Finite element method

45.1 Introduction

In 1994, a century-old ban on the construction of wooden buildings more than two storeys in height in Sweden was lifted, leading to the reintroduction of such buildings. The use of wood as a construction material has many advantages. The lightweight properties of wood, for example, lower the transportation costs involved and reduce the size of the foundations needed [1]. In addition, the energy consumption during the construction and the lifecycle of wooden buildings is lower than that of concrete buildings of comparable size [2]. At the same time, however, it is more difficult to build lightweight structures of wood such that noise and disturbing vibrations in the different storeys and rooms are avoided, especially at low frequencies [3]. The vibrations can be caused by, for example, footsteps, airborne sound, vibrating machines and external sources such as railway and road traffic.

Despite newly constructed multi-storey wood buildings fulfilling the requirements for sound insulation, many of the occupants perceive the impact sound as annoying [4]. In [5], an investigation is reported where vibrational and acoustical parameters were measured and the subjective ratings of occupants were evaluated, including a total of ten lightweight buildings of different construction types. The correlation between the impact sound insulation, evaluated according to ISO 717-2:2013 [6], and the perceived annoyance of the occupants was found to be weak. The ISO standard only considers frequencies above 50 Hz; the correlation was improved considerably by extending the range to include frequencies down to 20 Hz. This emphasises the need for updated regulations as well as improved low-frequency impact sound insulation in lightweight buildings.

45.1.1 Vibration Reduction Measures

In order to reduce the vibrations transmitted throughout the buildings, different measures can be taken. In [7], different types of vibration reduction measures are discussed, for example the tuned mass damper (TMD), consisting of a mass mounted to

O. Flodén (✉) • K. Persson • G. Sandberg
Faculty of Engineering, Department of Construction Sciences, Lund University, John Ericssons väg 1, 223 63 Lund, Sweden
e-mail: ola.floden@construction.lth.se

J. Caicedo, S. Pakzad (eds.), *Dynamics of Civil Structures, Volume 2*, Conference Proceedings
of the Society for Experimental Mechanics Series, DOI 10.1007/978-3-319-15248-6_45

the vibrating structure by some elastic material acting as a spring. The TMD is tuned to have a certain natural frequency and provides an effective way of cancelling the vibrations caused by a single vibration mode. Another example is the semi-active absorber, which can change its damping properties rapidly to adjust for changes in the excitation. An even more sophisticated measure is the active control system, which drives the system through feedback loops, an effective but costly procedure due to the energy required to drive the system. Moreover, an experimental investigation is presented in [7], studying the use of viscoelastic materials as vibration isolators in the junctions of a floor-ceiling structure in steel. It was found to be an effective method for reducing the vibrations caused by modes in which the floor and the ceiling move out of phase, and it was concluded that viscoelastic materials function well for wider frequency ranges, as compared to TMDs.

Many of the newly constructed multi-storey wood buildings in Sweden are composed of timber volume elements (TVEs), such buildings being described in more detail in Sect. 45.1.2. TVE buildings are constructed by stacking volume modules which are separated by layers of viscoelastic elastomer materials. In the studies presented here, the TVE buildings will serve as example case for studying the effect of different design choices for the elastomer layers. The use of elastomer materials in junctions is common in different types of lightweight buildings.

In [8], measurements on full-scale structures were carried out in order to investigate the effect of a number of measures for reducing the impact sound in TVE buildings. Measures that were found to be effective in reducing the vibrations were, for example, an extra layer of plaster board on the floor structure and the use of a floating floor, in which mineral wool is placed between the beams and the boards of a floor structure. The use of a heavier mineral wool as insulation, or a larger cavity between floors and ceilings, were found to be less effective measures for reducing the vibrations. Elastomer layers in the junctions were also tested, leading to ambiguous results from two different measurement setups; one resulting in reduced sound pressure levels, compared to having no elastomer material in the junctions, the other in increased sound pressure levels. The majority of the tested measures were found to change the impact sound less than 2 dB when evaluated according to the ISO standards. This should be compared with the measured variance of 1.1 dB between theoretically identical constructions due to the varying quality of the workmanship.

An experimental investigation of the effect of using elastomer layers in junctions of wooden constructions is reported in [9]. A mock-up consisting of a floor structure, supported by three walls, was used to study the vibration transmission from the floor to the walls of the storey below. Marked differences in the behaviour was found for certain vibration modes when inserting elastomer materials in the junctions, as compared to a setup with the floor mounted directly on the walls. For example, the damping is larger for mode shapes where large deformations occur in the elastomer layers. It was also concluded that the step sound insulation can decrease for low frequencies (20–70 Hz), possibly due to shear resonances in the elastomer layers. This points out the need for a careful design of the elastomer layers with respect to the structure, the vibration sources and the requirements in question.

45.1.2 Timber Volume Element Buildings

The lightweight properties of wood simplify the use of prefabrication in the construction process compared to conventional concrete buildings. The TVE buildings are prefabricated multi-storey buildings, increasing in popularity in Sweden. A TVE is a module consisting of floor-, roof- and wall elements completed with, for example, electrical installations, flooring, cabinets and wardrobes. Each TVE typically constitutes a small apartment, one room or part of a larger room. Prefabricated TVEs are transported to a construction site where they are stacked to form the complete building. In Fig. 45.1, the conceptual layout of a TVE building is illustrated, and in Fig. 45.2, drawings of junctions between a floor-ceiling structure and an apartment separating wall (to the left) and a facade wall (to the right) are shown. An advantage regarding vibrations and acoustic performance is that a floor is structurally separated from the ceiling of the storey below; the upper volume contains the floor whereas the lower volume comprises the ceiling. Elastomer blocks are placed on the flanks in between the TVEs in order to reduce the vibration transmission through the junctions. The major structural connection between adjacent volumes is by means of the elastomers, the only additional connection being through a few studs and tie plates, used to position and fixate the TVEs.

45.1.3 Objective

In this paper, a numerical investigation is presented, aiming at an increased understanding of how the design of elastomer layers in junctions of multi-storey wood buildings affects the vibration transmission between storeys and rooms.

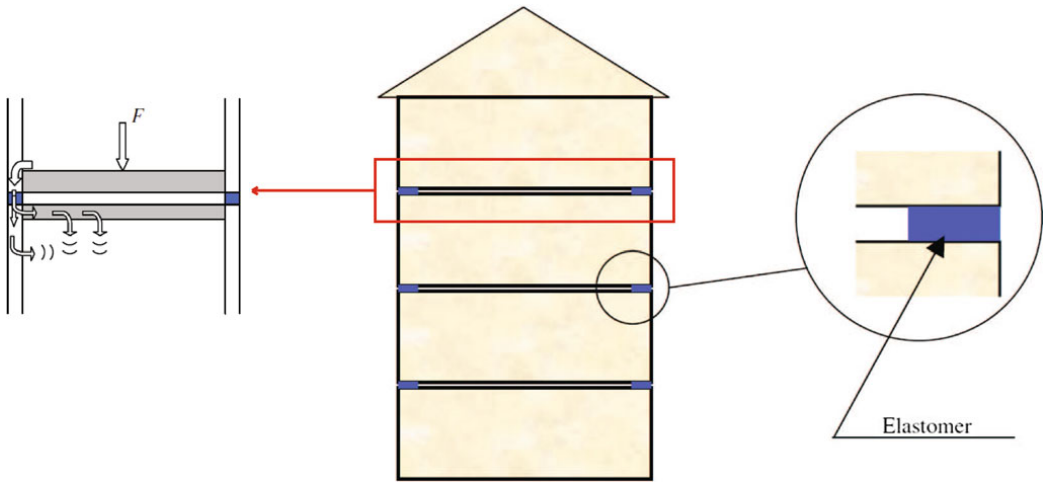

Fig. 45.1 Sketch of a TVE building [8]. The path of structural vibrations between storeys is illustrated in the figure to the *left* and an elastomer block is illustrated in the figure to the *right*

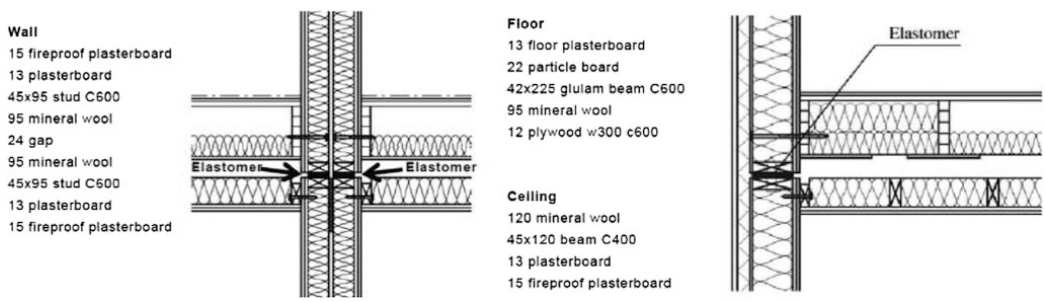

Fig. 45.2 Drawings of the TVE building system, showing sections of a floor-ceiling structure and junctions with an apartment separating wall (*left*) and a facade wall (*right*)

More specifically, parametric studies were carried out, considering different properties of the elastomer material and different placements of the elastomer blocks. The aim is to gain an understanding of the extent to which this type of design choices affect the vibration isolation. The result of the numerical investigation may then serve as input for designing experimental studies. A precise prediction of the sound insulation levels is outside the scope of the paper. The studies are limited to the low-frequency range, defined here as frequencies below 100 Hz.

In Sect. 45.2, the dynamic properties of the elastomer materials are discussed and investigated in order to provide input for the parametric studies. The numerical model employed is discussed in Sect. 45.3 and the parametric studies are presented in Sect. 45.4.

45.2 Properties of Elastomer Materials

In order to determine a realistic range for the properties of the elastomer materials, a type of elastomer often used in TVE buildings, *Sylodyn*, was studied. Sylodyn is a mixed cellular polyurethane dampening material developed by Getzner Werkstoffe GmbH, manufactured in five different types: NB, NC, ND, NE and NF. The stiffness of the materials are increasing from NB to NF, stiffer materials being used when the static loads are of higher magnitude. The elastomers are

normally exposed to static loads of such magnitude that the materials behave nonlinearly from a static point of view. The dynamic loads the buildings are exposed to are in most situations, however, of such magnitude that the nonlinear behaviour can be neglected. The dynamic response may then be regarded as a small perturbation of the static equilibrium. Linear and frequency-dependent viscoelastic material properties were determined for Sylodyn NE in [10]. The properties were calculated by finite element (FE) simulations, matching the results to experimental data found in data sheets provided by the manufacturer. The same procedure was employed here for Sylodyn NB and NF, respectively, in order to obtain the extreme values of the material parameters for the manufactured materials.

A linear viscoelastic material can be described by its bulk modulus K and shear modulus G, both being complex and frequency-dependent properties. The material is then described by four frequency-dependent parameters; $K_\mathrm{R}(f)$, $K_\mathrm{I}(f)$, $G_\mathrm{R}(f)$ and $G_\mathrm{I}(f)$, the subscripts R and I denoting the real and imaginary parts, respectively. Varying four different parameters in a parametric study is a time consuming procedure. Therefore, the possibility of using a single parameter to describe the variance in properties between the different materials was investigated. The idea was to scale the properties of Sylodyn NB to match the properties of both Sylodyn NE and NF. The following expressions were assumed for the scaling:

$$\begin{aligned} G_\mathrm{R}(x,f) &= (1+x)\, G_\mathrm{R}^\mathrm{NB}(f), \\ G_\mathrm{I}(x,f) &= \left(1+\alpha_1 x+\alpha_2 x^2\right) G_\mathrm{I}^\mathrm{NB}(f), \\ K_\mathrm{R}(x,f) &= \left(1+\alpha_3 x+\alpha_4 x^2\right) K_\mathrm{R}^\mathrm{NB}(f), \\ K_\mathrm{I}(x,f) &= \left(1+\alpha_5 x+\alpha_6 x^2\right) K_\mathrm{I}^\mathrm{NB}(f), \end{aligned} \tag{45.1}$$

where x is the scaling parameter and α_i are coefficients. The coefficients were determined by comparing the four parameters of Sylodyn NE and NF, respectively, to parameters obtained through Eq. (45.1), while adjusting the coefficients until the average difference between the spectra for each material parameter was minimised. During the minimisation process, the scaling parameters, x^NE and x^NF for Sylodyn NE and NF, respectively, were set to values obtained through normalisations of $G_\mathrm{R}(x,f)$ to $G_\mathrm{R}^\mathrm{NB}(f)$ at $f = 50\,\mathrm{Hz}$ (the mid-point of the studied frequency range) for both materials, such that

$$\begin{aligned} x^\mathrm{NE} &= \frac{G_\mathrm{R}^\mathrm{NE}(50\ \mathrm{Hz})}{G_\mathrm{R}^\mathrm{NB}(50\ \mathrm{Hz})} - 1 = 4.53, \\ x^\mathrm{NF} &= \frac{G_\mathrm{R}^\mathrm{NF}(50\ \mathrm{Hz})}{G_\mathrm{R}^\mathrm{NB}(50\ \mathrm{Hz})} - 1 = 9.63. \end{aligned} \tag{45.2}$$

The coefficients resulting from the minimisation process are given in Table 45.1. The frequency spectra for the shear modulus of Sylodyn NB, NE and NF and the scaled spectra of Sylodyn NB are shown in Fig. 45.3, and the corresponding plots for the bulk modulus are shown in Fig. 45.4. When comparing the scaled spectra to the original spectra for the material parameters of Sylodyn NE and NF, it was found that the error is below 6 % for the real parts of the bulk and shear moduli, and below 30 % for the imaginary parts. This shows that it is a relatively accurate approximation to use x as a single parameter for describing the variance in material properties between the different elastomer materials.

Moreover, the long-term bulk and shear moduli, $K_\infty = K_\mathrm{R}(0\ \mathrm{Hz})$ and $G_\infty = G_\mathrm{R}(0\ \mathrm{Hz})$, are required as input to the analyses. It was, for the scaled properties, assumed that $K_\infty = K_\mathrm{R}(x, 1\ \mathrm{Hz})$ and $G_\infty = G_\mathrm{R}(x, 1\ \mathrm{Hz})$ in the investigation of the material properties presented in Sect. 45.4.1.

Table 45.1 The values obtained for the coefficients of the scaling in Eq. (45.1)

α_1	α_2	α_3	α_4	α_5	α_6
1.57	0.005	1.14	0.011	1.80	0.019

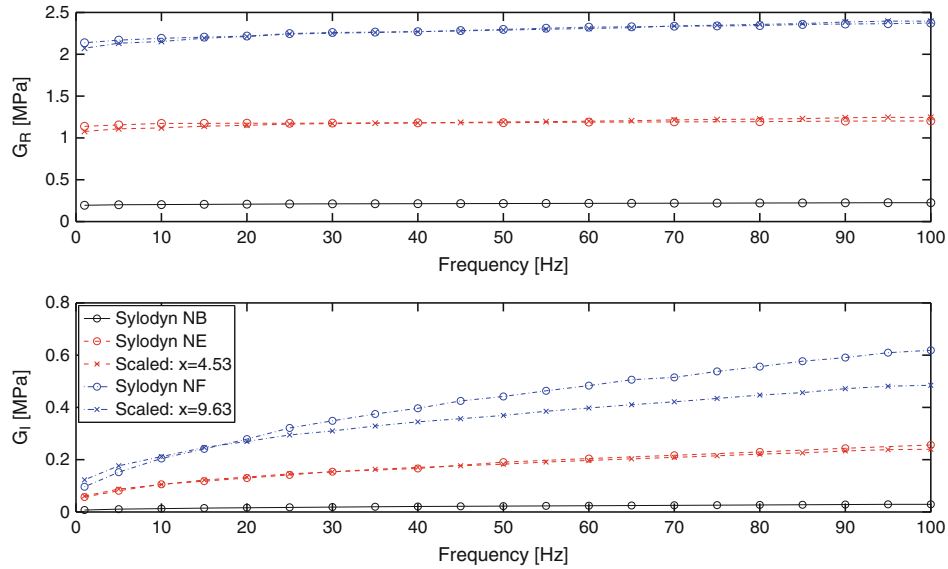

Fig. 45.3 The real and imaginary parts of the shear modulus for Sylodyn NB, NE and NF, together with the scaled spectra of Sylodyn NB. The legend is valid for both plots

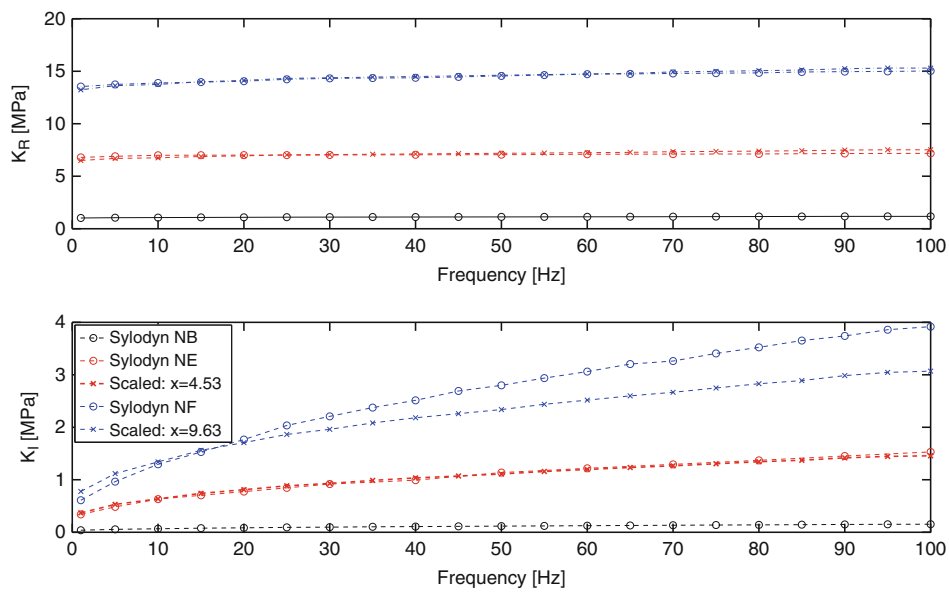

Fig. 45.4 The real and imaginary parts of the bulk modulus for Sylodyn NB, NE and NF, together with the scaled spectra of Sylodyn NB. The legend is valid for both plots

45.3 Numerical Modelling

The FE model, a quarter of it being shown in Fig. 45.5, was modelled in the commercial software Abaqus [11]. It includes two stacked TVEs, modelled according to the drawings in Fig. 45.2, separated by a number of elastomer blocks.

Each TVE is $9.0 \times 3.9 \times 3.4\,\mathrm{m}^3$ in size, the long side walls being apartment separating and the short side walls being facades. The facade walls are constructed in the same manner as the apartment separating walls, shown in Fig. 45.2, but with $95 \times 220\,\mathrm{mm}^3$ studs and a weatherboard covering the outside. The centre-to-centre distance for the beams in the floors and in the walls is 600 mm, whilst the distance is 400 mm for the beams in the ceiling. All the structural components listed in Fig. 45.2, except the mineral wools, were included in the model. All the interfaces between floors, walls and ceilings were modelled as fully fixed to each other, connecting the degrees of freedom at the interface surfaces by Lagrange multipliers. The exception is the connections between the walls and the floors, and between the walls and the ceilings, where only the beams in the floors and the ceilings were coupled to the walls; the particle and plaster boards being free at their ends.

The effect of modelling the air and the insulation in the cavity between the floor and the ceiling, in terms of acoustic media, was investigated in [12]. It was found to affect the vibration transmission appreciably, especially at low frequencies. The acoustic media is, however, neglected in the studies presented here as the objective is to investigate to which extent the structural transmission of vibrations can be affected by modifying the elastomer layers, assuming the acoustic media to have a negligible effect on the relative difference in structural transmission.

The particle board, the plaster board and the plywood were modelled as isotropic materials with properties according to Table 45.2, whereas the wood beams were modelled as orthotropic with properties according to Table 45.3. The weatherboard was assigned the same properties as the plaster board. The elastomer blocks modelled in this study were of dimensions $100 \times 95 \times 25\,\mathrm{mm}^3$ and placed along the walls between the two stacked TVEs with a centre-to-centre distance from one another of 600 mm.

The structure was meshed with 20-node solid hexahedral elements, employing quadratic interpolation and reduced integration, except for the elastomer blocks which were meshed with elements using a hybrid formulation in order to avoid volumetric locking. The mesh sizes were decided based on the wavelengths expected to occur at the highest frequency of interest, namely 100 Hz.

Due to the complexity when assessing damping in building structures, a global damping ratio of 6 % was assigned to all materials, as opposed to considering damping for each material and for the different connections, the exception being the viscoelastic properties of the elastomers. The damping ratio was determined in [13], with use of experimental data obtained from measurements in a TVE building [14], by fitting an exponential function to the transient response of a floor structure. The damping ratio was used to establish a damping matrix by means of Rayleigh damping, see e.g. [15]. The damping matrix was, hence, constructed as a linear combination of the mass and the stiffness matrices, selecting the proportionality constants to be 17.37 and $9.77 \cdot 10^{-5}$, respectively.

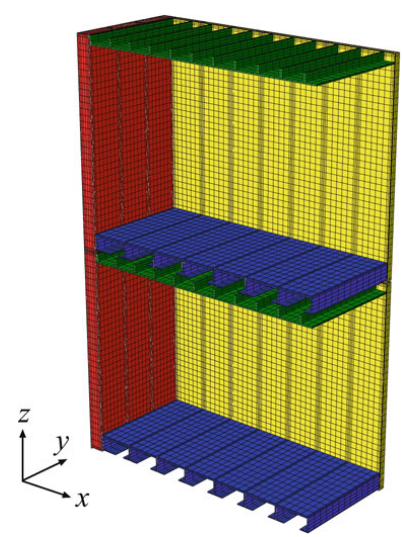

Fig. 45.5 A quarter of the FE model of two stacked TVEs. The apartment separating walls are shown in *yellow*, the facade walls in *red*, the ceiling in *green*, the floor in *blue* and the elastomer blocks in *grey*

Table 45.2 Material parameters used for the isotropic materials

Material	E (MPa)	ν (−)	ρ (kgm^{-3})
Particle board	3,000	0.3	767
Plaster board	2,000	0.2	692.3
Plywood	12,400	0.3	710

E is the Young's modulus, ν is the Poisson's ratio and ρ is the density

Table 45.3 Material parameters used for the wood beams

E_1 (MPa)	E_2	E_3	G_{12} (MPa)	G_{13}	G_{23}	ν_{12} (−)	ν_{13}	ν_{23}	ρ (kgm^{-3})
8,500	350	350	700	700	50	0.2	0.2	0.3	432

G is the shear modulus

The model was analysed in terms of steady-state frequency sweeps in order to study the vibration transmission from the floor in the upper TVE to the ceiling in the lower TVE at various frequencies. The surfaces at the four corners on the bottom of the lower TVE and on the top of the upper TVE, where elastomer blocks would be placed if further storeys were included, were modelled as clamped. A harmonic unit point load was applied in the vertical direction at the floor structure of the upper TVE, located in a point 300 mm in the x-direction (see Fig. 45.5) from the mid-point of the floor in order to be placed in the span between two beams.

The steady-state response was calculated for frequencies up to 100 Hz, the resulting acceleration amplitudes being evaluated at the surfaces of the floor in the upper TVE and the ceiling in the lower TVE. The magnitude of the complex acceleration amplitudes were calculated for the nodes at the surfaces. The accelerations were evaluated in a quarter of each surface due to conditions close to symmetry, the exception being the 300 mm shift of the position of the load. An RMS value was calculated for each frequency step in the analyses, and for each of the two surfaces, as

$$a_{\mathrm{RMS}}(f) = \sqrt{\frac{1}{n}\sum_{i=1}^{n} a_i^2(f)}, \tag{45.3}$$

where f is the frequency, a_i is the magnitude of the complex accelerations in each node and n is the number of nodes at a quarter of the floor surface or a quarter of the ceiling surface. All the RMS values presented in the paper are given in decibel with 1 μm/s^2 as reference value.

45.3.1 Model Reduction

In order to improve the computational efficiency of the FE model, substructuring [16] was applied by considering each TVE as a substructure. Both interface reduction and model order reduction were employed to establish an efficient reduced order system. The number of degrees of freedom at the interfaces between the TVEs and the elastomer blocks were reduced by employing the concept of using a condensation node [17] for each interface surface. The coupling between a condensation node and its interface surface can be realised in different ways, a number of alternatives being compared in [18] for a model of a wooden floor-ceiling structure involving an elastomer layer. It was concluded that a rigid coupling should be employed for the interface surfaces of the elastomer parts and that a uniformly distributed coupling should be employed for the interface surfaces of the wooden parts. The latter type of coupling distributes the forces acting on the condensation node uniformly to the nodes of its interface surface. The findings in [18] were employed for the interface surfaces in the model investigated here.

A number of methods for model order reduction, applied to wooden building structures, were compared in [19]. It was found that the Craig-Bampton method [20] provides reduced order models with adequate accuracy compared to other available methods, and this method was, hence, used in the present study to create reduce order models of the TVEs. The Craig-Bampton method generates reduced models containing the interface degrees of freedom of the full model together with generalised coordinates representing some of the fixed-interface eigenmodes of the model. Reduced models of the two stacked TVEs, involving different numbers of retained eigenmodes in the Craig-Bampton reduction, were investigated in order to find a reduced model with acceptable accuracy and reasonable computation time. In the comparison of the reduced models, the elastomer blocks were modelled with the viscoelastic properties determined in [10], i.e the material properties of Sylodyn NE. When employing a reduced model with 400 retained eigenmodes in each of the two TVEs, the error in RMS

values at the ceiling surface, compared to the full model, was found to be below 50 % up to 100 Hz. At the floor surface, the error in RMS values was found to be less than 20 % up to 100 Hz. These levels of error were considered acceptable, bearing in mind that the parametric studies carried out in this investigation aim at establishing the relative differences in vibrations for the different models under study, and not at a quantification of the vibration levels.

45.4 Parametric Studies

The numerical model described in Sect. 45.3 was used as a reference model for investigating the effects of varying the properties of the elastomer material and the positioning of the elastomer blocks.

45.4.1 Material Properties

The properties of the elastomer material were varied by using different values of the scaling parameter x, described in Sect. 45.2. Setting $x = 0$ and $x = 9.63$ results in the parameters for the softest and the stiffest of the investigated elastomer materials, Sylodyn NB and NF, respectively. In the parametric study, x was varied from -0.5 to 20, these values resulting in a span of G_R from half the value for Sylodyn NB to twice the value for Sylodyn NF. The material properties obtained when x is set to -0.5, 0.0, 10 and 20 are shown in Fig. 45.6. The RMS values of the acceleration amplitudes in the floor and in the ceiling, obtained for different values of x, are shown in Fig. 45.7 and Fig. 45.8, respectively. In the figures, the frequency spectra of the RMS values obtained for different values of x are plotted, as well as the mean value of the frequency spectra as function of x. Moreover, the RMS values obtained from a model with the two TVEs stacked directly on top of each other, without any elastomer layer in between, are also presented in the results.

It can be observed in Fig. 45.7 that the effect of the properties of the elastomer material, on the acceleration amplitudes in the floor, is weak. Varying the parameters of the elastomer material results in a negligible difference in RMS values; 0.01 dB when studying the mean value of the frequency spectra. Compared to having no elastomer layer in between the TVEs, the RMS values in the floor are reduced by about 1 dB for frequencies above 30 Hz.

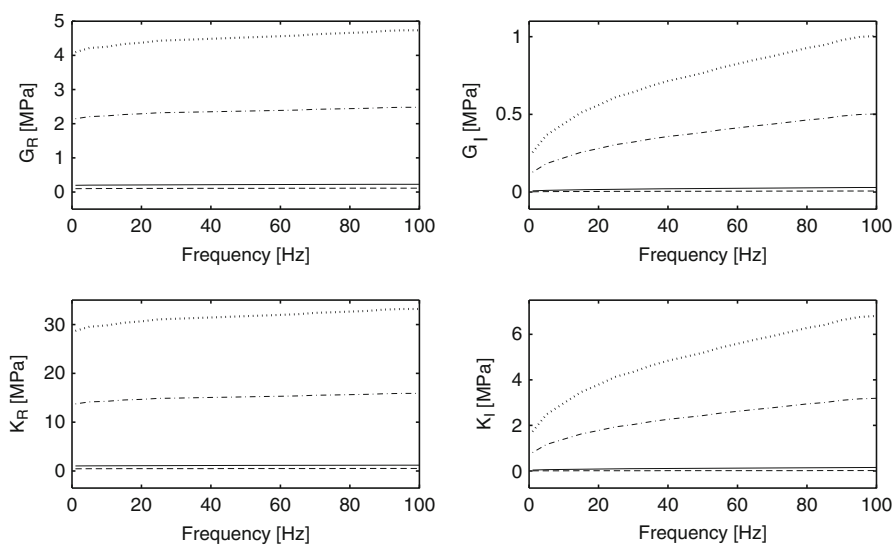

Fig. 45.6 The shear and bulk moduli obtained for $x = -0.5$ (*dashed line*), $x = 0.0$ (*solid line*), $x = 10$ (*dash-dot line*) and $x = 20$ (*dotted line*)

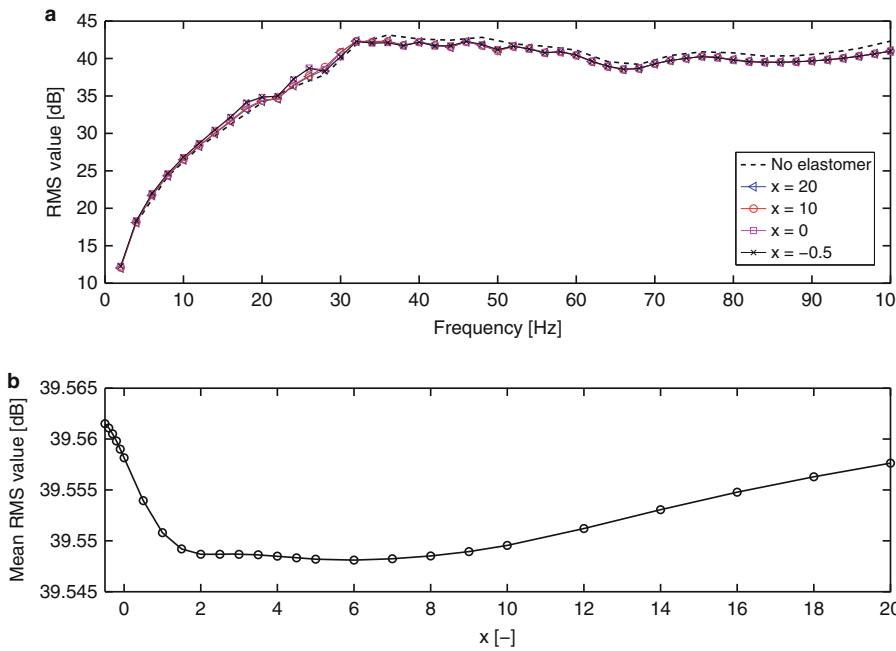

Fig. 45.7 The RMS values of the acceleration amplitudes at the floor surface presented as (**a**) function of frequency and (**b**) in terms of the mean value of each frequency spectrum, plotted versus the scaling parameter

The properties of the elastomer material have a larger effect on the RMS values in the ceiling, as can be observed in Fig. 45.7. The difference in mean value of the RMS values, when comparing the softest and the stiffest of the investigated material properties ($x = -0.5$ and $x = 20$, respectively), is about 9 dB. For frequencies below 50 Hz, there is a marked reduction in vibration levels compared to having no elastomer material in between the TVEs. Above 50 Hz, however, the use of elastomers in the junctions can lead to increasing acceleration amplitudes in the ceiling for certain frequencies. This observation is in agreement with the experimental results presented in [9]. Moreover, decreasing the stiffness of the elastomer material can lead to an amplification of the vibrations for certain, higher, frequencies and for certain degrees of stiffness of the material.

45.4.2 Placement

The placement of the elastomer blocks was varied by shifting all the blocks, except the blocks at the four corners, a certain distance along the gap between the walls of the two stacked TVEs, retaining the centre-to-centre distance of 600 mm. Three models were studied, in which the blocks were shifted 100, 200 and 300 mm, respectively. No model reduction was performed for the models compared in this study.

The RMS values of the acceleration amplitudes in the ceiling surface, obtained from the analyses of the different models, are shown in Fig. 45.9. It can be observed that the shifted placement of the elastomer blocks has a small effect on the vibration levels in the ceiling, resulting in acceleration amplitudes differing less than 0.5 dB from the reference model for all the investigated models and in the whole frequency range. This could be explained by the deformation pattern along the walls connecting to the elastomer blocks; the dominating wavelengths were larger than the centre-to-centre distance of the blocks. The effect of the placement is, therefore, low as long as the centre-to-centre distance of the blocks is retained.

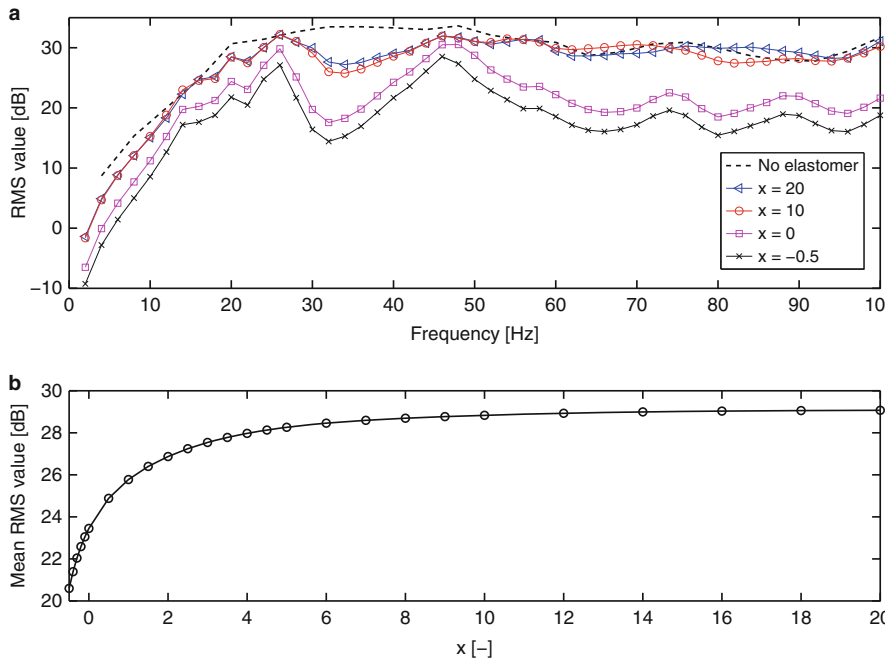

Fig. 45.8 The RMS values of the acceleration amplitudes at the ceiling surface presented as (**a**) function of frequency and (**b**) in terms of the mean value of each frequency spectrum, plotted versus the scaling parameter

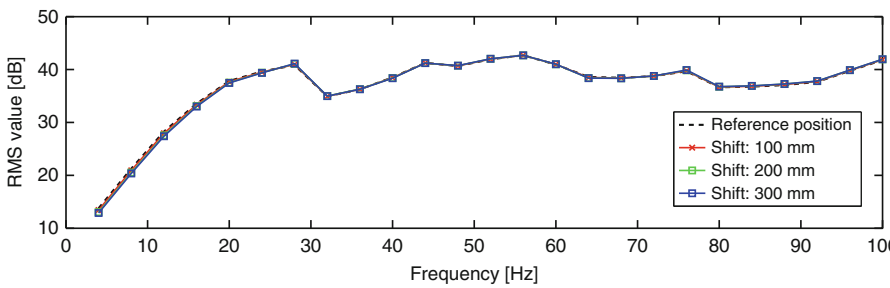

Fig. 45.9 The RMS values of the acceleration amplitudes in the ceiling for different placements of the elastomer blocks

45.5 Conclusions

The objective of the studies presented here was to investigate the extent to which the design of the elastomer layers involved in multi-storey wood buildings affects the vibration transmission between different storeys. This was carried out by performing parametric studies on numerical models of two storeys of a building, varying the material properties of the elastomer material within realistic ranges and modifying the placement of elastomer blocks, while studying the vibrations caused by a load acting on the floor of the upper storey.

The properties of the elastomer material were found to have a negligible effect on the acceleration amplitudes of the floor where the load is acting. For the transmission to the underlying ceiling, however, the properties of the elastomer material were found to affect the acceleration amplitudes appreciably. In general, softer elastomer materials result in decreased vibration

transmission to the ceiling, exceptions being found for certain frequencies. This indicates the importance of using elastomer materials which are no stiffer than what is required to withstand the static loads, in order to achieve the best possible vibration isolation in the buildings. In case a very stiff material is required, the elastomer layer can lead to an amplification of the vibration levels for some frequencies. For such situations, it could be preferable to develop other types of joints with better vibration isolation performance.

The placement of the elastomer blocks was found to have a small effect on the acceleration amplitudes both in the floor and in the ceiling, when assuming constant centre-to-centre distance between the blocks. This could be explained by the fact that the dominating wavelengths at the walls connecting to the blocks were larger than the centre-to-centre distance of the blocks. In order to affect the vibration transmission to a larger extent, through changes in the placement of the blocks, it is, hence, necessary to abandon the regular centre-to-centre distance between the blocks. The effect of adding or removing blocks at certain positions could be investigated for this purpose.

References

1. Stehn L, Rask LO, Nygren I, Östman B (2008) Byggandet av flervåningshus i trä – Erfarenheter efter tre års observation av träbyggandets utveckling. Technical Report, Luleå University of Technology, Sweden
2. Gustavsson L, Pingoud K, Sathre R (2006) Carbon dioxide balance of wood substitution: comparing concrete- and wood-framed buildings. Mitig Adapt Strateg Glob Change 11:667–691
3. Forssén J, Kropp W, Brunskog J, Ljunggren S, Bard D, Sandberg G, Ljunggren F, Ågren A, Hallström O, Dybro H, Larsson K, Tillberg K, Sjökvist LG, Östman B, Hagberg K, Bolmsvik Å, Olsson A, Ekstrand CG, Johansson M (2008) Acoustics in wooden buildings – State of the art 2008: Vinnova project 2007-01653. SP Technical Research Institute of Sweden, Report 2008:16
4. Simmons C, Hagberg K, Backman E (2011) Acoustical performance of apartment buildings – resident's survey and field measurements, AkuLite Report 2. SP Technical Research Institute of Sweden, Report 2011:58
5. Ljunggren F, Simmons S, Hagberg K (2014) Correlation between sound insulation and occupants' perception – Proposal of alternative single number rating of impact sound. Appl Acoust 85:57–68
6. ISO 717-2 (2013) Rating of sound insulation in buildings and of building elements – Part 2: impact sound insulation
7. Ljunggren F, Ågren A (2002) Development of a new damper to reduce resonant vibrations in lightweight steel joist floors. Appl Acoust 63:1267–1280
8. Ljunggren F, Ågren A (2011) Potential solutions to improved sound performance of volume based lightweight multi-storey timber buildings. Appl Acoust 72:231–240
9. Bolmsvik Å, Brandt A (2013) Damping assessment of light wooden assembly with and without damping material. Eng Struct 49:434–447
10. Negreira J (2013) Vibrations in lightweight buildings – Perception and prediction. Licentiate dissertation, Division of Engineering Acoustics, Lund University, Sweden
11. Dassault Systèmes (2012) Abaqus 6.12 documentation
12. Flodén O (2014) Vibrations in lighweight structures – Efficiency and reduction of numerical models. Licentiate dissertation, Division of Structural Mechanics, Lund University, Sweden
13. Negreira J, Bard D (2013) Finite element modelling of a Timber Volume Element based building with elastic layer insulators. SP Technical Research Institute of Sweden, Report 2013:27
14. AkuLite (2012) Mätrapport 10052. Brunnby Park, Upplands Väsby, Sweden
15. Chopra AK (2007) Dynamics of Structures. Prentice Hall, New Jersey
16. de Klerk D, Rixen DJ, Voormeeren SN (2008) General framework for dynamic substructuring: history, review and classification of techniques. AIAA J 46(5):1169–1181
17. Heirman GHK, Desmet W (2010) Interface reduction of flexible bodies for efficient modeling of body flexibility in multibody dynamics. Multibody Syst Dyn 24(2):219–234
18. Flodén O, Persson K, Sandberg G (2014) Coupling elements for substructure modelling of lightweight multi-storey buildings. In: Dynamics of Coupled Structures, vol 1, pp 113–124. Springer, New York
19. Flodén O, Persson K, Sandberg G (2014) Reduction methods for the dynamic analysis of substructure models of lightweight building structures. Comput Struct 138:49–61
20. Craig RR, Bampton M (1968) Coupling of substructures in dynamic analysis. AIAA J 6:1313–1319

Paper B

Engineering Structures 83 (2015) 7–16

Contents lists available at ScienceDirect

Engineering Structures

journal homepage: www.elsevier.com/locate/engstruct

The effect of modelling acoustic media in cavities of lightweight buildings on the transmission of structural vibrations

O. Flodén *, J. Negreira, K. Persson, G. Sandberg

Department of Construction Sciences, Lund University, P.O. Box 118, SE-22100 Lund, Sweden

ARTICLE INFO

Article history:
Received 20 February 2014
Revised 14 July 2014
Accepted 20 October 2014
Available online 21 November 2014

Keywords:
Structure–acoustic interaction
Porous materials
Vibration transmission
Lightweight buildings
Finite element method

ABSTRACT

Determining the dynamic behaviour of lightweight buildings by means of finite element analyses requires models representing the geometry involved in great detail, resulting in systems having many millions of degrees of freedom. It is, therefore, important to avoid unnecessarily detailed models by carefully considering what is essential to include in the models and the level of details required for describing the phenomena of interest accurately. In the study presented here, it was investigated whether or not air and insulation in cavities of multi-storey wood buildings affect the transmission of low-frequency structural vibrations. It was concluded, by means of numerical studies, that including air and insulation in cavities, modelled as acoustic media, affects the transmission from a floor to the underlying ceiling and surrounding walls.

1. Introduction

In 1994, a century-old ban on the construction of wooden buildings more than two storeys in height in Sweden was lifted, leading to the reintroduction of such structures. Compared to heavier structures, the lightweight buildings are more sensitive to vibrations, making it difficult to construct multi-storey wood buildings in such a way that noise and disturbing vibrations in the different storeys and rooms are avoided. Specifically problematic is the issue of low-frequency vibrations [1]. Wooden constructions involving long spans have low resonance frequencies that, in combination with low damping, are easily excited by loads with low-frequency content. The vibrations can be caused by, for example, footsteps, airborne sound, vibrating machines and external sources such as railway and road traffic. To design buildings of adequate performance regarding sound and vibrations, it is desirable to have tools for predicting the effects of structural modifications prior to construction. Testing prototypes and performing experiments are both time-consuming and expensive, the long-term aim therefore being to develop prediction tools that are valid for general load-cases by making use of finite element (FE) models.

Accurately assessing the dynamic behaviour of multi-storey lightweight buildings, even at lower frequencies, requires FE models representing the geometry in considerable detail, resulting in the models being very large. The number of degrees of freedom of such models easily exceeds the limits of computer capacity, at least for computations to be performed within reasonable time. It is, therefore, important to avoid unnecessarily detailed models by carefully considering what is essential to include in the models and the level of details required for describing the phenomena of interest accurately. The issue considered here is whether or not air and insulation in cavities of multi-storey wood buildings affect the transmission of structural vibrations.

The acoustic pressure field in a room can interact with the vibrations in the floor, ceiling and walls. For heavier structures, the acoustic pressure waves usually have a negligible effect on the structural vibrations. It is, therefore, possible to analyse the acoustic pressure field by applying the structural displacements, obtained from a precedent analysis of the structural domain, as boundary conditions. Moreover, the effect of the acoustic media in a structure, on the transmission of structural vibrations, depends on the flexibility of the structure, a more flexible structure tending to interact more with the acoustic media. It was concluded in [2] that the acoustic pressure field in the rooms is negligible also for lightweight buildings; studies on a 2D FE model of a two-storey wood building showing that the effect of including air in the rooms, on the displacements of the building, is small for frequencies below 250 Hz. The air was modelled to have a realistic acoustic damping, which is present in buildings due to objects and porous materials such as curtains and carpets.

In multi-storey wood buildings, there are acoustic media not only in the rooms, but also in the many cavities containing both air and insulation. The effect of modelling air in cavities of lightweight

* Corresponding author.
E-mail address: ola.floden@construction.lth.se (O. Flodén).

http://dx.doi.org/10.1016/j.engstruct.2014.10.037
0141-0296/

double-plate wall panels was investigated in [3,4]. In [3], the vibration transmission was investigated for a model including two double-plate wall panels connected in an L-shape, with and without air in the cavities. Both eigenvalue and steady-state analyses showed that the inclusion of air in the cavities of the structure has a large effect on its dynamic characteristics at high frequencies and a noticeable effect already at the first eigenfrequency. In [4], the response of a double-plate wall panel, with and without air in the cavities, exposed to diffuse field excitation was investigated. Simulations in terms of eigenvalue and steady-state analyses showed that the air has a negligible effect on the dynamic characteristics of the structure, contradicting the results in [3].

The studies presented here aim at determining whether or not air and insulation in cavities have to be considered when performing numerical analyses of the low-frequency vibration transmission in multi-storey lightweight buildings. The low-frequency range is defined here as frequencies below 200 Hz. As a first step, different porous material models for modelling of the insulation were compared, a frame of a double-plate wall panel being employed as a test model. Subsequently, numerical studies were carried out for a section of a multi-storey wood building constructed with timber volume elements (TVEs), such buildings being described in Section 1.1. The response of a floor, exposed to a harmonic point load, and the vibration transmission from the floor to the underlying ceiling and the surrounding walls were investigated, comparing FE models including air and insulation as acoustic media in cavities to models without acoustic media.

The models employed in the numerical studies are representative for a wide range of residential wood buildings of the type studied here, in terms of both dimensions and material properties. It is, therefore, believed that the conclusions presented in the paper are valid for such structures. Moreover, a wide range of frequencies are considered, resulting in the same phenomena being captured also for models having slightly different dimensions, as the shift in eigenfrequencies in such cases is small compared to the width of the frequency range.

1.1. Timber volume element buildings

The conceptual layout of a TVE building is illustrated in Fig. 1. A TVE is a prefabricated volume module consisting of wood framed floor-, roof- and wall-elements, each TVE typically constituting a small apartment, one room or part of a larger room. As much of the construction work as possible is performed indoors at a factory, including electrical installations, flooring, cabinets, wardrobes etc. The prefabricated modules are transported to the construction site where they are stacked to form a complete building. In between the TVEs, several elastomer blocks are introduced to reduce the flanking transmission of vibrations. Each elastomer block has an interface area of approximately 0.1×0.1 m^2 and is placed between the walls of two stacked modules. The only additional connection between modules is through a number of tie plates, ensuring the global stability of the building. Vibrations transmitted in TVE buildings are, therefore, mainly passing through the elastomer layers or through the air and the insulation in the cavities of the buildings. The FE models employed in the numerical studies presented here were constructed according to the drawings shown in Fig. 2.

2. Governing theory

2.1. Structure–acoustic analysis

Structure–acoustic systems can be analysed by deriving FE formulations for both the structural domain and the acoustic fluid domain. By imposing continuity conditions for displacements and pressures at domain-separating boundaries, the domains form a coupled FE equation system. Vibrations in lightweight buildings are usually of such amplitudes that any non-linear behaviour can be neglected and, therefore, linear behaviour is assumed here for both domains. In the following derivations, a subscript S denotes a quantity in the structural domain, whereas a subscript F indicates a quantity in the acoustic fluid domain.

2.1.1. Structural domain

The equations describing the structural domain follow the notation in [6]. For a detailed derivation of the FE formulation of a solid, see e.g. [6,7]. The differential equation of motion for the continuum formulation of a three-dimensional solid, occupying the domain Ω_S, is given by

$$\tilde{\mathbf{V}}^T\boldsymbol{\sigma}_S + \mathbf{b}_S = \rho_S \frac{\partial^2 \mathbf{u}_S}{\partial t^2}, \tag{1}$$

where $\boldsymbol{\sigma}_S$ is the matrix representation of the stress tensor, $\mathbf{b}_S$ is the body force vector, ρ_S is the mass density, $\mathbf{u}_S$ is the displacement vector, $\tilde{\mathbf{V}}$ is a differential operator matrix and t is the time [8]. A FE discretisation and use of Galerkin's method results in a FE formulation in the structural domain, given by

$$\mathbf{M}_S\ddot{\mathbf{a}}_S + \mathbf{K}_S\mathbf{a}_S = \mathbf{f}_{l,S} + \mathbf{f}_{b,S}, \tag{2}$$

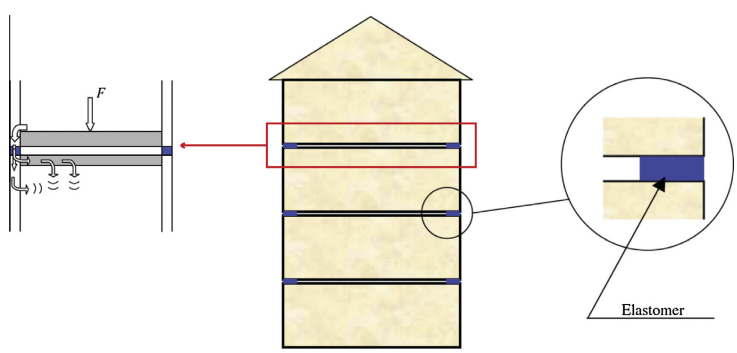

Fig. 1. Sketch of a TVE building [5]. The path of structural vibrations between storeys is illustrated in the figure to the left and an elastomer block is illustrated in the figure to the right.

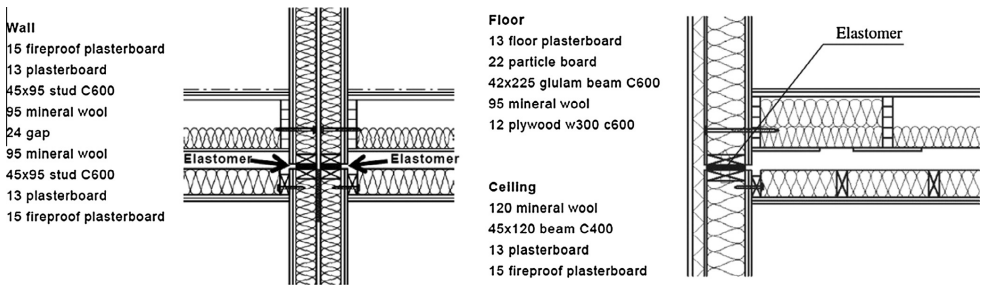

Fig. 2. Drawings of the TVE building system, showing sections of the floor and ceiling structures and the junctions with apartment separating wall (left) and façade wall (right).

$$\mathbf{M}_S = \int_{\Omega_S} \mathbf{N}_S^T \rho_S \mathbf{N}_S \, \mathrm{d}V, \quad \mathbf{K}_S = \int_{\Omega_S} (\widetilde{\nabla}\mathbf{N}_S)^T \mathbf{D}_S \widetilde{\nabla}\mathbf{N}_S \, \mathrm{d}V,$$
$$\mathbf{f}_{l,S} = \int_{\Omega_S} \mathbf{N}_S^T \mathbf{b}_S \, \mathrm{d}V, \qquad \mathbf{f}_{b,S} = \int_{\partial\Omega_S} \mathbf{N}_S^T \mathbf{t}_S \, \mathrm{d}S. \tag{3}$$

where $\mathbf{M}_S$ is the mass matrix, $\mathbf{K}_S$ is the stiffness matrix, $\mathbf{a}_S$ is the nodal displacement vector, $\mathbf{f}_{l,S}$ is the body load vector, $\mathbf{f}_{b,S}$ is the boundary load vector, $\mathbf{N}_S$ contains the FE interpolation functions, $\mathbf{D}_S$ is the constitutive stress-strain matrix and $\mathbf{t}_S$ is the surface traction vector. Normally, a term $\mathbf{C}_S\dot{\mathbf{a}}_S$, where $\mathbf{C}_S$ is the damping matrix, is added to the left-hand side of Eq. (2) to account for viscous forces present in the structure.

2.1.2. Acoustic fluid domain

In addition to the assumption of small displacements, the governing equations of the acoustic fluid are derived supposing the fluid to be irrotational. The motion of an acoustic fluid can be described using different primary variables, such as the fluid displacement or a fluid displacement potential. In the FE formulation presented here, the acoustic pressure is used as primary variable. A detailed description of the FE formulation of an acoustic fluid, and the structure-acoustic coupling, can be found in [9], for example. The motion of the fluid in the acoustic fluid domain Ω_F is governed by the equation of motion and the continuity equation

$$\rho_0 \frac{\partial^2 \mathbf{u}_F}{\partial t^2} + R\frac{\partial \mathbf{u}_F}{\partial t} + \nabla p_F = 0, \tag{4}$$

$$\frac{\partial p_F}{\partial t} + \rho_0 c_0^2 \nabla \cdot \frac{\partial \mathbf{u}_F}{\partial t} = 0, \tag{5}$$

where p_F is the acoustic pressure, ρ_0 is the static density, R is the flow resistivity, c_0 is the speed of sound and ∇ is the gradient operator. By differentiating Eq. (5) with respect to time and inserting Eq. (4), the wave equation in the acoustic fluid domain is obtained as

$$\frac{1}{c_0^2}\frac{\partial^2 p_F}{\partial t^2} + \frac{R}{\rho_0 c_0^2}\frac{\partial p_F}{\partial t} - \nabla^2 p_F = 0. \tag{6}$$

An FE discretisation and use of Galerkin's method results in an FE formulation in the acoustic fluid domain, given by

$$\mathbf{M}_F \ddot{\mathbf{p}}_F + \mathbf{C}_F \dot{\mathbf{p}}_F + \mathbf{K}_F \mathbf{p}_F = \mathbf{f}_{b,F}, \tag{7}$$

$$\mathbf{M}_F = \tfrac{1}{c_0^2}\int_{\Omega_F} \mathbf{N}_F^T \mathbf{N}_F \, \mathrm{d}V, \qquad \mathbf{C}_F = \tfrac{R}{\rho_0 c_0^2}\int_{\Omega_F} \mathbf{N}_F^T \mathbf{N}_F \, \mathrm{d}V,$$
$$\mathbf{K}_F = \int_{\Omega_F} (\nabla \mathbf{N}_F)^T \nabla \mathbf{N}_F \, \mathrm{d}V, \quad \mathbf{f}_{b,F} = \int_{\partial\Omega_F} \mathbf{N}_F^T \mathbf{n}_F^T \nabla p_F \, \mathrm{d}S, \tag{8}$$

where $\mathbf{p}_F$ is the nodal pressure vector, $\mathbf{f}_{b,F}$ is the boundary load vector and $\mathbf{n}_F^T$ is the boundary normal vector, pointing outwards from the acoustic fluid domain.

2.1.3. Coupling of domains

At interfaces connecting a structural domain to an acoustic fluid domain, denoted $\partial\Omega_{SF}$, there will naturally be a continuity in terms of both displacements and pressures. By imposing conditions of continuity as boundary conditions at the interfaces, the two equation systems describing the separate domains are coupled into a single system, including the interaction of the domains. The continuity in displacements and pressures at $\partial\Omega_{SF}$ can be expressed as

$$\mathbf{u}_S \mathbf{n}_F = \mathbf{u}_F \mathbf{n}_F, \tag{9}$$

$$\boldsymbol{\sigma}_S|_{n_F} = -p_F, \tag{10}$$

where $\boldsymbol{\sigma}_S|_{n_F}$ is the stress normal to $\partial\Omega_{SF}$. By introducing the spatial coupling matrix

$$\mathbf{H}_{SF} = \int_{\partial\Omega_{SF}} \mathbf{N}_S^T \mathbf{n}_F \mathbf{N}_F \, \mathrm{d}S, \tag{11}$$

the boundary load vectors at $\partial\Omega_{SF}$ can be rewritten as

$$\mathbf{f}_{b,S} = \mathbf{H}_{SF}\mathbf{p}_F, \tag{12}$$

$$\mathbf{f}_{b,F} = -\rho_0 \mathbf{H}_{SF}^T \ddot{\mathbf{a}}_S - R\mathbf{H}_{SF}^T \dot{\mathbf{a}}_S. \tag{13}$$

Using Eqs. (12) and (13) in combination with Eqs. (2) and (7) results in the structure-acoustic system of equations

$$\begin{bmatrix} \mathbf{M}_S & \mathbf{0} \\ \rho_0 \mathbf{H}_{SF}^T & \mathbf{M}_F \end{bmatrix} \begin{bmatrix} \ddot{\mathbf{a}}_S \\ \ddot{\mathbf{p}}_F \end{bmatrix} + \begin{bmatrix} \mathbf{C}_S & \mathbf{0} \\ R\mathbf{H}_{SF}^T & \mathbf{C}_F \end{bmatrix} \begin{bmatrix} \dot{\mathbf{a}}_S \\ \dot{\mathbf{p}}_F \end{bmatrix} + \begin{bmatrix} \mathbf{K}_S & -\mathbf{H}_{SF} \\ \mathbf{0} & \mathbf{K}_F \end{bmatrix} \begin{bmatrix} \mathbf{a}_S \\ \mathbf{p}_F \end{bmatrix} = \begin{bmatrix} \mathbf{f}_{l,S} \\ \mathbf{0} \end{bmatrix} + \begin{bmatrix} \mathbf{f}_{b,S} \\ \mathbf{f}_{b,F} \end{bmatrix}, \tag{14}$$

where $\mathbf{f}_{b,S}$ and $\mathbf{f}_{b,F}$ contain contributions from the parts of the domain boundaries $\partial\Omega_S$ and $\partial\Omega_F$, respectively, that are separated from the interface boundary $\partial\Omega_{SF}$.

2.2. Porous material models

The use of different types of mineral wool in facades and interior walls of lightweight buildings is common in order to improve both thermal and acoustic insulation. The interaction between air and fibres of the wool affects the propagation of pressure waves in the air, the porous structure forcing the waves to travel a longer distance and a dampening effect occurring due to friction at the surface of the fibres. Moreover, the pressure waves in the air interact with any potential motion of the fibres. Different approaches for modelling porous materials have been proposed in the literature, some being based on empirical studies, suggesting prediction formulae of acoustic properties based on parameter fitting to experimental data. Others are analytical and based on certain assumptions regarding the geometry and behaviour of the structural frame and the interaction with the air.

This section presents three porous material models, two of them empirical and one analytical, as well as brief literature reviews concerning other models within the two categories. The three models presented here consider the porous materials as equivalent acoustic fluids. They can, therefore, be analysed with the numerical methods employed for acoustic fluids and are integrated in a structure-acoustic model in a straightforward manner by modifying the, possibly complex, coefficients in Eq. (5).

In Eqs. (4) and (5), two material parameters describing an acoustic fluid were introduced, namely the speed of sound c_0 and the static density ρ_0. A common, alternative, way of describing an acoustic fluid is by its static density together with the bulk modulus K_0, related to the speed of sound according to

$$K_0 = \rho_0 c_0^2. \tag{15}$$

Another pair of material parameters that are frequently employed to describe an acoustic fluid are the characteristic impedance Z_0 and the wavenumber k_0. The two latter alternatives of material parameters are related according to

$$Z_0 = \sqrt{\rho_0 K_0}, \tag{16}$$

$$k_0 = \omega\sqrt{\frac{\rho_0}{K_0}}, \tag{17}$$

where ω is the angular frequency.

2.2.1. Empirical models

2.2.1.1. Delany–Bazley. Empirical models relating the real and imaginary parts of the complex characteristic impedance Z and the complex wavenumber k to the quotient (f/R), where f is frequency, were developed in [10]. Measurements of the characteristic impedance, the wavenumber and the flow resistivity were carried out for a range of mineral wools and the following power law relations were obtained by fitting the coefficients to experimental data:

$$Z = Z_0\left(1 + \alpha_1(f/R)^{-\beta_1} - i\ \alpha_2(f/R)^{-\beta_2}\right), \tag{18}$$

$$k = k_0\left(1 + \alpha_3(f/R)^{-\beta_3} - i\ \alpha_4(f/R)^{-\beta_4}\right), \tag{19}$$

where the coefficients are given in Table 1. Data in the range $0.01 \leqslant f/R \leqslant 1.0$ ($\mathrm{N^{-1}\,m^4\,s^{-2}}$) were used and it is advised not to extrapolate the power law relations outside this range.

2.2.1.2. Miki. The real part of the surface impedance when calculated according to the Delany–Bazley formulae sometimes becomes negative at low frequencies. To avoid this unphysical phenomenon, new power law relations were developed in [11], making use of the experimental data utilised in [10] and imposing constraints for the real part of the characteristic impedance to be positive, resulting in empirical formulae of the form in Eqs. (18) and (19) with the coefficients given in Table 2.

These empirical formulae are physically realisable at lower frequencies compared to the formulae by Delany and Bazley. Unphysical properties will, however, occur also in this case, the real part of the density becoming negative at low frequencies. As the power law relations were fitted to the experimental data used in [10], no conclusions can be made regarding the validity of the model outside the range $0.01 \leqslant f/R \leqslant 1.0$ ($\mathrm{N^{-1}\,m^4\,s^{-2}}$).

Table 1
Coefficients for the Delany–Bazley model.

α_1	α_2	α_3	α_4	β_1	β_2	β_3	β_4
0.0511	0.0768	0.0858	0.175	0.750	0.730	0.700	0.590

Table 2
Coefficients for the Miki model.

α_1	α_2	α_3	α_4	β_1	β_2	β_3	β_4
0.0699	0.107	0.109	0.160	0.632	0.632	0.618	0.618

2.2.1.3. Other empirical models. In addition to the formulae by Delany & Bazley and Miki, a number of empirical relations for Z and k have been suggested in the literature. The same procedure as in [10] was applied to measurement data for foam materials in [12]. In [13], measurements were performed for a wide range of glass and rock wools, concluding that prediction formulae involving logarithmic terms resulted in better correlation to the measurement data in comparison with power law relations developed in the same manner as in [10]. In [14,15], porous material models combining the empirical formulae by Delany and Bazley with analytical microstructure models, assuming parallel fibres, were presented, resulting in physically meaningful predictions also at lower frequencies.

2.2.2. Analytical models

Already in 1868, a theory for sound propagation in cylindrical tubes, including both viscous and thermal effects, was presented in [16], a simplified model later being presented in [17]. Porous materials generally have complex geometries, making it practically impossible to analyse the exact microstructure. This is why most porous material models are phenomenological, an approach being valid in case the wave lengths are much larger than the characteristic dimensions of the microstructure. Several analytical models for porous materials, involving different assumptions regarding the geometry and behaviour of the structural frame as well as the interaction between the frame and the acoustic fluid, have been proposed.

2.2.2.1. Equivalent acoustic fluid model – rigid structural frame. Phenomenological equivalent acoustic fluid models assuming the structural frame to be rigid have been presented in [17,18]. These models involve two properties of the structural frame, namely the porosity ϕ and the structure factor K_S, also known as the tortuosity. ϕ is the ratio of fluid volume to total volume, while K_S is defined as $\rho_e = K_S\rho_0$, relating the density of the acoustic fluid in the pores to an effective density ρ_e of the equivalent acoustic fluid. With a rigid structural frame, the equation of motion and the continuity equation in Eqs. (4) and (5), respectively, become

$$K_S\rho_0\frac{\partial^2 u_F}{\partial t^2} + R\frac{\partial u_F}{\partial t} + \nabla p_F = 0, \tag{20}$$

$$\phi\frac{\partial p_F}{\partial t} + \rho_0 c_0^2 \nabla\cdot\frac{\partial u_F}{\partial t} = 0. \tag{21}$$

By differentiating Eq. (21) with respect to time and inserting Eq. (20), the wave equation for the equivalent acoustic fluid is obtained as

$$\frac{K_S\phi}{c_0^2}\frac{\partial^2 p_F}{\partial t^2} + \frac{R\phi}{\rho_0 c_0^2}\frac{\partial p_F}{\partial t} - \nabla^2 p_F = 0, \tag{22}$$

which is similar to the wave equation for an acoustic fluid given in Eq. (6), the coefficients being modified by the properties of the structural frame. In Eq. (6), R accounts for the dissipation of energy in an acoustic fluid domain in a smeared approach while it is a property of the structural frame in Eq. (22).

2.2.2.2. Other analytical models. Most of the porous material models available in the literature assume the structural frame to be rigid, a thorough review of such models developed before and after 1980 being found in [19,20], respectively. A model assuming the structural frame to be limp is presented in [21]. In [22], a model assuming a rigid frame and one assuming a limp frame were compared to measurements, studying the high and low frequency limits of the resulting effective densities. Biot's theory [23] includes the flexibility of the structural frame at the cost of introducing displacement degrees of freedom, the porous material no longer being modelled as an equivalent acoustic fluid. The theory combines an elastic continuum formulation for the structural frame with the theory for sound propagation in a rigid structural frame by considering a coupling of the stress-strain relationships and the inertial and viscous forces.

3. Numerical studies

In the numerical studies presented here, the effect of modelling the air and the insulation in cavities of TVE buildings on the vibration transmission was investigated. First, a comparative study was carried out for the three porous material models introduced in Section 2.2, a section of a wooden double-plate wall panel being employed as test model. Furthermore, the vibrations induced by a load acting on a floor structure in a TVE-based building were analysed, comparing models including acoustic media in different ways. All models were created in the commercial FE software *Abaqus* [24].

Point loads were used as excitations in all the models, as the transmission of low-frequency vibrations in residential buildings mainly originate from structural excitations and not the acoustic pressure fields in the rooms, these being more dominant at higher frequencies. Structural loads, for example footsteps or rotating machines, are often distributed over small surfaces compared to the wavelengths of the structural vibrations, a point load therefore providing a good approximation.

In the models including air as an acoustic medium, it is assumed to be non-absorbing, i.e. the flow resistivity is zero ($R = 0$ in Eq. (4)). Hence, the energy dissipation in the acoustic media only takes place in the insulation.

The result plots presented below show the root mean square (RMS) values of the acceleration amplitudes, as a function of frequency, for a certain set of FE nodes. The RMS values are presented in decibel (dB) with 1 μm s^{-2} as reference value.

3.1. Comparative study – porous material models

The empirical models by Delany & Bazley and Miki as well as the equivalent acoustic fluid model with rigid structural frame were compared for a FE model of a section in a wooden double-plate wall panel, shown in Fig. 3. The three methods were compared in order to study if the selection of method affects the vibration transmission over cavities of lightweight buildings. The methods are fairly simple, but the objective here is not to create an accurate and validated model of the acoustic media, but rather to investigate whether it has to be considered in the models. If so, the models of the buildings, including acoustic media in the cavities, will have to be validated to measurement data, possibly resulting in the need for a more sophisticated porous material model.

The wall panel consisted of a $2500 \times 650 \times 120$ mm^3 wood frame covered with gypsum plates on both sides, creating a low-stiffness model with a cavity between the plates. The cavity was modelled in five different ways: (1) with no acoustic media, (2) filled with air and (3–5) filled with insulation, employing the three different porous material models. The coefficients in Eqs. (18) and (19) for the Delany & Bazley and Miki models are slightly modified in the implementation of the models in Abaqus, employed in the numerical calculations presented here. The coefficients used in Abaqus are shown in Table 3.

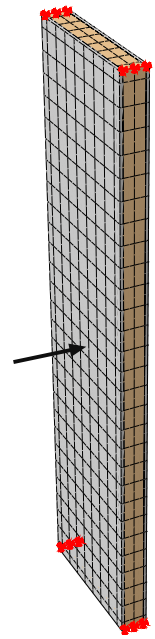

Fig. 3. FE model of a section in a wood-framed wall panel, employed for comparing different porous material models. The arrow illustrates the applied load.

Measured values for the porous material properties of glass- and mineral wools can be found in, for example, [13,25–28]. The measured values fall within the ranges $0.95 \leqslant \theta \leqslant 0.99, 1.01 \leqslant \alpha \leqslant 1.08$ and $6000 \leqslant R \leqslant 90,000$. The properties used in the comparative study are presented in Table 4. A relatively low value for the flow resistivity is selected in order for the empirical models to be physically valid in a major part of the frequency range of interest. Consequently, the energy dissipation in the insulation is relatively low compared to most glass- and mineral wools. For the selected flow resistivity, the models by Delany & Bazley and Miki are feasible for analysis above 70 Hz and 40 Hz respectively. Below those frequencies, unphysical values of the complex bulk modulus and complex density for the Delany & Bazley and Miki models, respectively, are obtained.

Steady-state analyses were performed up to 200 Hz, locking the displacements at the four corners of the panel. The wall panel was excited by a harmonic unit point load in the middle of one of the gypsum plates, the source plate, and the accelerations were evaluated at the opposite side of the other plate, the receiver plate. The acceleration amplitudes were evaluated in terms of an RMS value of the magnitude in all nodes of the receiver plate's outer surface, given by

$$a_{\mathrm{RMS}}(f) = \sqrt{\frac{1}{n}\sum_{i=1}^{n} a_i^2(f)}, \tag{23}$$

where a_i is the magnitude of the complex acceleration in node i and n is the number of nodes in the outer surface of the receiver plate.

Table 3
Coefficients used in Abaqus for the Delany & Bazley and Miki models.

	α_1	α_2	α_3	α_4	β_1	β_2	β_3	β_4
Delany–Bazley	0.0571	0.0870	0.0978	0.189	0.754	0.732	0.700	0.595
Miki	0.0786	0.121	0.123	0.179	0.632	0.632	0.618	0.618

Table 4
The porous material properties employed in the comparative study.

R (Nm^{-4} s)	ϕ (−)	α (−)
6000	0.96	1.1

An RMS value was calculated for each excitation frequency in the steady-state analysis.

In Fig. 4, the acceleration amplitudes for the different models of the wall cavity, in the frequency range 20–200 Hz, are shown. For frequencies below the first resonance frequency, located at 30 Hz, the acoustic media has a negligible effect on the acceleration amplitudes, whereas for frequencies in the range 30–90 Hz, there is a small effect of including air in the cavity. Including a porous material, however, lowers the acceleration amplitudes due to its viscous effects. Above 90 Hz, it is evident that a large part of the energy is transmitted through the acoustic media, since its inclusion increases the acceleration amplitudes significantly. Generally, using the porous material models results in lower acceleration amplitudes compared to the model with only air in the cavity. In their valid frequency ranges, the different methods for modelling the porous material yield very similar results. It is, hence, sufficient to include only one of the three models in the subsequent analyses and the model with rigid structural frame was selected due to the unphysical behaviour of the empirical models at lower frequencies.

3.2. Acoustic media in cavities of TVE buildings

A section of a TVE-based building was analysed in order to investigate the effect of modelling air and insulation, as acoustic media, in the cavities on the vibrations caused by a harmonic point load acting on a floor structure. Specifically, the response of the floor, as well as the transmission to the underlying ceiling and surrounding walls, was investigated for a model containing two stacked TVEs, a quarter of the model being shown in Fig. 5. Each TVE was 9000 x 3900 x 3400 mm^3 large (the long side walls being apartment separating and the short side walls being facades) and modelled according to the drawings in Fig. 2. Moreover, the walls of the neighbouring TVEs were included at the apartment separating walls, meaning that the cavities in those walls were included in the model as well. No structural connection to the walls of the neighbouring TVEs was, however, included.

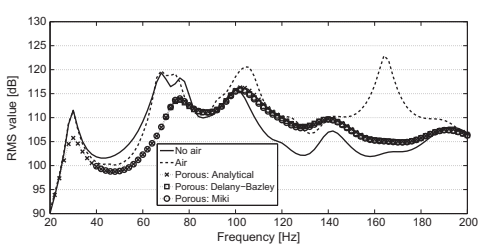

Fig. 4. RMS values of the acceleration amplitudes at the receiver plate of the wall panel model employed for comparing different porous material models.

The materials of the structural components are listed in Fig. 2; the particle board, plaster board and plywood being modelled as isotropic materials with properties according to Table 5, whereas the wood beams were modelled as orthotropic materials with properties according to Table 6. A type of elastomer often used in TVE buildings is Sylodyn, a mixed cellular polyurethane dampening material developed by Getzner Werkstoffe GmbH. The blocks modelled in this study were $100 \times 95 \times 25$ mm^3 large, of type Sylodyn NE, and placed along the walls between the two stacked TVEs with a centre-to-centre distance from one another of 600 mm. Frequency-dependent viscoelastic material properties for the elastomers were determined in [29] by performing laboratory testing and FE simulations to match experimental data. The porous material properties used for modelling the insulation were selected according to Table 7. The analytical porous material model assuming a rigid structural frame was employed for the insulation. In contrast to the comparative study in Section 3.1, a higher flow resistivity was used here, namely 40,000 Nm^{-4} s. The selected value falls within the mid-range of values for glass- and mineral wools found in the literature ($6000 \leqslant R \leqslant 90,000$). Hence, the damping in the porous material is higher compared to the FE model employed in the comparative study presented in Section 3.1. As the objective here is not to study a specific porous material, but rather to investigate whether this type of materials need to be considered in the models, it is sufficient to employ parameters that are realistic compared to the measured values found in the literature.

The structural parts were meshed with 20-node solid hexahedral elements, employing quadratic interpolation and reduced integration. For the elastomer blocks, elements with a hybrid formulation were used in order to avoid locking. The air and the insulation, in turn, were meshed with 20-node acoustic hexahedral elements, employing quadratic interpolation. The mesh sizes both for the structural and the acoustic parts were decided based on the wavelengths expected to occur at the highest frequency of interest, namely 200 Hz.

Due to the complexity when assessing damping in building structures, a global damping ratio of 6% was assigned to all materials, as opposed to considering damping for each material and in the different junctions. The damping ratio was determined in [30], with the use of experimental data obtained from measurements in a TVE building [31], by fitting an exponential function to the transient response of a floor structure. The damping ratio was used to establish a damping matrix by means of the Rayleigh method, see e.g. [32]. The C_S-matrix in Eq. (14) was, hence, constructed as a linear combination of the mass- and stiffness matrices, selecting the proportionality constants to be 17.37 and $9.77 \cdot 10^{-5}$, respectively. Since the damping ratio was calculated from measurements on a real building, involving insulation in the cavities, the damping in the structure may be overestimated as the insulation is modelled explicitly. The possible overestimation is, however, believed to have a negligible effect on the conclusions of the studies presented here.

In the analyses, the surfaces of the two TVEs, where elastomer blocks would be placed if further storeys were included, were modelled as clamped. Moreover, the walls of the neighbouring

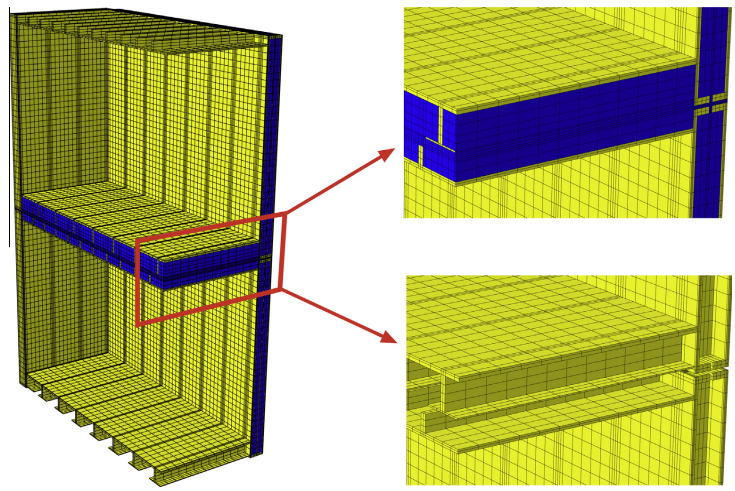

Fig. 5. A quarter of the model of two TVEs. The acoustic media are shown in blue. The junction between floor, ceiling and apartment separating walls is shown to the right, with and without acoustic media in the cavities.

Table 5
Material parameters used for the isotropic materials.

Material	E (MPa)	ν (−)	ρ (kg m^{-3})
Particle board	3000	0.3	767
Plaster board	2000	0.2	692.3
Plywood	12,400	0.3	710

Table 6
Material parameters used for the wood beams.

E_1 (MPa)	E_2	E_3	G_{12} (MPa)	G_{13}	G_{23}	ν_{12} (−)	ν_{13}	ν_{23}	ρ (kg m^{-3})
8500	350	350	700	700	50	0.2	0.2	0.3	432

Table 7
Porous material properties used in the numerical studies.

R (N/m^{-4} s)	ϕ (−)	α (−)
40,000	0.96	1.1

modules were clamped at the vertical edges. A vertical unit point load, acting on the middle of the floor in the upper TVE, was applied, and steady-state analyses were performed for frequencies up to 200 Hz in steps of 5 Hz.

3.2.1. Vibrations in the floor and the underlying ceiling

First, the vibrations in the floor of the upper TVE and the underlying ceiling were investigated for different ways of modelling air and insulation in the cavity between the floor and the ceiling. A model without acoustic media was compared to models with air alone and air together with insulation in the cavity, the insulation being placed according to the drawings in Fig. 2. All analyses were performed applying two different boundary conditions, $p = 0$ and $\nabla p = 0$, at the interfaces of the acoustic media bordering to surrounding cavities, in order to investigate their effect on the vibrations transmitted over the cavity. These interfaces are illustrated in Fig. 6, where the full TVEs are shown. At all boundaries of the acoustic media in contact with structural components, structure-acoustic coupling was considered.

The acceleration amplitudes obtained in the analyses of the different models were extracted from half of the nodes (due to the symmetry) at the floor surface and the ceiling surface, respectively, and RMS values of the complex acceleration magnitudes were calculated according to Eq. (23).

In Fig. 7, the RMS values of the acceleration amplitudes at the floor are shown. Including air alone in the cavity has a small effect on the levels of vibration in the floor, the RMS values being changed by just over 1% in average. An exception is found at 30 Hz, where the inclusion of air lowers the vibration amplitudes. Considering both air and insulation in the cavity leads to a dampening effect, lowering the levels of vibration by approximately 15% while the frequency response function is similar in shape to that obtained when including no acoustic media in the cavity. Moreover, it can be observed that the choice of boundary conditions for the acoustic media has a negligible effect on the acceleration amplitudes at the floor.

In Fig. 8, the RMS values of the acceleration amplitudes at the ceiling are shown. It can be observed that including air alone results in higher acceleration amplitudes, especially at lower frequencies. For low frequencies, the modelling of both air and insulation results in acceleration amplitudes in-between the case with air alone and the case with no acoustic media in the floor-ceiling cavity. At higher frequencies, the acceleration amplitudes obtained for the case with air and insulation are similar to those obtained for the case without acoustic media, deviating with less than a factor of 2. At some frequencies, the dampening effect of the insulation results in reduced vibration amplitudes when including both air and insulation, as compared to having no acoustic media. When air alone is considered, the levels of vibration are affected by the choice of boundary conditions for the acoustic medium, the effect, however, being relatively small when both air and insulation are included in the model.

3.2.2. Vibrations in the surrounding walls

Next, the vibrations in the walls of the lower TVE were investigated for different ways of modelling the air and insulation in the

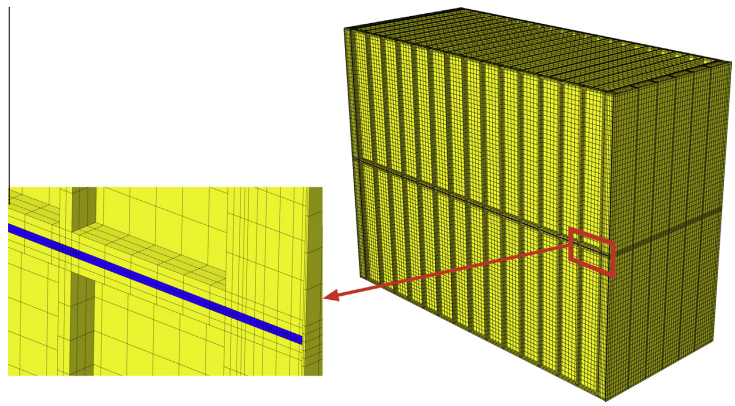

Fig. 6. The model of the two TVEs. The acoustic media in contact with the surrounding cavities, where different boundary conditions were applied, are shown to the left. The acoustic media are shown in blue.

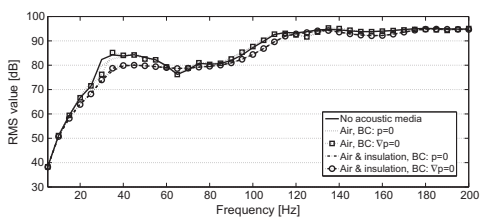

Fig. 7. RMS values of the acceleration amplitudes at the floor for the different models of the acoustic media in the floor-ceiling cavity.

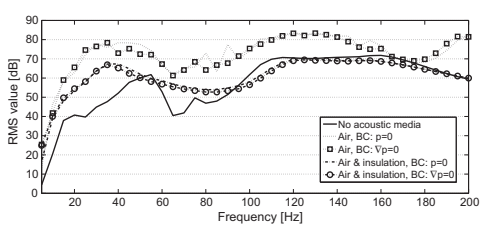

Fig. 8. RMS values of the acceleration amplitudes at the ceiling for the different models of the acoustic media in the floor-ceiling cavity.

cavity between the floor and the ceiling as well as the cavities in the apartment separating walls. Models including acoustic media either in the floor-ceiling cavity alone or in both the floor-ceiling cavity and the wall cavities were compared to a model without acoustic media. In the models including acoustic media, it was included as air alone or air together with insulation. The insulation in the walls was placed according to the drawings in Fig. 2, i.e. between the beams of each wall, having a small air gap between the walls of two neighbouring TVEs. Moreover, models having the floor-ceiling cavity and the wall cavities separated were created by introducing a separating wall in the junction between the cavities, the junction being shown in Fig. 5. These models were compared to the models with connected cavities in order to investigate if the acoustic pressure waves travelling between the cavities affect the vibration amplitudes in the walls.

At the boundaries to the acoustic media in surrounding cavities, only $\nabla p = 0$ was applied as it was observed in the evaluation of the ceiling vibrations that the boundary conditions have a small effect on the vibration transmission. The acceleration amplitudes obtained in the analyses of the different models were extracted in all nodes at the surface of an apartment separating wall of the lower TVE. RMS values of the complex acceleration magnitudes were calculated according to Eq. (23).

In Fig. 9, the RMS values of the acceleration amplitudes at the wall of the lower TVE are shown for the models where air alone was used as acoustic medium in the cavities. In Fig. 10, the RMS values are shown for the models where both air and insulation were included as acoustic media. The frequency range is divided into two parts, including frequencies in the ranges 0–100 Hz and 100–200 Hz, respectively. Observe that different scales are employed for the y-axes in the two frequency ranges.

It can be observed in Fig. 9 that including acoustic medium in terms of air alone in the cavities has a large effect on the vibration transmission from the floor to the walls of the TVE below. The system becomes more resonant when air is included and the acceleration amplitudes at the wall panel are generally higher, except at some frequencies between resonance peaks, where the amplitudes are reduced compared to the model with no acoustic media. At most frequencies, the acceleration amplitudes are higher when the floor-ceiling cavity is connected to the wall cavities compared to having the cavities separated. At low and high frequencies (below 15 Hz and above 155 Hz), the model with air in all cavities, having the cavities separated, results in acceleration amplitudes similar to the model with air only in the floor-ceiling cavity. Hence, if the cavities are separated, the inclusion of air in the wall panels has a negligible effect at those frequencies.

In Fig. 10, it can be observed that considering both air and insulation as acoustic media in the cavities results in smoother spectrums compared to including air alone. For most frequencies, with the exception being frequencies below 40 Hz, the acceleration amplitudes are decreased when including air and insulation in the cavities compared to having no acoustic media. A resonance frequency is observed at 20 Hz for the model with acoustic media only in the floor-ceiling cavity which is not present for any of the other models. Hence, a resonance occurs due to the inclusion of

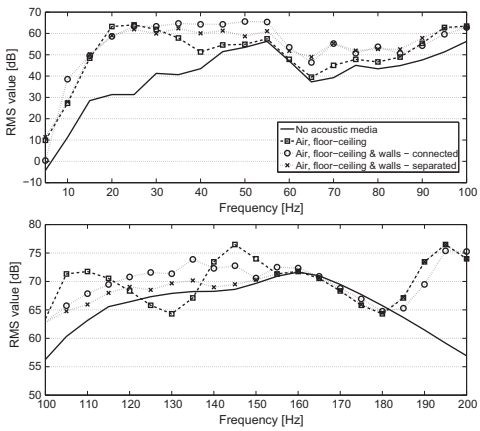

Fig. 9. RMS values of the acceleration amplitudes at the apartment separating wall of the lower TVE for the different models including air alone as acoustic medium. Note that the two plots employ different scales at the *y*-axis.

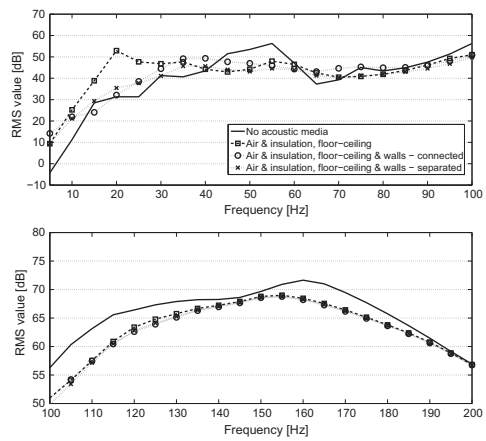

Fig. 10. RMS values of the acceleration amplitudes at the apartment separating wall of the lower TVE for the different models including both air and insulation as acoustic media. Note that the two plots employ different scales at the *y*-axis.

air and insulation in the floor-ceiling cavity which is cancelled when considering the acoustic media also in the wall cavities. In general, the acceleration amplitudes when considering both air and insulation, as compared to including air alone in the cavities, are closer to the case with no acoustic media. Above 60 Hz, the inclusion of air and insulation as acoustic media results in acceleration amplitudes deviating with a factor of less than 2 compared to having no acoustic media. Above 100 Hz, all three models with air and insulation in the cavities result in very similar acceleration amplitudes. This shows that at higher frequencies, the effect of including acoustic media in the wall cavities, on the vibration transmission to the wall panels, is small in case both air and insulation are considered.

4. Conclusions

The main conclusion from the numerical studies is that acoustic media in the cavities of wooden buildings affect the vibration transmission. It was observed that the vibrations transmitted from a load acting on a floor structure affected the acceleration amplitudes in both the underlying ceiling, structurally separated from the floor, and the walls of the storey below. The effect is especially distinct when air alone is considered as acoustic medium. Generally, including air alone results in a more resonant system with higher acceleration amplitudes while including both air and insulation introduces a dampening effect, especially at higher frequencies. The dampening effect of the insulation results in decreased acceleration amplitudes at higher frequencies as compared to including no acoustic media. In reality, the cavities normally contain insulation, the modelling of air alone, thus, leading to an overestimation of the transmitted vibrations.

The level of vibrations in the floor was only marginally affected by the inclusion of air alone as acoustic medium in the floor-ceiling cavity. When considering both air and insulation as acoustic media, the shape of the frequency response function did not change to any appreciable extent, while a dampening effect was observed in the floor vibrations.

In the analyses of the vibrations in the floor and in the ceiling, it was concluded that the choice of boundary conditions for the acoustic media bordering to surrounding cavities has a small effect in terms of vibration transmission from the floor to the ceiling below. This implies that the acoustic media in surrounding cavities has a weak effect on the vibrations transmitted locally over the floor-ceiling cavity.

In the analyses of the vibrations in the walls of the lower TVE, it was observed that including air and insulation in the wall cavities had no effect on the transmission to the wall panels above 100 Hz. If the vibrations transmitted from the floor to surrounding walls are studied for frequencies over 100 Hz, it is, hence, sufficient to include the air and insulation only in the floor-ceiling cavity. This result indicates that the effect of including acoustic media in cavities is decreasing with the distance from the load. It should be investigated further how far from the load the acoustic media has to be considered.

The porous material models investigated in this paper are only a few of many available in the literature. Specifically, no models assuming limp or elastic structural frame have been evaluated here. As it was concluded that acoustic media in cavities of multi-storey wood buildings have to be considered when performing low-frequency vibration analyses, the material model for the insulation should be validated.

Acknowledgement

The financial support for this work provided by the Silent Spaces project, a part of the EU program Interreg IV A, is gratefully acknowledged.

References

[1] Forssén J, Kropp W, Brunskog J, Ljunggren S, Bard D, Sandberg G, Ljunggren F, et al. Acoustics in wooden buildings – state of the art 2008. Vinnova project 2007-01653, report 2008:16, SP Trätek, Stockholm; 2008.
[2] Andersen L, Kirkegaard PH, Dickow KA, Kiel N, Persson K. Influence of wall surface and air modelling in finite-element analysis of sound transmission between rooms in lightweight buildings. In: Proceedings of the internoise 2012/ASME NCAD meeting, New York.
[3] Domadiya PG, Dickow KA, Andersen L, Sorokin SV. Mitigation of flanking noise in double-plate panel structures by periodic stiffening – finite element analysis in the low-frequency range. In: Proceedings of COMPDYN 2011, Corfu, Greece.
[4] Dickow KA, Gandalal PD, Andersen L, Kirkegaard PH. Transmission of sound through double-plate panel structures – a numerical study of coupling

parameters in lightweight panel structures. In: Proceedings of COMPDYN 2011, Corfu, Greece.
[5] Ljunggren F, Ågren A. Potential solutions to improved sound performance of volume based lightweight multi-storey timber buildings. Appl Acoust 2011;72:231–40.
[6] Ottosen N, Petersson H. Introduction to the finite element method. Harlow (United Kingdom): Pearson Education Ltd.; 1992.
[7] Bathe KJ. Finite element procedures. New York: Prentice Hall; 1996.
[8] Holzapfel GA. Nonlinear solid mechanics: a continuum approach for engineering. Chichester (United Kingdom): John Wiley & Sons Ltd.; 2000.
[9] Sandberg G. Finite element modelling of fluid-structure interaction. Ph.D. thesis. Division of Structural Mechanics, Lund University, Sweden; 1986.
[10] Delany ME, Bazley EN. Acoustical properties of fibrous absorbent materials. Appl Acoust 1970;3(2):105–16.
[11] Miki Y. Acoustical properties of porous materials-modifications of Delany–Bazley models. J Acoust Soc Jpn 1990;11(1):19–24.
[12] Dunn IP, Davern WA. Calculation of acoustic impedance of multi-layer absorbers. Appl Acoust 1986;19(5):321–34.
[13] Komatsu T. Improvement of the Delany–Bazley and Miki models for fibrous sound-absorbing materials. Acoust Sci Technol 2008;29(2):121–9.
[14] Mechel FP. Ausweitung der absorberformel von delany and bazley zu tiefen frequenzen. Acustica 1976;35(3):210–3.
[15] Kirby R, Cummings A. Prediction of the bulk acoustic properties of fibrous materials at low frequencies. Appl Acoust 1999;56(2):101–25.
[16] Kirchhoff G. On the influence of heat conduction in a gas on sound propagation. Annu Phys Chem 1868;134:177–93.
[17] Zwikker C, Kosten CW. Sound absorbing materials. Amsterdam: Elsevier; 1949.
[18] Morse PM, Ingard KU. Theoretical acoustics. New Jersey: Princeton University Press; 1968.
[19] Attenborough K. Acoustical characteristics of porous materials. Phys Rep 1982;82(3):179–227.
[20] Allard JF, Atalla N. Propagation of sound in porous media – modelling sound absorbing materials. 2nd ed. Chichester (United Kingdom): John Wiley & Sons Ltd.; 2009.
[21] Göransson P. Acoustic finite element formulation of a flexible porous material – a correction for inertial effects. J Sound Vib 1995;185(4):559–80.
[22] Panneton R. Comments on the limp frame equivalent fluid model for porous media. J Acoust Soc Am 2007;122(6):217–22.
[23] Biot MA. Theory of propagation of elastic waves in a fluid-saturated porous solid. I. Low-frequency range. J Acoust Soc Am 1956;28(2):168–78.
[24] Dassault Systèmes. Abaqus 6.12 documentation; 2012.
[25] Schiavi A, Guglielmone C, Miglietta P. Effect and importance of static-load on airflow resistivity determination and its consequences on dynamic stiffness. Appl Acoust 2011;72(9):705–10.
[26] Olny X, Panneton R. Acoustical determination of the parameters governing thermal dissipation in porous media. J Acoust Soc Am 2008;123(2):814–24.
[27] Sagartzazu X, Hervella-Nieto L, Pagalday JM. Review in sound absorbing materials. Arch Comput Methods Eng 2008;15(3):311–42.
[28] Kino N, Takayasu U. Experimental determination of the micro-and macrostructural parameters influencing the acoustical performance of fibrous media. Appl Acoust 2007;68(11):1439–58.
[29] Negreira J. Vibrations in lightweight buildings – perception and prediction. Licentiate dissertation. Division of Engineering Acoustics, Lund University, Sweden; 2013.
[30] Negreira J, Bard D. Finite element modelling of a timber volume element based building with elastic layer insulators. SP Technical Research Institute of Sweden, report 2013: 27.
[31] AkuLite. Mätrapport 10052. Brunnby Park, Upplands Väsby, Sweden; 2012.
[32] Chopra AK. Dynamics of structures. New Jersey: Prentice Hall; 2007.

Paper C

Chapter 18
Numerical and Experimental Studies on Scale Models of Lightweight Building Structures

Ola Flodén, Kent Persson, and Göran Sandberg

Abstract Lightweight buildings are sensitive to low-frequency vibrations, making it difficult to construct them in such a way that noise and disturbing vibrations are kept at an acceptable level. In the design of vibration reduction measures, it is desirable to have computational models for predicting the effects of structural modifications. Validations of the models to experimental data have to be performed to ensure reliable predictions. The experimental studies are simplified if full-scale models can be scaled down in size. In the paper, methods for designing scaled experimental models of building structures are discussed. An example, the scaling of a wooden building structure, is presented.

Keywords Lightweight buildings • Impact sound • Vibration transmission • Model validation • Scale models

18.1 Introduction

Noisy neighbours are a common cause of annoyance for residents in multi-family houses. Compared to heavier structures, lightweight buildings are more sensitive to vibrations, making it difficult to construct them in such a way that noise and disturbing vibrations are kept at an acceptable level. Despite newly constructed lightweight buildings complying with regulations for sound insulation, many of the residents perceive the impact sound as annoying [1]. Building regulations in most European countries take frequencies in the range 100–3150 Hz into account, whilst the lower limit in Sweden is 50 Hz. The measured sound insulation correlates much better to residents annoyance when extending the frequency range in the evaluations down to 20 Hz [1], pointing out the importance of improved sound insulation at lower frequencies. In wood buildings, for example, a common measure for reducing vibration transmission is to insert elastomers in-between building parts [2]. The design of such measures is based primarily on experience. To optimise the design, it is desirable to have computational models for predicting the effects of structural modifications. The models have to be calibrated, correlated and validated to measurement results for the predictions to be reliable. An alternative to employing full-scale experimental structures for performing the measurements is to design scaled experimental models that behave in a similar way.

In the paper, methods for designing scaled experimental models of building structures are discussed. The objective of the scaling procedure is to arrive at scaled experimental models that preserve the dynamic behaviour of the full structures. An example regarding the scaling of a wooden building structure is presented here.

18.2 Governing Theory

The equations of motion for a structure can be derived through its Lagrangian, which for an undamped system is given by

$$L(q_1, \ldots, q_n, t) = T(q_1, \ldots, q_n, t) - V(q_1, \ldots, q_n, t), \tag{18.1}$$

O. Flodén (✉) • K. Persson • G. Sandberg
Faculty of Engineering, Department of Construction Sciences, Lund University, John Ericssons väg 1, SE-223 63 Lund, Sweden
e-mail: ola.floden@construction.lth.se

M. Allen et al. (eds.), *Dynamics of Coupled Structures, Volume 4*, Conference Proceedings of the Society for Experimental Mechanics Series, DOI 10.1007/978-3-319-29763-7_18

where T is kinetic energy, V is potential energy, $q_1, \ldots, q_n$ is a set of n generalised coordinates and t is time. The equations of motion of the system is given by the Lagrange's equations

$$\frac{d}{dt}\left(\frac{\partial L}{\partial \dot{q}_j}\right) = \frac{\partial L}{\partial q_j}. \tag{18.2}$$

Scaling the size of a model affects its Lagrangian. The Lagrangian of a scale model, can be expressed as

$$L_s = T_s - V_s = a\left(T_f - bV_f\right), \tag{18.3}$$

where subscripts s and f denote quantities belonging to the scale model and to the full model, respectively, and a and b are constants. The resulting equations of motion are not affected by a, whilst $b = 1$ is required in order to preserve the equations of motion. A scale model should, hence, be constructed in such a way that b is as close to unity as possible. This approach for determining parameters of scale models is possible when expressions for the energies can be derived. For more complex structures, numerical models of the full and the scaled experimental models have to be analysed and compared in order to ensure accurate scaling.

18.3 Scale Models of Building Structures

The Lagrangians used in scaling procedures are constructed based on the physical phenomena expected to occur. Residential buildings are normally constructed using different types of beam-, column- and plate-like structures which are exposed to different types of deformations. To illustrate the scaling procedure, the scaling of a beam is derived by considering its bending, an important type of deformation in the dynamics of building structures. In the derivations presented here, the coordinate system in Fig. 18.1 is used. The beam is assumed to have rectangular cross-section; the width b, the height h and the length l of the beam is defined in Fig. 18.1. The kinetic energy of an Euler-Bernoulli beam in bending is given by

$$T = \frac{1}{2}\int_0^l \rho A \dot{u}^2 dx, \tag{18.4}$$

where $A = bh$ is the cross-sectional area, ρ is the density and u is the deflection in the z-direction. The potential energy is given by

$$V = \frac{1}{2}\int_0^l EI\left(\frac{\partial^2 u}{\partial x^2}\right)^2 dx, \tag{18.5}$$

where E is the Young's modulus and I is the moment of inertia of the cross-section,

$$I = \frac{bh^3}{12}. \tag{18.6}$$

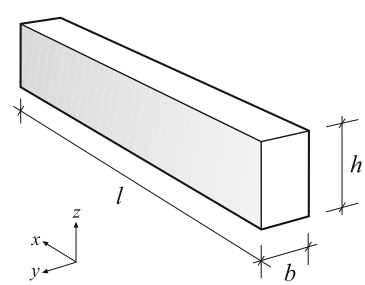

Fig. 18.1 Coordinate system and dimensions used in the derivations of the scaling of a beam

The scaling is introduced by defining the following dimensionless parameters:

$$\mu = \frac{A_s}{A_f}, \qquad \kappa = \frac{I_s}{I_f}, \qquad \chi = \frac{x_s}{x_f} = \frac{l_s}{l_f}. \tag{18.7}$$

By inserting the dimensionless parameters in the energy expressions for the scaled and the full models, it can be shown that

$$T_s = \mu\chi T_f \tag{18.8}$$

and

$$V_s = \frac{\kappa}{\chi^3} V_f. \tag{18.9}$$

Scaling parameters could be introduced also for the material properties (E and ρ) and the time. It is, however, assumed here that the same material is used for both models. Not scaling the time results in the eigenfrequencies being preserved. Inserting Eqs. (18.8) and (18.9) in the first equation in Eq. (18.3) results in

$$L_s = \mu\chi T_f - \frac{\kappa}{\chi^3} V_f = \mu\chi \left(T_f - \frac{\kappa}{\mu\chi^4} V_f \right). \tag{18.10}$$

By comparing the result to the second equation in Eq. (18.3), it is found that the scaling condition $b = 1$ results in

$$\frac{\kappa}{\mu\chi^4} = 1 \quad \Leftrightarrow \quad \left(\frac{l_s}{l_f}\right)^2 = \frac{h_s}{h_f}. \tag{18.11}$$

When using this condition for creating a scale model of a beam, the eigenfrequency of the bending modes are preserved. It can be seen that bending in the z-direction is unaffected by the width. Hence, if a length scaling is assumed, the scaled height can be determined or vice versa. A corresponding expression can be determined for the width by considering bending in the y-direction.

The procedure presented above can be employed for other types of deformations, such as the torsion of beams or the bending of plates. The type of deformation to consider in the scaling depends on the type that is expected to dominate the dynamics of the structure.

18.3.1 Example: Wooden Building Structure

The structure studied here was designed to represent the physics involved in low-frequency (below 100 Hz) vibration transmission in multi-storey wood buildings. Specifically, a type of construction called timber volume element (TVE) buildings was used as reference for designing the experimental model. A main feature of such buildings, from a dynamical point-of-view, is the use of elastomer layers for vibration isolation. The load-bearing structure in TVE buildings consists of wood frames covered by plasterboards and particleboards. The buildings are constructed by stacking box-like volume elements (the TVEs) with layers of elastomers in-between. The experimental model considered here, illustrated in Fig. 18.2, consists of parts of two TVEs, one comprising a floor with walls on top and the other comprising a ceiling with walls below. Only half the height of the walls, compared to complete TVEs, is included in the model. The floor and the ceiling consist of a number of primary beams (seven and ten, respectively) attached to edge beams and have surfaces of particleboard and plasterboard, respectively. The walls consist of seven primary beams each, attached to edge beams on one side, and have surfaces of plasterboard. Two sides of the model have one type of walls, apartment separating walls, and the other two sides have another type of walls, facade walls. In Table 18.1, the dimensions are shown for the floor, the ceiling and the two types of walls. Elastomer blocks of the material Sylodyn NB [3] are placed in-between the two TVE structures. A total of 28 elastomer blocks, each being $100 \times 95 \times 25\,\text{mm}^3$ large, are placed with a centre-to-centre distance (cc) of 600 mm along the walls. The outer dimensions of the full experimental model are $4000 \times 3600 \times 2800\,\text{mm}^3$.

The scaling of the beams was made using Eq. (18.11) for bending in the two directions, resulting in relations between the length and the height, and between the length and the width,

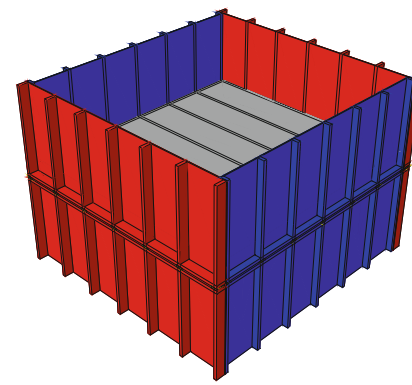

Fig. 18.2 The full-scale wooden building structure studied here. The floor is shown in *grey*, the apartment separating walls in *red*, the facade walls in *blue* and the elastomer blocks in *yellow*. The ceiling, placed under the floor, cannot be seen in the figure

Table 18.1 Length (l), centre-to-centre distance (cc) and cross-sectional dimensions ($b \times h$) of the primary beams, and thickness (t) of the plates in the full model and in the scale model. The unit is mm

	Full model					Scale model				
	l_f	cc_f	h_f	b_f	t_f	l_s	cc_s	h_s	b_s	t_s
Floor	3430	600	220	45	22	2330	408	95	21	10
Ceiling	3430	400	120	45	13	2330	272	55	21	6
Apartm sep wall	1390	600	95	45	13	950	408	45	21	6
Facade wall	1390	600	145	45	13	950	401	70	21	6

$$\left(\frac{l_s}{l_f}\right)^2 = \frac{h_s}{h_f}, \qquad \left(\frac{l_s}{l_f}\right)^2 = \frac{b_s}{b_f}. \tag{18.12}$$

The thickness of the plates (particleboards and plasterboards) were scaled by regarding them as beams spanning the cc between the primary beams, i.e. assuming one-dimensional deformations for the plates. By considering bending of the plates, Eq. (18.12) can be used to obtain the relation between cc and plate thickness t,

$$\left(\frac{cc_s}{cc_f}\right)^2 = \frac{t_s}{t_f}. \tag{18.13}$$

The scaling ratio for the cc is employed also for the length of the beams, i.e.

$$\frac{cc_s}{cc_f} = \frac{l_s}{l_f}. \tag{18.14}$$

Moreover, the floor, the ceiling and the walls have to be scaled so that their sizes match, i.e. using the same four scaling ratios (scaling of height, width, length and cc) for all structures. First, the scaling ratio for the thickness of the plates was chosen since particleboard and plasterboard are manufactured in only a few different thicknesses. Thereafter, Eqs. (18.12)–(18.14) were used to determine the remaining scaling ratios. The dimensions of the beams and of the plates in the scale model are shown in Table 18.1.

The final step in determining the dimensions of the scale model is to scale the elastomer blocks. The dimensions of the blocks were determined by regarding the two TVE structures as rigid masses and the elastomer layer as a spring. The eigenfrequency of a system with two masses, m_1 and m_2, connected by a spring with stiffness k is given by

$$f = \sqrt{k\frac{m_1 + m_2}{m_1 m_2}} = \sqrt{\frac{k}{m^{eff}}}, \qquad m^{eff} = \frac{m_1 m_2}{m_1 + m_2}, \tag{18.15}$$

where m^{eff} is the effective mass. The ratio between the eigenfrequencies of the full model and of the scale model is, consequently,

$$\frac{f_f}{f_s} = \sqrt{\frac{k_f}{k_s}\frac{m_s^{eff}}{m_f^{eff}}}. \tag{18.16}$$

The effective masses of the full and the scaled models, calculated using the densities found in [2], are 281 kg and 53 kg, respectively. It is assumed that the eigenfrequency of the two-mass-system is preserved, $f_s = f_f$. The ratio between the spring stiffness of the two models can then be calculated as

$$\frac{k_f}{k_s} = \left(\frac{f_f}{f_s}\right)^2 \frac{m_f^{eff}}{m_s^{eff}} = 5.30. \tag{18.17}$$

Assuming the elastomer blocks to be linear elastic, their combined stiffness is given by

$$k = \frac{EA}{d}, \tag{18.18}$$

where A is the total contact area of the blocks and d is the thickness of the blocks. The same type of elastomer was used for the scale model as for the full model, so that $E_s = E_f$. Consequently,

$$\frac{k_s}{k_f} = \frac{d_f}{d_s}\frac{A_s}{A_f}. \tag{18.19}$$

Combining Eqs. (18.17) and (18.19) results in

$$\frac{d_s}{d_f} = 5.30\frac{A_s}{A_f}. \tag{18.20}$$

Hence, if a thickness scaling is specified, an area scaling can be determined and vice versa. The thickness of the scaled elastomer blocks was chosen to be the same as for the full blocks, $d_s = d_f$. This results in the scaled area being $A_s = A_f/5.30 = 1800\,\text{mm}^2$. Assuming a squared shape for the blocks, their dimensions can be determined as $42 \times 42 \times 25\,\text{mm}^3$. In order to match the width of the beams in the apartment separating walls, the blocks were chosen to be $45 \times 45 \times 25\,\text{mm}^3$ large. The outer dimensions of the scale model are $2600 \times 2400 \times 1900\,\text{mm}^3$. The volume of the full model is, hence, reduced by 70 % in the scaling.

Finite element (FE) models of the full and the scaled experimental models were created to investigate how well the scaling procedure works when the scaled plates and beams are assembled to larger structures. The material properties found in [2] were used in the FE models. The element sizes were decided based on the accuracy in eigenfrequencies below 100 Hz, the highest frequency of interest. All connections in the FE models were modelled as fully tied. The comparison of the scale models to the full models was carried out in terms of free-free eigenfrequencies, i.e. eigenfrequencies calculated with no boundary conditions applied. The difference in eigenfrequencies was evaluated in terms of the normalised relative frequency difference (NRFD), defined as

$$\text{NRFD} = \frac{\left|f_i^s - f_i^f\right|}{f_i^f}, \tag{18.21}$$

where f_i^s and f_i^f are the ith eigenfrequencies of the scale model and of the full model, respectively. First, FE models of the floor, the ceiling and the walls were investigated. Eigenfrequencies below 100 Hz and the resulting NRFD values are shown in Figs. 18.3 and 18.4, respectively. The curves have different lengths along the horizontal axis since the structures have different numbers of eigenfrequencies below 100 Hz. The NRFD values are, with a few exceptions, below 10 %. The mean NRFD value is between 2 and 6 % for the different structures. The mode shapes were compared visually, most modes of the scale models being similar to those of the full models. Some of the higher frequency modes were found to be shifted in order. At higher frequencies, the mode shapes are more localised, for example due to resonances in each *cc*-section of the plates.

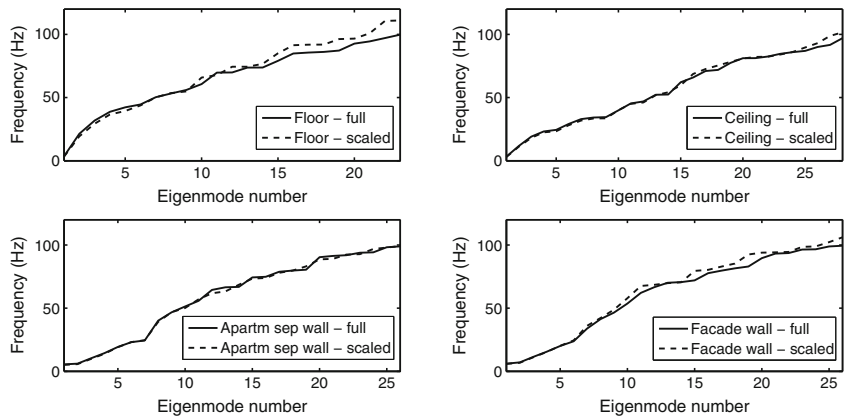

Fig. 18.3 Eigenfrequencies for the full and the scaled models of the floor, the ceiling and the walls

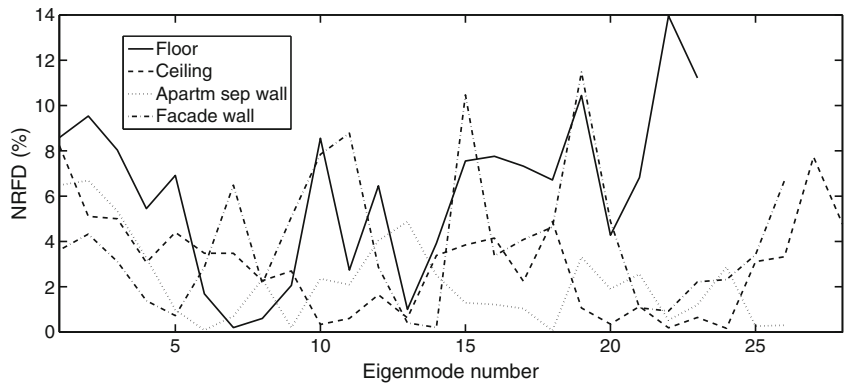

Fig. 18.4 NRFD values for the floor, the ceiling and the walls

Therefore, discrepancies between eigenfrequencies of the beams and of the plates can have larger impact on the resulting mode shapes. The global mode shapes at low frequencies are, however, well preserved in the scale models.

Second, FE models (full and scaled) of the complete structure were created. The elastomer blocks were modelled as linear viscoelastic with properties determined by employing the procedure developed in [4]. The free-free eigenfrequencies of the full and the scaled models are shown in Fig. 18.5, and the resulting NRFD values are shown in Fig. 18.6. The modal density is high, especially around 80 Hz, because of local resonances occurring primarily in the plates of the walls. It is therefore difficult to distinguish the mode shapes from each other. It can, however, be seen that similar trends in modal density are found for the full and the scaled models.

In addition to comparing eigenfrequencies, the vibration transmission from the floor to the TVE below was studied. A harmonic point load was applied in the vertical direction at the middle of the floor, free-free boundary conditions being used. A unit load was used for the scale model, whilst a load of 5.28 N was used for the full model since the ratio of total masses between the models is 5.28. The resulting complex acceleration amplitudes, $\hat{a}_i$ (i denoting node number), were evaluated at the surface of the ceiling and at the surface of one of the facade walls. Root-mean-square (RMS) values of the accelerations in all nodes of each surface were calculated as

$$a_{RMS}(f) = \sqrt{\frac{1}{n}\sum_{i=1}^{n} |\hat{a}_i(f)|^2}, \tag{18.22}$$

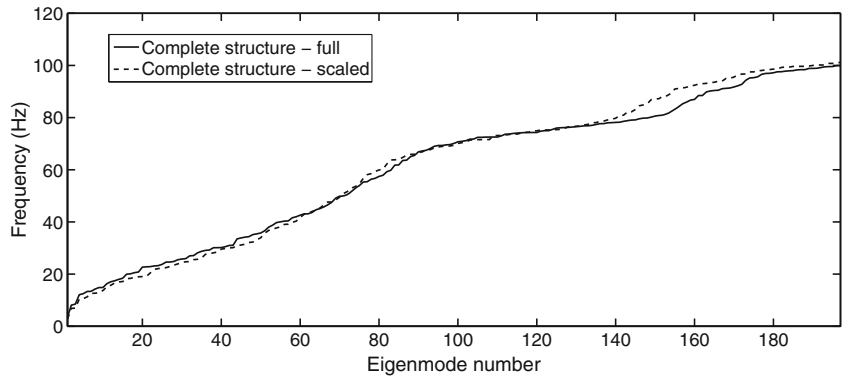

Fig. 18.5 Eigenfrequencies for the full and scaled models of the complete structure

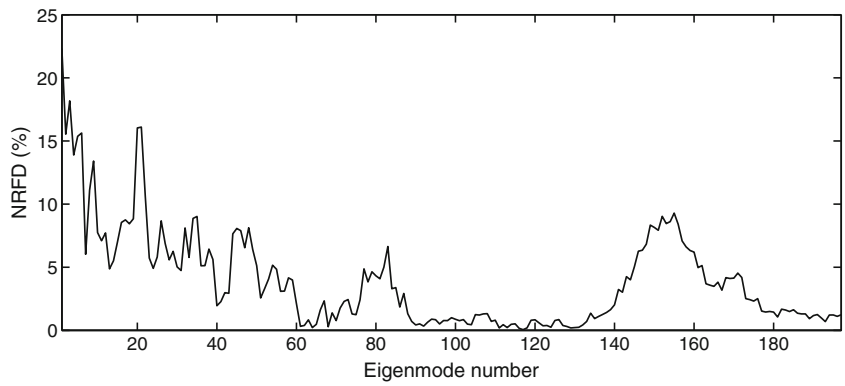

Fig. 18.6 NRFD values for the complete structure

where n is the number of FE nodes at the surface in question. The RMS values at the ceiling surface and at the wall surface are shown in Figs. 18.7 and 18.8, respectively. For frequencies below 50 Hz, the scaled and the full FE models produce similar results, the differences being larger at higher frequencies. Consequently, the scale model performs well below 50 Hz. Above that frequency, the effect of physical phenomena which were not considered in the scaling becomes larger.

18.4 Concluding Remarks

In the paper, the designing of scaled experimental models of building structures was discussed. The scaling is based on assumptions of basic physical phenomena, such as bending of beams, governing the dynamic behaviour. As an example, a wooden building structure representing parts of two storeys in a multi-storey building was considered. The vibration transmission from a floor to the storey below was studied, finding that the scale model produced results similar to the full model for frequencies below 50 Hz. The scale model needs to be developed if better correlation to the full model is desired for higher frequencies. The results may be improved by not using the same scaling ratios for the cc as for the length of the beams. Moreover, other phenomena such as shear deformations of the elastomer layers could be considered in order to improve the scaling.

The degree to which the full and the scaled models need to correlate depends on the aim of the experimental studies. If the scaled experimental structure is used for predicting absolute values of some sort, a high degree of correlation is required. The example structure studied here will be used for developing FE models by comparisons between simulations

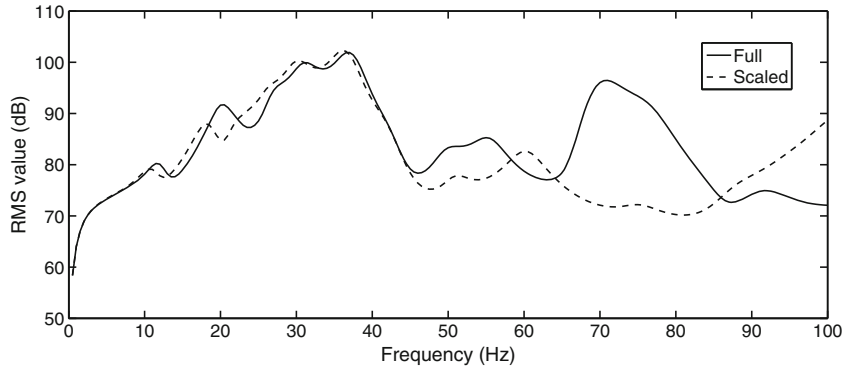

Fig. 18.7 RMS values of the acceleration amplitudes at the ceiling surface for the full and the scaled models of the complete structure

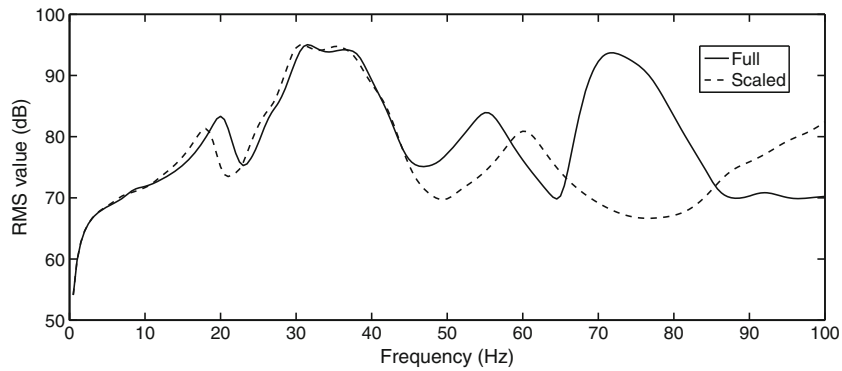

Fig. 18.8 RMS values of the acceleration amplitudes at the facade wall surface for the full and the scaled models of the complete structure

and measurements. In such situations, it is less important to have very good correlation between the full and the scaled models in terms of, for example, eigenfrequencies and amplitudes. It is instead sufficient to represent the physical phenomena governing the dynamic behaviour of the full experimental model, so that the FE models developed (with help of the scaled experimental model) are able to represent these phenomena.

A restriction in the methods discussed here for deriving scaled experimental models is that numerical modelling is employed for investigating their correlation to full-scale models. In the example, the joints were modelled in the same manner in the FE models of the full models and of the scale models. Hence, any difference in joint behaviour, which may be the case in reality, is neglected here.

References

1. Ljunggren F., Simmons S., Hagberg K. Correlation between sound insulation and occupants' perception – proposal of alternative single number rating of impact sound. Appl. Acoust. **85**, 57–68 (2014)
2. Flodén O., Persson K., Sandberg G. Numerical investigation of vibration reduction in multi-storey lightweight buildings. In: Dynamics of Civil Structures, vol. 2, pp. 443–453. Springer International Publishing, Berlin (2015)
3. Getzner W.: GmbH. Data sheet for Sylodyn NB, 2014
4. Negreira J., Austrell P.E., Flodén O., Bard, D.: Characterisation of an elastomer for noise and vibration insulation in lightweight timber buildings. Build Acoust. **21**(4), 251–276 (2014)

Paper D

A multi-level model correlation approach for low-frequency vibration transmission in wood structures

O. Flodén, K. Persson, G. Sandberg

Department of Construction Sciences, Lund University, P.O. Box 118, SE-22100 Lund, Sweden

Abstract

The main challenge in predicting structure-borne sound in wood buildings is to accurately model the vibration transmission between the source and the receiving room. A step towards establishing such models is to investigate the possibilities and limitations of using deterministic methods, which requires correlations between simulations and measurements. In the paper, we present a multi-level model correlation approach for low-frequency vibration transmission in wood buildings. The approach was applied to a scaled-size experimental structure representing a part of a two-storey wood building, considering frequencies up to 100 Hz. Correlations between simulations and measurements were performed at four different levels: structural components (viz. beams and boards), planar structures (viz. floor, ceiling and walls), room structures and the complete structure. The results indicate that the dynamic behaviour of the experimental structure was to a great extent captured by the developed model. Based on the observations made in the multi-level correlations, important model parameters are discussed and modelling guidelines are suggested. We conclude that it is relevant to employ deterministic methods in order to model the low-frequency vibration transmission in wood buildings provided that measurement data for calibration purposes is available. The developed numerical model can be used as a reference model for investigations on the effects of variations and uncertainties in the modelling.

Keywords: structure-borne sound, vibration transmission, wood buildings, finite element method, model correlation

1. Introduction

1.1 Background

Many of the residents in multi-storey wood buildings perceive the structure-borne sound as annoying even though the buildings fulfil regulations regarding sound insulation [1–7]. In [7], the impact sound insulation in eight wood buildings was measured according to standardised procedures. The measured impact sound insulation was compared to subjective ratings from residents. It was found that it is of essential importance to evaluate sound at frequencies below 100 Hz in order to correlate measurements to subjective ratings. These observations emphasise the need for improved low-frequency structure-borne sound insulation in wood buildings. To improve the sound insulation, and thus the

acoustic comfort for residents, it is valuable that accurate numerical models to predict the effects of noise reduction measures are available. Through numerical simulations, the performance of reduction measures can be optimised. Another benefit of using numerical simulations is that they provide additional insight into the physics governing noise and vibration transmission; the results of simulations can be visualised in more detail than experimental results, and parametric studies can demonstrate the effects of changes in design parameters.

Prediction of structure-borne sound in buildings can be divided into three tasks: (1) predicting the input force caused by the source, (2) predicting the transmission of structural vibrations from the source to the receiving room, and (3) predicting the sound pressure caused by the vibrations in the receiving room. Attempts to predict all three steps for low-frequency sound transmission in wood buildings, excited using an ISO tapping machine [8], are presented in [9–12]. Comparisons between results from finite element (FE) analyses and measurements unveil poor accuracy in all of the studies. In [11], the structure-borne sound transmission through a cross-laminated timber structure was tested in a laboratory and compared to simulated results. It was concluded that the radiated sound power in the receiving room can be predicted with good accuracy when measured vibrations in the ceiling of the receiving room are used as input. Hence, the main challenge in predicting structure-borne sound in wood buildings is to accurately model the structural vibration transmission between the source and the receiving room.

The model correlation studies we present in the paper were performed for an example case representing a part of a timber volume element (TVE) building. Such buildings are constructed by stacking pre-fabricated volume elements with elastomeric isolators between storeys to reduce vibration transmission. The volume elements are composed of frames of wood beams covered with plates, usually particleboards and plasterboards. TVE buildings account for about 10% of the newly produced multi-family housings in Sweden and their construction is increasing rapidly [13].

There are several publications presenting model correlation studies for finite element (FE) models of low-frequency vibrations in wood buildings. Those publications focus on, for example, joints between beams and boards [14, 15] and elastomeric vibration isolators used in wood buildings [16–18]. However, there is a lack of studies on model correlation for the vibration transmission between different storeys, which is the topic we discuss in the paper. It is a challenging task to develop deterministic models of wood buildings because of several uncertainties, for example, how to model the many joints between various structural components. Another uncertainty is how to account for the variations in material properties of wood and in mechanical behaviour of joints, which cause variations in vibration transmission among buildings with identical geometry. Variations can be considered in deterministic models by using, for example, Monte Carlo simulations. However, it is inevitable that the deterministic strategy fails outside a certain frequency range because of the increasing effects of small details at higher frequencies. The question is to what extent the deterministic strategy is relevant for the frequency range of interest, and when to accept a less detailed modelling strategy, such as statistical energy analysis (SEA). SEA methods are widely used for analysing high-frequency noise transmission in residential buildings. Such methods consider the energy flow between subsystems and require high modal density of the subsystems to yield accurate results. This is not the case at lower frequencies in which small sets of vibration modes govern the response. Compared to SEA methods, deterministic

methods have the advantage of allowing for a more detailed description of the structure under study and therefore facilitate studies on design modifications.

1.2 Aim and objective

The aim of the research presented in the paper is to develop numerical models and strategies for predicting low-frequency (0–100 Hz) vibration transmission in wood buildings. A step towards establishing such models is to investigate the possibilities and limitations of using deterministic methods, which requires correlations between model output and measurement data. In this paper, we present a multi-level model correlation approach for low-frequency vibration transmission in wood buildings. The multi-level approach is applied to an experimental wooden building structure representing a part of a two-storey building. The objective is to establish a correlated deterministic numerical model that can be used as a reference model for investigations on the effects of variations and uncertainties in the modelling. The accuracy of the model developed in the paper is evaluated to determine its capability of predicting vibration transmission when measurement data for calibration purposes is available. Based on the observations made in the multi-level correlations, important model parameters are discussed and modelling guidelines are suggested.

1.3 Outline of the multi-level approach

Model correlations were performed for the experimental wooden building structure shown in Figure 1. An FE model of the structure was calibrated and correlated to measurements by employing the multi-level approach illustrated in Figure 2. The term 'model correlation' is defined here as the process of comparing simulated and measured results to unveil and reduce errors in the modelling. The comparisons presented in the paper are based on the normalised relative frequency difference (NRFD) and the modal assurance criterion (MAC), which are objective measures of the errors in eigenfrequencies and mode shapes. Calibration, on the other hand, is defined as the procedure of improving estimates of uncertain model parameters. The steps in the multi-level approach can be summarised as follows:

1. **Initial numerical model.** An initial FE model was created by using material parameters from the literature and by connecting parts using simple joint models. The model was used as a starting point for the model correlation studies and to perform pre-test analyses of the experimental setups.

2. **Correlation of structural components.** FE models of the wood beams, particleboards and plasterboards were calibrated to obtain the material parameters that result in the best correlation between simulated and measured eigenfrequencies.

3. **Correlation of planar structures.** Simulated eigenfrequencies and mode shapes of the floor, ceiling and walls were correlated to measurement results. The effects of using the optimised material parameters obtained in step 2 were investigated and errors in the modelling of the joints between beams and boards were identified. The FE models were updated to improve the correlation.

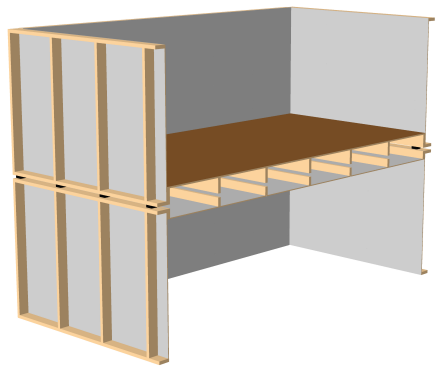

(a) *Rendering of the structure cut perpendicular to the primary beams in the floor and in the ceiling. Wood beams are shown in beige, particleboards in brown, plasterboards in grey and elastomer blocks in black.*

(b) *Photograph of the experimental setup for the structure.*

Figure 1. *The experimental wooden building structure studied in the paper. The structure represents part of a two-storey TVE building.*

4. **Correlation of room structures.** Simulated eigenfrequencies and mode shapes of the two room structures were correlated to measurement results to identify errors in the modelling of the joints between planar structures. The FE models were updated to improve the correlation.

5. **Correlation of vibration transmission in the complete structure.** A damping model based on measured modal damping ratios was assigned to the materials in the two room structures. The elastomers placed between the rooms were modelled using frequency-dependent viscoelastic material properties. Frequency response functions (FRFs) for the experimental structure were simulated and compared to measured FRFs. The FE model was updated by including acoustic media in the cavity between floor and ceiling to improve the correlation.

More detailed descriptions of both the experimental structure, the measurements and the calibrations of structural components than are presented in the paper can be found in [19] (which is written by the corresponding author of this paper).

1.4 Numerical analysis methods and error metrics

The calibrations and correlations performed for the FE models of the structural components, planar structures and room structures were based on eigenfrequencies and mode shapes. The eigenfrequencies from simulations and measurements were compared by using NRFD values, defined as

$$\text{NRFD} = \frac{f_i^{sim} - f_j^{exp}}{f_j^{exp}}, \tag{1}$$

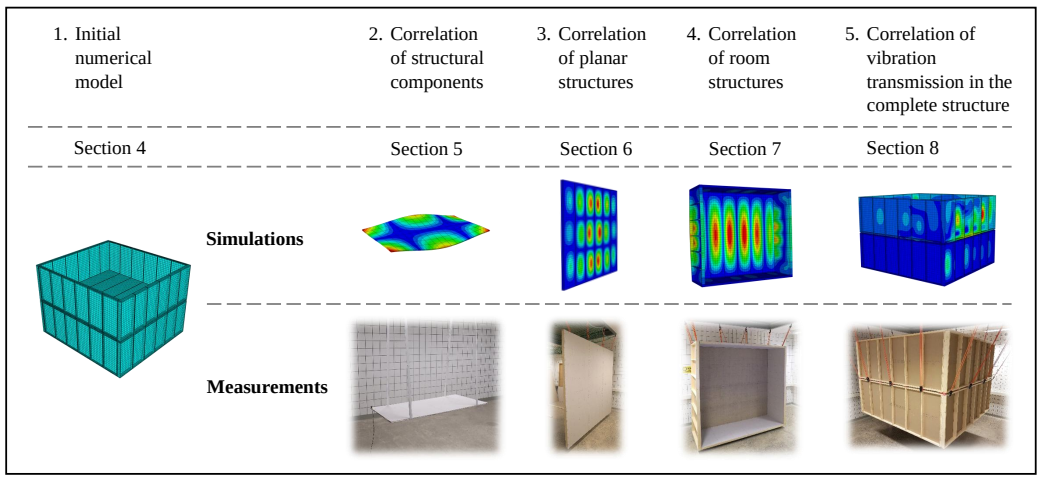

Figure 2. *Illustration of the multi-level approach used for developing a numerical model of the experimental structure.*

where f_i^{sim} is the ith simulated eigenfrequency and f_j^{exp} is the jth measured eigenfrequency. The NRFD value is relevant only if the simulated and measured eigenfrequencies belong to corresponding mode shapes. MAC values were employed to quantify the similarity in mode shapes. The MAC value is defined as

$$\text{MAC} = \frac{\left|(\Phi_i^{sim})^T(\Phi_j^{exp})\right|^2}{(\Phi_i^{sim})^T(\Phi_i^{sim})(\Phi_j^{exp})^T(\Phi_j^{exp})}, \tag{2}$$

where Φ_i^{sim} is the ith simulated mode shape and Φ_j^{exp} is the jth measured mode shape. The MAC value falls between 0 and 1, where 1 implies perfect correlation between the two mode shapes. By calculating the MAC values for all possible combinations of modes between two sets, the so-called cross-MAC matrix is obtained. If a mode set is compared to itself, the resulting matrix is referred to as the auto-MAC matrix.

To obtain FRFs for the vibration transmission in the complete structure, steady-state analyses were performed between 0–100 Hz in steps of 0.25 Hz when applying unit amplitude loads. No objective measure was used to quantify the errors between simulated and measured FRFs. Instead, visual comparisons were made to identify similarities and discrepancies.

2. Experimental structure

The experimental structure, shown in Figure 1, represents a part of a two-storey TVE building. It was a scaled-size structure consisting of two stacked room. The upper room comprised a floor and four walls whereas the lower room comprised a ceiling and four walls. The two rooms were

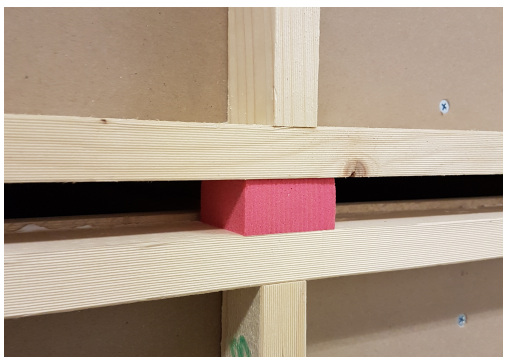

Figure 3. *Photograph of the elastomer blocks placed between the walls of the two stacked rooms.*

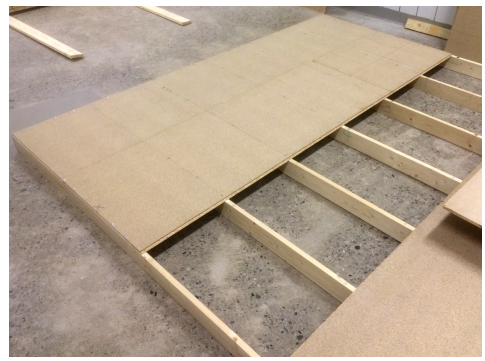

Figure 4. *Photograph of the floor during attachment of the particleboards. The seven primary wood beams are shown.*

connected via 28 elastomer blocks placed between the walls of the rooms, as shown in Figure 3. The planar structures (viz. floor, ceiling and walls) consisted of wood frames with seven primary beams attached to edge beams placed perpendicular to their ends. The floor was covered by particleboards, while the ceiling and walls were covered by plasterboards. Figure 4 shows the floor during attachment of the particleboards. The walls were of two different types, which differed in the dimensions of the wood beams: apartment separating walls and facade walls. The two rooms contained two walls of each type. The apartment separating walls were placed along the edge beams of the floor and the ceiling, whereas the facade walls were placed along the outermost primary beams.

2.1 Idealisations and scaling of the structure

The structure was designed based on drawings of a TVE building. Compared to the real building, a number of idealisations were made and the structure was scaled-down in size. The idealisations were made to facilitate the model correlations, whereas the scaling was necessary to obtain a structure that fitted within available laboratory facilities.

There were seven primary wood beams in the experimental floor structure; floors in real TVE buildings normally contain 2–3 times as many beams. Each room in the experimental structure included half the height of a TVE, i.e. the walls were of half height. No details or irregularities in the geometry, such as windows, doors, interior walls or floor surfaces, were included in the structure. Hence, only the load-bearing structures of the TVEs were represented in the experimental structure. Mineral wool for thermal and sound insulation purposes was not included in the structure.

The scaling of the structure was performed using the procedure presented in [20], written by the authors of this paper. The objective of the procedure is to reduce the size of experimental building structures while preserving their dynamic behaviour. By adopting the procedure, the reduced dimensions are calculated analytically by considering the bending modes of beams and boards in the building

structures. In [20], the scaling procedure was applied to a structure similar to the structure studied in this paper; both representing parts of two-storey TVE buildings. The accuracy of the scaling was investigated by comparing FE analyses of the full- and scaled-size structures. It was found that the eigenfrequencies and mode shapes between the full- and scaled-size structures were well-correlated for frequencies up to 100 Hz. Steady-state analyses showed that the vibration transmission between storeys was well-correlated up to 50 Hz, while discrepancies in resonance frequencies were found at higher frequencies.

2.2 Dimensions and materials

The outer dimensions of the structure were 2600×2400×1900 mm^3. Table 1 presents the dimensions of the floor, ceiling and walls in terms of the cross-sectional dimensions of the beams ($h \times b$), the length and centre-to-centre distance of the primary beams (l and c/c, respectively), and the thickness of the boards (t). The elastomer blocks were 45×44×24 mm^3 in size and of the type Sylodyn NB [21]. The wood beams were made of spruce and of type G4-2 according to SS-EN 1611-1 [22]. The particleboards were of type P1 according to SS-EN 312 [23] and the plasterboards were of type A according to SS-EN 520 [24].

Table 1. *Dimensions of the beams and boards in the floor, ceiling and walls. l and c/c are the length and centre-to-centre distance of the primary beams, $h \times b$ is the cross-sectional dimensions of the beams, and t is the thickness of the boards. Dimensions are in the unit of mm.*

	l	c/c	h	b	t
Floor	2280	408	93	21	10
Ceiling	2280	272	54	21	6.5
Apartment separating walls	860	408	44	22	6.5
Facade walls	860	401	69	21	6.5

2.3 Construction

The wood frames in the floor, ceiling and walls were assembled by screwing the edge beams into the ends of the primary beams. The wood frames were covered with one layer of particleboards or plasterboards. The particleboards on the floor were glued to each other at their grooved-and-tongued edges and attached to the beams using both screws and glue. The plasterboards on the ceiling and walls were attached to the wood frames using only screws, i.e. no glue. The walls contained one plasterboard each, whereas the ceiling contained three plasterboards placed next to each other. The joints between them were located on top of wood beams.

The upper room was assembled by first screwing the apartment separating walls into the sides of the edge beams of the floor. The facade walls were then screwed into the sides of the outermost primary beams of the floor and of the apartment separating walls. The lower room was constructed in the same manner. The elastomer blocks placed between the rooms were kept in place solely by frictional forces.

Figure 5. *Photograph of the measurement setup used for the upper room structure.*

3. Experimental procedure

Experimental modal analysis (EMA) was performed for the structural components, the planar structures and the room structures to extract eigenfrequencies, mode shapes and modal damping ratios. The vibration transmission in the complete structure was measured in terms of FRFs. All tests were performed with impact hammers (Brüel & Kjær 8206 and 8208) as excitation sources and piezoelectric accelerometers (Brüel & Kjær 4507-001 and 4524) to measure the vibrations. The data acquisition was performed using Brüel & Kjær LAN-XI 3050 A-060/A-042 frontends and the signal processing was carried out in PULSE Labshop/Reflex 19.0 [25]. The measurements were performed in a laboratory where the relative humidity was 50±5% and the temperature was 18±3°C for at least 48 h prior to measurements.

The structures were suspended from the laboratory ceiling using elastic bands to mimic free boundary conditions; Figure 5 shows the setup used for the upper room structure. The rigid body modes, which had frequencies between 0–1.5 Hz, were significantly lower than the elastic modes, except for the first elastic mode of the floor and of the ceiling (which were global torsion modes).

Pre-test analyses were performed to determine suitable excitation points and measurement points for the EMA. The pre-test analyses were performed by studying simulated mode shapes. These were obtained by using the initial FE model described in Section 4. Uniform grids of excitation points were used. The resolution of these grids were selected by studying the auto-MAC values of the simulated mode sets to ensure that the mode shapes could be separated from each other. Up to six accelerometers were used in each measurement and these were placed in a subset of the excitation points. Their positions were determined by finding the set of measurement points for which the minimum amplitude of the simulated mode shapes was maximised.

The measured acceleration time signals were windowed with exponential functions, while the force signals were windowed with cosine tapered functions. The modal parameters were estimated by employing methods implemented in PULSE Reflex 19.0 (rational fraction polynomial and polyreference methods). The resulting mode shapes were normalised to obtain real-valued vectors.

More details on the measurement procedure and a comprehensive presentation of the measurement results can be found in [19].

4. Initial numerical model

The first step in the multi-level approach is to create an initial FE model. This FE model was used for pre-test analyses of the experimental setups and as a starting point for the model correlations. All modelling and analyses presented in the paper were performed using Abaqus/Standard 6.13 [26].

4.1 Material models

The materials were assumed to be linear elastic, homogeneous and orthotropic. Elastic parameters were collected from a wide range of publications to identify a feasible interval for each parameter. In some publications, the parameters are presented as normal distributions; the 95% confidence limits were taken from those publications. The parameters in the initial model were chosen as the mid-points in the feasible intervals. However, the densities of the different materials were determined by weighing and measuring the dimensions of the structural components used in the experimental structure.

Parameters of spruce were collected from [27–30]. The intervals and the values used in the initial model are shown in Table 2. The parameters are given in terms of cylindrical coordinates (the longitudinal direction, L, the tangential direction, T, and the radial direction, R). E is the Young's modulus, G is the shear modulus, ν is the Poisson's ratio and ρ is the density. The parameters in the radial and tangential directions were assumed to be equal, i.e. $E_T = E_R$, $G_{LT} = G_{LR}$ and $\nu_{LT} = \nu_{LR}$.

Table 2. *Material parameters of spruce in terms of the intervals identified from literature and the values used in the initial model. Stiffness parameters are in the unit of MPa and density in kg/m^3.*

	E_L	E_T, E_R	G_{LT}, G_{LR}	G_{RT}	ν_{LT}, ν_{LR}	ν_{TR}	ρ
Lower limit	5600	230	440	21	0.34	0.20	-
Upper limit	17000	1200	1600	125	0.72	0.60	-
Initial model	11000	700	1000	73	0.53	0.40	460

Parameters of particleboard were collected from [31–33]. In [33], the parameters are distinguished between the surface layers and the core layer of the boards. In [31, 32], however, the presented parameters are independent of the thickness direction. The intervals presented here are based on all types of values. In the FE model of the experimental structure, the parameters were assumed to be independent of the thickness direction. The intervals and the values used in the initial model are presented in Table 3. Directions 1 and 2 are the in-plane directions, while 3 is the out-of-plane

direction. Direction 1 is the stiffer of the in-plane directions and was assigned to the lengthwise direction of the boards in the FE model of the experimental structure.

Table 3. *Material parameters of particleboard in terms of the intervals identified from literature and the values used in the initial model. Stiffness parameters are in the unit of MPa and density in kg/m^3.*

	E_1	E_2	E_3	G_{12}	G_{13}	G_{23}	ν_{12}	ν_{13}	ν_{23}	ρ
Lower limit	1300	1200	200	570	170	150	-0.06	0.23	0.20	-
Upper limit	5500	4800	570	1800	400	370	0.44	1.32	1.27	-
Initial model	3400	3000	390	1200	290	260	0.19	0.78	0.74	750

Parameters of plasterboard were collected from two manufacturers [34, 35] and two research papers [36, 37]. Only the Young's moduli are presented in the references; [34–36] present orthotropic parameters for the in-plane directions of the boards, while [37] presents isotropic parameters. The intervals for the remaining parameters were chosen without any a priori knowledge. The out-of-plane Young's modulus, E_3, is likely to be lower than the in-plane moduli, E_1 and E_2, because of the paper-coating of the boards, which contributes to the bending stiffness. The lower limit was therefore set to 10% of the limit for the in-plane parameters. The interval for E_3 was used also for the three shear moduli. The intervals and the values used in the initial model are presented in Table 4. Direction 1 was assigned to the length-direction of the boards in the FE model of the experimental structure.

Table 4. *Material parameters of plasterboard in terms of the intervals identified from literature and the values used in the initial model. Stiffness parameters are in the unit of MPa and density in kg/m^3.*

	E_1	E_2	E_3	G_{12}	G_{13}	G_{23}	ν_{12}	ν_{13}	ν_{23}	ρ
Lower limit	1600	1600	150	150	150	150	0.0	0.0	0.0	-
Upper limit	2500	2000	2500	2500	2500	2500	0.5	0.5	0.5	-
Initial model	2000	1800	1000	1000	1000	1000	0.25	0.25	0.25	760

The elastomers were assigned frequency-dependent viscoelastic material properties. The parameters of the material model were determined by applying the procedure presented in [18] to Sylodyn NB. In the procedure, results from FE analyses are combined with experimental data provided by manufacturers valid for the geometry of the tested elastomers and for the boundary conditions applied during the tests. The material parameters of Sylodyn NB, obtained by using the procedure, are shown in Figure 6 in terms of the real and imaginary parts of the bulk modulus, K, and the shear modulus, G.

4.2 Joints

The joints in the structure were modelled as fully coupled in the initial FE model. For the joints between beams and boards, full coupling was implemented by using one single mesh for each planar structure, so that the beams and boards shared mesh nodes. For the joints between planar structures,

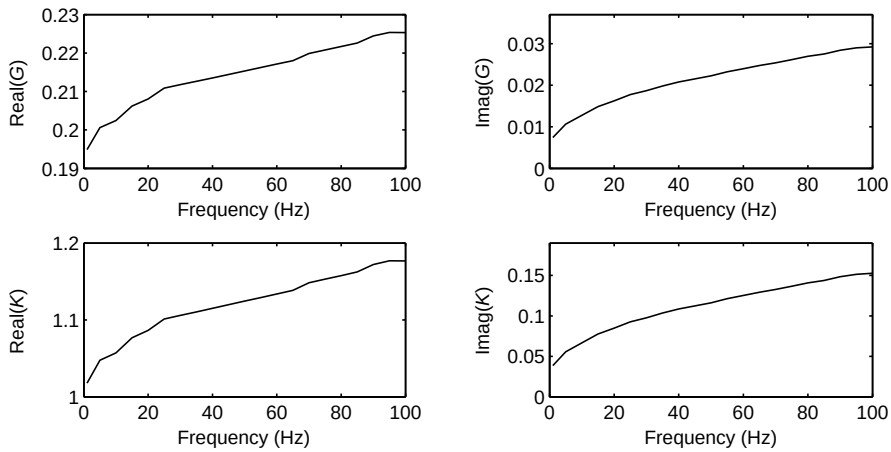

Figure 6. *Real and imaginary parts of the shear modulus, G, and of the bulk modulus, K, employed for the elastomers in the FE model. The parameters are in the unit of MPa.*

full coupling was implemented by using constraint equations tying the nodes on one part to the surface at the other part. The same approach was used for the interfaces between elastomers and room structures. The three plasterboards in the ceiling were modelled as a single continuous board in the initial model.

4.3 Finite element discretisations

The experimental structure was meshed with 20-node solid hexahedral elements with quadratic interpolation and reduced integration. The elastomer elements were, however, fully integrated to avoid spurious modes. Mesh convergence analyses were performed for the FE models of the structural components (viz. wood beams, particleboards and plasterboards) by ensuring that the errors in the eigenfrequencies in Section 5, relative to densely meshed models, were less than 0.1%. The element size for the elastomers was determined by analysing the complete structure and ensuring that the errors in the eigenfrequencies below 100 Hz were less than 0.1%. In total, the initial model was meshed with about 50,000 elements and contained approximately 830,000 DoFs.

5. Correlation of structural components

The second step in the multi-level approach is to calibrate the FE models of the structural components to obtain the material parameters that result in the best correlation between simulated and measured eigenfrequencies. Calibrations were performed for each wood beam in the structure and for two specimen each of particleboard and plasterboard. For the wood beams, the two first bending modes in each direction and the two first torsional modes were used in the calibrations. For the particleboards and plasterboards, the six lowest eigenmodes were used in the calibrations.

5.1 Calibration procedure

The calibrations were performed using the sum of the squared NRFD values as the objective function. It was ensured that the NRFD values were based on well-correlated mode shapes between simulations and measurements. For the particleboards and plasterboards, the MAC values were higher than 0.9. For the wood beams, the MAC values were higher than 0.7 and about 0.9 in average. The calibrations did not have any appreciable effect on the MAC values.

The material parameters were optimised in three steps:

1. **Sensitivity analysis.** The parameters were varied one at a time within the interval limits presented in Section 4.1, and the effects on the simulated eigenfrequencies were studied. Only the parameters with appreciable effect on the NRFD values were optimised in steps 2 and 3. For the remaining parameters, the initial values were used.

2. **Grid search.** The intervals for the material parameters given in Section 4.1 were divided into ten steps each and the objective function was evaluated for all combinations of parameter values. The results provided an estimate of the optimal parameters.

3. **Newton optimisation.** The parameters from step 2 were used as initial values for a multi-dimensional Newton optimisation. Iterations were performed until each of the parameters were updated with a maximum of 0.1% of its value.

5.2 Results

The NRFD values obtained using the calibrated models were below 4% for each measured eigenfrequency and about 1% in average. The sensitivity analyses for the wood beams unveiled that two parameters have appreciable effect on the eigenfrequencies of the wood beams, E_L and $G_{LR} = G_{LT}$. The remaining parameters affect the NRFD values with less than 0.5%. Calibrations were performed for all 90 wood beams in the experimental structure. Figure 7 shows the normal distributions of the optimised parameters; each dot along the curve represents an optimised value. For the particleboards and plasterboards, three parameters were found to have an appreciable effect on the eigenfrequencies:

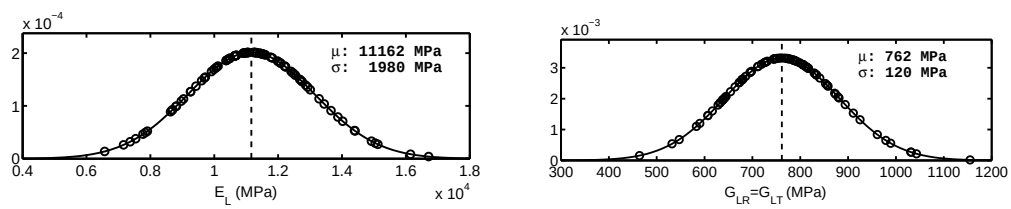

(a) *Young's modulus* E_L. (b) *Shear modulus* $G_{LR} = G_{LT}$.

Figure 7. *Normal distributions for the optimised material parameters of the wood beams. The circles represent optimised values.* μ *is the mean value and* σ *is the standard deviation.*

E_1, E_2 and G_{12}. The remaining parameters affected the NRFD values with less than 1%, except for ν_{12}, which affected the NRFD values with up to 8%. This is, however, low compared to E_1, E_2 and G_{12}, which affected the NRFD values with up to 130%. Table 5 presents mean values of the optimised parameters for the two measured specimens of particleboard and of plasterboard.

Table 5. *Optimised Young's and shear moduli for the particleboards and plasterboards. The parameters are in the unit of MPa.*

	E_1	E_2	G_{12}
Particleboard	4600	4400	1900
Plasterboard	4000	3100	1300

6. Correlation of planar structures

The third step in the multi-level approach is to correlate the FE models of the floor, ceiling and walls to measurements. The initial models were updated by involving optimised material parameters and, for some structures, the modelling of joints between beams and boards was modified. The objective of the correlations was to maximise the average of the MAC values for the measured mode shapes.

6.1 Floor

First, the effect of involving optimised material parameters were investigated by comparing three different models: (1) the initial model, denoted 'Initial', (2) a model with optimised parameters for each individual floor beam, denoted 'Individual' and (3) a model with the mean value of the optimised parameters for all floor beams, denoted 'Mean'. In the two latter models, the optimised parameters of particleboard were used. Cross-MAC matrices for the three models are shown in Figure 8. Only the 'Individual' model was able to accurately represent the mode shapes at higher frequencies; the MAC values for that model were above 0.79 for all measured eigenmodes and 0.94 in average. In comparison, the MAC values for the 'Mean' model were 0.87 in average while the lowest value was 0.41. The reason for the large difference in correlation is that the variation in material parameters among beams causes mode shapes that are neither symmetric nor asymmetric. As an example, the 12^{th} measured mode shape of the floor is shown in Figure 9 along with the corresponding simulated mode shape of the 'Individual' model. In all subsequent analyses presented in the paper, individual material parameters were used for the wood beams. Because of the high correlation obtained for the mode shapes, the joints in the floor model were not modified. Simulated and measured eigenfrequencies, and the resulting NRFD values, are shown in Figure 10. The results shown in the figure are those obtained for the 'Individual' model.

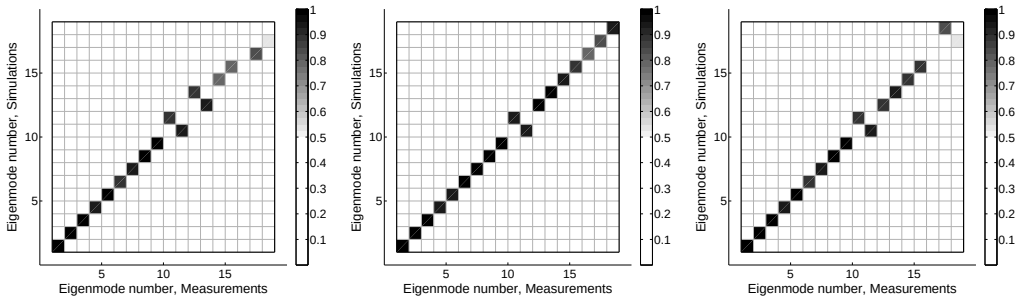

(a) *Model: Initial.* (b) *Model: Individual.* (c) *Model: Mean.*

Figure 8. *Cross-MAC for the FE models of the floor.*

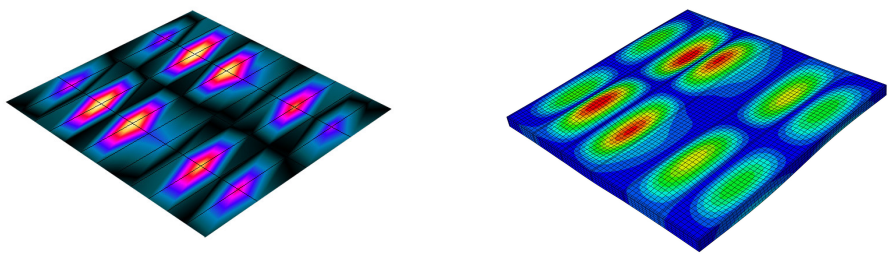

(a) *Measured mode shape at 80.0 Hz.* (b) *Simulated mode shape at 83.6 Hz, obtained using the 'Individual' model.*

Figure 9. *The 12^{th} mode shape of the floor.*

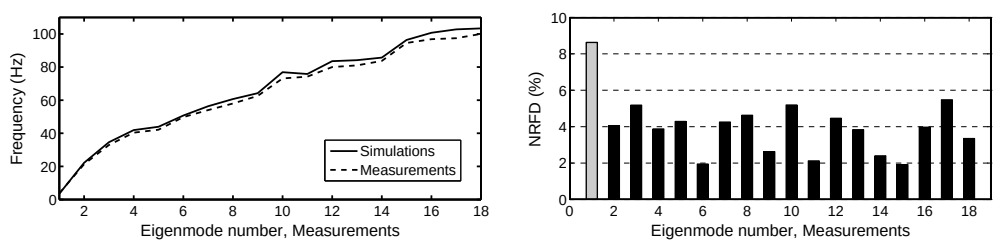

(a) *Eigenfrequencies.* (b) *NRFD values. Positive values in black and negative values in grey.*

Figure 10. *Simulated and measured eigenfrequencies, and the resulting NRFD values, for the floor. The average of the NRFD values is 4.6%.*

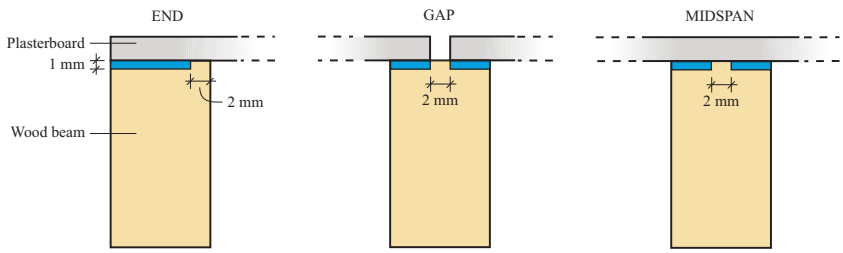

Figure 11. *Fictitious materials used for the modelling of joints between plasterboards and wood beams. The fictitious materials are shown in blue.*

6.2 Ceiling

The FE model of the ceiling was updated with the optimised material parameters for each individual wood beam. The resulting correlations were, however, not as good as for the floor. To obtain higher MAC values at higher frequencies, the modelling of the joints had to be modified. In the updated model, the gaps between the three plasterboards in the experimental structure were included by modelling them as 2 mm wide. Moreover, as illustrated in Figure 11, the joints between beams and plasterboards were modelled with interlayers of fictitious materials to obtain couplings with lower rotational stiffness. Three different fictitious materials were used, one for each type of joint shown in the figure; namely, end joints, gap joints and midspan joints. It should be noted that the end and midspan joints provide non-zero rotational stiffness for a fictitious materials with zero stiffness. The material parameters of wood were assigned to the fictitious materials, except the Young's modulus in the transversal direction, which was optimised to improve the MAC values. The Young's modulus of the three materials were optimised one at a time by maximising the average of the MAC values for the measured mode shapes. The optimisation process was re-iterated until no further improvement in the average of the MAC values was found. The Young's modulus of the fictitious materials ended up lying between 0.3–1.3% of the value for wood ($E_T = E_R$ =700 MPa).

Cross-MAC matrices for the ceiling, before and after updating the modelling of the joints, are shown in Figure 12. It can be seen that the MAC values for the higher modes were improved substantially by updating the modelling of the joints. The MAC values for the updated model were 0.90 in average and 0.59 for the least correlated mode shape; a substantial improvement when compared to 0.81 and 0.42 for the model with initial joints. Eigenfrequencies from simulations and measurements, and the resulting NRFD values, are shown in Figure 13. The results shown in the figure are those obtained after updating the modelling of the joints.

In addition to updating the rotational coupling, it was investigated if any possible slip between plasterboards and wood beams affected the correlation. The slip was represented in the ceiling model by lowering the shear modulus of a thin layer introduced between the wood beams and the plasterboards. It was found that the average of the MAC values was decreased when modelling the slip. Therefore, slip was not considered in the models discussed in the remaining part of the paper. It should be noted that the correlations were performed by considering the average of the MAC values, and that slip may improve the correlation for certain mode shapes.

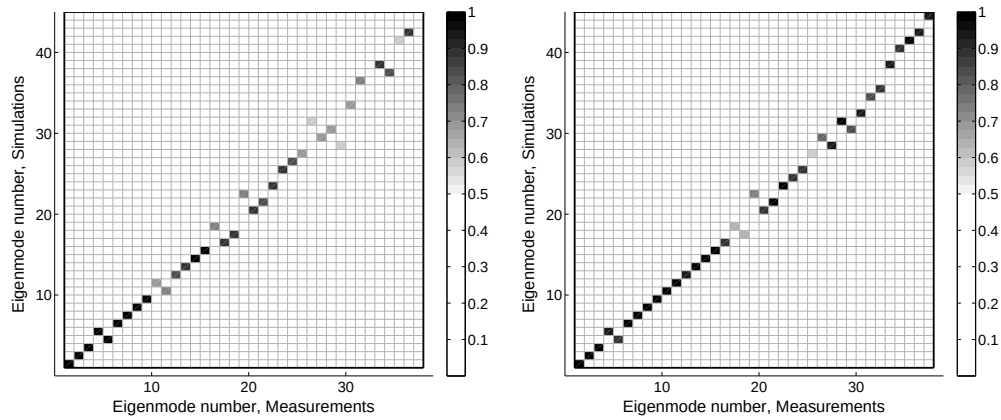

(a) *Model: Initial joints between beams and plasterboards.* (b) *Model: Updated joints between beams and plasterboards.*

Figure 12. *Cross-MAC for the FE models of the ceiling.*

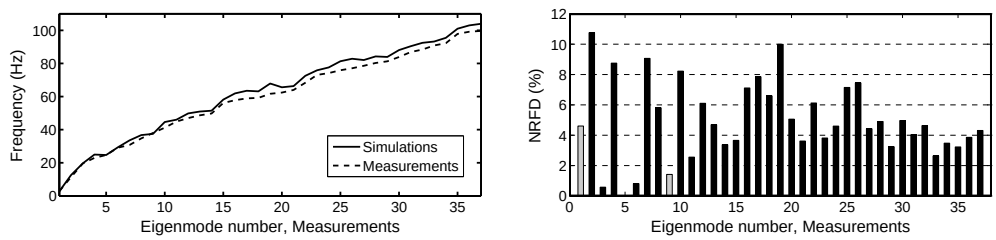

(a) *Eigenfrequencies.*

(b) *NRFD values. Positive values in black and negative values in grey.*

Figure 13. *Simulated and measured eigenfrequencies, and the resulting NRFD values, for the ceiling. The average of the NRFD values is 5.0%.*

6.3 Walls

The initial FE models of the eight walls were updated with the optimised material parameters for each individual wood beam. The joints between the wood beams and the plasterboards were modelled in the same way as for the ceiling. The walls in the experimental structure contained one plasterboard each and, therefore, no gaps between plasterboards were present. Consequently, only two fictitious material configurations were used for each wall; one for midspan joints and one for end joints (see Figure 11). The parameters of the fictitious materials were optimised for each wall. The resulting Young's modulus of the fictitious materials varied significantly among the different walls; the obtained

values were between 0.007–100% of the value for wood ($E_T = E_R$ =700 MPa). A reason for the large variations is that the measured mode shapes at higher frequencies differ substantially among the eight walls. It should be pointed out again that the models of the joints provide rotational stiffness also in the extreme case when the stiffness of the fictitious materials is zero. However, the variations in optimised values indicate that there were large variations in mechanical behaviour of the joints in the different walls.

The correlation between simulations and measurements, in terms of average and extreme values of the MAC and NRFD values, for the eight walls are presented in Table 6. The results presented in the table are those obtained after updating the modelling of the joints.

Table 6. *MAC values and NRFD values for the eight walls, presented in terms of average and extreme values for the sets of measured eigenmodes. Among the eight walls, the MAC and NRFD values are in average 0.94 and 8.5%, respectively. *Number of measured eigenmodes.*

	Apartment separating walls				Facade walls			
	1	2	3	4	1	2	3	4
No. of modes*	14	13	12	12	10	11	11	8
Model: Initial joints								
MAC, avg	0.92	0.92	0.93	0.96	0.85	0.81	0.94	0.93
MAC, min	0.73	0.52	0.62	0.77	0.50	0.43	0.71	0.81
NRFD, avg	10	10	10	11	10	11	9.6	12
NRFD, max	19	17	20	18	17	18	16	20
Model: Updated joints								
MAC, avg	0.94	0.97	0.98	0.96	0.88	0.87	0.94	0.94
MAC, min	0.72	0.85	0.85	0.78	0.67	0.52	0.73	0.85
NRFD, avg	8.7	7.6	8.8	11	4.4	7.1	9.2	11
NRFD, max	15	16	20	17	12	14	15	15

7. Correlation of room structures

In the fourth step of the multi-level approach, the simulated eigenfrequencies and mode shapes of the two room structures were correlated to measurements. The correlations were performed for frequencies below 50 Hz because the measured mode shapes at higher frequencies had high complexity, i.e. they could not be approximated as real-valued. The initial FE models of the two room structures were updated by replacing the initial FE models of the floor, ceiling and walls with the correlated models described in Section 6. When modelling full interaction of the joints between the planar structures, the correlation between simulations and measurements was poor for several mode shapes. Visual comparison of the mode shapes unveiled that the joints between planar structures were too stiff in the models of the room structures. Therefore, elastic rotational coupling was introduced between the pla-

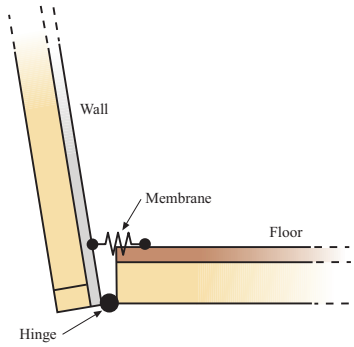

Figure 14. *Cross section of the models used for the joints between planar structures.*

nar structures by using the approach illustrated in Figure 14; the translations were constrained along a line in the joints, and an elastic membrane was inserted along the other end of the joints. By changing the stiffness of the membranes, the rotational stiffness of the joints can be modified. This modelling approach was used for the floor-to-wall, ceiling-to-wall and wall-to-wall joints. In the model of each room structure, two membrane materials were used; one for the wall-to-wall joints and one for the floor/ceiling-to-wall joints. The stiffness of the two membranes were optimised one at a time, and the optimisation process was re-iterated until no further improvement in the average of the MAC values was found. The resulting rotational stiffness was 20 kNm/rad per meter for the floor-to-wall joints, 10 kNm/rad per meter for the ceiling-to-wall joints and 15 kNm/rad per meter for the wall-to-wall joints in the upper room structure. For the wall-to-wall joints in the lower room structure, it was optimal to have no rotational stiffness.

Cross-MAC matrices for the two room structures, before and after the modelling of the joints were updated, are shown in Figure 15 (for the upper room structure) and Figure 16 (for the lower room structure). For the upper room structure, the average of the MAC values was increased from 0.77 to 0.88 when updating the models of the joints. For the lower room structure, it was increased from 0.68 to 0.85. Eigenfrequencies from the simulations and measurements, and the resulting NRFD values, are shown in Figure 17 (for the upper room structure) and in Figure 18 (for the lower room structure). The results shown in the figures are those obtained after updating the models of the joints.

8. Correlation of vibration transmission in the complete structure

In the fifth and final step of the multi-level approach, the accuracy of the predicted vibration transmission in the experimental structure was investigated by comparing simulated and measured FRFs. The transmission from three excitation points at the floor in the upper room to four measurement points in the lower room was investigated. Also, the driving point FRFs were determined by measuring the accelerations in the excitation points. The locations of the excitation points and the measurement points are shown in Figure 19. Point 3 was placed on a facade wall and point 4 was placed on an apartment separating wall.

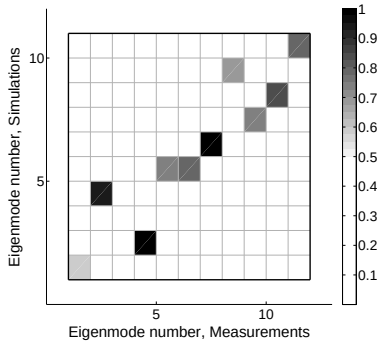

(a) *Model: Initial joints between planar structures.*

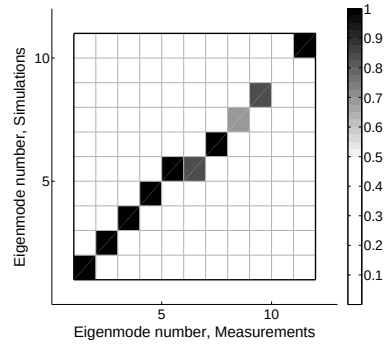

(b) *Model: Updated joints between planar structures.*

Figure 15. *Cross-MAC for the FE models of the upper room structure.*

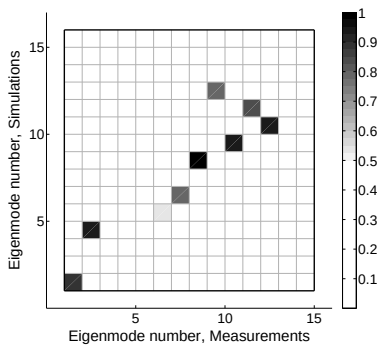

(a) *Model: Initial joints between planar structures.*

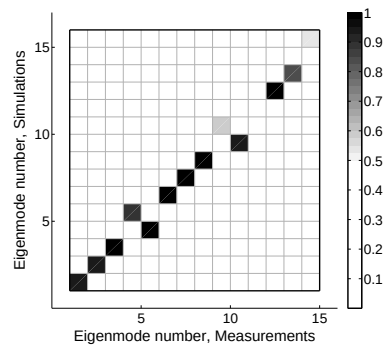

(b) *Model: Updated joints between planar structures.*

Figure 16. *Cross-MAC for the FE models of the lower room structure.*

The correlated models of the room structures were used in the model of the complete structure. A Rayleigh damping model [38] was established based on the measured modal damping ratios of the two room structures. In Rayleigh damping, the damping matrix is constructed as a linear combination of the mass matrix, $\mathbf{M}$, and stiffness matrix, $\mathbf{K}$,

$$\mathbf{C} = a_0\mathbf{M} + a_1\mathbf{K}, \tag{3}$$

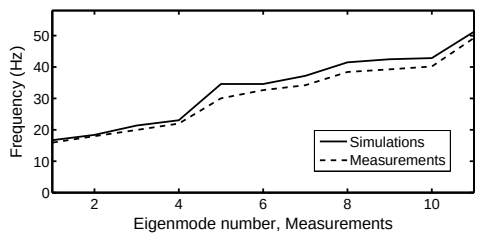

(a) *Eigenfrequencies.*

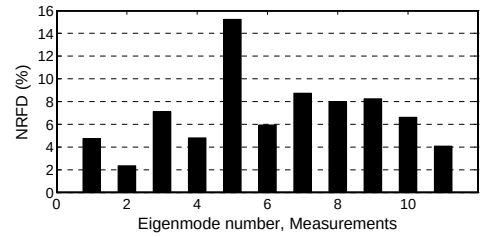

(b) *NRFD values. Positive values in black and negative values in grey.*

Figure 17. *Simulated and measured eigenfrequencies, and the resulting NRFD values, for the upper room structure. The average of the NRFD values is 6.9%.*

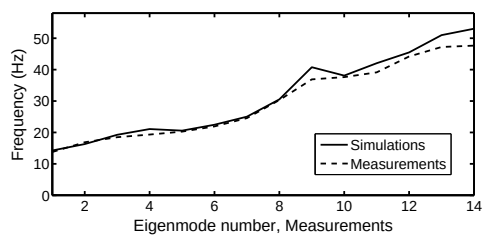

(a) *Eigenfrequencies.*

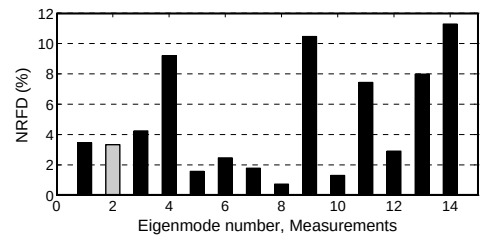

(b) *NRFD values. Positive values in black and negative values in grey.*

Figure 18. *Simulated and measured eigenfrequencies, and the resulting NRFD values, for the lower room structure. The average of the NRFD values is 4.4%.*

where a_0 and a_1 are coefficients. It can be shown that the damping ratio of the nth mode, when using Rayleigh damping, is given by

$$\zeta_n = \frac{a_0}{2\omega_n} + \frac{a_1\omega_n}{2}, \tag{4}$$

where ω_n is the angular frequency of the nth mode. The damping model for the experimental structure was established by adjusting a_0 and a_1 to obtain a function $\zeta_n(\omega_n)$ that fits well to the measured modal damping ratios of the room structures. The resulting Rayleigh damping model, obtained for $a_0 = 3.06$ and $a_1 = 3.22 \cdot 10^{-5}$, is plotted in Figure 20 along with the modal damping ratios. The damping model was assigned to the materials in the two room structures, while the damping of the elastomers was modelled through the viscoelastic material parameters shown in Figure 6.

In [39], it was shown through structure-acoustic FE simulations that the air and insulation in cavities of wood buildings affect the transmission of structural vibrations. Therefore, we investigated if the modelling of air in the cavity between the floor and the ceiling in the experimental structure affected the vibration transmission. The air cavity was discretised into 3000 acoustic finite elements with 20

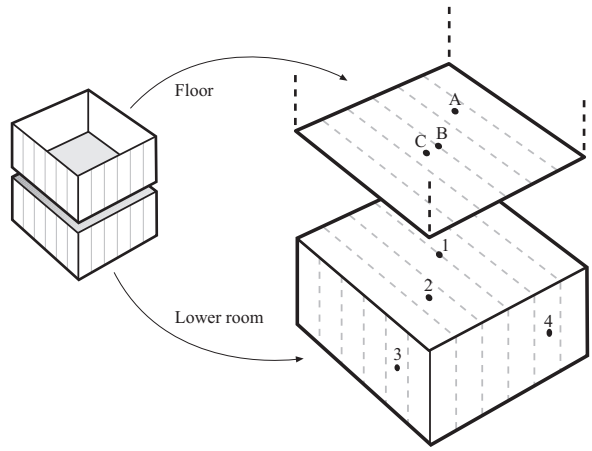

Figure 19. *Excitation and measurement points employed in the measurements of FRFs in the experimental structure. The grey dashed lines indicate wood beams. The black dashed lines indicate the walls in the upper room.*

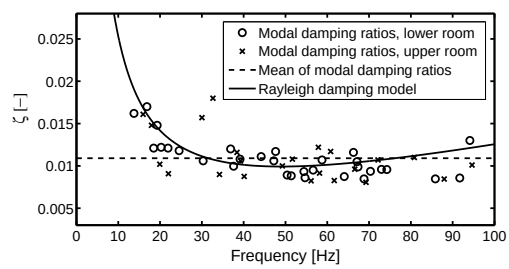

Figure 20. *Rayleigh damping model fitted to the measured modal damping ratios of the two room structures.*

nodes each and pressure as primary variable. At the boundary between the cavity and the surrounding air, atmospheric pressure was applied. Figure 21 shows simulated FRFs, obtained with and without the acoustic medium in the model, and the corresponding measured FRF. It can be observed that by modelling the air in the cavity, the simulated transmission to the lower room was increased substantially at higher frequencies. Therefore, acoustic elements were included in the model for the final comparisons between simulated and measured FRFs.

The driving point FRFs are shown in Figure 22, whereas the FRFs between floor and lower room are shown in Figure 23. It can be observed that the driving point FRFs, in general, are well correlated; the simulated and measured results display similar amplitudes and resonance peaks, although frequency shifts occur. The simulated resonance peaks are shifted about 5% towards higher frequencies compared to the measurements. Similar observations can be made for the FRFs to the lower room.

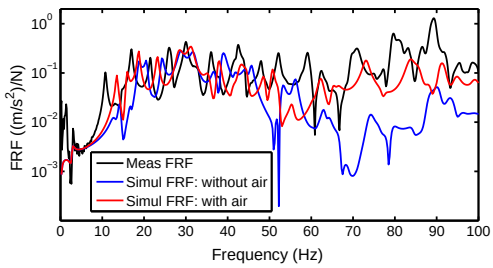

Figure 21. *Simulated FRFs with and without acoustic medium in the cavity between floor and ceiling, along with the corresponding measured FRF. The FRFs shown are for the transmission between excitation point A and measurement point 2.*

However, the simulated transmission is less accurate for frequencies above 50 Hz, where the simulated FRFs are generally of lower amplitude than the measured ones. The discrepancies are especially large for the measurement points on the walls (points 3 and 4).

The effect of the frequency shift is illustrated in Figure 24, where the frequency axis of the simulated results is scaled. The scaling was performed by multiplying the frequency axis with a linear function increasing from 0.92 to 0.97 between 0–100 Hz. Consequently, the frequencies of the simulated FRFs are decreased by 3–8%. The figure shows the simulated and measured driving point FRFs for excitation point C and the FRFs for the transmission from excitation point C to measurement point 2. It can be seen that after scaling the frequency axis, the simulated FRFs capture most of the resonance peaks in the measured data. An interpretation of the results is that the dynamic behaviour of the experimental structure was to a great extent captured by the model, but that the model had a higher stiffness. This is in line with the results of the correlations for the planar structures and the room structures, where it was found that the mode shapes were well-correlated while the simulated eigenfrequencies were about 5% higher than the measured ones.

9. Discussion

9.1 Accuracy of deterministic approach

One of the objectives in the paper is to investigate the possibilities and limitations of using deterministic methods to model low-frequency vibration transmission in wood buildings. The results presented show that the dynamic behaviour of the experimental structure was to a great extent captured by the developed model, although appreciable discrepancies were found for the vibration transmission between rooms at frequencies above 50 Hz. The errors can most likely be reduced by considering the possible sources of error discussed below. Based on the promising results, we conclude that it is relevant to employ deterministic methods provided that measurement data for calibration purposes is available. Since the correlated model captures the dynamic behaviour of the experimental structure, the simulation results can be used to understand the physics governing the vibration transmission. This

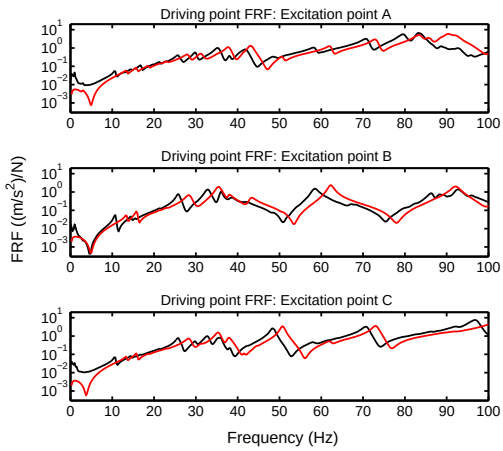

Figure 22. *Simulated and measured FRFs for the response in the excitation points on the floor. Simulated FRFs are shown in red and measured FRFs in black.*

is valuable when designing and studying measures for noise and vibration reduction. However, to obtain reliable deterministic models that can be used for predicting the relative efficiency of different designs, it should be investigated how variations in material properties and mechanical behaviour of joints affect the model output. Also, it should be investigated to what extent the many details present in real buildings, but not included in the idealised experimental structure, (for example, windows, doors, interior walls and floor surfaces) affect the results.

The effects of variations and uncertainties on the model output depend on the frequency content of the load. If, for example, the experimental structure would be subjected to single-frequency harmonic excitation, the simulated vibration levels could be several orders of magnitude wrong because of shifted resonance peaks. The errors are, in general, smaller for broadband excitations since the response is a sum of the responses at multiple frequencies, which reduces the errors caused by frequency shifts. The lightly damped properties of the experimental structure makes the errors in the simulated results especially sensitive to frequency shifts, as the resonance peaks are narrow. It should be noted that the damping in real buildings can be expected to be higher than in the experimental structure because of, for example, the mineral wool insulation and interfaces between subfloor and parquet.

9.1.1. Sources of error

A possible source of error is the assumption of atmospheric pressure for the acoustic medium at interfaces to surrounding air. The numerical investigations in [39] do, however, imply that the effect of the boundary conditions is relatively small. Another source of error related to the transmission through acoustic medium is the reflection of sound waves at the walls of the laboratory; the measurements were performed in a small laboratory ($6\times6\times3$ m^3 in size) with tiled walls.

Two possible transmission paths between the rooms in the structure exist: through the air and

through the elastomers. The dynamic properties of the elastomers were determined by using the procedure in [18], which was validated through an example case with a significantly stiffer type of elastomer than the one used in the experimental structure. Both types of elastomers are closed-cell polyurethane materials from the same manufacturer; the main difference between them is the size of the air cells, which are much larger in the elastomers used in the experimental structure. It is not verified that the procedure in [18] is equally well-suited for the elastomers in the experimental structure and this can affect the simulated vibration transmission between the rooms.

We suspect that a major source of error for the vibration transmission between rooms is that the simulated eigenfrequencies of the room structures were shifted as compared to the measured eigenfrequencies. If the two room structures have coinciding eigenfrequencies, the transmission is likely to be higher at that frequency. Consequently, if eigenfrequencies coincide in the experimental structure but not in the FE model, or the other way around, it may cause large errors. This would explain why the resonance peaks in the driving point FRFs were well represented in the simulations while discrepancies were found for the vibration transmission between the rooms.

The frequency shifts are likely to be caused mainly by the type of model used for the joints between beams and boards and between planar structures. For example, only the rotational stiffness of the joints were optimised and those optimisations were performed by studying errors in mode shapes, but not in eigenfrequencies.

9.2 Modelling guidelines and suggestions for further work

It was shown that it is important to use optimised material parameters of each individual beam to accurately simulate the mode shapes up to 100 Hz. The reason is that the variation in material parameters among beams causes mode shapes that are neither symmetric nor asymmetric. When employing statistical methods such as Monte Carlo simulations for analysing the effects of variations in material parameters, random parameters should be generated for each individual wood beam instead of using equal parameters for all beams.

The correlation studies for the floor showed that the mode shapes can be simulated with high accuracy by employing full interaction for the screwed and glued joints between wood beams and particleboards. This supports the conclusions in [15], where experimental setups of joints between wood beams and particleboards were investigated numerically and experimentally. The correlation studies for the ceiling and walls showed that modelling full interaction is erroneous for the joints between wood beams and plasterboards, which were screwed and not glued. Instead, elastic joints should be considered for the rotational coupling. This was found also for the joints between planar structures. To implement the rotational coupling in models of wood buildings, a possible approach is to optimise the parameters of different types of joints for simplified experimental setups. By performing such optimisations for a series of theoretically identical structures, statistical distributions for model parameters of joints can be obtained.

The correlation of simulated and measured vibration transmission between rooms showed that it is important to model acoustic media in cavities between floor and ceiling, especially at higher frequencies. This supports the conclusions of the numerical investigation in [39], where models with and without air and insulation in cavities of wood buildings were compared. The experimental structure

studied in the paper did not contain insulation, which is used in real buildings for thermal and sound insulation purposes. To determine suitable methods for modelling insulation in cavities, correlations between simulations and measurements could be performed for simplified setups.

An important step in the development of deterministic models for vibration transmission in wood buildings is to propagate the variations in material parameters of wood and in mechanical behaviour of joints to the model output. When statistical distributions for the stochastic parameters have been established, statistical analyses should be performed by considering the variations simultaneously. The variations in vibration transmission can thereby be estimated. The extent of the variations govern the possibilities and limitations of using deterministic methods. Large variations make it difficult to predict absolute vibration levels and to draw conclusions regarding relative effects of different designs. The models can, however, still be useful for understanding the governing physics, which is important when designing measures for noise and vibration reduction. The stochastic parameters should not only be investigated simultaneously, but also one at a time to determine the necessity of modelling them as stochastic.

10. Concluding remarks

In the paper, we present a multi-level model correlation approach for low-frequency vibration transmission in wood buildings. The approach was applied to an experimental building structure that represents a part of a two-storey building. Calibrations and correlations between simulations and measurements were performed at four levels: structural components, planar structures, room structures and the complete structure. Simulated and measured FRFs were compared for the experimental building structure and it was found that the driving point FRFs for excitations points on the floor of the experimental structure were well correlated; the simulated and measured results displayed similar amplitudes and resonance peaks, although frequency shifts were found. Similar observations were made for the vibration transmission from the floor to the ceiling and walls of the lower room, except that larger errors were found at frequencies above 50 Hz. The results indicate that the dynamic behaviour of the experimental structure was to a great extent captured by the developed model, but that the model had a higher stiffness. Based on the promising results, we conclude that it is relevant to employ deterministic methods in order to model the vibration transmission provided that measurement data for calibration purposes is available. The developed numerical model can be used as a reference model for investigations on the effects of variations and uncertainties in the modelling, and on the possibilities and limitations of using deterministic methods.

Acknowledgements

This work was supported by the Urban Tranquility project, a part of the EU program Interreg V.

References

[1] Hveem S. Nordic multi-storey timber buildings for residential housing. Internoise 2000, Nice, France.

[2] Forssén J., Kropp W., Brunskog J., Ljunggren S., Bard D., Sandberg G., Ljunggren F., Ågren A., Hallström O., Dybro H., Larsson K., Tillberg K., Sjökvist L.G., Östman B., Hagberg K., Bolmsvik Å., Olsson A., Ekstrand C.G., Johansson M. Acoustics in wooden buildings – State of the art 2008. Vinnova project 2007-01653, Report 2008:16, SP Technical Research Institute of Sweden, Stockholm.

[3] Simmon S., Hagberg K., Backman K. Acoustical performance of apartment buildings – Resident's survey and field measurements, Report 2011:58. SP Technical Research Institute of Sweden, Stockholm.

[4] Hveem S., Homb A., Hagberg K., Rindel J.H. Low-frequency footfall noise in multi-storey timber frame buildings, Report 1996:12E. NKB Work and Committee Reports, Helsinki, Finland.

[5] Sipari P. Sound insulation of multi-storey houses – A summary of Finnish impact sound insulation results. Build Acoust, 2000;7(1):15–30.

[6] Guigou-Carter C., Balanant N., Villenave M. Acoustic comfort evaluation in lightweight wood-based buildings. Forum Acusticum 2014, Krakow, Poland.

[7] Ljunggren F., Simmons S., Hagberg K. Correlation between sound insulation and occupants' perception – Proposal of alternative single number ratings of impact sound. Appl Acoust, 2014;85:57–68.

[8] International Organization for Standardization. ISO 10140-3: Acoustics – Laboratory measurement of sound insulation of building elements – Part 3: Measurements of impact sound insulation. ISO, Geneva, Switzerland, 2010.

[9] Cougenanff C. Robust design of lightweight wood-based systems in linear vibroacoustics. Doctoral thesis, Universite Paris-Est, France, 2015.

[10] Rabold A. FEM based prediction model for the impact sound level of floors. Acoustics'08, Paris, France.

[11] Kohrmann M., Buchschmid M., Müller G., Vøltl R., Schanda, U. Numerical models for the prediction of vibro-acoustical characteristics of light-weighted ceiling. Internoise 2013, Innsbruck, Austria.

[12] Buchschmid M., Müller G., Kohrmann M., Schanda U. Vibroacoustic investigation of lightweight ceilings – Modeling aspects and design guidelines. Euronoise 2015, Maastricht, Netherlands.

[13] Freij J. Genombrott för flerfamiljshus i trä. In: Skog & Ekonomi – Nyheter från Danske Bank, Nummer 1. Danske Bank Sweden, 2016.

[14] Jiang L., Hu L., Chui Y.H. Finite-element model for wood-based floors with lateral reinforcement. J Struct Eng, 2004;130(7):1097–1107.

[15] Negreira J., Sjöström A., Bard D. Low frequency vibroacoustic investigation of wooden T-junctions. Appl Acoust, 2016;105:1–12.

[16] Bolmsvik Å., Linderholt A., Brandt A., Ekevid T. FE modelling of light weight wooden assemblies – Parameter study and comparison between analyses and experiments. Eng Struct, 2014;73:125–142.

[17] Bolmsvik Å., Linderholt A. Damping elastomers for wooden constructions – Dynamic properties. Wood Mater Sci Eng, 2015;10(3):245–255.

[18] Negreira J., Austrell P.E., Flodén O., Bard D. Characterisation of an elastomer for noise and

vibration insulation in lightweight timber buildings. Build Acoust, 2014;21(4):251–276.
[19] Flodén O. Vibration measurements of a wooden building structure. Report TVSM-7162, Division of Structural Mechanics, Lund University, 2016.
[20] Flodén O., Persson K., Sandberg G. Numerical and experimental studies on scale models of lightweight building structures. In: Dynamics of Coupled Structures, Volume 4 (173–180). Springer International Publishing, 2016.
[21] Getzner Werkstoffe GmbH. Sylodyn NB, product data sheet. https://www.getzner.com/en/products/sylodyn, 2016-10-25.
[22] Swedish Standards Institute. SS-EN 1611-1: Sawn timber – Appearance grading of softwoods – Part 1: European spruces, firs, pines and Douglas firs. SIS, Stockholm, Sweden, 2000.
[23] Swedish Standards Institute. SS-EN 312: Particleboards – Specifications. SIS, Stockholm, Sweden, 2010.
[24] Swedish Standards Institute. SS-EN 520: Gypsum plasterboards – Definitions, requirements and test methods. SIS, Stockholm, Sweden, 2009.
[25] Brüel & Kjær. PULSE Reflex 19.0. 2014.
[26] Dassault Systèmes SIMULIA. Abaqus 6.13 documentation. 2013.
[27] Larsson D., Ohlsson S., Perstorper M., Brundin J. Mechanical properties of sawn timber from Norway spruce. Holz als Roh- und Werkstoff, 1998;56:331–338.
[28] Berbom Dahl K. Mechanical properties of clear wood from Norway spruce. Doctoral thesis, Norwegian University of Science and Technology, Trondheim, 2009.
[29] Kretschmann D. Wood handbook – Wood as an engineering material: Chapter 5 – Mechanical properties of wood. US Dept of Agriculture, Forest Service, Forest Products Laboratory, 2010.
[30] Danielsson H. Perpendicular to grain fracture analysis of wooden structural elements – Models and application. Doctoral thesis, Lund University, 2013.
[31] Najafi S.K., Bucur V., Ebrahimi G. Elastic constants of particleboard with ultrasonic technique. Mater Lett, 2005;59:2039–2042.
[32] Nemli G., Aydin I., Zekovic E. Evaluation of the properties of particleboard as function of manufacturing parameters. Mater Des, 2007;28:1169–1176.
[33] Wilczyński A., Kociszewski M. Determination of elastic constants of particleboard layers by compressing glued layer specimens. Wood Res, 2011;56(1):77–92.
[34] Knauf Danogips. Classic Board, product data sheet. http://byggsystem.knaufdanogips.se/index.php/filbibliotek/produktdatablad/details/24/2/produktdatablad-classic-board, 2016-10-11.
[35] Gyproc Saint-Gobain. GNE Normal, product data sheet. http://gyproc.se/node/2057, 2016-10-11.
[36] Cramer S.M., Friday O.M., White R.H., Sriprutkiat G. Mechanical properties of gypsum board at elevated temperatures. Fire and materials 2003 conference, San Fransicso, US.
[37] Rahmanian I. Thermal and mechanical properties of gypsum boards and their influence on fire resistance of gypsum board based systems. Doctoral thesis, University of Manchester, UK, 2011.
[38] Chopra A.K. Dynamics of structures. Prentice Hall, New Jersey, US, 2007.
[39] Flodén O., Negreira J., Persson K., Sandberg G. The effect of modelling acoustic media in cavities of lightweight buildings on the transmission of structural vibrations. Eng Struct 2015;83:7–16.

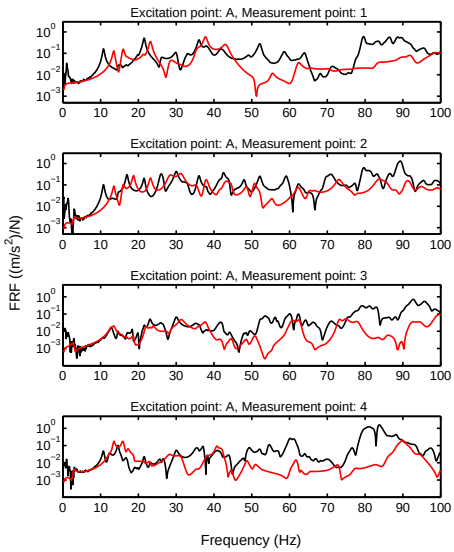

(a) *Excitation point A.*

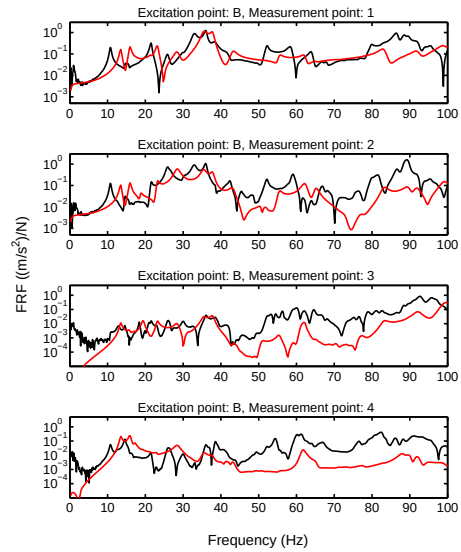

(b) *Excitation point B.*

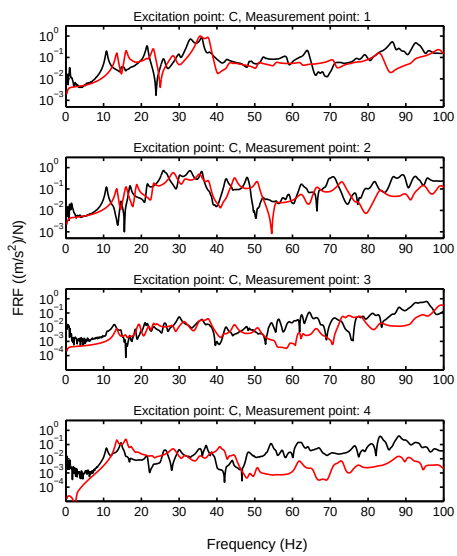

(c) *Excitation point C.*

Figure 23. *Simulated and measured FRFs for the vibration transmission from the floor to the lower room. Simulated FRFs are shown in red and measured FRFs in black.*

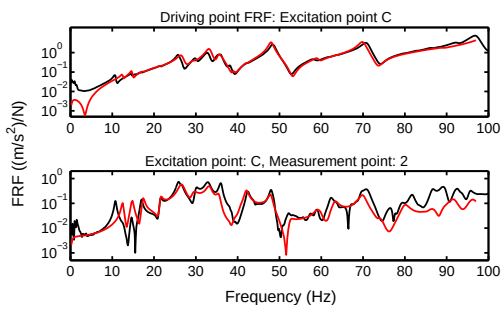

Figure 24. *Illustration of the frequency shift between simulated and measured FRFs; the frequency axis of the simulated results is scaled. Simulated FRFs are shown in red and measured FRFs in black.*

Paper E

Modelling of elastomeric vibration isolators in dynamic substructuring

O. Flodén, K. Persson, G. Sandberg

Department of Construction Sciences, Lund University, P.O. Box 118, SE-22100 Lund, Sweden

Abstract

Elastomers are used for vibration isolation in many types of structures. When performing vibration analyses of such structures, there is a need to model the elastomers in an accurate and computationally efficient manner. In this paper, we present a procedure for creating coupling elements that represent elastomers in dynamic substructuring. The coupling elements are constructed on the basis of 3D finite element models of elastomers, and they are intended for use in assembling reduced substructure models. The developed procedure involves methods for interface reduction and for a reduction of the number of internal degrees of freedom of the finite element models. A model of a wooden building structure with elastomeric vibration isolators is used as an example case to investigate the effects of using the different methods to create coupling elements. In addition, the effects of modelling features such as rotational coupling and frequency-dependent material properties in the coupling elements were investigated. It was found that the procedure for creating coupling elements can be used for establishing accurate and efficient assemblies of reduced substructure models provided that suitable methods are employed.

Keywords: elastomers, vibration isolation, dynamic substructuring, finite element method, model order reduction, interface reduction

1. Introduction

Elastomers are used for vibration isolation between structures because of their low stiffness and high strain capacity. The low stiffness is beneficial for reducing the transmission of high-frequency vibrations from a source to surrounding structures. The size of the elastomers is often small compared to the structural components between which they are placed. This is illustrated in Figure 1, and examples of such structures are machines that are placed on elastomer foundations and multi-storey buildings with elastomers between storeys. In this paper, we present research that focuses on structures where the elastomeric isolators are small compared to the structure itself.

To design structures having adequate performance in terms of vibrations and structure-borne sound, it is desirable to have tools that predict the effects of structural modifications prior to construction. The finite element (FE) method is used to create prediction models in many engineering disciplines as it allows for detailed analyses of complex problems. To accurately assess the dynamic behaviour of structures, FE models that represent the geometry in considerable detail are required. However, the models are often too large for simulations to be performed within a reasonable time, implying the

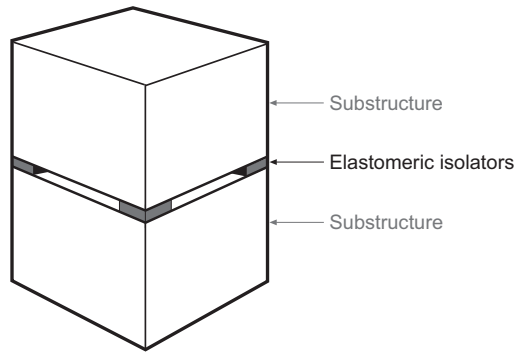

Figure 1. *Illustration of a structure involving elastomeric vibration isolators that are small compared to the structure itself.*

need for model order reduction. A methodology that is frequently used to reduce the size of the FE models is dynamic substructuring [1], which is based on a division of structures into substructures that are reduced in size and assembled to form reduced global models. The reduced system matrices are in general densely populated, especially if there is a large number of interface degrees of freedom (DOFs). Consequently, more than a few thousand DOFs per substructure can make analyses unfeasible. The structure shown in Figure 1 is preferably partitioned into substructures by making divisions at the elastomer interfaces. The resulting substructures have interface surfaces that are small relative to the complete geometry, which is an advantage when striving for a small number of interface DOFs. Furthermore, if experimental structures are available, it is often possible to divide them in the same manner. Each substructure can then be analysed both numerically and experimentally, enabling model correlation to be performed at the substructure level.

Elastomeric vibration isolators are often modelled using linear springs and dashpots. Such work can be found in, for example, [2–5]. Spring-dashpot systems are suitable for coupling substructure models as this type of system results in a small number of interface DOFs for the substructures. However, it is difficult to determine appropriate constants for the springs and dashpots; it is common that material data provided by manufacturers are valid for certain elastomer geometries and for the boundary conditions applied during specific tests. The material data obtained from manufacturers can be used to determine viscoelastic material models by employing a procedure such as the one presented in [6]. Such material models can be used in 3D FE models of elastomeric isolators with arbitrary geometries. FE models of the elastomers account for features such as rotational coupling, frequency-dependent material properties and the mass of the elastomers. However, modelling the elastomers using FE models can result in a large number of interface DOFs for the substructures, which in turn can have significant negative effects on the computational efficiency of the analyses.

In this paper, we present a procedure for creating reduced coupling elements that replace 3D FE models of elastomeric vibration isolators in dynamic substructuring. The aim of the procedure is to improve the computational efficiency of FE analyses with elastomers without impairing the accuracy

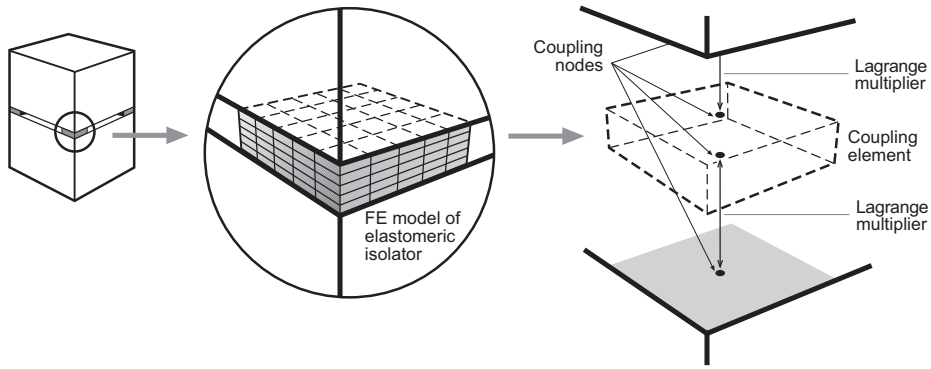

Figure 2. *Illustration of coupling elements representing elastomeric vibration isolators in dynamic substructuring.*

of the analyses. A coupling element replaces the FE model of an elastomer with a set of coupling nodes and a reduced description of its internal structure, as illustrated in Figure 2. The coupling element has one coupling node for each substructure to which the elastomer is connected. The coupling nodes have both translational and rotational DOFs, thus containing six DOFs per node. The assembling of the substructures is realised by tying the nodes of the coupling elements to adjacent substructures using Lagrange multipliers [7]. The procedure for creating coupling elements involves two steps: 1) a reduction of the number of interface DOFs and 2) a reduction of the number of internal DOFs of the elastomer models.

1.1 Outline of paper

In Section 2, we discuss the dynamic properties of elastomers and how these are accounted for in the coupling elements. In Section 3, we provide a brief introduction to dynamic substructuring, and we present the theory for the methods discussed in Section 4. In Section 4, we explain the procedure for creating coupling elements, and we discuss different methods for reducing the number of DOFs of elastomer models. In Section 5, we analyse an example case to demonstrate the effects of replacing full FE models of elastomers with coupling elements in dynamic substructuring. The example case is an FE model of a wooden building structure with elastomeric vibration isolators. The analyses were performed in the frequency domain to better account for the frequency-dependent properties of the elastomers. In Section 6, we present a general discussion of the effects of using coupling elements on the accuracy and efficiency of dynamic substructure analysis.

2. Dynamic properties of elastomers

Elastomers are a class of polymers that have high strain capacity. The long and tangled molecular chains of elastomers can stretch and align with the direction of straining, resulting in yield strains of up to several hundred percent. Examples of other characteristic properties are high vibration damping

due to energy loss from hysteresis and low stiffness compared to common construction materials such as steel, concrete and wood. Therefore, elastomers are suitable for vibration isolation. The low stiffness implies a large difference in the impedance at the interfaces to surrounding structures, thus increasing the amount of reflected vibration energy. Furthermore, the damping properties result in energy dissipation in the elastomeric vibration isolators. The dynamic properties of elastomers depend on various parameters such as temperature, frequency and the strain level. This complicates analyses where large variations of those conditions occur. For further information about the dynamic properties of elastomers, see for example [8, 9].

In the studies presented here, the elastomer properties are assumed to be frequency dependent, but independent of strain level and temperature. In other words, it is assumed that variations in strain level and temperature during steady-state dynamics have no significant effect on the response. For the example case studied here, which is a wooden building structure representing part of a residential building, such assumptions do not imply any significant limitations; vibrations are of low amplitude during serviceability conditions and the temperature is fairly constant within a building envelope. In problems where the temperature varies slowly compared to the vibration frequencies, the variations can be accounted for by creating coupling elements for each temperature of interest. The same applies for variations in the static load. The procedure presented in this paper for creating coupling elements allows for an arbitrary frequency dependence of the elastomer properties. In the example case, the frequency dependence is considered by adopting a linear viscoelastic material model for the elastomers. The material parameters employed were established in [6] for a type of elastomer that is commonly used for vibration isolation in residential buildings. The parameters, which are the complex shear modulus, G, and complex bulk modulus, K, are shown in Figure 3. The frequency dependence is the same for the two real parts and the two imaginary parts, respectively. This is a consequence of assuming Poisson's ratio to be independent of frequency. For the specific elastomer, the frequency dependence of the real parts is relatively weak, varying with 5% in the frequency range of interest. The frequency dependence of the imaginary parts is stronger, varying with 600%.

3. Governing theory

3.1 Dynamic substructuring

Substructuring is a methodology that is employed to perform analyses of structures by regarding them as assemblies of substructures. In the analysis, each substructure can be represented by a numerical model or experimentally determined functions. A historical review on dynamic substructuring and a classification of different methods can be found in [1]. In many applications, substructuring is suitable for reducing the size of numerical models. The theory presented here describes how such a reduction is performed.

In an assembly of substructure models, each substructure is described by the equation of motion as follows.

$$\mathbf{M}\ddot{\mathbf{u}} + \mathbf{C}\dot{\mathbf{u}} + \mathbf{K}\mathbf{u} = \mathbf{f}, \tag{1}$$

where $\mathbf{M}$, $\mathbf{C}$ and $\mathbf{K} \in \mathbb{R}^{n\times n}$ are the mass, damping and stiffness matrices, respectively, $\mathbf{f} = \mathbf{f}(t) \in \mathbb{R}^{n\times 1}$ is the load vector and $\mathbf{u} = \mathbf{u}(t) \in \mathbb{R}^{n\times 1}$ is the state vector. The objective of model order re-

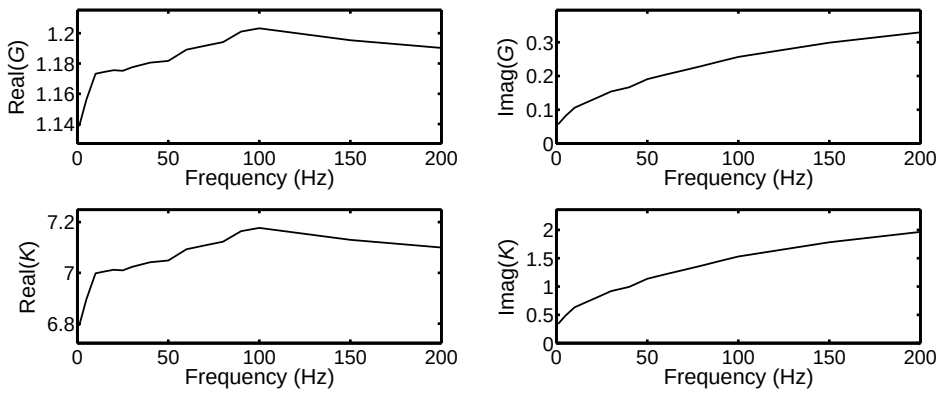

Figure 3. *Real and imaginary parts of the shear modulus, G, and of the bulk modulus, K, for the elastomer used in the example case. The parameters are in the unit of MPa.*

duction is to obtain a system of m DOFs (where $m << n$) that preserves the dynamic characteristics of the full equation system. The general approach is to approximate the state vector using the transformation $\mathbf{u} = \mathbf{T}\mathbf{u}_R$, where $\mathbf{T} \in \mathbb{R}^{n\times m}$ is the transformation matrix and $\mathbf{u}_R \in \mathbb{R}^{m\times 1}$ is the reduced state vector. This is a Ritz approximation [10] with the columns of the transformation matrix being the basis vectors. Applying the transformation to Eq. (1) results in

$$\mathbf{M}_R\ddot{\mathbf{u}}_R + \mathbf{C}_R\dot{\mathbf{u}}_R + \mathbf{K}_R\mathbf{u}_R = \mathbf{f}_R, \tag{2}$$

where the reduced mass, damping and stiffness matrices $\mathbf{M}_R, \mathbf{C}_R, \mathbf{K}_R \in \mathbb{R}^{m\times m}$ and the reduced load vector $\mathbf{f}_R \in \mathbb{R}^{m\times 1}$ are given by

$$\mathbf{M}_R = \mathbf{T}^T\mathbf{M}\mathbf{T}, \quad \mathbf{C}_R = \mathbf{T}^T\mathbf{C}\mathbf{T}, \quad \mathbf{K}_R = \mathbf{T}^T\mathbf{K}\mathbf{T}, \quad \mathbf{f}_R = \mathbf{T}^T\mathbf{f}. \tag{3}$$

In recent decades, many different methods for model order reduction have been proposed in the literature. Guyan reduction [11], improved reduction system (IRS) [12] and component mode synthesis (CMS) by Craig and Bampton [13] and by MacNeal [14] are examples of methods that were developed specifically for problems in structural dynamics. These methods generate reduced models that preserve the displacement DOFs at the interface surfaces, and they are therefore referred to as structure preserving. Moreover, reduction methods which originate from control theory, making use of Krylov subspace iterations [15] or balanced truncation [16], have gained in popularity among structural dynamic engineers in recent years. However, such methods are not structure preserving in their original form. A wide range of methods was investigated in [17] by comparing the accuracy and computation time of reduced FE models.

The DOFs in the reduced-state vector can be divided into two categories: interface DOFs and generalised coordinates. Interface DOFs can be, for example, displacements or forces in the nodes of

the substructure interfaces. Generalised coordinates generally have no physical interpretation other than being amplitudes of basis vectors contained in the transformation matrix. The coupling of substructures is normally realised by using Lagrange multipliers [7] in order to tie the interface DOFs of neighbouring substructures to each other, and thereby enforcing compatibility requirements and force equilibrium. The procedure presented in this paper for creating coupling elements assumes the reduction methods to be structure preserving. The coupling of substructures is then realised by tying the nodal displacements of neighbouring substructures to each other.

3.2 Guyan reduction

In Guyan reduction, the internal DOFs of the model are eliminated, resulting in a reduced-state vector containing only the interface DOFs. In the following derivations of the transformation matrix, the damping matrix is neglected. Partitioning the state vector in terms of the interface DOFs (also known as boundary DOFs, denoted here by subscript b) and the DOFs to be eliminated, the internal DOFs (denoted by subscript e), enables the system matrices in Eq. (1) to be partitioned into sub-blocks as

$$\begin{bmatrix} \mathbf{M}_{bb} & \mathbf{M}_{be} \\ \mathbf{M}_{eb} & \mathbf{M}_{ee} \end{bmatrix} \begin{bmatrix} \ddot{\mathbf{u}}_b \\ \ddot{\mathbf{u}}_e \end{bmatrix} + \begin{bmatrix} \mathbf{K}_{bb} & \mathbf{K}_{be} \\ \mathbf{K}_{eb} & \mathbf{K}_{ee} \end{bmatrix} \begin{bmatrix} \mathbf{u}_b \\ \mathbf{u}_e \end{bmatrix} = \begin{bmatrix} \mathbf{f}_b \\ \mathbf{f}_e \end{bmatrix}. \tag{4}$$

Solving the equation in the second row for $\mathbf{u}_e$ with the assumption that no loads are applied to the internal DOFs, $\mathbf{f}_e = \mathbf{0}$, results in

$$\mathbf{u}_e = -\mathbf{K}_{ee}^{-1} \left(\mathbf{M}_{eb}\ddot{\mathbf{u}}_b + \mathbf{M}_{ee}\ddot{\mathbf{u}}_e + \mathbf{K}_{eb}\mathbf{u}_b \right). \tag{5}$$

The inertia terms in Eq. (5) are neglected, resulting in the transformation of the state vector for Guyan reduction

$$\begin{bmatrix} \mathbf{u}_b \\ \mathbf{u}_e \end{bmatrix} = \begin{bmatrix} \mathbf{I} \\ -\mathbf{K}_{ee}^{-1}\mathbf{K}_{eb} \end{bmatrix} \mathbf{u}_b = \mathbf{T}_{\text{Guyan}}\mathbf{u}_b. \tag{6}$$

Models reduced by Guyan reduction do not introduce errors in static analysis. However, for dynamic analysis, large errors can be expected at frequencies that are close to and above the first fundamental frequency of the structure.

3.3 Component mode synthesis by Craig and Bampton

Component mode synthesis (CMS) by Craig and Bampton, which is referred to in this paper as CMS, is believed to be the most popular method for model order reduction among structural dynamic engineers. In CMS, a set of generalised coordinates, $\boldsymbol{\xi}$, is included to compensate for the inertia terms that are neglected in Guyan reduction. The generalised coordinates represent the amplitudes of eigenmodes calculated with the boundary DOFs constrained. Setting $\mathbf{u}_b = \mathbf{0}$ and $\mathbf{f}_e = \mathbf{0}$ in Eq. (4) and assuming a harmonic solution results in the eigenvalue problem

$$\mathbf{K}_{ee}\boldsymbol{\Phi} = \lambda\mathbf{M}_{ee}\boldsymbol{\Phi}, \tag{7}$$

which can be solved for the eigenmodes $\boldsymbol{\Phi}$ and the eigenvalues λ. A subset of the eigenmodes, referred to as retained eigenmodes, are selected as additional basis vectors to the approximation of the internal

DOFs in Eq. (6), resulting in

$$\mathbf{u}_e = -\mathbf{K}_{ee}^{-1}\mathbf{K}_{eb}\mathbf{u}_b + \sum_i \mathbf{\Phi}_i \xi_i = \overline{\mathbf{\Psi}}\mathbf{u}_b + \overline{\mathbf{\Phi}}\boldsymbol{\xi}. \tag{8}$$

The transformation of the state vector is then given by

$$\begin{bmatrix}\mathbf{u}_b \\ \mathbf{u}_e\end{bmatrix} = \begin{bmatrix}\mathbf{I} & \mathbf{0} \\ \overline{\mathbf{\Psi}} & \overline{\mathbf{\Phi}}\end{bmatrix}\begin{bmatrix}\mathbf{u}_b \\ \boldsymbol{\xi}\end{bmatrix} = \mathbf{T}_{\text{CMS}}\begin{bmatrix}\mathbf{u}_b \\ \boldsymbol{\xi}\end{bmatrix}. \tag{9}$$

The reduced system matrices are generally densely populated. This is caused by the basis vectors that belong to the interface DOFs. The eigenmodes, on the other hand, diagonalise the mass and stiffness matrices. Therefore, the main issue regarding computational efficiency is often the number of interface DOFs.

3.4 Interface reduction

For substructure models that have a large number of interface DOFs, it is necessary to perform an interface reduction before using one of the methods for model order reduction described above. There are essentially two methodologies for reducing the number of interface DOFs of substructures. The first is based on the concept of interface modes; deformation shapes of the interfaces that are extracted from eigenmodes of the substructure assembly [18]. The coupling of adjacent substructures is then realised by coupling the sets of generalised coordinates through Lagrange multipliers. However, the methodology is not structure preserving and the reduced substructures are not created independent of each other. Therefore, it is not investigated further here.

In the second methodology, an additional node, which is referred to as the condensation node [19], is introduced for each interface surface. A condensation node represents the motion of its interface surface, and has both translational and rotational DOFs, resulting in six DOFs per interface. The coupling of adjacent substructures is realised by coupling the condensation nodes through Lagrange multipliers. The condensation nodes can be coupled to the DOFs of their respective interface surfaces in different ways. The simplest approach is to use rigid-body constraints for the interface surface, and this is referred to as rigid coupling in this paper. Alternatively, the forces and moments acting on the condensation node can be distributed to the nodes of the interface surface by certain weight factors, and this is referred to as distributed coupling in this paper. This results in the motion of the condensation node being a weighted average of the motion of the interface nodes. The governing equations of the coupling methods are outlined below.

3.4.1. Rigid coupling

When rigid-body constraints are imposed for the interface surface and small deformations are assumed, the displacements of node j at the interface surface can be described by

$$\mathbf{u}_j = \mathbf{u}_c + \mathbf{\Theta}_c \times \mathbf{r}_{cj}, \tag{10}$$

where $\mathbf{u}_c$ and $\mathbf{\Theta}_c$ are the displacements and rotations, respectively, of the condensation node, and $\mathbf{r}_{cj}$ is the vector from the condensation node to node j at the interface surface.

3.4.2. Distributed coupling

In distributed coupling, the forces and moments acting on the condensation node, $\mathbf{f}_c$ and $\mathbf{m}_c$, respectively, are distributed to the nodes of the interface surface according to

$$\mathbf{f}_j = \hat{v}_j \left(\mathbf{f}_c + \left(\mathbf{P}^{-1} \left(\mathbf{m}_c + \mathbf{r}_c \times \mathbf{f}_c \right) \right) \times \mathbf{r}_j \right), \tag{11}$$

where $\mathbf{f}_j$ is the force acting on node j of the interface surface [20]. $\hat{v}_j$ represents the normalised value of the weight v_j in the node and is given by

$$\hat{v}_j = \frac{v_j}{\sum_j v_j}, \tag{12}$$

while $\mathbf{P}$ is given by

$$\mathbf{P} = \sum_j \hat{v}_j \left(\left(\mathbf{r}_j^T \mathbf{r}_j \right) \mathbf{I} - \left(\mathbf{r}_j \mathbf{r}_j^T \right) \right). \tag{13}$$

The spatial vectors $\mathbf{r}_c$ and $\mathbf{r}_j$ point from the weighted centre of the interface, $\bar{\mathbf{x}}$, to the condensation node and node j, respectively. They are consequently given by

$$\mathbf{r}_c = \mathbf{x}_c - \bar{\mathbf{x}} \tag{14}$$

and

$$\mathbf{r}_j = \mathbf{x}_j - \bar{\mathbf{x}}, \tag{15}$$

where

$$\bar{\mathbf{x}} = \sum_i \hat{v}_j \mathbf{x}_j. \tag{16}$$

$\mathbf{x}_c$ and $\mathbf{x}_j$ are the coordinates of the nodes. By distributing the forces and moments according to Eq. (11), the motion of the condensation node becomes a weighted average of the displacements of the nodes at the interface, according to

$$\mathbf{u}_c = \sum_j \hat{v}_j \mathbf{u}_j \tag{17}$$

and

$$\mathbf{\Theta}_c = \sum_j \hat{v}_j \frac{\mathbf{r}_{cj}}{|\mathbf{r}_{cj}|^2} \times \mathbf{u}_j, \tag{18}$$

where $\mathbf{r}_{cj}$ is the vector from the condensation node to node j at the interface surface.

The weight factors can be defined arbitrarily. Four different methods that can be used to determine the weight factors are presented below. The most straightforward method of distributed coupling is uniform weighting, which involves distributing the load equally to all nodes at the interface surface. The remaining methods employ weight factors which decrease with the distance to the condensation node by using polynomials of different degrees.

Uniform weighting

$$v_j = 1. \tag{19}$$

Linearly decreasing weighting

$$v_j = 1 - \frac{|\mathbf{r}_{cj}|}{|\mathbf{r}_{c0}|}, \tag{20}$$

where $\mathbf{r}_{c0}$ is the vector from the condensation node to the furthest node at the interface surface.

Quadratically decreasing weighting

$$v_j = 1 - \left(\frac{|\mathbf{r}_{cj}|}{|\mathbf{r}_{c0}|}\right)^2. \tag{21}$$

Cubically decreasing weighting

$$v_j = 1 - 3\left(\frac{|\mathbf{r}_{cj}|}{|\mathbf{r}_{c0}|}\right)^2 + 2\left(\frac{|\mathbf{r}_{cj}|}{|\mathbf{r}_{c0}|}\right)^3. \tag{22}$$

3.5 Steady-state analysis

The steady-state response of dynamic systems is obtained by assuming harmonic loading $\mathbf{f} = \hat{\mathbf{f}}e^{\mathrm{i}\omega t}$ and a harmonic response $\mathbf{u} = \hat{\mathbf{u}}e^{\mathrm{i}\omega t}$ in the equation of motion defined in Eq. (1). $\hat{\mathbf{f}}$ and $\hat{\mathbf{u}}$ are complex frequency-dependent amplitudes, i is the imaginary unit and ω is the angular frequency. Introducing this assumption results in the equation of motion in the frequency domain

$$\mathbf{D}(\omega)\,\hat{\mathbf{u}} = \hat{\mathbf{f}}, \tag{23}$$

where the dynamic stiffness matrix $\mathbf{D}(\omega)$ is given by

$$\mathbf{D}(\omega) = -\omega^2\mathbf{M} + \mathrm{i}\omega\mathbf{C} + \mathbf{K}. \tag{24}$$

4. Procedure for creating coupling elements

In this section, we present a procedure for creating coupling elements which represent elastomeric vibration isolators in dynamic substructuring. The procedure uses 3D FE models as the input, and consists of two steps, as illustrated in Figure 4 for an elastomer in the shape of a block. The elastomer in the figure has two interface surfaces, one on its top and one on its bottom. In the first step of the procedure, interface reduction is performed by introducing condensation nodes (marked by black dots in the figure). The second step consists of a reduction of the number of internal DOFs by replacing the nodal DOFs of the FE model with a reduced description of the interaction between the condensation nodes. The methods listed in Figure 4 are discussed in Sections 4.1 and 4.2, and are used for

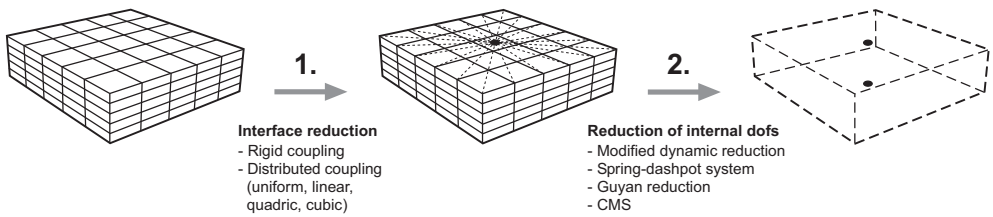

Figure 4. *Illustration of the procedure for creating coupling elements representing elastomers.*

an example case in Section 5. In the derivations of the methods presented here, the elastomers are each assumed to have two interface surfaces. However, the methods can be employed for elastomers with more than two interface surfaces. The methods can be used in several commercial FE software packages, e.g. Abaqus [20] and Nastran [21]; some methods are implemented and others require user-implemented functionality to be used in the software. Methods other than those which are discussed here can, if necessary, be used in the procedure.

4.1 Interface reduction

The reduction of the number of DOFs at interfaces between elastomers and adjacent substructures is performed by introducing one condensation node for each interface surface of the elastomers and of the substructures. The coupling of substructures is then realised by connecting the condensation nodes of the coupling elements to those of the substructures through Lagrange multipliers, as illustrated in Figure 2. The coupling between a condensation node and the DOFs at its interface surface, as illustrated in Figure 4, can be performed by using one of the coupling methods described in Section 3.4. Other types of distributed coupling, which are obtained by selecting the weights in alternative ways, could also be used. The constraints between the condensation node and the DOFs at the interface surface are enforced through Lagrange multipliers. The number of constraint equations resulting from rigid coupling depends on the number of DOFs at the interface surface, whereas distributed coupling requires only six equations per condensation node. Each constraint equation requires a Lagrange multiplier and, consequently, rigid coupling requires a larger number of DOFs to be realised.

4.2 Reduction of internal DOFs

Here, we discuss three methods which are employed to reduce the number of internal DOFs of elastomers. The equation of motion in the frequency domain for an interface-reduced FE model can be partitioned in terms of interface DOFs and internal DOFs, resulting in

$$\begin{bmatrix} \mathbf{D}_{bb}\left(\omega\right) & \mathbf{D}_{be}\left(\omega\right) \\ \mathbf{D}_{eb}\left(\omega\right) & \mathbf{D}_{ee}\left(\omega\right) \end{bmatrix} \begin{bmatrix} \hat{\mathbf{u}}_b \\ \hat{\mathbf{u}}_e \end{bmatrix} = \begin{bmatrix} \hat{\mathbf{f}}_b \\ \hat{\mathbf{f}}_e \end{bmatrix}, \tag{25}$$

where

$$\hat{\mathbf{u}}_b = \begin{bmatrix} \hat{u}_x^1 & \hat{u}_x^2 & \hat{u}_y^1 & \hat{u}_y^2 & \hat{u}_z^1 & \hat{u}_z^2 & \hat{\Theta}_x^1 & \hat{\Theta}_x^2 & \hat{\Theta}_y^1 & \hat{\Theta}_y^2 & \hat{\Theta}_z^1 & \hat{\Theta}_z^2 \end{bmatrix}^{\mathrm{T}} \tag{26}$$

and

$$\hat{\mathbf{f}}_b = \begin{bmatrix} \hat{f}_x^1 & \hat{f}_x^2 & \hat{f}_y^1 & \hat{f}_y^2 & \hat{f}_z^1 & \hat{f}_z^2 & \hat{m}_x^1 & \hat{m}_x^2 & \hat{m}_y^1 & \hat{m}_y^2 & \hat{m}_z^1 & \hat{m}_z^2 \end{bmatrix}^{\mathrm{T}}. \tag{27}$$

u_l^k and Θ_l^k are the displacements and rotations, respectively, in the condensation nodes, and f_l^k and m_l^k are the corresponding forces and moments, respectively. k specifies the direction (x, y or z) and l denotes the node number (1 or 2). The methods discussed below are structure preserving, i.e they can be used to construct reduced systems where $\mathbf{u}_b$ is preserved.

4.2.1. Modified dynamic reduction

The use of Guyan reduction on the dynamic stiffness matrix is known as dynamic reduction [22]. When performing dynamic reduction, the dynamic stiffness matrix is evaluated at a chosen frequency. The resulting reduced system yields fully accurate results for steady-state analysis at that specific frequency. The idea of the method proposed here is to perform such a reduction for all frequencies of interest, resulting in the internal DOFs of the elastomers being eliminated without introducing errors. The dynamically reduced system of an elastomer is given by

$$\mathbf{D}^{red}(\omega)\,\hat{\mathbf{u}}_b = \hat{\mathbf{f}}_b, \tag{28}$$

where the reduced dynamic stiffness matrix, $\mathbf{D}^{red}(\omega)$, contains the inverse of the transfer functions between forces and displacements, and between moments and rotations. Because of the frequency-dependent stiffness and damping properties of elastomers, the dynamic stiffness matrix takes the form

$$\mathbf{D}^{red}(\omega) = -\omega^2\mathbf{M}^{red} + \mathrm{i}\omega\mathbf{C}^{red}(\omega) + \mathbf{K}^{red}(\omega). \tag{29}$$

In practice, $\mathbf{D}^{red}(\omega)$ is obtained by performing steady-state analyses for the interface-reduced elastomer models, i.e. solving Eq. (25) for a range of frequencies. The analyses are performed when applying a unit amplitude in each DOF in $\mathbf{u}_b$, whilst constraining its remaining DOFs, such that

$$\hat{\mathbf{u}}_b = \mathbf{I}_j = [0 \ldots 0 \underset{j}{1} 0 \ldots 0]^{\mathrm{T}} \tag{30}$$

for $j = 1, \ldots 12$. Moreover, no loads are applied to the internal DOFs, $\hat{\mathbf{f}}_e = \mathbf{0}$. Consequently, Eq. (25) can be written as

$$\begin{bmatrix} \mathbf{D}_{bb}(\omega) & \mathbf{D}_{be}(\omega) \\ \mathbf{D}_{eb}(\omega) & \mathbf{D}_{ee}(\omega) \end{bmatrix} \begin{bmatrix} \mathbf{I}_j \\ \hat{\mathbf{u}}_e \end{bmatrix} = \begin{bmatrix} \hat{\mathbf{f}}_b \\ \mathbf{0} \end{bmatrix}, \tag{31}$$

from which $\hat{\mathbf{f}}_b$ can be determined. Using Eq. (28), the jth column of $\mathbf{D}^{red}(\omega)$ is given by

$$\mathbf{D}^{red}_{:,j}(\omega) = \mathbf{D}^{red}(\omega)\,\mathbf{I}_j = \hat{\mathbf{f}}_b. \tag{32}$$

Therefore, the reduced dynamic stiffness matrix is determined by evaluating forces and moments in the condensation nodes. To resolve the frequency dependence of $\mathbf{D}^{red}(\omega)$, the analyses should be performed for a sufficiently large number of frequencies.

To employ dynamic reduction for models developed in commercial FE software, user-defined ele-

ments can be implemented so that the dynamic stiffness matrix is read from a file for each frequency in steady-state analysis. In Abaqus/Standard 6.13, which is used in the numerical studies presented here, damping cannot be implemented in user-defined elements for analyses in the frequency domain. Consequently, only the stiffness and mass matrices in Eq. (29) were implemented in the user-defined elements. Damping was accounted for by using six dashpot elements, as described for the spring-dashpot system in Section 4.2.2. Errors are thus introduced in the reduced representation of the elastomers. In this study, dynamic reduction, which accounts for damping by using dashpots, is referred to as *modified dynamic reduction*.

4.2.2. Spring-dashpot system

This method is based on the one employed in [2], where elastomeric vibration isolators were modelled using three spring-dashpot elements which couple the displacements in the three axial directions. The couplings are modified here to include rotational DOFs and frequency-dependent properties. Hence, the internal DOFs of an elastomer model are replaced by six frequency-dependent spring-dashpot elements which couple the displacements and rotations of the two condensation nodes. The equation of motion in Eq. (25) is then reduced to

$$\mathbf{D}^{sd}(\omega)\,\hat{\mathbf{u}}_b = \hat{\mathbf{f}}_b, \tag{33}$$

where

$$\mathbf{D}^{sd}(\omega) = \mathrm{i}\omega\mathbf{C}^{sd}(\omega) + \mathbf{K}^{sd}(\omega) \tag{34}$$

and the superscript sd denotes matrices belonging to the spring-dashpot system. The damping and stiffness matrices are given by

$$\mathbf{C}^{sd}(\omega) = \begin{bmatrix} \mathbf{C}_{ux}(\omega) & \mathbf{0} & \cdots & & \cdots & \mathbf{0} \\ \mathbf{0} & \mathbf{C}_{uy}(\omega) & & & & \\ \vdots & & \mathbf{C}_{uz}(\omega) & & & \\ & & & \mathbf{C}_{\Theta x}(\omega) & & \vdots \\ \vdots & & & & \mathbf{C}_{\Theta y}(\omega) & \mathbf{0} \\ \mathbf{0} & \cdots & & \cdots & \mathbf{0} & \mathbf{C}_{\Theta z}(\omega) \end{bmatrix} \tag{35}$$

and

$$\mathbf{K}^{sd}(\omega) = \begin{bmatrix} \mathbf{K}_{ux}(\omega) & \mathbf{0} & \cdots & & \cdots & \mathbf{0} \\ \mathbf{0} & \mathbf{K}_{uy}(\omega) & & & & \\ \vdots & & \mathbf{K}_{uz}(\omega) & & & \\ & & & \mathbf{K}_{\Theta x}(\omega) & & \vdots \\ \vdots & & & & \mathbf{K}_{\Theta y}(\omega) & \mathbf{0} \\ \mathbf{0} & \cdots & & \cdots & \mathbf{0} & \mathbf{K}_{\Theta z}(\omega) \end{bmatrix}. \tag{36}$$

The six subsystems, one for each spring-dashpot element, have the same form. The one describing u_x is given by

$$i\omega \mathbf{C}_{ux}(\omega) \begin{bmatrix} \hat{u}_x^1 \\ \hat{u}_x^2 \end{bmatrix} + \mathbf{K}_{ux}(\omega) \begin{bmatrix} \hat{u}_x^1 \\ \hat{u}_x^2 \end{bmatrix} = \begin{bmatrix} \hat{f}_x^1 \\ \hat{f}_x^2 \end{bmatrix}, \tag{37}$$

where

$$\mathbf{C}_{ux}(\omega) = c_{ux}(\omega) \begin{bmatrix} 1 & -1 \\ -1 & 1 \end{bmatrix}, \quad \mathbf{K}_{ux}(\omega) = k_{ux}(\omega) \begin{bmatrix} 1 & -1 \\ -1 & 1 \end{bmatrix}. \tag{38}$$

$c_{ux}(\omega)$ and $k_{ux}(\omega)$ are the frequency-dependent damping and stiffness coefficients, respectively. To determine the coefficients, it is assumed that $\hat{u}_x^1 = 1$ and $\hat{u}_x^2 = 0$, resulting in

$$\mathrm{i}\omega c_{ux}(\omega) + k_{ux}(\omega) = \hat{f}_x^1(\omega). \tag{39}$$

$\hat{f}_x^1(\omega)$ is obtained by adopting the procedure for determining the reduced dynamic stiffness matrix, see Section 4.2.1. The coefficients can then be calculated as

$$c_{ux}(\omega) = \frac{1}{\omega}\mathrm{Im}\left(\hat{f}_x^1(\omega)\right), \quad k_{ux}(\omega) = \mathrm{Re}\left(\hat{f}_x^1(\omega)\right). \tag{40}$$

The coefficients for the remaining five subsystems can be determined in the same manner. From Eq. (29) and Eq. (32), it is found that

$$\hat{f}_x^1(\omega) = -\omega^2 \mathbf{M}_{11}^{red} + \mathrm{i}\omega \mathbf{C}_{11}^{red}(\omega) + \mathbf{K}_{11}^{red}(\omega), \tag{41}$$

which results in

$$\mathrm{Im}\left(\hat{f}_x^1(\omega)\right) = \omega \mathbf{C}_{11}^{red}(\omega), \quad \mathrm{Re}\left(\hat{f}_x^1(\omega)\right) = -\omega^2 \mathbf{M}_{11}^{red} + \mathbf{K}_{11}^{red}(\omega). \tag{42}$$

By comparing Eq. (40) with Eq. (42), it can be seen that the spring coefficients contain contributions from both the stiffness and the mass of the full elastomer model.

4.2.3. Guyan reduction and component-mode synthesis

The elastomers can be treated in the same way as the substructures to which they are connected by using one of the reduction methods developed for constant system matrices, e.g. Guyan reduction or CMS. The material properties then have to be evaluated at a discrete frequency so that the frequency dependence of the damping and stiffness matrices in Eq. (34) is eliminated.

5. Example case

As an example case, we used an FE model of a wooden building structure. It was used for studying the effects of replacing FE models of elastomeric vibration isolators with reduced coupling elements in dynamic substructuring. The example model represents a cut-out from a common type of multi-storey wood building, timber volume element building (for more details, see [23]). The model consists of a floor and a ceiling with elastomeric isolators in-between. We investigated the effects of using the

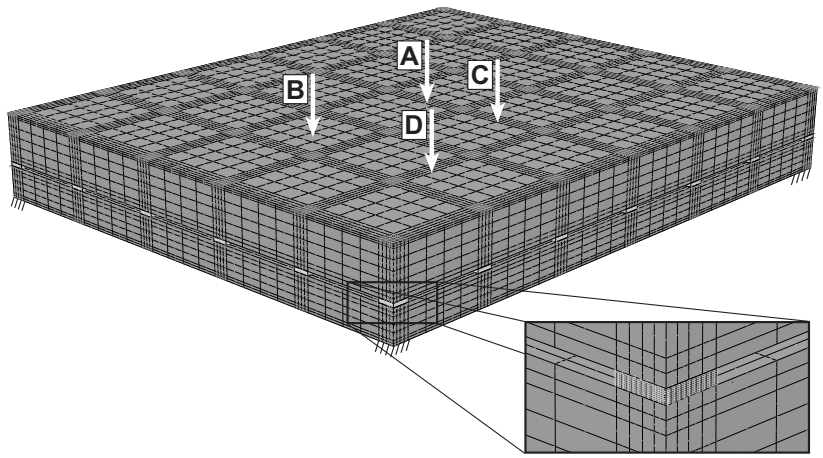

Figure 5. *FE mesh for the model of the floor–ceiling structure. The floor and the ceiling are shown in grey and the elastomer blocks in white.*

reduced models on the accuracy and efficiency of analyses of the vibration transmission from the floor to the ceiling.

In Sections 5.2 and 5.3, we present results regarding the use of different methods for interface reduction and for the reduction of internal DOFs of the elastomer models. In Section 5.4, we present the results obtained when using the coupling elements together with reduced substructure models of the floor and of the ceiling. Moreover, we investigated the effects of considering different modelling features for the elastomers (mass, damping, frequency-dependence and rotational coupling) in the coupling elements; the results are presented in Section 5.5. We employed Abaqus/Standard 6.13 to create the model and perform the analyses.

5.1 FE model

The FE model is shown in Figure 5 and consists of two wood-framed structures: a floor and an underlying ceiling. The two structures are coupled through 28 elastomer blocks. The floor and the ceiling each consist of five load-bearing wood beams (having cross-sections of 95×220 mm^2 and 95×120 mm^2, respectively), separated by centre-to-centre distances of 600 mm. A 22 mm thick particleboard covers the floor beams, while a 13 mm thick plasterboard is attached to the underside of the ceiling beams. Furthermore, wood beams are placed at the ends of the load-bearing beams, perpendicular to these, creating box-like structures. The elastomer blocks, which are $95\times100\times25$ mm^3 large, provide the only connection between the floor and the ceiling, and are placed with a centre-to-centre distance of 600 mm along the outermost beams. The outer dimensions of the complete model are $3700\times3000\times510$ mm^3.

The orthotropic material properties listed in Table 1 were used for the wood beams, and the isotropic properties listed in Table 2 were used for the particleboard and the plasterboard. The frequency-

dependent viscoelastic material properties shown in Figure 3 were used for the elastomers. The FE mesh consists of 20-node solid hexahedral elements with quadratic interpolation. Reduced integration was used for the elements of the wood structures, while full integration and independent interpolation of the hydrostatic pressure was used for the elastomer elements. The model contains 630,000 DOFs, of which 300,000 belong to the elastomer blocks. The beams and the plates were fully fixed to each other by having common interface DOFs. Before introducing the coupling elements in the model, the interfaces between elastomers and wood structures were modelled by tying the DOFs of the elastomer interfaces to the wood interfaces using Lagrange multipliers. The elastomers have 1000 DOFs per interface surface, and the wood structures have 200 DOFs per interface surface. A global damping ratio of 6% was determined from the measurement data presented in [24], and this was assigned to all materials except for the elastomers. A damping matrix was constructed using the Rayleigh method, see for example [25], selecting the constants for the mass- and stiffness proportionality to be 17 and $9.8 \cdot 10^{-5}$, respectively.

Table 1. *Material parameters used for wood beams. Stiffness parameters in MPa and density in kg/m^3.*

E_1	E_2	E_3	G_{12}	G_{13}	G_{23}	ν_{12}	ν_{13}	ν_{23}	ρ
8500	350	350	700	700	50	0.2	0.2	0.3	430

Table 2. *Material parameters used for particleboard and plasterboard. Stiffness parameters in MPa and density in kg/m^3.*

	E	ν	ρ
Particleboard	3000	0.3	770
Plasterboard	2000	0.2	690

The properties of the elastomers result in frequency-dependent system matrices. Therefore, eigenvalue analyses are not applicable for comparing the performance of the coupling elements. Instead, steady-state analyses were performed for frequencies up to 200 Hz in steps of 1 Hz. Vertical point loads with unit amplitude were applied at four different positions on the floor surface, as shown in Figure 5, while the displacements at the four corners of the ceiling surface were clamped. The four loads are referred to here as loads A–D. Three of the loads, A–C, were in-between beams, while load D was on top of a beam. Accelerations were evaluated in the nodes at the ceiling surface. Root-mean-square (RMS) values of the accelerations in all nodes at the surface were calculated as

$$a_{RMS}(f) = \sqrt{\frac{1}{n}\sum_{i=1}^{n} |\hat{a}_i\,(f)\,|^2}, \tag{43}$$

where f is the frequency, $\hat{a}_i$ is the complex acceleration amplitude in node i and n is the number of nodes. The accuracy when using the coupling elements was evaluated by studying errors in RMS

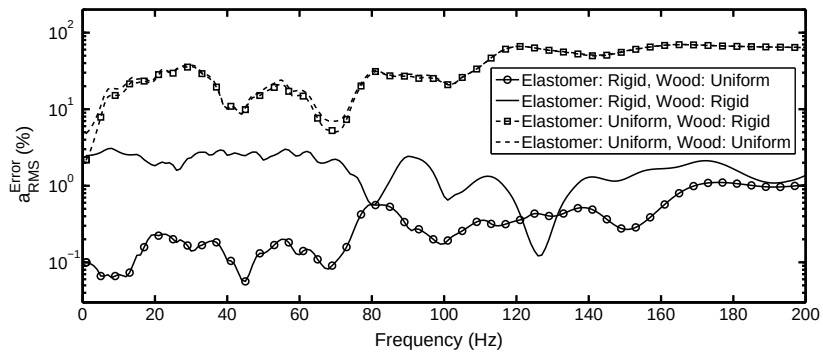

Figure 6. *Error spectra obtained when applying load A and using different combinations of rigid coupling and uniformly distributed coupling for the interfaces of the elastomers and of the wood structures. The full model was used as reference.*

values compared to a reference model. In Sections 5.2–5.4, the reference models are specified. Error spectra were calculated as

$$a^{Error}_{RMS}(f) = \frac{\left| a_{RMS}(f) - a^{Ref}_{RMS}(f) \right|}{a^{Ref}_{RMS}(f)}, \tag{44}$$

where $a^{Ref}_{RMS}(f)$ is the spectrum of RMS values of the reference model. To simplify the interpretation of the result plots presented here, the error spectra were averaged by sweeping a 10 Hz window over the frequency range and calculating the average value within the window for each frequency step. Below 6 Hz and above 195 Hz, smaller windows were used to fit within the analysed frequency range, 1–200 Hz.

5.2 Interface reduction

The various methods presented in Section 3.4 for coupling a condensation node to an interface surface were investigated for the floor-ceiling model with full FE models of the elastomers. Different combinations of rigid coupling and distributed coupling were employed for the interfaces of the elastomers and of the wood structures. The same coupling type was applied for all interface surfaces of each material. Figure 6 shows the error spectra obtained when using the full model as reference and applying load A. Only one type of distributed coupling, uniform weighting, is included in the figure. It can be seen that distributed coupling for the elastomer interfaces resulted in large errors as compared to rigid coupling, irrespective of the coupling method used for the wood interfaces.

Figure 7 shows the error spectra obtained when applying load A and using the different coupling methods for the wood structures. Rigid coupling was used for the elastomers. It can be observed that rigid coupling for the wood structures resulted in the largest errors at lower frequencies. For frequencies above 120 Hz, the error levels are similar among the different types of coupling. Of

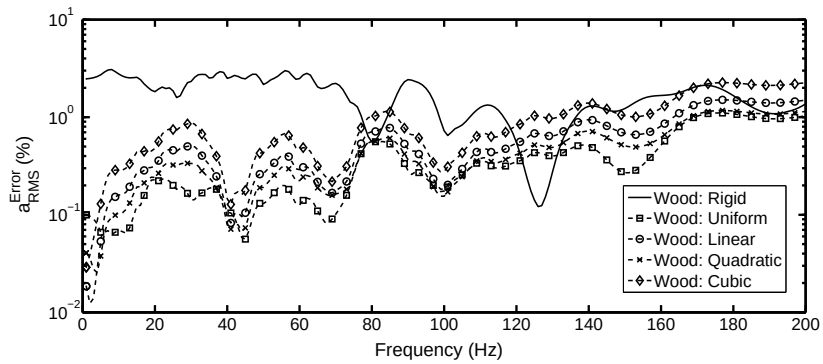

Figure 7. *Error spectra obtained when applying load A and using different coupling methods for the wood structures and rigid coupling for the elastomers. The full model was used as reference.*

the distributed coupling types, uniform weighting was the most accurate. The error spectra for the responses to loads B–D show the same trends. Table 3 shows the mean and maximum values of the error spectra for the responses to the different loads. For all loads, uniformly distributed coupling resulted in the lowest error levels in terms of both mean and maximum values. The maximum error was then below 2% for all the investigated loads.

Table 3. *Mean and maximum values of the error spectra obtained when employing different coupling methods for the wood structures and rigid coupling for the elastomers.*

	Mean error (%)				Maximum error (%)			
Coupling method	Load A	Load B	Load C	Load D	Load A	Load B	Load C	Load D
Rigid	1.7	1.5	1.4	1.4	5.4	6.4	4.9	6.3
Uniform	0.4	0.5	0.4	0.2	1.1	1.3	1.1	0.5
Linear	0.6	0.7	0.6	0.3	1.5	1.8	1.4	0.9
Quadratic	0.5	0.5	0.5	0.2	1.2	1.4	1.1	0.7
Cubic	0.9	1.0	1.0	0.4	2.3	2.7	2.0	1.6

5.3 Reduction of internal DOFs of elastomers

The methods for reducing the number of internal DOFs discussed in Section 3.4 were employed for the floor–ceiling model with reduced interfaces. For Guyan reduction and CMS, the material properties were evaluated at 100 Hz. The CMS model contained 10 retained eigenmodes. Figure 8 shows the error spectra when applying load A. The errors were calculated using the interface-reduced model as reference. It can be observed that modified dynamic reduction resulted in the lowest error levels for all frequencies. Guyan reduction and CMS resulted in error spectra that are nearly identical to each other. The spring-dashpot system resulted in error levels that are similar to those for Guyan reduction, except at low frequencies where the errors are smaller.

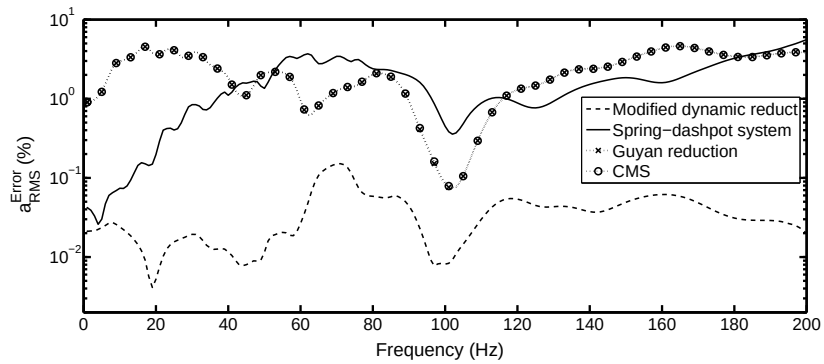

Figure 8. *Error spectra obtained when applying load 1 and using different methods to reduce the internal DOFs of the elastomers. The interface-reduced model was used as reference.*

The mean and maximum values of the error spectra for the responses to the different loads are shown in Table 4. The errors introduced by modified dynamic reduction are small compared to those from the interface reduction. However, the errors introduced by the remaining three methods are relatively dominant.

Table 4. *Mean and maximum values of the error spectra obtained when employing different methods to reduce the internal DOFs of the elastomers.*

	Mean error (%)				Maximum error (%)			
Method	Load A	Load B	Load C	Load D	Load A	Load B	Load C	Load D
Modif dyn reduct	0.04	0.03	0.03	0.02	0.3	0.1	0.2	0.1
Spring-dashpot syst	1.8	1.4	1.8	1.6	6.5	4.1	7.0	7.0
Guyan reduct	2.3	2.4	2.3	2.5	7.4	7.9	8.5	7.9
CMS	2.3	2.4	2.3	2.5	7.4	7.9	8.5	7.9

5.4 Assembly of reduced substructures

Reduced substructure models of the floor and of the ceiling were created by employing CMS. The objective is to demonstrate the accuracy and efficiency of substructure models in which the elastomers are regarded as coupling elements. Reduced substructures with 150 and 390 retained eigenmodes were created, both for the floor and the ceiling. For both structures, the eigenfrequencies of the 150th and the 390th eigenmodes are approximately 400 Hz and 800 Hz, respectively. Using 150 eigenmodes follows the common rule of thumb of including eigenmodes up to twice the highest frequency of interest. The reduction methods employed to create the coupling elements were the ones found to be the most accurate in Sections 5.2 and 5.3: rigid coupling for the elastomers interfaces, uniformly distributed coupling for the wood interfaces and modified dynamic reduction for the internal DOFs.

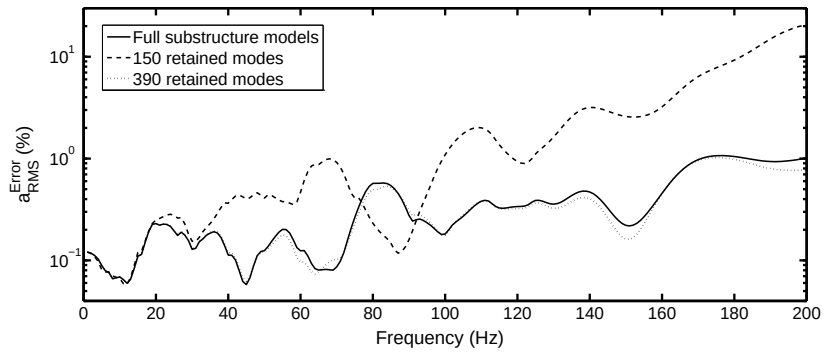

Figure 9. *Error spectra obtained when applying load A and using reduced substructure models of the floor and the ceiling. The full model was used as reference.*

Figure 9 shows the error spectra calculated for load A. The full model, i.e. the model with full FE models of the elastomers and of the substructures, was used as reference. The errors for a model with full FE models of the substructures, and with coupling elements for the elastomers, are included in the figure. Below 100 Hz, the models resulted in small errors. However, for higher frequencies, the error spectrum for the model with 150 retained eigenmodes in the substructures peaks at 20%. The model with 390 retained eigenmodes in the substructures is more accurate, with the error spectrum being virtually equal to the spectrum obtained when using full substructure models.

In Tables 5 and 6, the mean and maximum values, respectively, of the error spectra are presented. Table 5 also shows the number of DOFs of the models and the computation times of the analyses. Direct-solution steady-state analyses were ran using Abaqus/Standard 6.13 on a quad-core 2.80 GHz Intel Xeon W3530 CPU having 10 GB of RAM available. The computation times for the models with 150 and 390 retained eigenmodes in the reduced substructure models are 0.1% and 0.2%, respectively, of the time for the full model. Hence, by employing the coupling elements in substructure modelling of the example case, the computation time can be reduced by 99.8% at the cost of introducing errors of approximately 1%.

Table 5. *Mean values of the error spectra obtained when using reduced substructure models of the floor and the ceiling. The number of DOFs in the models and the CPU time of the analyses are shown.*

	Number		Mean error (%)			
Model	of DOFs	CPU time (s)	Load A	Load B	Load C	Load D
Full model	630,000	260,000	-	-	-	-
Full substructures	290,000	38,000	0.4	0.5	0.4	0.2
150 retained eigenmodes	1100	320	3.0	2.1	1.8	0.6
390 retained eigenmodes	1600	480	0.4	0.4	0.4	0.2

Table 6. *Maximum values of the error spectra obtained when using reduced substructure models of the floor and the ceiling.*

	Maximum error (%)			
Model	Load A	Load B	Load C	Load D
Full substructures	1.1	1.3	1.1	0.6
150 retained eigenmodes	20.4	9.1	7.6	3.7
390 retained eigenmodes	1.0	1.3	1.1	0.6

5.5 Modelling features in coupling elements

The effect of considering different modelling features for the coupling elements (mass, damping, frequency-dependent material properties and rotational coupling) was investigated by excluding them from the elastomer models one at a time. Interface reduction was employed during the investigations; rigid coupling for the elastomer interfaces and uniformly distributed coupling for the wood interfaces. Damping was excluded by removing the imaginary part of the viscoelastic material properties. The frequency dependence was omitted by evaluating the material properties at 100 Hz. Rotational coupling was excluded by locking the rotational DOFs at the elastomer interfaces and not connecting them to the rotational DOFs at the wood interfaces.

The error spectra that were obtained when applying load A are shown in Figure 10. It can be seen that different modelling features are important at different frequencies. As expected, the exclusion of the mass or the damping had a relatively small effect at low frequencies, while resulting in larger errors at higher frequencies. When excluding rotational coupling, the largest errors were produced at low frequencies. The exclusion of frequency dependence yielded accurate results around 100 Hz, which is the frequency at which the material properties were evaluated. The mean and maximum values of the error spectra for the responses to the different loads are shown in Table 3. It can be seen that by excluding each of the features, maximum errors of at least 7–8% were produced.

Table 7. *Mean and maximum values of the error spectra obtained when excluding different modelling features from the coupling elements.*

	Mean error (%)				Maximum error (%)			
Excluded feature	Load A	Load B	Load C	Load D	Load A	Load B	Load C	Load D
Mass	1.4	1.0	1.3	1.4	6.5	3.4	6.7	7.2
Damping	16.6	16.2	17.1	17.5	48.5	36.7	38.0	41.4
Freq depend	2.4	2.4	2.3	2.6	7.3	7.7	8.4	7.8
Rotat coupling	2.4	1.3	2.5	2.0	23.0	13.5	18.9	13.4

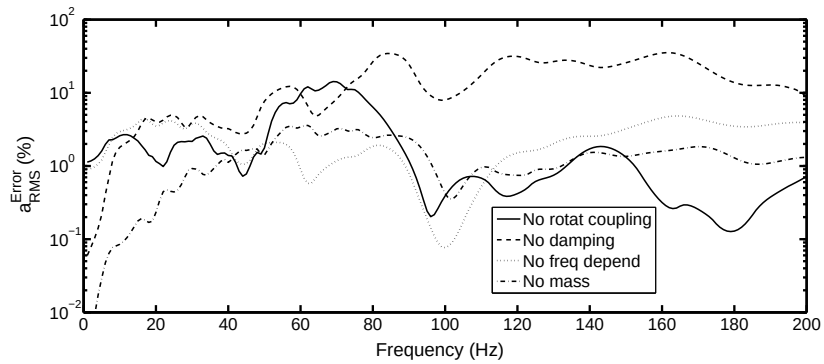

Figure 10. *Error spectra obtained when applying load A and excluding different modelling features from the coupling elements. The interface-reduced model was used as reference.*

5.6 Summary and conclusions

In this section, we summarise the results from the studies of the example case and present the conclusions.

Interface reduction

The use of distributed coupling for the elastomers resulted in large errors, while rigid coupling provided far more accurate results. The interface reduction of the wood structures was less sensitive to the choice of coupling method. Rigid coupling was the least accurate method for the wood structures, with the maximum errors being approximately five times higher than those obtained by using distributed coupling. With the use of rigid coupling for the elastomers and uniformly distributed coupling for the wood structures, maximum errors of approximately 1% were obtained in the frequency range of interest. Therefore, we can conclude that the methodology involving the use of condensation nodes is adequate for the model under study.

Reduction of internal DOFs of elastomers

Modified dynamic reduction resulted in errors of negligible magnitude compared to those stemming from the interface reduction. Guyan reduction and CMS resulted in error spectra that are nearly identical to each other. Hence, it can be concluded that the eigenmodes retained in the CMS reduction did not improve the accuracy of the coupling elements. The error spectra obtained when employing Guyan reduction and CMS are similar to that obtained when excluding the frequency dependence of the material properties. This shows that the omitted frequency dependence is the main source of error for those methods. The spring-dashpot system resulted in errors that have the same magnitude as those obtained with Guyan reduction and CMS, but with higher accuracy at low frequencies.

Assembly of reduced substructures

When the coupling elements were used along with reduced substructure models of the floor and ceiling, the computation time of the example model was reduced by 99.8% at the cost of introducing errors

of approximately 1% in the frequency range of interest. This shows the potential of using coupling elements for the elastomers. Such a reduction in computation time would not be possible if the full interfaces of the reduced substructure models were retained, as they would result in several thousand interface DOFs per substructure.

Modelling features in coupling elements

It was important to include damping and rotational coupling in the coupling elements, as their exclusions resulted in errors of up to 50% and 20%, respectively. The exclusion of the mass or the frequency dependence of the material properties resulted in errors of up to 7–8% and mean errors of a few percent.

6. General discussion

The effect of using coupling elements on the accuracy and efficiency of dynamic substructure analyses depends on the application being considered. For example, the accuracy is affected by the geometry and material properties of the structure and of the elastomers, and the loads to which the structure is subjected. The relative difference in accuracy and efficiency when using different methods for interface reduction and for a reduction of the number of internal DOFs is not necessarily the same in different applications. Consequently, it is preferable to perform comparative studies such as the one presented in Section 5 for each type of application for which the coupling elements are used.

For many problems, the interface reduction is the most important step in the procedure for creating coupling elements. It reduces the number of interface DOFs to six per interface surface, both for the elastomers and for the substructure models. A large number of interface dofs leads to densely populated matrices in the reduced system. The second step in the procedure, reducing the number of internal DOFs of the elastomers, is important when a large proportion of the DOFs in the substructure assembly belongs to the elastomers.

6.1 Interface reduction

In general, distributed coupling underestimates the stiffness of an interface surface, whereas rigid coupling overestimates the stiffness. The error levels introduced by the coupling methods depend on the extent to which the interfaces deform relative to the deformations of the internal structure. If the stiffness of two connecting structures differs substantially, rigid coupling can be expected to perform well for the interface of the softer structure because the deformations of its interface are relatively small. Distributed coupling, on the other hand, is likely to be more accurate for the interface of the stiffer structure. This is demonstrated in the analyses of the example model. In the limiting case, where one of the structures is infinitely stiff, rigid coupling does not introduce any errors if the two connecting structures are fully tied to each other. For two structures with similar stiffness values, it is a more difficult task to predict suitable coupling methods.

In rigid coupling, a larger number of Lagrange multipliers is required than in distributed coupling. However, the number of Lagrange multipliers is not important for the computational efficiency if a reduction of the number of internal DOFs succeeds the interface reduction because the multipliers are treated as internal DOFs.

6.2 Reduction of internal DOFs of elastomers

Of the methods investigated, modified dynamic reduction is generally the most accurate method. Unlike original dynamic reduction, which yields exact results, the use of modified dynamic reduction introduces errors through the dashpot model of the damping in the elastomers. The errors introduced are generally smaller than those obtained when using the spring-dashpot system because the stiffness and mass of the elastomer models are preserved in modified dynamic reduction. The size of the errors introduced by the spring-dashpot system depends on the validity of assuming block-diagonal system matrices. The assumption implies that there exists no coupling between different DOFs of the condensation nodes; e.g. forces do not cause reaction moments. Employing Guyan reduction or CMS is likely to result in larger errors owing to the neglected frequency dependence of the material properties. The size of the errors depends on the extent of the frequency dependence.

The effect on the computation time of analyses of substructure models is similar among the different methods for the reduction of internal DOFs. All of the methods eliminate the internal DOFs of the elastomer models, resulting in only the interface DOFs being preserved in the coupling elements. The exception is CMS, which includes additional DOFs which represent eigenmodes of the elastomers.

7. Concluding remarks

In this paper, we present a procedure for creating coupling elements that represent elastomeric vibration isolators in dynamic substructuring. We discussed several methods for interface reduction and to reduce the number of internal DOFs of the elastomers in terms of their effect on the accuracy and efficiency of the analyses. To investigate the effects of using the coupling elements, we used an example case consisting of an FE model of a wooden building structure. The results showed that the use of coupling elements can reduce the computation time significantly without impairing the accuracy of the analysis. The conclusion holds if suitable reduction methods are employed when creating the coupling elements. If the procedure for creating coupling elements is to be used for applications other than the one studied in the example case, it is preferable to perform comparative studies to determine suitable reduction methods for creating the coupling elements and to ensure that the resulting errors are sufficiently small.

The proposed procedure for creating coupling elements is well suited for elastomeric isolators that have small-size interface surfaces relative to the size of the full structure. For elastomers with larger interface surfaces, such as strips or mats, or with more complex geometries, the coupling elements are likely to introduce larger errors in the analyses. A possible solution is to divide each interface into multiple surfaces. Such an approach requires further investigations to ensure accurate and efficient analyses.

Acknowledgements

This work was supported by the Urban Tranquility project, a part of the EU program Interreg V.

References

[1] de Klerk D, Rixen DJ, Voormeeren SN. General framework for dynamic substructuring: history, review and classification of techniques. AIAA J 2008;46(5):1169–1181.

[2] Bolmsvik Å, Linderholt A, Brandt A, Ekevid T. FE modelling of light weight wooden assemblies – Parameter study and comparison between analyses and experiments. Eng Struct 2014;73:125–142.

[3] Whelan MJ, Janoyan KD. Assessment of simplified linear dynamic analysis of a multispan skew bridge on steel-reinforced elastomeric bearings. J Bridge Eng 2012;17(1):151–160.

[4] Mola E, Paksoy MA, Rebecchi G, Busca G, Scaccabarozzi M, Berardengo M. Tuning of finite element models of multi-girder composite structures. In: Dynamics of Civil Structures, Volume 2 (157–170). New York: Springer International Publishing; 2015.

[5] Lee DH, Hwang WS, Kim CM. Noise sensitivity analysis of an engine mount system using the transfer function synthesis method. SAE Paper No. 2001-01-1532.

[6] Negreira J, Austrell PE, Flodén O, Bard D. Characterisation of an elastomer for noise and vibration insulation in lightweight timber buildings. Build Acoust 2014;21(4):251–276.

[7] Bathe KJ. Finite element procedures. New York: Prentice Hall; 1996.

[8] Austrell PE. Modeling of elasticity and damping for filled elastomers. Doctoral thesis. Division of Structural Mechanics, Lund University, Sweden; 1997.

[9] Sjöberg M. On dynamic properties of rubber isolators. Doctoral thesis. Department of Vehicle Engineering, Royal Institute of Technology, Stockholm, Sweden; 2002.

[10] Arnold RR, Citerley RL, Chargin M, Galant D. Application of Ritz vectors for dynamic analysis of large structures. Comput Struct 1985;21(3):461–467.

[11] Guyan RJ. Reduction of stiffness and mass matrices. AIAA J 1965;3(2):380.

[12] O'Callahan J. A procedure for an improved reduced system (IRS) model. Proc 7th Int Modal Anal Conf, Las Vegas, 1989:17–21.

[13] Bampton MCC, Craig RR. Coupling of substructures for dynamic analysis. AIAA J 1968;6:1313–1319.

[14] MacNeal RH. A hybrid method of component mode synthesis. Comput Struct 1971;1(4):581–601.

[15] Salimbahrami B, Lohmann B. Order reduction of large scale second-order systems using Krylov subspace methods. Linear Algebr Appl 2006;415(2):385–405.

[16] Reis T, Stykel T. Balanced truncation model reduction of second-order systems. Math Comput Model Dyn Syst 2008;14(5):391–406.

[17] Flodén O, Persson K, Sandberg G. Reduction methods for the dynamic analysis of substructure models of lightweight building structures. Comput Struct 2014;138:49–61.

[18] Tran DM. Component mode synthesis methods using interface modes. Application to structures with cyclic symmetry. Comput Struct 2001;79(2):209–222.

[19] Heirman GHK, Desmet W. Interface reduction of flexible bodies for efficient modeling of body flexibility in multibody dynamics. Multibody Syst Dyn 2010;24(2):219–234.

[20] Dassault Systèmes. Abaqus 6.13 Documentation; 2013.

[21] MSC Software. MSC Nastran 2016, Superelements User's Guide.

[22] Leung AYT. An accurate method of dynamic condensation in structural analysis. Int J Numer Meth Eng 1978;12(11):1705–1715.
[23] Flodén O, Negreira J, Persson K, Sandberg G. The effect of modelling acoustic media in cavities of lightweight buildings on the transmission of structural vibrations. Eng Struct 2015;83:7–16.
[24] AkuLite. Mätrapport 100526. Brunnby Park, Upplands Väsby, Sweden; 2012.
[25] Chopra AK. Dynamics of structures. New Jersey: Prentice Hall; 2007.

Paper F

Computers and Structures 138 (2014) 49–61

Contents lists available at ScienceDirect

Computers and Structures

journal homepage: www.elsevier.com/locate/compstruc

Reduction methods for the dynamic analysis of substructure models of lightweight building structures

O. Flodén *, K. Persson, G. Sandberg

Department of Construction Sciences, Lund University, P.O. Box 118, SE-22100 Lund, Sweden

ARTICLE INFO

Article history:
Received 30 July 2013
Accepted 28 February 2014
Available online 27 March 2014

Keywords:
Model order reduction
Finite element modeling
Substructure modeling
Vibration analysis
Lightweight building structures

ABSTRACT

In the present study, different model order reduction methods were compared in terms of their effects on the dynamic characteristics of individual building components. A wide variety of methods were employed in two numerical examples, both being models of wooden floor structures, in order to draw conclusions regarding their relative efficiency when applied to models of such structures. It was observed that a comparison of the methods requires the reduced models to be exposed to realistic boundary conditions, free–free eigenvalue analyses being insufficient for evaluating the accuracy of the reduced models when employed in an assembly of substructures.

1. Introduction

Lightweight buildings are often constructed using prefabricated planar or volume elements, often with use of low-stiffness panels mounted on high-stiffness beams. Accurately assessing the dynamic behaviour of these elements when rather high vibration frequencies are involved requires use of finite element (FE) models representing the geometry in considerable detail. Assembling the individual elements of multi-storey lightweight buildings within the framework of global FE models of entire buildings results in very large models, the number of degrees of freedom (dofs) of which easily exceeds the limits of computer capacity, at least for computations to be performed within reasonable lengths of time. The question arises then of how such FE models can be reduced in size while at the same time being able to represent the dynamic characteristics of the building or buildings in question with sufficient accuracy. The method of dividing a large model into components and creating a global model through coupling models of reduced size of each component is referred to as substructuring. In the present study, low-frequency vibrations in multi-storey lightweight buildings are modelled by adopting a substructuring approach.

In recent decades, a number of methods for model order reduction of dynamic problems have been developed within the area of structural mechanics, mode-based methods being the methods most frequently used. Fairly recently, methods originating from control theory, designated here as modern reduction methods, have been employed within structural mechanics. In contrast to mode-based methods which have an explicit physical interpretation, the modern reduction methods are developed from a purely mathematical point of view. Some mode-based methods are implemented in commercial FE software which enables them to be applied to large-scale problems directly. In order to apply other methods to models created in commercial FE software, the system matrices involved need to be exported from the software and be reduced in another environment.

A number of comparative studies have been published in which the performance of different reduction methods has been evaluated, in connection with mechanical engineering problems. In [1,2], modern reduction methods were compared with mode-based methods. In [1], a rack consisting of steel beams was used as a numerical example, the reduction methods involved being compared by studying the structural response within the time domain and the Frobenius norm of the transfer function matrix for different load cases. It was concluded that the modern reduction methods produce excellent reduction results and are more effective than mode-based methods are. In [2], a crankshaft of a piston served as a numerical example, the Frobenius norm of the transfer function matrix being used to compare the reduction methods in question. It was concluded that substantial benefits can be achieved by use of the modern reduction methods. In [3], a wide range of methods was compared by studying the eigenfrequencies and eigenmodes of an elastic rod. The modern reduction methods were found to perform better for mechanical problems than several of the classic methods. In [4], however, in which a clamped

* Corresponding author. Tel.: +46 462229493.
E-mail address: ola.floden@construction.lth.se (O. Flodén).

http://dx.doi.org/10.1016/j.compstruc.2014.02.011
0045-7949/

beam structure served as a numerical example, it was concluded that mode-based methods are better suited for the analysis of multibody systems than modern reduction methods are. The eigenfrequencies and eigenmodes were analysed with different boundary conditions applied at the interface of the reduced models. It was concluded that mode-based methods are less dependent than the modern reduction methods are on variations in the boundary conditions, something which would clearly be an important advantage in multibody dynamics.

In the comparative studies just referred to, conclusions were drawn on the basis of numerical examples involving relatively simple structures. Lightweight floor and wall structures, however, generally have a much more complex geometry, making it difficult to extrapolate the conclusions in question. Also, in the comparative studies referred to, different types of analyses were used for evaluating the performance of the reduction methods employed, this providing diverse information that can be evaluated in a variety of ways. By applying analyses of multiple types to a given numerical example it should be possible to obtain a broader understanding of the behaviour of different reduction methods than a single type of analysis would provide. Moreover, analysing the reduced models with realistic boundary conditions is necessary since the boundary conditions employed can have a strong influence on the performance of different reduction methods, as demonstrated in [4].

The objective of the analyses carried out in the present investigation was to evaluate the performance of a rather wide range of model order reduction methods by comparing their accuracy and computational cost when applied to detailed FE models of floor and wall structures. The conclusions will be of value in the process of constructing efficient substructure models for vibration analysis of multi-storey lightweight buildings. The reduced models employed are in this paper evaluated in terms of eigenfrequencies and eigenmodes in a free-free state, as well as in terms of vibration transmission behaviour when the structures in question are exposed to realistic boundary conditions, obtained by connecting them with other building components. New insight is offered regarding both the efficiency of the reduction methods when employed in the analysis of complex structures and the effect of applying realistic boundary conditions to the reduced models.

Commercial FE software of different kinds represent convenient tools for both pre- and post-processing, such as in the coupling of substructures and in the visualisation of results. Since some reduction methods reported on in the literature are incompatible with such software, methods of this sort are either excluded from the analyses here or are used in a modified fashion. A broad range of model order reduction methods presented in the literature will be discussed and the theories behind them taken up. The performance of the reduction methods, applied to lightweight building structures, was evaluated for frequencies of less than 100 Hz by studying two numerical examples. The first example is a model of moderate size of a wooden floor structure, a model created in the commercial FE software Abaqus, from which the system matrices were exported to Matlab, in which various of the reduction methods described in Section 2 were employed. The second example is a large and detailed model of an experimental wooden floor structure, analysed with use of model order reduction methods implemented in Abaqus as well as by use of an alternative approach employing structural elements. Although the conclusions presented in this paper are based in principle on the results of the two numerical examples, many wooden floor and wall structures have geometries and materials similar to those of the structures studied in the two examples. Accordingly, the main conclusions arrived at would appear to be applicable to a wide variety of wooden floor and wall structures similar in topology to these two floors.

2. Model order reduction

An FE formulation of a structural dynamics problem results in a linear equation of motion of the following form [5]:

$$\mathbf{M}\ddot{\mathbf{u}} + \mathbf{C}\dot{\mathbf{u}} + \mathbf{K}\mathbf{u} = \mathbf{F}, \tag{1}$$

where $\mathbf{M}, \mathbf{C}, \mathbf{K} \in \mathbb{R}^{n\times n}$ are the mass, damping and stiffness matrices respectively, $\mathbf{F} = \mathbf{F}(t) \in \mathbb{R}^{n\times 1}$ is the load vector and $\mathbf{u} = \mathbf{u}(t) \in \mathbb{R}^{n\times 1}$ is the state vector which is sought. A dot denotes differentiation with respect to time, t. The objective of model reduction here is to find a system of m dofs in which $m \ll n$, one which preserves the dynamic characteristics of the full model. The general approach is to approximate the state vector by use of the transformation $\mathbf{u} = \mathbf{T}\mathbf{u}_R$, where $\mathbf{T} \in \mathbb{R}^{n\times m}$ is a transformation matrix and $\mathbf{u}_R \in \mathbb{R}^{m\times 1}$ is a reduced state vector. Applying the transformation in question to Eq. (1) results in

$$\mathbf{M}_R\ddot{\mathbf{u}}_R + \mathbf{C}_R\dot{\mathbf{u}}_R + \mathbf{K}_R\mathbf{u}_R = \mathbf{F}_R, \tag{2}$$

$$\mathbf{M}_R = \mathbf{T}^T\mathbf{M}\mathbf{T}, \quad \mathbf{C}_R = \mathbf{T}^T\mathbf{C}\mathbf{T}, \quad \mathbf{K}_R = \mathbf{T}^T\mathbf{K}\mathbf{T}, \quad \mathbf{F}_R = \mathbf{T}^T\mathbf{F}, \tag{3}$$

where $\mathbf{M}_R, \mathbf{K}_R, \mathbf{C}_R \in \mathbb{R}^{m\times m}$ are the reduced mass, damping and stiffness matrices, respectively, and $\mathbf{F}_R \in \mathbb{R}^{m\times 1}$ is the reduced load vector. In recent decades, many different methods for model order reduction, involving procedures of varying types for establishing the transformation matrix and the reduced state vector involved, have been proposed in the literature. The dofs in the reduced state vector can be divided into two categories: physical dofs and generalised coordinates. Physical dofs are the dofs of the full system that are retained in the reduction process, whereas the generalised coordinates represent the amplitudes of various Ritz basis vectors [6] that describe the deflection shapes that are allowed in the reduced system. The reduction methods can be categorised according to the type of dofs generated in the reduction process, where *condensation methods* involve only physical dofs, *generalised coordinate methods* are based solely on generalised coordinates, and *hybrid reduction methods* employ a combination of dofs of both types. A number of important methods within each category are listed below:

- Condensation methods
  - Guyan reduction [7]
  - Dynamic reduction [8]
  - Improved reduction system (IRS) [9,10]
  - System equivalent expansion reduction process (SEREP) [11]
- Generalised coordinate methods
  - Modal truncation [5,12]
  - Component mode synthesis by Craig–Chang [12,13]
  - Krylov subspace methods [14,15]
  - Balanced truncation [16,17]
- Hybrid methods
  - Component mode synthesis by Craig–Bampton [12,18]
  - Component mode synthesis by MacNeal [19]
  - Component mode synthesis by Rubin [20]

The methods just referred to, except for the Krylov subspace methods and balanced truncation, which have their origin in control theory and are considered to be modern reduction methods, were developed specifically for structural mechanics. Modal truncation and component mode synthesis by Craig–Chang, Craig–Bampton, Rubin or MacNeal are all mode-based methods, which means that structural eigenmodes of some sort are employed as Ritz basis vectors. In commercial FE software, generalised coordinates are treated as internal dofs and the coupling of substructures is usually realised at the physical dofs by use of Lagrange multipliers [5]. Consequently, if the global model involved is to be analysed and post-processed in commercial FE software, any methods for

model order reduction based solely on generalised coordinates are excluded. However, such methods can be combined with condensation methods to obtain hybrid versions of the methods. Component mode synthesis by Craig–Bampton, for example, is modal truncation combined with Guyan reduction. Moreover, variants of component mode synthesis in which Krylov subspace methods instead of modal truncation are combined with Guyan reduction have been described in [21,22]. Model order reduction methods that result in reduced models in which the physical dofs at the interfaces are preserved are often referred to as structure-preserving methods.

In the present study, five of the above-listed reduction methods are investigated: Guyan reduction, dynamic reduction, IRS and component mode synthesis, the latter both in the mode-based Craig–Bampton form and in the Krylov subspace version. Out of the mode-based component mode synthesis methods, the Craig–Bampton version, the most commonly employed method among structural engineers, is selected. The Krylov subspace version is included in the studies to investigate the potential improvement in efficiency offered by the increasingly popular methods from control theory when employed for the type of problems studied here. Moreover, modified versions of the component mode synthesis methods are investigated using IRS instead of Guyan reduction as the condensation method, these being referred to as improved component mode synthesis methods [21]. In addition, a set of alternative methods termed generalised methods [23], obtained by deriving the above mentioned methods in a slightly different manner, are investigated.

In the derivations of the reduction methods presented below, the case considered is an undamped one. Since the damping ratio of the structures analysed in the study is relatively low, it has a negligible effect on the eigenfrequencies and the eigenmodes. Also, the damping matrix employed provides only a rough approximation of all the damping phenomena occurring in the structures as a whole. Accordingly, as an alternative to its being reduced in the same way as the mass and stiffness matrices, the damping matrix can be constructed in the reduced system directly.

2.1. Original methods

As mentioned above, the model order reduction methods can be derived in a slightly different manner than in their original versions, this resulting in methods referred to as generalised methods, as presented in Section 2.2. Below, the original versions of the methods investigated here are presented.

2.1.1. Guyan reduction

In the condensation methods, the dofs are separated into masters (m) and slaves (s), the slave dofs being condensed in the reduction process, resulting in a reduced state vector containing only the master dofs. Partitioning the state vector in terms of the master and slave categories enables the system matrices in Eq. (1) to be partitioned into sub-blocks as follows:

$$\begin{bmatrix} \mathbf{M}_{mm} & \mathbf{M}_{ms} \\ \mathbf{M}_{sm} & \mathbf{M}_{ss} \end{bmatrix} \begin{bmatrix} \ddot{\mathbf{u}}_m \\ \ddot{\mathbf{u}}_s \end{bmatrix} + \begin{bmatrix} \mathbf{K}_{mm} & \mathbf{K}_{ms} \\ \mathbf{K}_{sm} & \mathbf{K}_{ss} \end{bmatrix} \begin{bmatrix} \mathbf{u}_m \\ \mathbf{u}_s \end{bmatrix} = \begin{bmatrix} \mathbf{F}_m \\ \mathbf{F}_s \end{bmatrix}. \tag{4}$$

Solving the equation in the second row in Eq. (4) for $\mathbf{u}_s$ results in

$$\mathbf{u}_s = -\mathbf{K}_{ss}^{-1}(\mathbf{M}_{sm}\ddot{\mathbf{u}}_m + \mathbf{M}_{ss}\ddot{\mathbf{u}}_s + \mathbf{K}_{sm}\mathbf{u}_m), \tag{5}$$

where it has been assumed that there are no loads acting on the slave dofs, so that $\mathbf{F}_s = \mathbf{0}$. Neglecting the inertia terms in Eq. (5) results in the transformation of the state vector for Guyan reduction

$$\begin{bmatrix} \mathbf{u}_m \\ \mathbf{u}_s \end{bmatrix} = \begin{bmatrix} \mathbf{I} \\ -\mathbf{K}_{ss}^{-1}\mathbf{K}_{sm} \end{bmatrix} \mathbf{u}_m = \mathbf{T}_{\text{Guyan}}\mathbf{u}_m, \tag{6}$$

where the transformation matrix $\mathbf{T}_{\text{Guyan}}$ can be used in Eq. (3) to obtain the reduced system matrices and the reduced load vector. Guyan reduction is often referred to as static condensation, since models reduced with Guyan reduction do not result in any errors in static analysis. Due to its static nature, Guyan reduction can be expected to only produce acceptable results for frequencies close to the lowest eigenfrequencies of the system. At higher frequencies, the neglected inertia terms have a stronger influence, resulting in errors of larger size. The performance of this method is highly dependent upon the approach for selecting master dofs. In the numerical examples studied here, only the dofs needed to connect the substructures to the surroundings serve as masters, although additional dofs can be employed as master dofs as well, various methods for selecting such dofs having been proposed [24,25].

2.1.2. Dynamic reduction

If a harmonic time-dependent load, $\mathbf{F} = \hat{\mathbf{F}}exp(i\omega t)$, is assumed, this results in a harmonic response, $\mathbf{u} = \hat{\mathbf{u}}exp(i\omega t)$, where $i = \sqrt{-1}$ is the imaginary unit, ω is the angular frequency and $\hat{\mathbf{F}}$ and $\hat{\mathbf{u}}$ are the complex load and displacement amplitudes, respectively. Introducing this assumption into Eq. (4) results in the equation of motion applying to the frequency domain

$$\begin{bmatrix} \mathbf{D}_{mm}(\omega) & \mathbf{D}_{ms}(\omega) \\ \mathbf{D}_{sm}(\omega) & \mathbf{D}_{ss}(\omega) \end{bmatrix} \begin{bmatrix} \hat{\mathbf{u}}_m \\ \hat{\mathbf{u}}_s \end{bmatrix} = \begin{bmatrix} \hat{\mathbf{F}}_m \\ \hat{\mathbf{F}}_s \end{bmatrix}, \tag{7}$$

$$\mathbf{D}(\omega) = -\omega^2\mathbf{M} + \mathbf{K}. \tag{8}$$

Solving the equation in the lower row in Eq. (7) for $\hat{\mathbf{u}}_s$, assuming $\hat{\mathbf{F}}_s = \mathbf{0}$, results in

$$\hat{\mathbf{u}}_s = -\mathbf{D}_{ss}^{-1}(\omega)\mathbf{D}_{sm}(\omega)\hat{\mathbf{u}}_m \tag{9}$$

and, consequently, the transformation of the state vector for dynamic reduction is given by

$$\begin{bmatrix} \hat{\mathbf{u}}_m \\ \hat{\mathbf{u}}_s \end{bmatrix} = \begin{bmatrix} \mathbf{I} \\ -\mathbf{D}_{ss}^{-1}(\omega)\mathbf{D}_{sm}(\omega) \end{bmatrix} \hat{\mathbf{u}}_m = \mathbf{T}_{\text{Dynamic}}\hat{\mathbf{u}}_m, \tag{10}$$

where the transformation matrix $\mathbf{T}_{\text{Dynamic}}$ requires a selection of ω in order to be established. The special case of dynamic reduction in which $\omega = 0$ results in the transformation of Guyan reduction shown in Eq. (6). For harmonic load cases in which the excitation frequency has the same value as ω, dynamic reduction provides exact results. This suggests dynamic reduction to be an effective scheme for analysing a structure subjected to load cases having narrow frequency content. For steady-state analyses, fully accurate reduced models can be obtained by reducing the system matrices at each discrete frequency, yet this is a costly procedure that requires the availability of large memory resources for storing the resulting matrices.

2.1.3. Improved reduction system (IRS)

The term *improved* in the name improved reduction system refers to a perturbation of the transformation taking place in Guyan reduction, Eq. (6). The previously neglected inertia terms are then included as pseudo-static forces. The occurrence of free undamped vibrations of a system reduced by means of a Guyan reduction results in the following expression for the acceleration of the master dofs:

$$\ddot{\mathbf{u}}_m = -\mathbf{M}_{\text{Guyan}}^{-1}\mathbf{K}_{\text{Guyan}}\mathbf{u}_m, \tag{11}$$

where $\mathbf{M}_{\text{Guyan}}$ and $\mathbf{K}_{\text{Guyan}}$ are the reduced stiffness- and mass matrices obtained by employing Guyan reduction. Differentiating Eq. (6) and making use of the relationship expressed in Eq. (11) results in the following expression for acceleration of the slave dofs:

$$\ddot{\mathbf{u}}_s = -\mathbf{K}_{ss}^{-1}\mathbf{K}_{sm}\ddot{\mathbf{u}}_m = \mathbf{K}_{ss}^{-1}\mathbf{K}_{sm}\mathbf{M}_{\text{Guyan}}^{-1}\mathbf{K}_{\text{Guyan}}\mathbf{u}_m. \tag{12}$$

Inserting Eqs. (11) and (12) into Eq. (5) results in the approximation of the slave dofs

$$\mathbf{u}_s = \mathbf{K}_{ss}^{-1}\left(\mathbf{M}_{sm}\mathbf{M}_{\text{Guyan}}^{-1}\mathbf{K}_{\text{Guyan}} - \mathbf{M}_{ss}\mathbf{K}_{ss}^{-1}\mathbf{K}_{sm}\mathbf{M}_{\text{Guyan}}^{-1}\mathbf{K}_{\text{Guyan}} - \mathbf{K}_{sm}\right)\mathbf{u}_m. \tag{13}$$

This rather complicated expression can be written in more compact form so as to obtain the transformation matrix for IRS

$$\mathbf{T}_{\text{IRS}} = \mathbf{T}_{\text{Guyan}} + \mathbf{S}\mathbf{M}\mathbf{T}_{\text{Guyan}}\mathbf{M}_{\text{Guyan}}^{-1}\mathbf{K}_{\text{Guyan}}, \tag{14}$$

$$\mathbf{S} = \begin{bmatrix} \mathbf{0} & \mathbf{0} \\ \mathbf{0} & \mathbf{K}_{ss}^{-1} \end{bmatrix}. \tag{15}$$

In the IRS transformation, the reduced system matrices that Guyan reduction provides are utilised so as to produce updated reduced matrices. As a further extension of this, the updated matrices can be used to create an iterative scheme where the transformation for the ith iteration is given by

$$\mathbf{T}_{\text{IRS},i} = \mathbf{T}_{\text{Guyan}} + \mathbf{S}\mathbf{M}\mathbf{T}_{\text{IRS},i-1}\mathbf{M}_{\text{IRS},i-1}^{-1}\mathbf{K}_{\text{IRS},i-1} \tag{16}$$

and the iterations are started by calculating $\mathbf{T}_{\text{IRS},1}$ according to Eq. (14). $\mathbf{K}_{\text{IRS},i-1}$ and $\mathbf{M}_{\text{IRS},i-1}$ are the reduced stiffness- and mass matrices of iteration $i-1$, obtained by using $\mathbf{T}_{\text{IRS},i-1}$ in Eq. (3). The iterative scheme converges to form the transformation matrix of SEREP [11], creating a reduced system that reproduces exactly the lowest eigenfrequencies and eigenmodes of the full system. The rate of convergence depends upon the selection of master dofs. In contrast to Guyan reduction, however, IRS does not reproduce the static behaviour of the full system exactly.

2.1.4. Component mode synthesis by Craig–Bampton (CMS)

Use of component mode synthesis by Craig–Bampton, here denoted CMS, compensates for the neglected inertia terms in Guyan reduction through its including a set of generalised coordinates $\boldsymbol{\xi}$. These generalised coordinates represent the amplitudes of a set of eigenmodes for the slave structure, calculated with the master dofs being fixed. Setting $\mathbf{u}_m = \mathbf{0}$ and $\mathbf{F}_s = \mathbf{0}$ in Eq. (4) and assuming a harmonic solution results in the following eigenvalue problem:

$$\mathbf{K}_{ss}\Phi = \lambda\mathbf{M}_{ss}\Phi, \tag{17}$$

which can be solved for the eigenvalues $\lambda = \omega^2$ and the eigenmodes Φ. A number of eigenmodes obtained from Eq. (17), referred to as retained eigenmodes, are selected as additional basis vectors to the approximation of the slave dofs in Eq. (6), resulting in

$$\mathbf{u}_s = -\mathbf{K}_{ss}^{-1}\mathbf{K}_{sm}\mathbf{u}_m + \sum \Phi_i\xi_i = \boldsymbol{\Psi}\mathbf{u}_m + \boldsymbol{\Phi}\boldsymbol{\xi}. \tag{18}$$

This gives the following transformation of the state vector for CMS:

$$\begin{bmatrix} \mathbf{u}_m \\ \mathbf{u}_s \end{bmatrix} = \begin{bmatrix} \mathbf{I} & \mathbf{0} \\ \boldsymbol{\Psi} & \boldsymbol{\Phi} \end{bmatrix}\begin{bmatrix} \mathbf{u}_m \\ \boldsymbol{\xi} \end{bmatrix} = \mathbf{T}_{\text{CMS}}\begin{bmatrix} \mathbf{u}_m \\ \boldsymbol{\xi} \end{bmatrix}, \tag{19}$$

which defines the transformation matrix $\mathbf{T}_{\text{CMS}}$. As for Guyan reduction, the accuracy of CMS depends upon the selection of master dofs, this affecting both the static modes and the eigenmodes of the slave structure. Also, the accuracy depends upon the selection of retained eigenmodes, certain eigenmodes having a larger influence than others on the solution of a specific problem. To obtain a reduced model with as great an accuracy for general load distributions as possible, however, all the eigenmodes up to some given limit that is chosen should be included.

2.1.5. Krylov subspace component mode synthesis (KCMS)

The Krylov subspace is defined as

$$K_q(\mathbf{A},\mathbf{b}) = span\left\{\mathbf{b}, \mathbf{A}\mathbf{b}, \ldots, \mathbf{A}^{q-1}\mathbf{b}\right\}, \tag{20}$$

where $\mathbf{A} \in \mathbb{R}^{n\times n}$, $\mathbf{b} \in \mathbb{R}^{n\times 1}$ is called the starting vector and q is a positive integer. $\mathbf{b}$ can also be a block of vectors, in which case each Krylov projection generates a new block of vectors. Since methods originating from control theory are ones developed for systems of an input–output form, the equation of motion is rewritten here as a system of this sort of the following form:

$$\mathbf{M}\ddot{\mathbf{u}} + \mathbf{K}\mathbf{u} = \mathbf{B}\mathbf{x}, \tag{21}$$

$$\mathbf{y} = \mathbf{N}^T\mathbf{u}, \tag{22}$$

where $\mathbf{x} = \mathbf{x}(t) \in \mathbb{R}^{x\times 1}$ is the input vector, $\mathbf{y} = \mathbf{y}(t) \in \mathbb{R}^{y\times 1}$ the output vector, $\mathbf{B} \in \mathbb{R}^{n\times x}$ a matrix describing the spatial load distributions and $\mathbf{N} \in \mathbb{R}^{n\times y}$ a matrix relating the state vector to the output vector. A Laplace transformation of the input–output system yields the transfer function $\mathbf{G}(s)$:

$$\mathbf{G}(s) = \mathbf{N}^T(s^2\mathbf{M} + \mathbf{K})^{-1}\mathbf{B}. \tag{23}$$

Krylov subspace methods, which have their origin in the area of control theory, are based on so-called *moment matching*. The moments involved are defined as the coefficients of a Taylor series expansion of $\mathbf{G}(s)$ around $s = 0$. It can be shown that the first q moments of the full system and of a reduced system match if the reduced basis is selected as the Krylov subspace generated by $\mathbf{A} = \mathbf{K}^{-1}\mathbf{M}$ and $\mathbf{b} = \mathbf{K}^{-1}\mathbf{B}$ [15]. In the present study it is required that the reduction methods employed are structure-preserving, i.e. retains the physical dofs at the interfaces. Accordingly, the approach of using Krylov subspace vectors in a component mode synthesis manner, as described in [21,22], here denoted KCMS, is adopted. Inserting $\mathbf{u}_m = 0$ and $\mathbf{F}_s = \mathbf{B}_s\mathbf{x}_s$ into Eq. (4) results in the following equation of motion for the slave structure:

$$\mathbf{M}_{ss}\ddot{\mathbf{u}}_s + \mathbf{K}_{ss}\mathbf{u}_s = \mathbf{B}_s\mathbf{x}_s. \tag{24}$$

A Krylov subspace is generated for the slave structure by selecting $\mathbf{A} = \mathbf{K}_{ss}^{-1}\mathbf{M}_{ss}$ and $\mathbf{b} = \mathbf{K}_{ss}^{-1}\mathbf{B}_s$:

$$K_q\left(\mathbf{K}_{ss}^{-1}\mathbf{M}_{ss}, \mathbf{K}_{ss}^{-1}\mathbf{B}_s\right) = span\left\{\underbrace{\mathbf{K}_{ss}^{-1}\mathbf{B}_s}_{V_k^1}, \underbrace{\left(\mathbf{K}_{ss}^{-1}\mathbf{M}_{ss}\right)\mathbf{K}_{ss}^{-1}\mathbf{B}_s}_{V_k^2}, \ldots, \underbrace{\left(\mathbf{K}_{ss}^{-1}\mathbf{M}_{ss}\right)^{q-1}\mathbf{K}_{ss}^{-1}\mathbf{B}_s}_{V_k^q}\right\} \tag{25}$$

and the approximation of the slave dofs in KCMS is given by

$$\mathbf{u}_s = -\mathbf{K}_{ss}^{-1}\mathbf{K}_{sm}\mathbf{u}_m + \sum V_k^i\xi_i = \boldsymbol{\Psi}\mathbf{u}_m + \mathbf{V}_k\boldsymbol{\xi}, \tag{26}$$

one which is similar to that of component mode synthesis by Craig–Bampton shown in Eq. (18), but with the eigenmodes of the slave structure exchanged for the Krylov subspace vectors as defined in Eq. (25). This results in the transformation of the state vector for KCMS

$$\begin{bmatrix} \mathbf{u}_m \\ \mathbf{u}_s \end{bmatrix} = \begin{bmatrix} \mathbf{I} & \mathbf{0} \\ \boldsymbol{\Psi} & \mathbf{V}_k \end{bmatrix}\begin{bmatrix} \mathbf{u}_m \\ \boldsymbol{\xi} \end{bmatrix} = \mathbf{T}_{\text{KCMS}}\begin{bmatrix} \mathbf{u}_m \\ \boldsymbol{\xi} \end{bmatrix} \tag{27}$$

defining the transformation matrix $\mathbf{T}_{\text{KCMS}}$. In order to avoid numerical issues, the Krylov subspace is generated by using the Arnoldi algorithm with modified Gram-Schmidt orthogonalization [14], which creates a set of linearly independent vectors. Calculating the starting vector $\mathbf{b}$ requires that $\mathbf{B}_s$, which describes the spatial load distribution on the slave structure, be selected. In the present study, a substructuring approach for the modelling of multi-storey buildings is adopted. Smaller parts of such buildings are considered as being substructures of these, most of these substructures having no loads that act upon the slave structure. Accordingly, a fictitious load needs to be selected, in the present study a random distribution being used for this.

In contrast to CMS, which includes eigenmodes of the full model as Ritz basis vectors, no eigenvalue extraction is required for creating reduced models by means of the KCMS method. Consequently, it is less costly to create the reduced models employing KCMS and in application where the computation time of this process is of importance, this gives KCMS an advantage over CMS.

2.1.6. Improved component mode synthesis

The two component mode synthesis methods described above are obtained by complementing Guyan reduction by a set of Ritz basis vectors for the slave structure, these being either eigenmodes or Krylov subspace vectors. IRS can be seen as representing an improvement as compared to Guyan reduction, an improvement that can also be applied to the component mode synthesis methods employed here. The transformation matrices of the improved component mode synthesis methods, improved CMS and improved KCMS (ICMS and IKCMS, respectively), can be obtained by simply replacing the basis vectors of Guyan reduction by the basis vectors of IRS:

$$\mathbf{T}_{\text{ICMS}} = \begin{bmatrix} \mathbf{T}_{\text{IRS}} & \hat{\mathbf{\Phi}} \end{bmatrix}; \quad \hat{\mathbf{\Phi}} = \begin{bmatrix} \mathbf{0} \\ \mathbf{\Phi} \end{bmatrix}, \tag{28}$$

$$\mathbf{T}_{\text{IKCMS}} = \begin{bmatrix} \mathbf{T}_{\text{IRS}} & \hat{\mathbf{V}}_{\text{k}} \end{bmatrix}; \quad \hat{\mathbf{V}}_{\text{k}} = \begin{bmatrix} \mathbf{0} \\ \mathbf{V}_{\text{k}} \end{bmatrix}, \tag{29}$$

where $\mathbf{T}_{\text{IRS}}$ can be given either by the original form of IRS, Eq. (14), or its iterated version, Eq. (16). The use of IRS instead of Guyan reduction can be expected to improve the dynamic behaviour of the reduced models, at the expense of introducing errors in static analyses.

2.2. Generalised methods

The generalised versions of the reduction methods (denoted here by a "g-" in the method names) are obtained by re-formulating the equation of motion. Instead of using the block-partitioning of the system matrices in Eq. (4), the following partitioning is employed:

$$\begin{bmatrix} \mathbf{M}_m & \mathbf{M}_s \end{bmatrix} \begin{bmatrix} \ddot{\mathbf{u}}_m \\ \ddot{\mathbf{u}}_s \end{bmatrix} + \begin{bmatrix} \mathbf{K}_m & \mathbf{K}_s \end{bmatrix} \begin{bmatrix} \mathbf{u}_m \\ \mathbf{u}_s \end{bmatrix} = \begin{bmatrix} \mathbf{F}_m \\ \mathbf{F}_s \end{bmatrix}, \tag{30}$$

with the non-square submatrices $\mathbf{K}_m, \mathbf{M}_m \in \mathbb{R}^{n\times m}$ and $\mathbf{K}_s, \mathbf{M}_s \in \mathbb{R}^{n\times s}$. A drawback of the generalised versions of the methods, in comparison to the original versions, is the increased computational resources needed to construct the reduced models, since this requires the generalised inverses of matrices that are very large.

2.2.1. Generalised Guyan reduction

In the same manner as in Eqs. (5) and (6), the inertia terms in Eq. (30) are neglected when solving for the slave dofs, resulting in the following transformation of the state vector for generalised Guyan (g-Guyan) reduction:

$$\begin{bmatrix} \mathbf{u}_m \\ \mathbf{u}_s \end{bmatrix} = \begin{bmatrix} \mathbf{I} \\ -\mathbf{K}_s^{+}\mathbf{K}_m \end{bmatrix} \mathbf{u}_m = \mathbf{T}_{\text{g-Guyan}} \mathbf{u}_m, \tag{31}$$

where $\mathbf{K}_s^{+} = \left(\mathbf{K}_s^T \mathbf{K}_s\right)^{-1} \mathbf{K}_s^T$ is the generalised left-inverse of $\mathbf{K}_s$ and $\mathbf{T}_{\text{g-Guyan}}$ is the transformation matrix. Note that in the approximation of the slave dofs it is assumed that there are no loads that act on either the master dofs or the slave dofs, $\mathbf{F}_m = \mathbf{0}$ and $\mathbf{F}_s = \mathbf{0}$, respectively, in contrast to the original Guyan reduction, in which only $\mathbf{F}_s = \mathbf{0}$ needs to be assumed.

2.2.2. Generalised dynamic reduction

Through use of an approach corresponding to the derivation of g-Guyan reduction, the transformation matrix of generalised dynamic (g-dynamic) reduction, $\mathbf{T}_{\text{g-Dynamic}}$, can be defined as

$$\begin{bmatrix} \hat{\mathbf{u}}_m \\ \hat{\mathbf{u}}_s \end{bmatrix} = \begin{bmatrix} \mathbf{I} \\ -\mathbf{D}_s^{+}(\omega)\mathbf{D}_m(\omega) \end{bmatrix} \hat{\mathbf{u}}_m = \mathbf{T}_{\text{g-Dynamic}} \hat{\mathbf{u}}_m, \tag{32}$$

where $\mathbf{D}_s(\omega) = -\omega^2\mathbf{M}_s + \mathbf{K}_s$ and $\mathbf{D}_m(\omega) = -\omega^2\mathbf{M}_m + \mathbf{K}_m$.

2.2.3. Generalised improved reduction system (g-IRS)

The transformation matrix of generalised IRS is obtained by including the inertia terms found in Eq. (30) as pseudo-static forces, using approximations corresponding to those employed in Eqs. (11) and (12), resulting in

$$\mathbf{T}_{\text{g-IRS}} = \mathbf{T}_{\text{g-Guyan}} + \hat{\mathbf{S}}\mathbf{M}\mathbf{T}_{\text{g-Guyan}}\mathbf{M}_{\text{g-Guyan}}^{-1}\mathbf{K}_{\text{g-Guyan}}, \tag{33}$$

$$\hat{\mathbf{S}} = \begin{bmatrix} \mathbf{0} \\ \mathbf{K}_s^{+} \end{bmatrix}, \tag{34}$$

where $\mathbf{M}_{\text{Guyan}}$ and $\mathbf{K}_{\text{Guyan}}$ are the reduced stiffness- and mass matrices obtained by employing g-Guyan reduction. g-IRS can also be extended to produce an iterative scheme in the same manner as in the original IRS, where the transformation matrix for the ith iteration is given by

$$\mathbf{T}_{\text{g-IRS},i+1} = \mathbf{T}_{\text{g-Guyan}} + \hat{\mathbf{S}}\mathbf{M}\mathbf{T}_{\text{g-IRS},i}\mathbf{M}_{\text{g-IRS},i}^{-1}\mathbf{K}_{\text{g-IRS},i} \tag{35}$$

and the iterations are started by calculating $\mathbf{T}_{\text{g-IRS},1}$ according to Eq. (33).

2.2.4. Generalised component mode synthesis

The generalised versions of Guyan reduction and IRS can be used to obtain the transformation matrices for the generalised versions of CMS, KCMS, ICMS and IKCMS (g-CMS, g-KCMS, g-ICMS and g-IKCMS, respectively)

$$\mathbf{T}_{\text{g-CMS}} = \begin{bmatrix} \mathbf{T}_{\text{g-Guyan}} & \hat{\mathbf{\Phi}} \end{bmatrix}, \tag{36}$$

$$\mathbf{T}_{\text{g-KCMS}} = \begin{bmatrix} \mathbf{T}_{\text{g-Guyan}} & \hat{\mathbf{V}}_{\text{k}} \end{bmatrix}, \tag{37}$$

$$\mathbf{T}_{\text{g-ICMS}} = \begin{bmatrix} \mathbf{T}_{\text{g-IRS}} & \hat{\mathbf{\Phi}} \end{bmatrix}, \tag{38}$$

$$\mathbf{T}_{\text{g-IKCMS}} = \begin{bmatrix} \mathbf{T}_{\text{g-IRS}} & \hat{\mathbf{V}}_{\text{k}} \end{bmatrix}, \tag{39}$$

where $\hat{\mathbf{\Phi}}$ and $\hat{\mathbf{V}}_{\text{k}}$ are defined in Eqs. (28) and (29), respectively.

2.3. Summary of methods

Table 1 summarises the methods for model order reduction which are presented above and investigated in the numerical examples.

3. Numerical examples

This section considers two numerical examples in which different model order reduction methods are applied to FE models of wooden floor structures. In the first example, a model of moderate size created in Abaqus is studied. The system matrices were exported to Matlab, where the reduction methods described in Section 2 were employed, the reduced models that resulted being analysed. The second example concerns a large and detailed model that was both created and analysed in Abaqus, using reduction methods implemented in the software together with an alternative approach involving use of structural elements. In both examples, two types of analyses were performed: eigenvalue analysis and steady-state analysis. The eigenvalue analysis was performed in a free-free state, i.e. without any displacements of the physical dofs being prescribed. The rigid body eigenmodes that occur in a free-free state are disregarded in the results that are presented. A steady-state analysis was performed to investigate the vibration

Table 1
The model order reduction methods presented in Section 2 and investigated in Section 3.

Method name	Abbrevation
Condensation methods	
Guyan reduction	–
Dynamic reduction	–
Improved reduction system	IRS
Generalised Guyan reduction	g-Guyan reduction
Generalised dynamic reduction	g-dynamic reduction
Generalised IRS	g-IRS
Hybrid methods	
Component mode synthesis by Craig–Bampton	CMS
Improved CMS	ICMS
Krylov subspace component mode synthesis	KCMS
Improved KCMS	IKCMS
Generalised CMS	g-CMS
Generalised ICMS	g-ICMS
Generalised KCMS	g-KCMS
Generalised IKCMS	g-IKCMS

transmission found in the reduced floor models when realistic boundary conditions were involved, these being accomplished by connecting the reduced models to the top of a pair of wall panel models. The displacement spectrum for one of the wall panels was analysed when a unit load was applied to the other panel.

3.1. Error quantities

Both the eigenfrequencies and the eigenmodes of the reduced models were studied in the eigenvalue analysis carried out. The eigenfrequencies were compared with those of the full (non-reduced) model in terms of the normalised relative frequency difference (NRFD) and the eigenmodes with those of the full model in terms of the modal assurance criterion (MAC). To obtain a measure for the displacement spectrum of the whole receiver wall panel in the steady-state analysis, a root mean square (RMS) value for the displacement magnitudes in all the nodes of the panel was calculated for each of the frequency steps.

3.1.1. Normalised relative frequency difference (NRFD)

The NRFD of the ith eigenfrequency is defined as

$$\mathrm{NRFD} = \frac{\left|f_i^{red} - f_i^{full}\right|}{f_i^{full}} \cdot 100, \tag{40}$$

where f_i^{full} is the eigenfrequency of the full model and f_i^{red} is the eigenfrequency of the reduced model. This quotient is multiplied by 100 to obtain the NRFD value as a percentage.

3.1.2. Modal assurance criterion (MAC)

The MAC value for the jth eigenmode of the reduced model, Φ_j^{red}, as compared with the ith eigenmode of the full model, Φ_i^{full}, is defined as

$$\mathrm{MAC} = \frac{\left|(\Phi_j^{red})^T(\Phi_i^{full})\right|^2}{(\Phi_j^{red})^T(\Phi_j^{red})(\Phi_i^{full})^T(\Phi_i^{full})}. \tag{41}$$

The eigenmodes of a reduced model often appear in shifted order as compared with the full model. Accordingly, each of the eigenmodes of a reduced model is compared with each of eigenmodes of the full model, within the frequency range which is specified.

3.1.3. Root mean square (RMS)

For any given excitation frequency f in the steady-state analysis, the RMS value is defined here as

$$U_{RMS}(f) = \sqrt{\frac{1}{n_{dof}}\sum_{i=1}^{n_{dof}} U_i(f)^2}, \tag{42}$$

where $U_i(f)$ is the magnitude of the complex amplitude for the ith displacement dof and n_{dof} is the number of displacement dofs of the receiver wall panel. A normalised error of the RMS value for a reduced model, U_{RMS}^{red}, as compared with the RMS value for the full model, U_{RMS}^{full}, can be calculated as

$$U_{RMS}^{error}(f) = \frac{\left|U_{RMS}^{red}(f) - U_{RMS}^{full}(f)\right|}{U_{RMS}^{full}(f)} \cdot 100. \tag{43}$$

Calculating the error for each excitation frequency enables an error spectrum to be obtained. Since the error spectra typically fluctuate to a marked degree, the result plots used for comparing the different reduction methods make use of averaged error spectra. The errors are averaged by sweeping a 20 Hz wide window over the frequency range and calculating the mean value of the spectrum inside the window for each frequency. Accordingly, the frequency range of the plots is one of 10–90 Hz.

3.2. Numerical example 1: a moderate-sized floor structure

In the first numerical example, a model of a $2445 \times 4090\ \mathrm{mm}^2$ large floor structure was studied. The structure consisted primarily of five load-bearing wooden beams, using a centre-to-centre distance of the successive beams from one another of 600 mm, supporting a particle board surface. At the two shorter sides of the floor, wooden beams were placed perpendicular to the five beams just referred to, creating a box-like structure. Each of these wood beams had a cross-section of $45 \times 220\ \mathrm{mm}^2$ and was modelled using an orthotropic material model possessing the properties shown in Table 2. The particle board had a thickness of 22 mm and was modelled using an isotropic material model having the properties shown in Table 3. The structure was meshed using 20-node brick elements with quadratic interpolation, resulting in 30,807 dofs. The mesh, viewed from below, is shown in Fig. 1. The structural components shared mesh nodes at the intersections, the connections thus being modelled as fully interactive.

All the dofs along the centre line on the underside of the outermost beams were selected as master dofs, resulting in there being 576 master dofs altogether, this representing the minimum number of dofs in the reduced models. Reduced models of the full floor-structure model were created by employing the 14 methods for model order reduction listed in Table 1. The dynamic reduction involved a frequency shift of 53.1 Hz, this being the eigenfrequency of the full model closest to 50 Hz, located at the centre of the frequency range. IRS, ICMS and IKCMS were employed in their iterated versions, using three iterations. A total of 50 generalised coordinates were made use of in the hybrid reduction methods employed. Accordingly, 50 eigenmodes were included in the mode-based methods and 50 Krylov vectors in the Krylov-based methods, resulting in reduced models having 626 dofs.

The reduced models established by employing all of the reduction methods listed in Table 1 resulted in very similar computation times, the condensation methods resulting in marginally shorter times compared to the component mode synthesis methods. The similarity can be explained by the size of the reduced models being

Table 2
The material parameters used for the wooden beams [26], the stiffness parameters being given in terms of MPa and the density in $\mathrm{kg/m}^3$.

E_1	E_2	E_3	G_{12}	G_{13}	G_{23}	ν_{12}	ν_{13}	ν_{23}	ρ
8500	350	350	700	700	50	0.2	0.2	0.3	432

Table 3
The material parameters used for the particle board [26], the modulus of elasticity being given in terms of MPa and the density in kg/m^3.

E	ν	ρ
3000	0.3	767

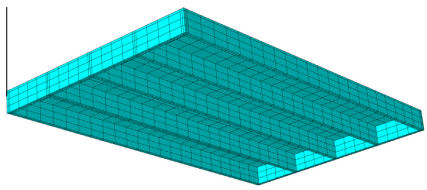

Fig. 1. The mesh of the floor structure in numerical example 1.

similar and the band width of the matrices being very large for all methods. The computation time for the eigenvalue analysis of each of the reduced models was approximately 3% of the computation time for the full model.

3.2.1. Eigenvalue analysis

The NRFD values for the original methods are shown in Fig. 2, 19 eigenfrequencies being included there, this being the number of eigenfrequencies of less than 100 Hz contained in the full model. The red, yellow and green dashed lines in the figure represent the error levels 10%, 1% and 0.1%, respectively. Guyan reduction provides an acceptable accuracy only for the first eigenfrequency of the full model, whereas dynamic reduction yields high NRFD values for each of the eigenfrequencies. CMS and KCMS provide relatively good and very similar results, the improved variants of both methods increasing the performance appreciably due to the high degree of accuracy of iterated IRS, quite to be expected since the eigenfrequencies iterated IRS provides converge in such a way as to reproduce the eigenfrequencies of the full model exactly.

The NRFD values for the generalised methods are shown in Fig. 3. As is evident there, the generalised versions of Guyan reduction and dynamic reduction improve the accuracy as compared with the original versions. The accuracy of IRS decreases for the lower frequencies when its generalised version is employed and, consequently, the accuracy of ICMS and IKCMS decreases as well. The results obtained when employing CMS and KCMS are slightly improved, however, when use is made of the generalised versions of the two.

In Fig. 4, the MAC values for the seven original methods and for the generalised versions of Guyan reduction, dynamic reduction, CMS and KCMS are shown. A plot comparing the full model with itself is included in order to demonstrate the orthogonality properties of the eigenmodes. Since the eigenmodes are non-orthogonal in the dot product, the off-diagonal terms are not generally zero in value, although this is the case in the example given here (within the discretization of the MAC plots, the off-diagonal terms being less than 0.1). In agreement with the NRFD results, the MAC values for the original versions of the Guyan reduction and the dynamic reduction correlate poorly with the full model, whereas the generalised versions show a relatively high degree of accuracy. All of the other original reduction methods, except for CMS, show a high degree of correlation with the full model for each of the eigenmodes.

3.2.2. Steady-state analysis

The setup for the steady-state analysis is shown in Fig. 5. The floor models were connected to the top of two wall panels, the one a source panel and the other a receiver panel, supporting each end of the load-bearing beams. The wall panels were modelled as shells provided with beam stiffeners at successive spacings from one another of 600 mm each, representing a 2500 mm high wood-framed wall having a plaster board surface. The floor models were tied to the displacement dofs of the wall panels by use of Lagrange multipliers, the bottom edge of the wall panels being fixed. A unit point load in all three directions, shown by the yellow arrows in the figure, was applied to the source panel. The displacements of the receiver wall panel were evaluated in accordance with Eq. (42) for excitation frequencies of up to 100 Hz.

The averaged error of the RMS values obtained using the original methods and the generalised methods is shown in Figs. 6 and 7, respectively. The dashed black line in both figures indicates the 10% error level. In studying Fig. 6, one can note that the frequency shift in dynamic reduction strongly affect the performance. Whereas Guyan reduction (corresponding to a 0 Hz shift) generates lower errors when the frequencies involved are lower, dynamic reduction results in the degree of errors being lowest at around 50 Hz, close to the frequency shift selected. CMS and KCMS can be seen to behave very similarly at the higher frequencies, whereas at the lower frequencies the latter is more accurate. In contrast to the results of the eigenvalue analysis, ICMS and IKCMS lower the level of performance for most frequencies as compared with conventional CMS and KCMS. In Fig. 7, one can note that the accuracy of Guyan reduction and of dynamic reduction is appreciably

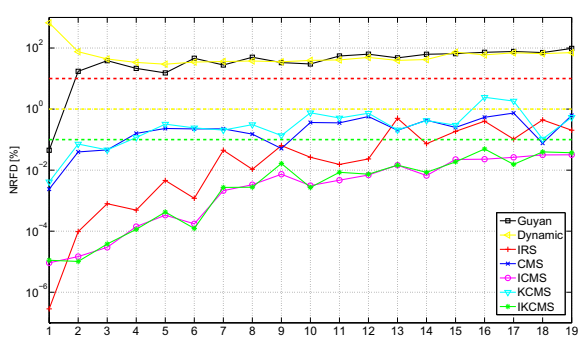

Fig. 2. NRFD values for the original model order reduction methods applied to numerical example 1.

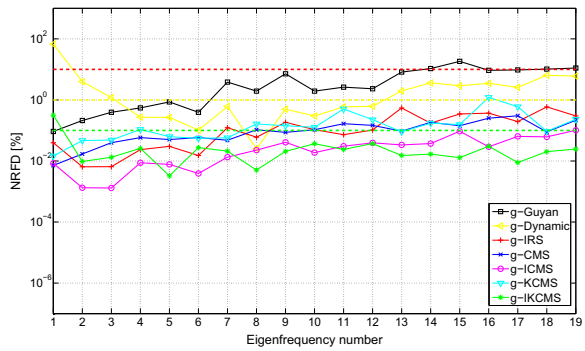

Fig. 3. NRFD values for the generalised model order reduction methods applied to numerical example 1.

greater with use of the generalised versions of these. The accuracy of KCMS decreases markedly at lower frequencies and increases at the higher frequencies when the generalised version of it is employed. As can be seen by comparing the results in Figs. 6 and 7, there is, generally speaking, a lesser degree of spread among the results for the different reduction methods when their generalised versions are employed.

In Table 4, the maximum and the mean errors for the frequency range as a whole (without averaging) are shown for both the original and the generalised methods. As is evident, using the generalised versions only has a strong positive effect in the case of Guyan reduction and of dynamic reduction. For most of the hybrid methods, use of the generalised versions leads to a reduction in performance. Of all the reduction methods, it is KCMS that provides the most accurate results in terms both of average and of maximum error levels.

3.3. Numerical example 2: a large two-span floor structure

In the second numerical example, a model of an experimental floor structure that was compared with measurements in [26] was studied. The 3645×9045 mm^2 large floor structure consists of seven load-bearing wooden beams, at a centre-to-centre distance of the successive beams from one another of 600 mm, supporting a particle board surface, secondary spaced boarding being attached to the underside of the beams. In the FE model, the wooden beams were placed perpendicular to the load-bearing beams at the two short sides of the floor, creating a box-like structure, in contrast to the experimental structure in which the ends of the beams were free. Each of the wooden beams had a cross-section of 45×220 mm^2 and was modelled using an orthotropic material model having the properties shown in Table 2. The secondary spaced boarding had a cross-section of 28×70 mm^2 and was modelled as having the same material properties as the wooden beams. The particle board had a thickness of 22 mm and was modelled using an isotropic material model possessing the properties shown in Table 3. The structure was meshed using 20-node brick elements with quadratic interpolation, resulting in 632,820 dofs. The mesh, as viewed from below, is shown in Fig. 8. The structural components shared mesh nodes at the intersections, the connections thus being modelled as fully interactive.

For reasons of efficiency, it is desirable to connect the floor structure to other structures at discrete points so as to minimise the number of physical dofs retained in the reduced models. Discrete point connections require that rotational dofs fulfil conditions of compatibility. To create rotational coupling in the case of the solid elements, 173 additional nodes, indicated by the yellow crosses in Fig. 8, having both displacement dofs and rotational dofs, were created. These nodes were connected to the neighbouring mesh nodes under conditions of rigid beam constraints, the rotational dofs thus being connected to the rotations of the structure as a whole. The experimental structure has both a mid-span support and end supports. To provide for a modelling of all of the supports, the model has additional nodes possessing rotational dofs both along the underside of the outermost beams and at the middle of the load-bearing beams. The dofs at the 173 additional nodes served as master dofs in the model order reduction, resulting in 1038 master dofs. The model was reduced by use of the two model order reduction methods implemented in Abaqus: Guyan reduction and CMS. The number of eigenmodes retained in the CMS reduction was varied so as to study the convergence of errors.

When employing the model order reduction methods, computationally effective models are obtained by reducing the size of the large system matrices obtained by use of detailed FE models. As an alternative, smaller systems can be constructed directly by use of structural finite elements, beam or shell elements, for example, assumptions being made regarding the kinematic relations and the equilibrium equations involved. These assumptions can turn out to have no more than a negligible effect in static analysis if one or two dimensions of the structure are significantly smaller than the other or others. In dynamic analysis, however, the constraints implied by beam and shell theory can have a strong effect on the structural behaviour in the case of higher frequencies. A structural FE model of the floor structure was created by modelling the panels and the wooden beams in terms of Reissner–Mindlin shell elements, and the secondary spaced boarding in terms of Timoshenko beam elements. The two theories involved allow for shear deformation of the normal to the shell plane and of the beam axis, respectively. Further discussion of the beam and the shell theory can be found in e.g. [5,27]. The structural-element model was meshed with 720 beam elements and 3312 shell elements, resulting in 24,762 dofs.

Table 5 shows the size (number of dofs) of the reduced models as well as the computation times obtained for a Lanczos eigenvalue analysis of the 55 first eigenmodes and a steady-state analysis involving 200 steps. The analyses were carried out employing Abaqus/Standard. It can be observed that the computation times are affected by increasing the number of eigenmodes retained in the CMS reduction, the retaining of 1000 eigenmodes (a duplication of the number of dofs compared to Guyan reduction) resulting in the computation times being increased significantly. The number of eigenmodes retained is, of course, a trade-off between accuracy

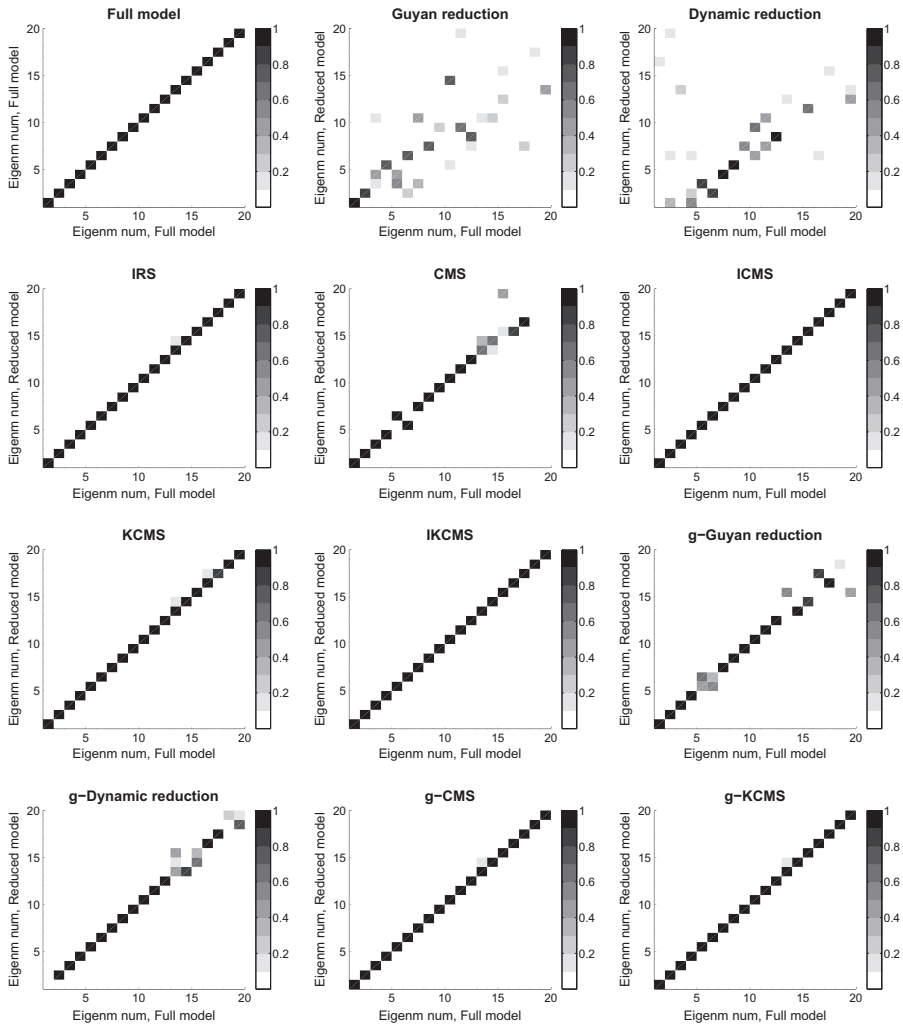

Fig. 4. MAC values for the different model order reduction methods applied to numerical example 1.

and computational cost, the gain in accuracy being illustrated in the analysis results presented below. It is, however, not possible to estimate the number of eigenmodes required for obtaining a certain accuracy without analysing the full model. Moreover, it can be observed that the computation times for both types of analyses of the structural elements model is similar to those for a model reduced with CMS where 500–1000 eigenmodes are retained, in spite of the former model being over 10 times larger. This is a consequence of the transformation of the system matrices involved in model order reduction, destroying the narrow bandwidth of matrices constructed with the FE method.

3.3.1. Eigenvalue analysis

Fig. 9 shows the NRFD values for the reduced models, including CMS when 10, 100 and 1000 eigenmodes are retained. The red, yellow and green dashed lines in the figure show the error levels of 10%, 1% and 0.1%, respectively. The results included 55 eigenfrequencies, which is the number of eigenfrequencies of the full model up to 100 Hz. Guyan reduction assesses only the lowest eigenfrequencies of the full model with an acceptable level of accuracy. Use of CMS in which 10 eigenmodes are retained improves the accuracy obtained for the first 20 eigenmodes, but is inaccurate for the remaining eigenmodes. When 100 eigenmodes are retained,

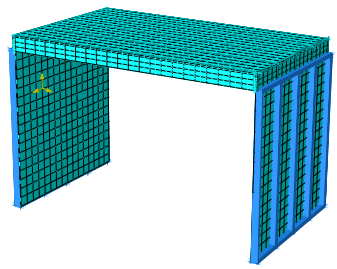

Fig. 5. The setup for the steady-state analysis in numerical example 1.

relatively accurate results can be obtained for all of the eigenfrequencies, the retaining of 1000 eigenmodes resulting in very small errors. Use of structural elements results in relatively large errors, although the errors are less frequency-dependent than when any of the model order reduction methods are employed.

Fig. 10 shows the MAC values obtained with use of the reduced models, including CMS when 10, 50, 100, 500 and 1000 eigenmodes are retained, as well as the full model being compared with itself. For practical reasons, only the master dofs of the reduced models were used for evaluating the eigenmodes. In comparing the plots, it could be noted that the MAC values of the higher eigenmodes were improved with use of CMS when the number of eigenmodes retained was increasing. Whereas Guyan reduction (no eigenmodes retained) only succeeds in modelling a few of the eigenmodes in the full model accurately, the MAC plot for CMS when 1000 eigenmodes are retained is identical to the MAC plot

Table 4
Average and maximum error levels of the RMS values obtained for the reduction methods applied to numerical Example 1.

Model	Mean error (%)	Maximum error (%)
Guyan reduction	37.7	276
g-Guyan reduction	8.26	35.0
Dynamic reduction	106	1120
g-dynamic reduction	7.49	54.6
IRS	6.52	39.4
g-IRS	5.70	37.5
CMS	3.26	20.9
g-CMS	3.35	27.0
ICMS	4.81	63.4
g-ICMS	4.18	33.9
KCMS	2.92	20.2
g-KCMS	3.21	27.8
IKCMS	4.96	42.6
g-IKCMS	7.67	98.1

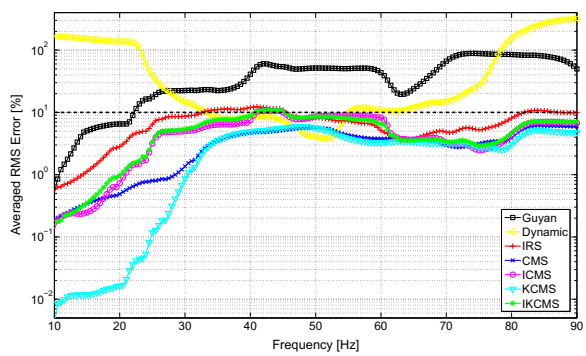

Fig. 6. Averaged errors of the RMS values for numerical example 1, as determined with use of the original model order reduction methods.

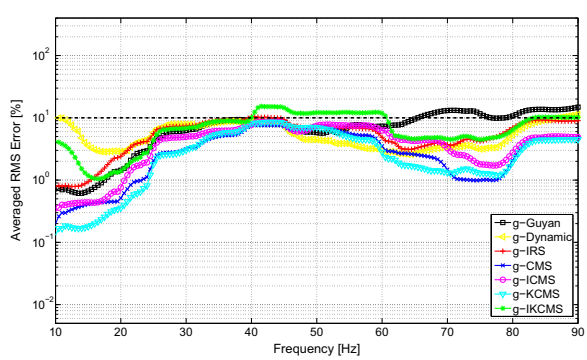

Fig. 7. Averaged errors of the RMS values for numerical example 1, as determined with use of the generalised model order reduction methods.

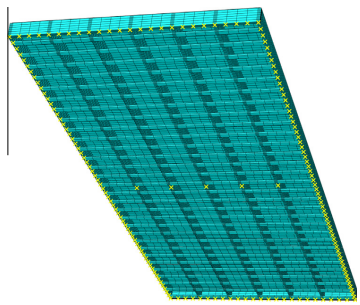

Fig. 8. The mesh of the floor structure model in numerical example 2.

Table 5
The size and computation times, both for eigenvalue analyses and steady-state analyses, of the reduced models analysed in connection with numerical example 2, the analyses running on one core of an Intel Xeon W3530 CPU of 2.80 GHz, having 10 GB of RAM memory available.

Model	Size (number of dofs)	Time (s) (eigenvalue anal.)	Time (s) (steady-state anal.)
Full model	632820	590	220000
Structural elements	24762	7.6	1200
Guyan reduction	1038	3.1	410
CMS, 10 re[a]	1048	3.2	410
CMS, 20 re[a]	1058	3.2	410
CMS, 50 re[a]	1088	3.7	420
CMS, 100 re[a]	1138	5.5	440
CMS, 200 re[a]	1238	5.7	480
CMS, 500 re[a]	1538	8.5	620
CMS, 1000 re[a]	2038	15	970

[a] Retained eigenmodes.

for the full model. The structural element model only models a few of the eigenmodes of the full model with a high degree of accuracy. The correlation there with results of the full model is better for the higher frequencies, however, than is the case of Guyan reduction or CMS when only a few eigenmodes are retained.

3.3.2. Steady-state analysis

The transmission of vibrations was studied using the same approach as in the first numerical example, shown in Fig. 5, where the floor models were connected to the top of two wall panels, the one a source panel and the other a receiver panel, supporting each end of the load-bearing beams. The floor models were, in the second numerical example, connected to a third wall panel located at the centre of the floor models through the nodes in the middle of the load-bearing beams. Both the displacement dofs and rotational dofs of the wall panels were linked to the floor models by use of Lagrange multipliers, except in the case of the mid-span wall panel, at which only the displacement dofs were connected. A unit point load in all three directions was applied to the source panel, the displacements at the receiver panel being evaluated for excitation frequencies of up to 100 Hz by use of Eq. (42).

The averaged error of the RMS values for the reduced models, including CMS when 10, 100 and 1000 eigenmodes are retained, is shown in Fig. 11. The dashed black line indicates the 10% error level. Guyan reduction was found to produce large errors for most of the frequencies. Use of CMS in which 10 eigenmodes were retained was found to produce large errors as well, whereas CMS in which 100 eigenmodes were retained was found to be relatively accurate for most of the frequencies. A reduced model in which close to 1000 eigenmodes were retained was needed, however, to obtain satisfactory results for higher frequencies. As in the eigenvalue analysis, the structural element model was found to produce relatively large errors, but with a lesser frequency dependence than for the other methods.

The maximum and the mean error values obtained for the frequency range as a whole (without averaging) are shown in Table 6. As can be seen, the levels of error converge when the number of retained eigenmodes employed in the CMS reduction is increased. When as many as 50 eigenmodes are included, there is a large reduction in the error as compared with Guyan reduction, in spite of the CMS model being only 5% larger. The convergence is slower when a greater number of eigenmodes are retained, but as shown in Fig. 11, at higher frequencies a greater number of eigenmodes are required in order to obtain accurate results. It could also be observed that including a greater number of retained eigenmodes can result in an increase in the maximum error. Consequently, for a given frequency, increasing the number of retained eigenmodes does not necessarily result in a decrease in the level of error involved.

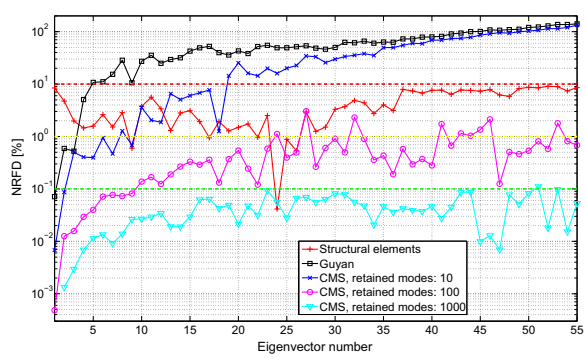

Fig. 9. NRFD values for the different reduction methods applied to numerical example 2.

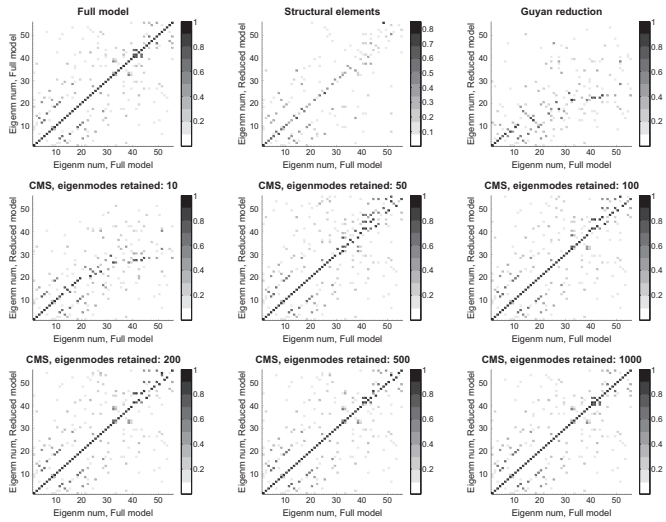

Fig. 10. MAC values for the reduction methods employed in connection with numerical example 2.

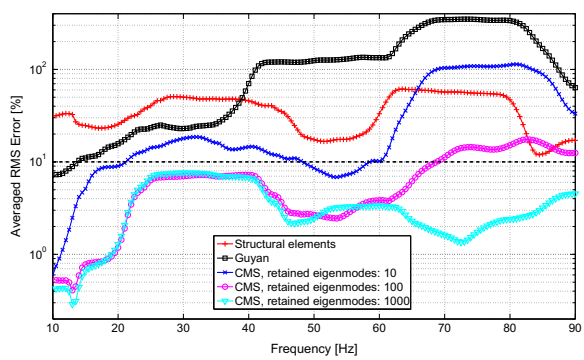

Fig. 11. Averaged errors of RMS values obtained for the model order reduction methods used in connection with numerical example 2.

Table 6
Average and maximum errors of the RMS values obtained in connection with numerical example 2.

Model	Mean error (%)	Maximum error (%)
Structural elements	34.9	61.4
Guyan reduction	113	349
CMS, 10 retained eigenmodes	33.1	114
CMS, 20 retained eigenmodes	11.5	38.4
CMS, 50 retained eigenmodes	7.75	16.3
CMS, 100 retained eigenmodes	6.88	21.4
CMS, 500 retained eigenmodes	3.86	8.92
CMS, 1000 retained eigenmodes	3.38	7.61

4. Conclusions

The objective of the analyses carried out in the present investigation was to evaluate the performance of a wide range of methods for model order reduction by comparing their accuracy and computational cost when applied to detailed FE models of floor and wall structures. In the first numerical example, it was evident that an eigenvalue analysis of the structure in a free-free state is insufficient for analysing the performance of the different reduction methods. A sensitivity of certain of the reduction methods to boundary conditions was demonstrated, differing observations being made regarding the accuracy of the methods in question in the two analyses: the eigenvalue analysis and the steady-state analysis. This shows the need for the reduced models to be analysed with use of realistic boundary conditions, such as in the case of the steady-state analyses that were considered here.

As was expected, Guyan reduction delivered acceptable results only at frequencies close to the lowest eigenfrequencies of the system, due to the method's static nature. Dynamic reduction was only found to be accurate close to the frequency shift selected

and provided inaccurate results at frequencies differing to any appreciable extent from this. Iterated improved reduction system (IRS) provided considerably better results than the other condensation methods.

In both numerical examples, component mode synthesis by Craig–Bampton (CMS) proved to be an effective method. The Krylov subspace component mode synthesis (KCMS) method used in the present study was found to be a good alternative as compared with CMS, the two methods offering comparable accuracy. Using IRS to create the improved variants of CMS and KCMS (ICMS and IKCMS, respectively) enabled the accuracy in terms of eigenfrequencies and eigenmodes to be improved appreciably, although at the same time the errors in the steady-state analysis were found to increase, indicating the improved variants to possibly be more sensitive to the boundary conditions introduced in the analysis.

The performance of Guyan reduction and of dynamic reduction was found to clearly be improved by use of the generalised versions of these methods. For the remaining methods, the accuracy was only marginally affected by use of the generalised versions and, for most of the methods, it was decreased at lower frequencies.

The alternative approach of using structural finite elements was found to result in relatively large errors, the computation time, however, being significantly shorter considering the size of the model. The structural element model can, however, be optimised further regarding such matters as the selection of structural element types and the connections involved.

Acknowledgments

The financial support for this work provided by the Silent Spaces project, a part of the EU program Interreg IV A, is gratefully acknowledged.

References

[1] Fehr J, Eberhard P. Simulation process of flexible multibody systems with non-modal model order reduction techniques. Multibody Syst Dyn 2011;25(3):313–34.
[2] Nowakowski C, Kürschner P, Eberhard P, Benner P. Model reduction of an elastic crankshaft for elastic multibody simulations. J Appl Math Mech 2013;93(4):198–216.
[3] Koutsovasilis P, Beitelschmidt M. Comparison of model reduction techniques for large mechanical systems. Multibody Syst Dyn 2008;20(2):111–28.
[4] Witteveen W. On the modal and non-modal model reduction of metallic structures with variable boundary conditions. World J Mech 2012;2(6):311–24.
[5] Bathe KJ. Finite element procedures. New York: Prentice Hall; 1996.
[6] Arnold RR, Citerley RL. Application of Ritz vectors for dynamic analysis of large structures. Comput Struct 1985;21(5):901–7.
[7] Guyan RJ. Reduction of stiffness and mass matrices. AIAA J 1965;3:380.
[8] Leung AYT. An accurate method of dynamic condensation in structural analysis. Int J Numer Methods Eng 1978;12:1705–15.
[9] O'Callahan J. A procedure for an improved reduced system (IRS) model. Proc Seventh Int Modal Anal Conf 1989:17–21.
[10] Friswell MI, Garvey SD, Penny JET. Model reduction using dynamic and iterated IRS techniques. J Sound Vib 1995;186:311–23.
[11] O'Callahan J, Avitabile P, Riemer R. System equivalent reduction expansion process (SEREP). Proc Seventh Int Modal Anal Conf 1989:29–37.
[12] Craig RR. Structural dynamics; an introduction to computer methods. New York: John Wiley & Sons Inc.; 1981.
[13] Craig RR, Chang CJ. A review of substructure coupling methods for dynamic analysis. Adv Eng Sci 1976;2:393–408.
[14] Lohmann B, Salimbahrami B. Introduction to Krylov subspace methods in model order reduction. Methods Appl Autom 2003:1–13.
[15] Salimbahrami B, Lohmann B. Order reduction of large scale second-order systems using Krylov subspace methods. Linear Algebra Appl 2006;415(2):385–405.
[16] Benner P. Numerical linear algebra for model reduction in control and simulation. GAMM Mitt 2006;29(2):275–96.
[17] Reis T, Stykel T. Balanced truncation model reduction of second-order systems. Math Comput Model Dyn Syst 2008;14(5):391–406.
[18] Craig RR, Bampton M. Coupling of substructures in dynamic analysis. AIAA J 1968;6:1313–9.
[19] MacNeal RH. A hybrid method of component mode synthesis. Comput Struct 1971;1(4):581–601.
[20] Rubin S. Improved component-mode representation for structural dynamic analysis. AIAA J 1975;13:995–1006.
[21] Koutsovasilis P, Beitelschmidt M. Model order reduction of finite element models: improved component mode synthesis. Math Comput Model Dyn Syst 2010;16(1):57–73.
[22] Häggblad B, Eriksson L. Model reduction methods for dynamic analyses of large structures. Comput Struct 1993;47(4):735–49.
[23] Koutsovasilis P. Improved component mode synthesis and variants. Multibody Syst Dyn 2013;29:343–59.
[24] Bouhaddi N, Fillod R. A method for selecting master dof in dynamic substructuring using the Guyan condensation method. Comput Struct 1992;45(5):941–6.
[25] Shah V, Raymund M. Analytical selection of masters for the reduced eigenvalue problem. Int J Numer Methods Eng 1982;18(1):89–98.
[26] Flodén O, Ejenstam J. Vibration analyses of a wooden floor-wall structure – experimental and finite element studies. Report TVSM-5176, Division of Structural Mechanics, Lund University, Sweden; 2011.
[27] Zienkiewicz OC, Taylor RL. The finite element method, 5th ed., vol. 2. London: MacGraw-Hill; 1994.